Engineered polysaccharide-based nanoparticles as hybrid fertilizer for efficient plant nutrition and stress tolerance

B.C Zungu



orcid.org 0000-0002-9369-3189

Thesis submitted in fulfilment of the requirements for the degree *Doctor of Philosophy in Science with Chemistry* at the North-West University

Promoter: Prof. Katata-Seru

Co-promoter: Dr. Kamdem Paumo

Graduation ceremony: 20 May 2024

DECLARATION

I, Bongiwe Colleen Zungu, declare herewith that the thesis entitled “Engineered polysaccharide-based nanoparticles as hybrid fertilizer for efficient plant nutrition and stress tolerance”, which I submit to the North-West University as completion of the requirements set for the Doctoral degree, is my own work and has not been submitted to any other university.

Signature of candidate: BC Zungu

University number: 25548867

Signed at: North-West University On this 27th day of November 2023

ACKNOWLEDGEMENTS

I want to forward my sincere gratitude to all, who have contributed to accomplishing this exciting project. It would not have been possible without your kindness, encouragement, and support.

- Firstly, I give thanks to the Almighty God, Shembe UNyaziLweZulu, for the opportunity granted, knowledge, and strength to keep on going forward despite the challenges.
- To my supervisor, Prof L Katata-Seru, I want to acknowledge your dedication, guidance, and continuous support.
- Special and sincere thanks go to my co-supervisor Dr H Kamdem Paumo for his invaluable scientific and technical advice.
- I want to thank Prof O Ruzvidzo for his thoughtful input and technical assistance during germination testing.
- My acknowledgements also go to my lab mates, Mr Rebaone Makaudi and Mr Joseph Gaorongwe, for their consistent interest in my study.
- I want to express my deepest gratitude and heartfelt thanks to my parents (Thokozile Dhlamini and Promise Pooe), siblings (Sibusiso Dhlamini and Busisiwe Dhlamini), and husband (Thembinkosi Zungu) for raising my confidence and aspirations.
- I also sincerely thank the North-West University, Sasol-Inzalo, and National Research Foundation (NRF) for financial support.

DEDICATION

I want to dedicate this thesis to my mother (Thokozile Dhlamini), children (Zanenhlanhla, Lindani, and Nqobile Zungu), and husband (Thembinkosi Zungu).

RESEARCH CONTRIBUTIONS

Bongiwe Dhlamini, Hugues Kamdem Paumo, Boniface Pone Kamdem, Lebogang Katata-Seru, and Indra Bahadur. Nano-engineering metal-based fertilizers using biopolymers: An innovative strategy for a more sustainable agriculture. **Journal of Environmental Chemical Engineering**, 2022, 10: 107729.

Bongiwe Zungu, Hugues Kamdem Paumo, Joseph Lesibe Gaorongwe, Gaborone Neo Tsuene, Oziniel Ruzvidzo, and Lebogang Katata-Seru, Zn nutrients-loaded chitosan nanocomposites and their efficacy as nanopriming agents for maize (*Zea mays*) seeds, ***Frontier in Chemistry***, 2023, 11: 1243884.

Bongiwe Dhlamini, Hugues Kamdem Paumo, and Lebogang Katata-Seru, *Helichrysum odoratissimum*-mediated ZnO nanoparticles as nano-priming agent for improving seed germination in maize (*Zea mays*). Manuscript under consideration for publication in **Journal of nanomaterials**.

Bongiwe Dhlamini, Hugues Kamdem Paumo, and Lebogang Katata-Seru. Nano-engineered metal-based nutrients using chitosan for efficient plant nutrition and growth. **4th edition of World Nanotechnology Conference** (Virtual Event - Oral presentation), Las Vegas, USA, 25-27 April 2022.

Bongiwe Colleen Zungu, Hugues Kamdem Paumo, and Lebogang Katata-Seru. Bio-developed nanofertilizers for improved crop productivity. **Three Minute (3MT) Thesis competition (Institutional)**(contact presentation), North-West University, 14 October 2022. 1st runner-up winner.

Bongiwe Colleen Zungu, Hugues Kamdem Paumo, and Lebogang Katata-Seru. Bio-developed nanofertilizers for improved crop productivity. **Three Minute (3MT) Thesis National Competition** (virtual), University of Free State, 28 October 2022. Winner (1st position overall winner).

TABLE OF CONTENTS

DECLARATION i

ACKNOWLEDGEMENTS ii

DEDICATION iii

RESEARCH CONTRIBUTIONS iv

ABSTRACT ix

LIST OF ABBREVIATIONS AND ACRONYMS xii

LIST OF FIGURES xiv

LIST OF SCHEMES xviii

LIST OF TABLES xix

CHAPTER 1 1

INTRODUCTION 1

1.1 Rationale and scope of the study 1

1.2 Effects of zinc and iron micronutrients for plant growth 4

1.3 Maize crop production and importance 6

1.4 Environmental impact of conventional fertilizers 7

1.5 Nanotechnology in agriculture 9

1.6 Problem statement 10

1.7 Research aim and objectives 11

1.8 Overview of the thesis 12

REFERENCES 15

CHAPTER 2 26

LITERATURE REVIEW 26

2.1 Metal-based nanoparticles in agriculture 26

2.2 Metal-based nanoparticles and their phytotoxicity 34

2.3 Biopolymer-based nanomaterials for agricultural practices 39

2.4 Nanomaterials and their pesticidal activity 44

REFERENCES 47

CHAPTER 3 64

RESEARCH METHODOLOGY 64
3.1 Materials 64
3.2 Experimental methods 64
3.2.1 Preparation and characterization of *H. odoratissimum* aqueous extract 64
3.2.2 *H. odoratissimum* aqueous extract-mediated synthesis of nano-metal oxides (ZnO and Fe_3O_4) 65
3.2.3 Encapsulation of the pre-synthesized metal oxides within chitosan nanoparticles 66
3.3 Characterization of nano-metal oxides (ZnO and Fe_3O_4) and nutrient-loaded chitosan nanoparticles 68
3.3.1 Electrochemical measurements 68
3.3.2 Dynamic light scattering (DLS) and zeta potential 68
3.3.3 Fourier transform infrared spectroscopy (FTIR) 68
3.3.4 X-ray diffraction spectroscopy (XRD) 69
3.3.5 Electron microscopy 69
3.3.6 X-ray photoelectron spectroscopy (XPS) 70
3.3.7 Thermogravimetric analysis (TGA) 70
3.4 Release behaviour of the prepared nanomaterials in water 71
3.5 Seed germination study 71
3.5.1 Seed decontamination and stratification 71
3.5.2 Seed priming 72
3.6 Antifungal activity 73
REFERENCES 75
CHAPTER 4 76
CHARACTERIZATION OF *H. ODORATISSIMUM* EXTRACT-MEDIATED NANO-METAL OXIDES 76
4.1 Phytochemical screening of *H. Odoratissimum* aqueous extract 76
4.2 Reduction potential of *H. Odoratissimum* aqueous extract and time monitoring for the formation of nanoparticles using absorption spectra 79

4.3 Microscopic and spectroscopic analysis of the nano-metal oxides (ZnO & Fe_3O_4) 82
4.3.1 Electron microscopy 82
4.3.2 Average particle size and surface charge 83
4.3.3 FTIR spectral analysis 86
4.3.4 XRD patterns analysis 87
REFERENCES 91
CHAPTER 5 98
CHARACTERIZATION OF NUTRIENT-LOADED CHITOSAN NANOPARTICLES . 98
5.1 Microscopic and spectroscopic analysis of the nutrient-loaded chitosan nanoparticles 98
5.1.1 Electron microscopy 98
5.1.2 Average particle size and surface charge 101
5.1.3 FTIR spectral analysis 105
5.1.4 Thermogravimetric analysis 106
5.1.5 XPS spectra analysis 107
5.2 Nutrient release behaviour in water 114
REFERENCES 116
CHAPTER 6 121
EFFECTS OF DEVELOPED ZINC OXIDE AND ZINC LOADED CHITOSAN NANOPARTICLES ON MAIZE SEED GERMINATION 121
6.1 Nanopriming technology for enhancing seed germination in sustainable agriculture 121
6.2 Germination traits of maize seeds primed with ZnO nanoparticles 125
6.2.1 Effects on germination of non-stressed seeds 125
6.2.2 Effects on germination of salt-stressed seeds 129
6.3 Germination traits of maize seeds primed with zinc-loaded chitosan nanoparticles 133
6.3.1 Effects on germination of non-stressed seeds 133

6.3.2 Effects on germination of salt-stressed seeds 138
REFERENCES 144
CHAPTER 7 150
ANTIFUNGAL PROPERTIES OF THE DEVELOPED IRON OXIDE AND IRON LOADED CHITOSAN NANOPARTICLES 150
7.1 Antifungal potential of metal oxide and chitosan nanoparticles 150
7.2 Activities against selected plant pathogenic fungi 153
7.3 Activities against selected fungal pathogens of humans 155
REFERENCES 157
CHAPTER 8 162
CONCLUSION AND PERSPECTIVES 162
APPENDIX 165

ABSTRACT

According to the Food and Agriculture Organization of the United Nations report 2022, nearly 828 million people were reported to suffer from chronic undernourishment in 2021-2022, with over 250 million affected in Africa. These figures demonstrate that achieving the United Nations Sustainable Development Goal 2 remains an elusive utopia unless it has happened in Africa. According to the global agriculture leaders in the 2023 Dakar 2 Summit, the continent should draw on its vast potential to feed on itself. However, the agricultural sector in the most populated continent, after Asia, is also increasingly facing the negative impacts of changing climates due to various stress conditions. Low-risk practices such as decreasing fertilizer inputs and seed priming have been promoted to curb this scenario. Breakthroughs in agricultural research have led to the development of nanofertilizers as priming agents that could contribute less to environmental pollution while promoting the early growth stages of plants, even under stress.

In this study, nano-metal oxides (ZnO and Fe_3O_4) were developed following the phyto-assisted procedure. Aqueous extracts of the South Africa's sacred herb *Helichrysum odoratissimum* (Impepho) were used, at different concentrations. The chemical profiles of these extracts were obtained using the colorimetric assessments complemented with the high-performance thin layer chromatography (HPTLC) analysis. The synthesized nano-metal oxides were characterized microscopically; scanning electron microscopy (SEM) and transmission electron microscopy (TEM) and spectroscopically; ultraviolet-visible spectroscopy (UV-Vis), Fourier-transform infrared spectroscopy (FTIR), and X-ray diffraction (XRD) techniques. Results revealed spherical ZnO and Fe_3O_4 nanoparticles from microscopic techniques. For UV-Vis, the absorption bands were observed at 370 nm (ZnO) and 416 nm (Fe_3O_4). The FTIR analysis confirmed the formation of nano-metal oxides and XRD patterns depicted crystalline structures for the nano-oxides. Furthermore, the electrochemical measurements established that the tested phytoconstituents (flavonoids, phenolic compounds, alkaloids, and terpenoids) acted as reducer and oxygen providers to convert the di-cationic Zn(II) and Fe(II) species into ZnO and Fe_3O_4 nanoparticles. Dynamic light scattering (DLS) technique revealed negatively charged and relatively

stable particles (surface charge < -26 mV) with average hydrodynamic sizes in the range of 144.6 ± 2.6 – 321.2 ± 6.2 nm.

The developed metal oxides and their metal ionic precursors were integrated into tripolyphosphate (TPP)-crosslinked chitosan (CS/TPP) biopolymeric nanostructures by ionic gelation. The physicochemical characterization techniques SEM-EDX, TEM, DLS, FTIR, TGA, and XPS were exploited to report the integrated nanomaterials' morphology, hydrodynamic size, surface charge, and structural organization. These revealed positively charged particles with average hydrodynamic sizes of 149.4 ± 22.3 - 498.8 ± 12.3 nm. The nutrient release behaviour of the developed polysaccharide-based nanoparticles was investigated by ICP-MS technique. The ZnO[15S], ZnO[15s]-loaded CS/TPP, and Zn(II)-laden CS/TPP nanoparticles were used as models. A slow change in zinc concentration of ZnO[15s]-loaded CS/TPP in water was observed as compared to other specimens during the study.

It has been argued that priming seeds with ZnO nanoparticles and TPP-crosslinked CS nanoparticles enhanced seed germination and seedling growth. Therefore, in this study, the developed ZnO nanoparticles and zinc integrated CS/TPP nanoparticles were used as nanopriming agents to stimulate the germination and early seedling growth of maize seeds. The seeds were soaked in the prepared treatments, arranged in triplicates inside the growth chamber in a complete randomized design (CRD). Ten days after priming *Zea mays* seeds with the ZnO nanoparticles at 0.04%, more than 3-fold increase in radicle elongation and number of lateral roots was recorded relative to the control treatment. Under salinity, ZnO nanoparticles (0.01%) improved the radicle length by 78% and 84% compared to the control and NaCl treatment, respectively. Moreover, the CS/TPP, Zn(II)-laden CS/TPP, and ZnO-loaded CS/TPP nanoparticles at 0.01%, significantly promoted the early seedling development under salinity stress.

Nanotechnology, by virtue of the important properties of nanoscale particles, has potential applications for the development of alternative pesticides. Iron oxide nanoparticles have demonstrated higher value in preventing and treating fungal infections in both plants and humans. Therefore, the antifungal properties of the prepared iron oxide nanoparticles and iron integrated CS/TPP nanoparticles were

evaluated against selected plant and human pathogens. The Fe_3O_4-loaded CS/TPP nanoparticles exhibited noteworthy activities with minimum inhibitory concentrations lower than 1.0 mg/mL against four phytopathogenic fungal strains, namely, *Aspergillus niger*, *Fusarium solani*, *Alternaria solani*, and *Aspergillus flavus*. The Fe(II)-laden CS/TPP nanoparticles were also found to show a better inhibitory effect against *F. solani* (MIC 0.3125 mg/mL) and *A. flavas* (MIC 0.625 mg/mL). Furthermore, the prepared Fe_3O_4-loaded CS/TPP nanoparticles showed the potential as therapeutic agents against *Candida* species (*Candida tropicallis* and *Candida glabrata*). This study envisaged promotion of the usage of phytoassisted procedures for the preparation of non-toxic nano-metal oxides for sustainable agriculture and food security.

Keywords: *Helichrysum odoratissimum*, nano-metal oxide, chitosan nanoparticles, seed priming, early seedlings development, antifungal activity.

LIST OF ABBREVIATIONS AND ACRONYMS

ALG	Alginate
CE	Complexation efficiency
CS	Chitosan
CDW	Coleoptile dry weight
CL	Coleoptile length
DLS	Dynamic light scattering
DNA	Deoxyribonucleic acid
EDX	Energy dispersive X-ray spectroscopy
FTIR	Fourier-transform infrared spectroscopy
GDP	Gross domestic product
HPTLC	High-performance thin layer chromatography
ICP-MS	Inductively coupled plasma-mass spectrometry
LoR	Length of roots
MIC	Minimum inhibitory concentration
MO	Metal oxide
NLR	Number of lateral roots
NR	Number of roots
NPs	Nanoparticles
PA	Phenolic acids
PDI	Polydispersity index
PVA	Polyvinyl alcohol
RDW	Radicle dry weight
RL	Radicle length
ROS	Reactive oxygen species
RDW	Root dry weight
RWC	Relative water content
FE-SEM	Field emission scanning electron microscopy
SDG	Sustainable Development Goals
SDW	Shoot dry weight
SL	Shoot length
TEM	Transmission electron microscope

TGA	Thermogravimetric analysis
TPP	Tripolyphosphate
UN	United Nations
UV-Vis	Ultraviolet-visible spectroscopy
USA	United States of America
WHO	World Health Organization
XPS	X-ray photoelectron spectroscopy
XRD	X-ray diffraction
ZP	Zeta potential

LIST OF FIGURES

Figure 1. 1: The world map of Zn deficiency showing the major countries and regions with low Zn soils. 2
Figure 1. 2: World map showing areas at high risk of iron deficiency. 3
Figure 1. 3: The importance and deficiency symptoms of zinc micronutrients on plant growth. 5
Figure 1. 4: The environmental effects of conventional fertilizers and the proposed solutions. 9
Figure 1. 5: Benefits of nanotechnology and nutrient-loaded nanomaterials. 10
Figure 1. 6: Interplay between plants and nanoparticles. 13

Figure 2. 1: Preparation of metal-rich nanofertilizers by biological means. 28
Figure 2. 2: Techniques reported for the preparation of nanofertilizers. 30
Figure 2. 3: The main functional groups in CS, ALG, and zein biopolymers. 39
Figure 2. 4: Hypothetical illustrations of ZnO- and Cu^{2+}-entrapped CS NPs indicating the metal chelation, ionic interactions, and nutrient release. 42

Figure 3. 1: Schematic presentation of the preparation of ZnO NPs and Fe_3O_4 NPs. 66
Figure 3. 2: Schematic illustration of the development of nutrient-loaded CS/TPP NPs. 67

Figure 4. 1: Image of *H. odoratissimum* grown in South Africa. 77
Figure 4. 2: Colourimetric test for the phytoconstituents (terpenoids (1), flavonoids (2), phenols and tannins (3), and alkaloids (4)). 78
Figure 4. 3: (a) UV-Vis absorption spectrum of *H. odoratissimum* extract and (b) HPTLC fingerprints observed under UV light 366 nm. 79
Figure 4. 4: Voltammetric characterization of solutions obtained after 20 min, 2 h stirring and 24 h aging in a three-electrode system at a scan rate of 25 mV/s. 81
Figure 4. 5: UV-Vis absorption spectra of the ZnO NPs and Fe_3O_4 NPs developed in *H. odoratissimum* extract by monitoring time. 82
Figure 4. 6: SEM images of the developed nano-metal oxides. 83

Figure 4. 7: TEM images of the developed zinc and iron nano-metal oxides. 83
Figure 4. 8: DLS and zeta potential analysis of the nano-zinc oxides. 85
Figure 4. 9: DLS and zeta potential analysis of the nano-iron oxides. 86
Figure 4. 10: FTIR spectra of the developed nano-metal oxides (a) ZnO and (b) Fe_3O_4. 87
Figure 4. 11: XRD patterns of the developed nano-metal oxides. 88
Figure 4. 12: Wurtzite ZnO structure and inverse spinel structure of Fe_3O_4. 88

Figure 5. 1: SEM images of CS/TPP NPs at two different magnifications of (a) 50 and (b) 100. 99
Figure 5.2: SEM images of (a) ZnO-loaded CS/TPP NPs and (b) Fe_3O_4-loaded CS/TPP NPs. 99
Figure 5. 3: TEM images of (a) ZnO-loaded CS/TPP NPs and (b) Fe_3O_4-loaded CS/TPP NPs. 100
Figure 5. 4: SEM images of Zn(II)-laden CS/TPP and Fe(II)-laden CS/TPP NPs.. 100
Figure 5. 5: Elemental maps (Zn, P, O, C, and Na) and EDX spectrum of Zn(II)-laden CS/TPP NPs. 101
Figure 5. 6: DLS and zeta potential analysis of the CS/TPP, ZnO-loaded CS/TPP, and Zn(II)-laden CS/TPP NPs. 103
Figure 5. 7: DLS and zeta potential analysis of the Fe_3O_4-loaded CS/TPP and Fe(II)-laden CS/TPP NPs. 104
Figure 5. 8: FTIR spectra of pristine CS/TPP NPs and nutrient-loaded CS/TPP NPs. 106
Figure 5. 9: TGA-DSC thermograms of ZnO-loaded CS/TPP NPs. 107
Figure 5. 10: XPS survey spectrum of ZnO-loaded CS/TPP NPs. 108
Figure 5. 11: XPS survey spectrum of Zn(II)-laden CS/TPP NPs. 109
Figure 5. 12: High-resolution XPS spectra of Zn 2p, C 1s, O 1 s, N 1s, and P 2p of ZnO-loaded CS/TPP NPs. 110
Figure 5. 13: High-resolution XPS spectra of Zn 2p, C 1s, O 1 s, and N 1s of Zn(II)-laden CS/TPP NPs. 111
Figure 5. 14: XPS survey spectrum of Fe_3O_4-loaded CS/TPP NPs. 112
Figure 5. 15: High-resolution XPS spectra of Fe 2p, C 1s, O 1s, N 1s, and P 2p of Fe_3O_4-loaded CS/TPP NPs. 113

Figure 5. 16: Plot depicting the release behaviour of the synthesized ZnO[15s], ZnO[15s]-loaded CS/TPP NPs, and Zn(II)-laden CS/TPP NPs in deionized water showing the variation of zinc concentration for 2 weeks. 115

Figure 6. 1: Germination process of maize seed. 122
Figure 6. 2: Effects of the seed nanopriming with ZnO NPs and Zn-loaded CS/TPP NPs. 124
Figure 6. 3: Effects of biogenic ZnO NPs and $Zn(NO_3)_2$ on the coleoptile and roots length with a significance difference (*P ≤ 0.05*). 126
Figure 6. 4: Effects of biogenic ZnO NPs and $Zn(NO_3)_2$ on the number of roots and lateral roots with a significance difference (*P ≤ 0.05*). 127
Figure 6. 5: Effects of biogenic ZnO NPs and $Zn(NO_3)_2$ on the radicle and shoot length with a significance difference (*P ≤ 0.05*). 128
Figure 6. 6: Effects of ZnO NPs 0.01% + NaCl 600 mM on the coleoptile and roots length with a significance difference (*P ≤ 0.05*). 130
Figure 6. 7: Effects of ZnO NPs 0.01% + NaCl 600 mM on the number of roots and lateral roots with a significance difference (*P ≤ 0.05*). 131
Figure 6. 8: Effects of ZnO NPs 0.01% + NaCl 600 mM on the radicle and shoot length with a significance difference (*P ≤ 0.05*). 132
Figure 6. 9: Effects of the prepared CS/TPP, Zn(II)-laden CS/TPP, and ZnO-loaded CS/TPP NPs at 0.01% on selected growth parameters with a significance difference (*P ≤ 0.05*). 135
Figure 6. 10: Effects of the prepared CS/TPP, Zn(II)-laden CS/TPP, and ZnO-loaded CS/TPP NPs at 0.04% on selected growth parameters with a significance difference (*P ≤ 0.05*). 136
Figure 6. 11: Effects of the prepared CS/TPP, Zn(II)-laden CS/TPP, and ZnO-loaded CS/TPP NPs at 0.01% on the growth parameters under salt stress (600 mM). Means were recorded from replicates for each treatment and significantly different at *P ≤ 0.05*. 140
Figure 6. 12: Effects of the prepared CS/TPP, Zn(II)-laden CS/TPP, and ZnO-loaded CS/TPP NPs at 0.04% on the growth parameters under salt stress (NaCl 600 mM). Means were recorded from replicates for each treatment and significantly different at *P ≤ 0.05*. 141

Figure 7. 1: Schematic representation of the possible processes occurring at the surface of nano-metal oxide for the formation of ROS in biological settings. 152

LIST OF SCHEMES

Scheme 4. 1: A plausible reaction mechanism for the development of metal oxide (MO) NPs in *H. odoratissimum* extract. 90

Scheme 5. 1: Interactions of the metal oxide surface with CS and TPP under acidic conditions. 104

LIST OF TABLES

Table 2. 1: Reported metal-based nanoparticles for plant growth and development. 31
Table 2. 2: Reported phytotoxicity of metal and metal-oxide NPs. 35
Table 2. 3: Reported biopolymeric nanomaterials for plant development and growth. 42

Table 4. 1: Phytochemical screening results. 78
Table 4. 2: Average hydrodynamic size, polydispersity index (PDI) and zeta potential (ZP) of colloidal suspensions of the nano-metal oxides. 165

Table 5. 1: Average hydrodynamic size, polydispersity index (PDI) and zeta potential (ZP) of colloidal suspensions of CS/TPP and nutrient-laden CS/TPP NPs. 165
Table 5. 2: Characteristics of the XPS peaks observed for ZnO-loaded CS/TPP NPs. 166
Table 5. 3: Characteristics of the XPS peaks observed for Zn(II)-laden CS/TPP NPs. 167
Table 5. 4: Characteristics of the XPS peaks observed for Fe_3O_4-loaded CS/TPP NPs. 168

Table 6. 1: Effect of $Zn(NO_3)_2$ and ZnO NPs on dry matter yield (g). 129
Table 6. 2: Effects of NaCl and ZnO NPs on dry matter yield (g). 132
Table 6. 3: Growth traits for 10-day-old seedlings under non-stress conditions. 137
Table 6. 4: Effects of pristine chitosan NPs and Zn-loaded chitosan NPs on dry matter yield (g) for the seeds germinated under normal conditions. 138
Table 6. 5: Growth traits for 10-day-old seedlings under salt stress conditions. 142
Table 6. 6: Effects of pristine chitosan NPs and Zn-loaded chitosan NPs on dry matter yield (g) for the seeds germinated under salinity stress. 143

Table 7. 1: Antifungal activity of the prepared nanomaterials. 154
Table 7. 2: Antifungal activity of the prepared nanomaterials on human pathogens. 156

CHAPTER 1
INTRODUCTION

1.1 Rationale and scope of the study

Micronutrient deficiency in sub-Saharan African soils has frequently been reported to impact crop production [1]. This situation reduces crop yield and contributes to negative effects on animal and human health [2]. Plants require micronutrients such as boron (B), copper (Cu), manganese (Mn), iron (Fe), and zinc (Zn) in small amounts. However, their presence in the soil is just as critical for plant growth as macronutrients (nitrogen (N), phosphorus (P), potassium (K), Calcium (Ca), and sulfur (S)). The micronutrients play vital roles in organisms' biological processes by interacting with various enzymes and other physiologically active molecules [3]. Notably, Fe and Zn promote the catalytic value of enzymes by forming enzyme-substrate complexes. Boron increases flowering, fruit, and seed development. On the other hand, copper aids in cell wall metabolism, protein synthesis, respiration, and photosynthesis. Manganese also acts as a cofactor for a variety of antioxidative enzymes.

Zinc and iron are the most abundant transition metals in organisms. Micronutrient malnutrition due to Zn and/or Fe deficiency affects approximately three billion people worldwide, with the greatest impact reported in developing countries [4,5]. Figure 1.1 shows that 75% of arable soil in sub-Saharan Africa is affected by Zn deficiency, whereas Figure 1.2 displays all areas at considerable risk of iron deficiency [6,7]. This is attributed to poor soil quality and inappropriate use of N, P, and K fertilizers [8,9], which do not replenish micronutrients in the soil. In human development, Zn and Fe deficiencies contribute to adverse functional disorders [10,11]. Given the effects of Zn and Fe deficiencies on human physical and psychological development, a recent report by the World Bank estimates that these etiological factors have a significant impact on annual gross domestic product (GDP) in developing countries (estimated loss of 2–5%) [12]. The NIH Office of Dietary Supplements (ODS) recommends dietary supplements for Zn of 2-3 mg in infants, 5 mg in children, 8-11 mg in adolescents and adults, and 11-13 mg in pregnant and breastfeeding women. Growth retardation (more severe in children), hypogonadism in males, changes in

neuro-sensory (abnormal taste sensation), and delayed wound healing are all consequences of Zn deficiency [13]. Hair loss and colour change from black to reddish-brown are other manifestations of Zn deficiency [14]. Increased oxidative stress, impaired cognitive function, and increased production of inflammatory cytokines have also been described as clinical effects of Zn deficiency [15]. Epidemiological evidence has shown a correlation between Zn deficiency and the risk of cancer due to the involvement of Zn in DNA synthesis and cell differentiation [16]. Inadequate intake of Zn can also result in a low sperm count and male infertility. It is worth noting that Zn deficiency is frequently associated with Fe deficiency. The latter has been documented to increase the risk for cognitive alterations in women of reproductive age and foster infant mortality rate [17].

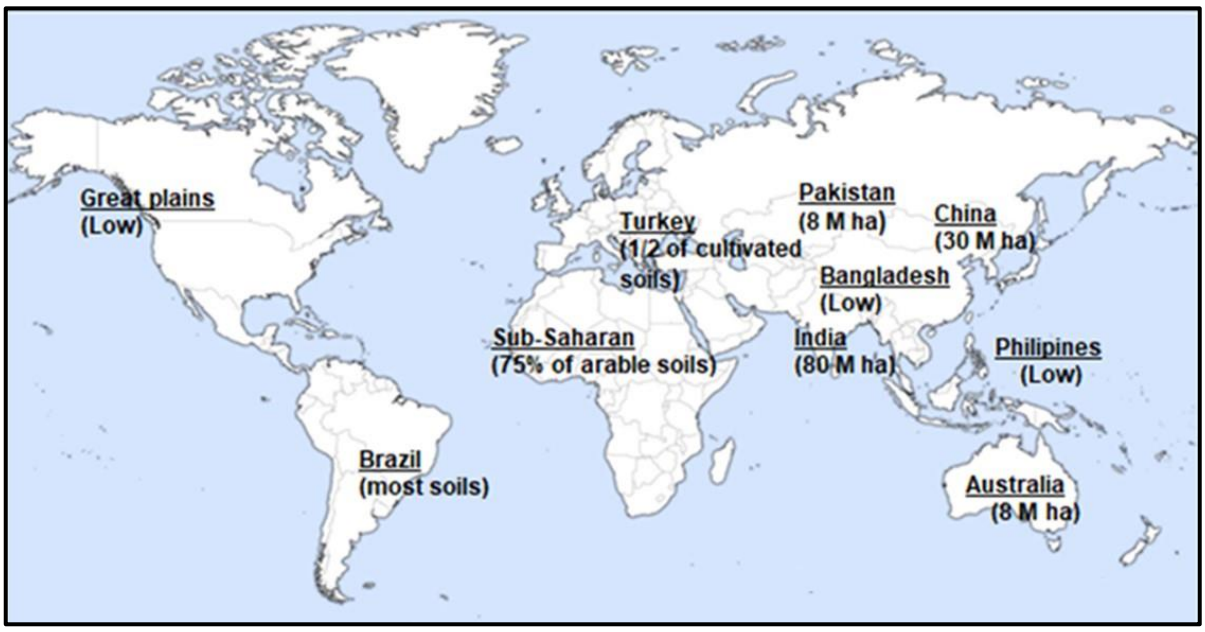


Figure 1. 1: The world map of Zn deficiency showing the major countries and regions with low Zn soils [6].

Anaemia caused by Fe deficiency in women of reproductive age and children under five is a global public health issue associated with increased morbidity and mortality [18-19]. Globally, more than 35% of women of reproductive age are iron-deficient, denoting an increased risk for maternal mortality [20,21]. Recent compelling data also established that nearly 40% of children aged 6-59 months suffer from Fe deficiency anemia [22,23]. Particularly, Africa has the highest levels of anaemia for pregnant women (57%), followed by South-East Asia (48%), according to the World

Health Organization (WHO) [20]. Malnutrition represents the leading cause of higher Fe deficiency anaemia in Africa. Nutritional Fe deficiency is caused by increased iron demand and/or iron loss and low bioavailability of Fe in the diets [24-26]. Most poor households in Africa, particularly in South Africa, consume highly repetitive diets consisting of foods with high concentrations of starch and low micronutrients. Previous anthropometric investigation on South African children in Free State and Limpopo provinces indicates a higher incidence of stunting because of micronutrient Fe and Zn deficiencies [27]. On this basis, micronutrient fertilization could be important in improving crop nutritional quality and alleviating the negative impact of deficiencies on human health.

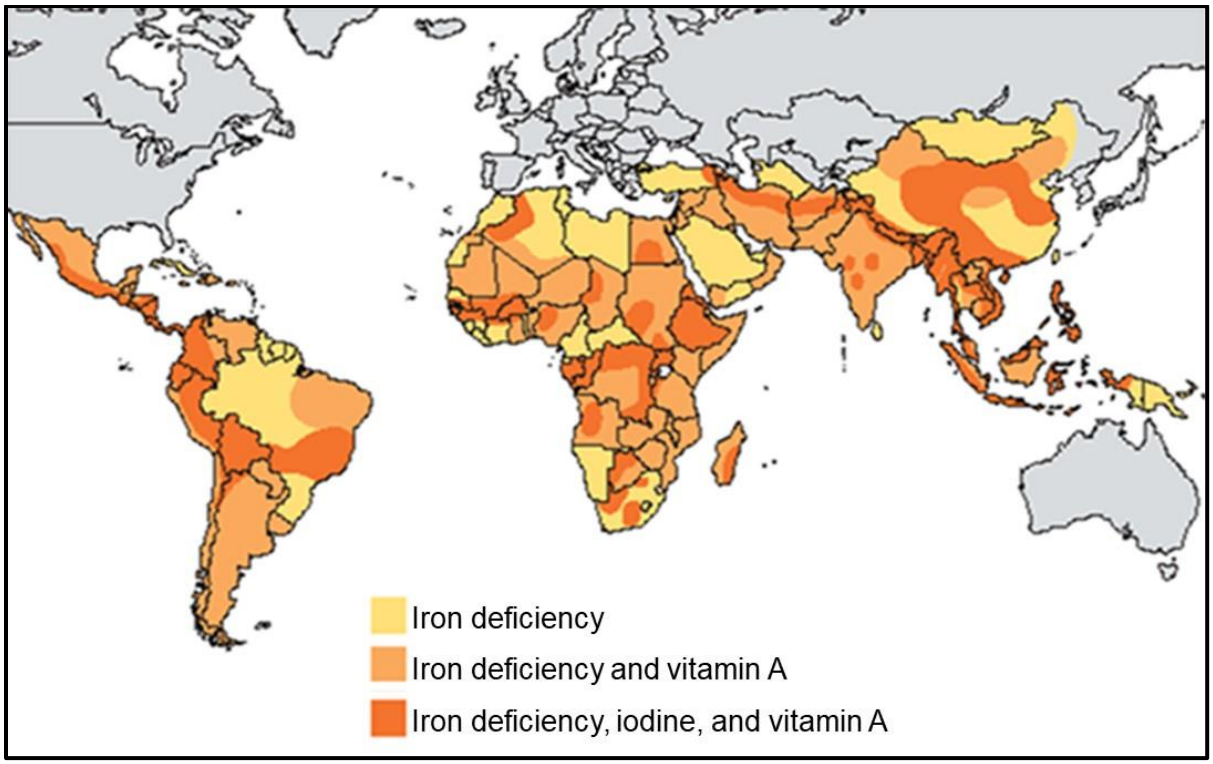


Figure 1. 2: World map showing areas at high risk of iron deficiency [7].

Currently, farmers use N, P, and K fertilizers to produce more food. However, the excessive application of these conventional inputs leads to environmental pollution [28]. Moreover, Russia is the world's largest producer of NPK fertilizers [29]. Africa is heavily dependent on fertilizer imports from Russia, and the conflict between Russia and Ukraine has affected the supply chain of these agricultural commodities. Therefore, affordable ways of developing fertilizers, which can replenish

micronutrients in agricultural soils sustainably, is of significance for farmers. The present study used a green strategy to synthesize Zn/Fe-rich nutrients for plant growth and development. Packaging these nutrients within nanoscale carriers is anticipated to generate materials with slow-release properties [30]. Formulation of plant nutrients in the nanoscale range represents a recent strategy that could revolutionize the agricultural sector and provide solutions for current/future challenges surrounding sustainable development and climate change. Furthermore, the traditional techniques of supplying nutrients, namely soil fertilization and foliar spraying, depend on environmental circumstances that can diminish their effectiveness. Seed pre-treatment in nutrient-rich solutions has also been described as an eco-efficient strategy that can contribute in mitigating the adverse effects of biotic and abiotic stressors, and by doing so, increasing crop performance.

1.2 Effects of zinc and iron micronutrients for plant growth

Zinc is involved in mediating the activities of many enzymes and is required for various redox reactions and metabolic processes [5]. This micronutrient contributes to carbohydrate metabolism, maintains cellular membrane integrity, participates in protein synthesis, and increases the biosynthesis of auxin (Figure 1.3) [16]. Zn is implicated in the synthesis of tryptophan, an essential amino acid in forming auxins. Furthermore, Zn triggers chlorophyll biosynthesis and stimulates the production of defense metabolites. Research indicates that Zn^{2+} stabilizes the thiol (-SH) groups in membrane proteins and regulates plant responses to biotic stresses [31,32]. Zinc nutrition has also been reported to improve plant resistance to environmental stressors, such as salinity and cold [33].

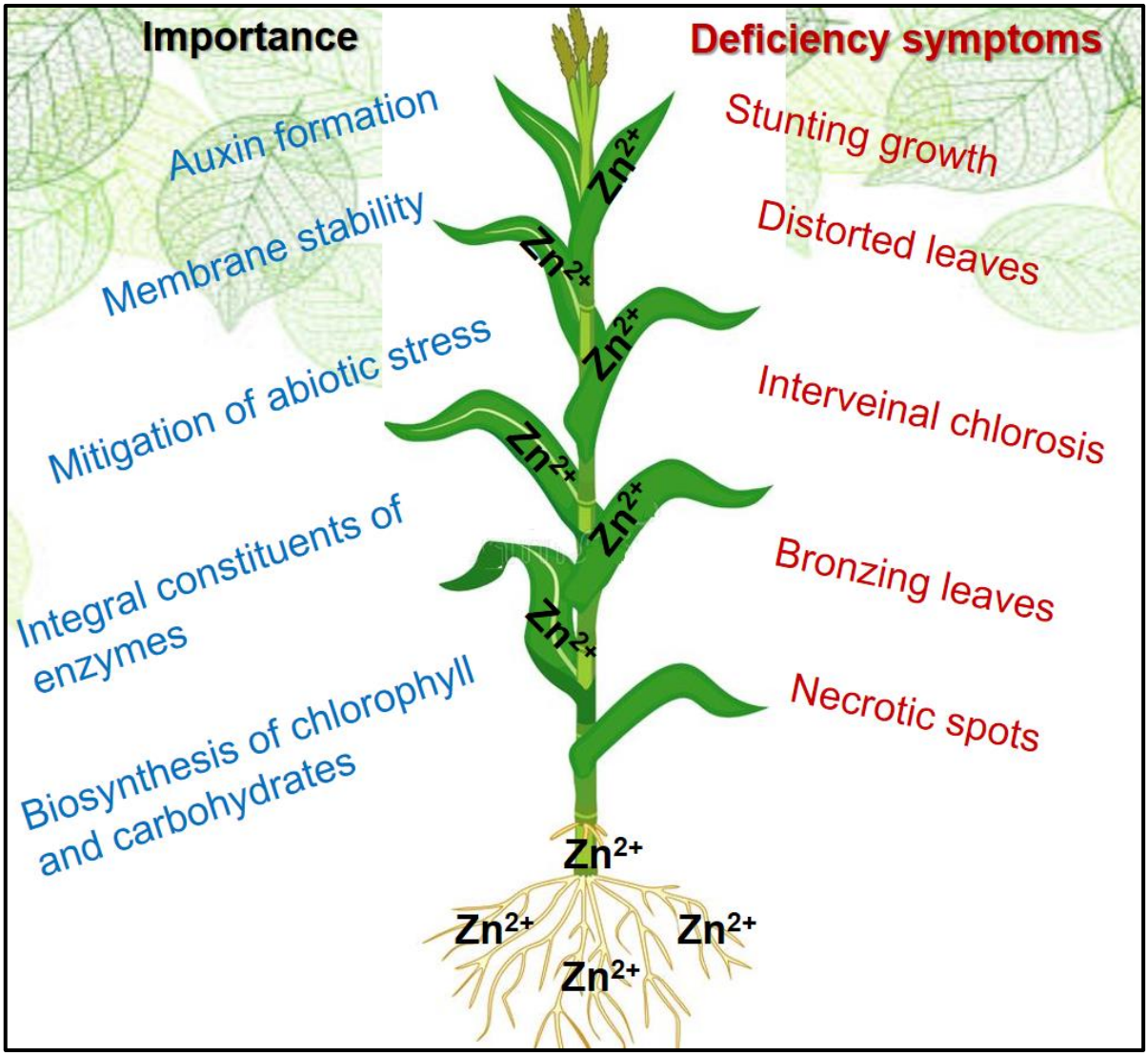


Figure 1. 3: The importance and deficiency symptoms of zinc micronutrients on plant growth.

Plants can easily absorb zinc as a divalent cation (Zn^{2+}) or organic Zn-ligand complexes, and a lack of this micronutrient can cause impairments in plant physiological and biochemical traits. Zn deficiency in plants result in smaller leaf size, chlorosis, inhibited stem growth, foliar necrosis, and internode shortening (Figure 1.3). These manifestations are mainly attributed to the oxidative effect of reactive oxygen species (ROS) [34]. These free radicals can alter proteins functions and structures via oxidative reactions with the -SH groups. Zinc uptake from the soil solution by roots to shoots through the xylem is the primary step for the Zn fluxes within plants [35,36]. Zinc fertilizers include disodium zinc ethylene diamine tetra-acetic acid $Na_2ZnEDTA$, zinc sulphate ($ZnSO_4$), zinc carbonate ($ZnCO_3$), zinc nitrate ($Zn(NO_3)_2$), zinc phosphate ($Zn_3(PO_4)_2$), and zinc oxide (ZnO). Among these Zn-

containing fertilizers, ZnO exhibits the highest percentage of Zn content (50-80%) [37,38].

Another central component in plant metabolism is Fe. This micronutrient is required to synthesise plant enzymes, such as 1-aminocyclopropane acid-1-carboxylic oxidase and lipoxygenases [39]. The latter catalyses the formation of fatty acids that improve plant tolerance to biotic and abiotic stresses, while the former acts as substrate for ethylene biosynthesis as a plant growth regulator. Owing to its ability to lose and gain electrons, Fe serves as a cofactor for enzymes engaged in redox reactions like DNA synthesis, hormone synthesis, respiration, and photosynthesis [40-42]. Fe is involved in the chlorophyll production and the maintenance of photosynthetically active tissue. Although abundant in the lithosphere, low Fe availability is frequently reported in alkaline and calcareous soils [43-45]. Generally, this micronutrient occurs in ferromagnesium silicates and hydroxides that are not readily available for plant uptake.

In plants, the typical symptoms of Fe deficiency also include chlorosis, which affects the developmental processes and product quality [46,47]. Fe-ethylenediamine-*N,N'*-bis-(hydroxyphenylacetic) acid (EDDHA/Fe^{3+}), ferrous ammonium phosphate ($FeNH_4PO_4$), ferric sulfate ($Fe_2(SO_4)_3$), ferrous sulfate ($FeSO_4$), and ferrous ammonium sulfate ($Fe(NH_4)_2(SO_4)_2$), are the most popular Fe-rich fertilizers [48]. Deficiencies of Fe and Zn are common issues affecting cereal crop productivity in sub-Saharan Africa [49,50]. Moreover, Zn and Fe dietary shortages have been related to anaemia, stunted growth, impaired physical and cognitive development, depressed immune function, severity of infection, neurobehavioral abnormalities; and adverse outcomes of pregnancy [51-53].

1.3 Maize crop production and importance

One of the most important agronomic crops worldwide is maize (*Zea mays* L.), a member of the grass family Poaceae. This plant was initially domesticated by native Mexicans around 10,000 years ago before getting proliferated to all suitable parts of the world [54]. The product of this plant is commonly utilized as a raw material in human diets, livestock feeds, pharmaceuticals, and biofuels [55]. In South Africa,

maize production substantially contributes to job creation and GDP [56,57]. For human nutrition, maize kernels are traditionally consumed as boiled or roasted. These are also processed into numerous products like flour, grits, starch, snack, alcoholic beverages, and oil [58]. The maize germ contains over 45% of oil high in polyunsaturated, monounsaturated, and saturated fatty acids. The kernels are a good source of carbohydrates and vitamins (C, E, K, B_1, B_2, B_3, B_5, and B_6). The maize kernels also supply dietary fibre and essential minerals, magnesium and phosphorus, lowering blood sugar and cholesterol levels [59]. The high carbohydrate content of maize allows their use in brewing and animal feeding. The rapid population growth and absolute increases in poultry production in Africa are major factors contributing to the increased interest in maize cultivation in South Africa.

Maize is cultivated in a range of agro-ecological environments; however, its growth and yield are hugely affected by several environmental constraints [60]. Drought and salinity, for example, are the main abiotic stresses hampering maize production in Africa. Drought conditions are well-known to reduce the growth rate, cause losses of dry weight, and reduce the number of kernels per plant. Under these conditions, salt accumulation is also anticipated in soil, leading to plant ion toxicity. Conventional NPK fertilisers were previously reported to improve *Zea mays* productivity even under drought and salt stress [61,62].

1.4 Environmental impact of conventional fertilizers

Hitherto, chemical fertilizers have been used to improve the development of crops and ensure sufficient food production. Plants need the primary (N, P, and K) and secondary macronutrients (Ca, Mg, and S) to thrive and develop [63]. Traditionally, these fertilizers are processed in bulky forms and can boost crop yield through soil-less hydroponic cultivation, foliar spray, or soil application. Nucleic acids and chlorophyll molecules both depend on nitrogen as an essential component. Nucleic acids are the macromolecules that enable production plants' enzymes and proteins, whereas chlorophylls facilitate photosynthesis by mediating plant-light interactions [64]. Phosphorus, a nucleic acid backbone, regulates protein synthesis in plants. Potassium maintains the osmotic potential in plants and is essential for ensuring optimum plant growth under drought stress [65]. Calcium has been reported to

improve the structural rigidity of cell walls and affect membrane stabilisation [66]. The insufficient sulfur in soil was found to result in decreased chlorophyll content and inhibition of the *Zea mays* plant's ability to produce protein [67]. Metalloid Si is essential to increase plant development and productivity by strengthening the stiffness of the cell wall and boosting the plant's tolerance to abiotic and biotic stressors [68–70].

Metal elements (Cu, Mg, Mn, Fe, and Zn) are imperative for plants to complete their life cycle [71,72]. The adequate application of salts or oxides containing these micronutrients improves seed germination and the plant's physiological processes. Despite these qualities, soil amendments with conventional fertilizers (processed in bulky forms) have also been linked to freshwater pollution, ozone depletion, and soil acidification, as illustrated in Figure 1.4 [73,74]. According to the literature, the overall distributive efficiency of fertilizers is <50% due to runoff and volatilization [75]. Organic fertilisers have also been put forth to limit the adverse effects of chemical inputs on the environment [76-78]. These fertilizers are derived from animal and plant wastes and are expected to degrade over time to release the plant nutrients, indicating a slow action. So far, composted organic residues have been used in high loadings for improving soil fertility, which also results in environmental concerns, as shown in Figure 1.3 [79]. The hydroponic cultivation is a soil-free technique recently explored in Africa to circumvent the issue of changing climates [80]. This method is based on vertical farming under controlled environments and necessitates using high-energy-consuming equipment, which may be costly for developing countries.

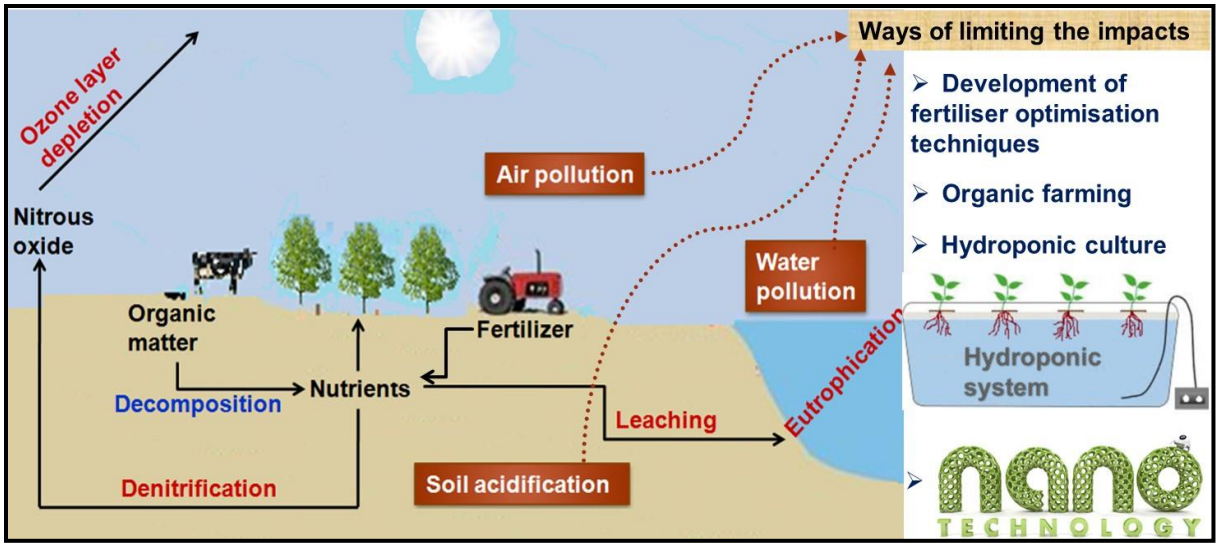


Figure 1. 4: The environmental effects of conventional fertilizers and the proposed solutions.

1.5 Nanotechnology in agriculture

There is a growing interest in advanced materials for sustainable agriculture. The fertilizers processed in nanoscale can facilitate nutrient uptake by plants from hydroponic systems, leaf surfaces, or soil. Nanoscale materials (nanomaterials) as new types of fertilizers can be obtained by breaking down the bulk fertilizers into nanoparticles or growing from nutrients at the atomic scale to form continuous nanostructures. Recently, it has been argued that nano-engineered fertilizers can improve plant mineral nutrition and environmental outcomes. Nanotechnology is a contemporary research area that involves studying and manipulating materials at the atomic and molecular levels. This expanding field of research and invention has been applied to numerous industries, including medicine, cosmetics, water purification, food, and agriculture [81]. Nanotechnology has offered a commendable opportunity for enhancing the efficiency of nutrient use and promoting eco-sustainable agriculture [82,83]. As compared with bulk materials, nanomaterials display unique characteristics, such as adhesion to the plant surface, ease of adsorption, and high reactivity. These properties improve plant responses to abiotic and biotic stresses (Figure 1.5) [84]. Moreover, the nanomaterials may act as carriers to encapsulate nutrients and enable smart fertilizers [85].

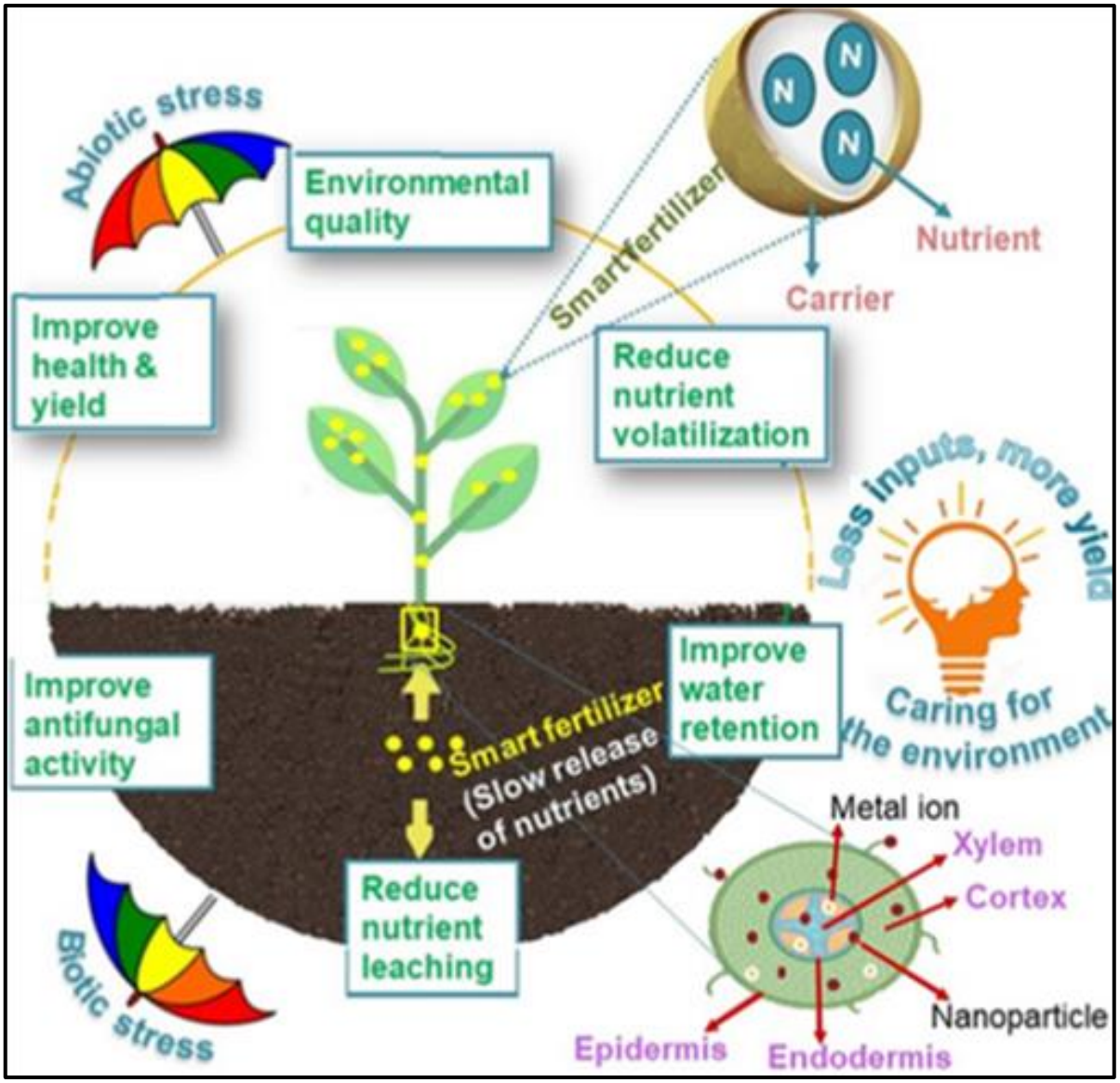


Figure 1. 5: Benefits of nanotechnology and nutrient-loaded nanomaterials.

1.6 Problem statement

Food insecurity and malnutrition remain some of the major concerns in Africa and around the world due to rapid population growth and changing climates. According to goal 2 of the Sustainable Development Goals (SDGs), a world free of hunger should be achieved by 2030. This can be made possible by increasing agricultural productivity and maintaining healthy soil quality [85]. The use of chemically processed fertilizers and pesticides in the agricultural sectors has long been considered to improve food productivity, contributing to nearly 60% of the crop production across the world [86]. However, the major concern with these agricultural

inputs is their detrimental ability to promote environmental burdens such as soil salinity, land deterioration, and water pollution [87, 88]. Lately, maize production in South Africa has been reported to be under the threat of soil salinity [89]. According to a report by Nell and van Huyssteen (2018) [90], nearly 30% of South African soils are now considered as saline. The disastrous impact of soil salinity is not only limited to agricultural productivity in South Africa but also poses a serious threat to the aquatic species distribution and diversity [91]. On the other hand, numerous studies have reported the presence of salts and pesticides in non-target environments in South Africa, based on their mobility in soil [92].

Given these facts, this research was thus set to look for innovative strategies and products that can help in increasing agricultural productivity with the least negligible environmental impact. Solutions containing metal oxide nanoparticles have attracted much research consideration to optimize the metabolic processes of plants in lieu of the conventional water-soluble chemical fertilizers. Additionally, the use of metal oxide nano-products has been growing extensively in the field of plant pathology [93]. However, scientific communities speculate that there is also a risk associated with the release of nanomaterials into the environment [94]. This project envisaged that integrating the metal (Zn or Fe) oxide nanoparticles within non-toxic chitosan polysaccharide nanostructures may alter their risk profile by means of sustained release behaviour. These polysaccharide-based nanomaterials may also combine the unique attributes of metal oxide nanoparticles with the essentiality of chitosan to advance the physiological characteristics of maize plant and improve crop management.

1.7 Research aim and objectives

The present study aimed to achieve the development of metal oxide nanoparticles loaded in chitosan biopolymer and assess their effects on the germination of *Z. mays* seeds stressed with salt. The engineered nanomaterials were envisaged to possess slower release properties and antifungal activities.

The specific objectives of the study were to:

- achieve the synthesis of nano-metal oxides (ZnO and Fe_3O_4) using a phyto-assisted methodology and characterize them,
- encapsulate the pre-synthesized nano-metal oxides using nontoxic and biodegradable chitosan biopolymer crosslinked with tripolyphosphate, then conduct their characterization,
- evaluate the nutrient release behaviour of the as-prepared nanocomposites in water,
- assess their effects on the germination traits of non-stressed and salt-stressed maize seeds and,
- appraise their biological activities against plant and human pathogenic fungi.

1.8 Overview of the thesis

Nanotechnology has the potential to promote precision agriculture and better environmental security. This attractive area of research also offers benefits of plant protection under abiotic and/or biotic stresses. Plant-mediated methods have been praised to generate nanoparticles in the process of reducing hazardous wastes. These highlight mutually beneficial outcomes between nanotechnology and plant research (Figure 1.6).

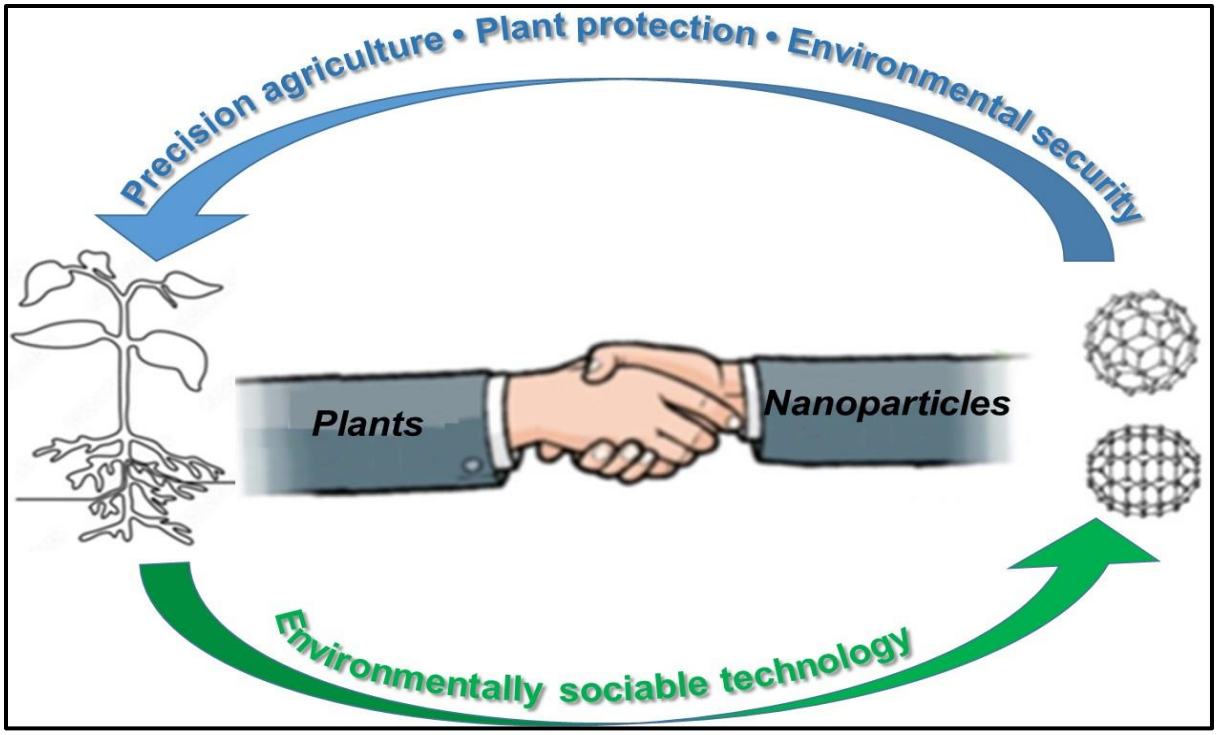


Figure 1. 6: Interplay between plants and nanoparticles.

This thesis consists of eight chapters, outlined as follows:

Chapter	Description
1	Provides an overview of the micronutrient deficiencies in soils and their impact on human health. This chapter is also devoted to the adverse impacts confronted by conventional fertilizers and the purpose of the study.
2	Presents a thorough literature survey on developing metal-based nanoparticles for advanced agriculture. Efforts made to ensure agricultural production in a sustainable manner are also discussed here.
3	Outlines the research methodology employed for synthesising and characterising the desired nanomaterials and their application.
4	Presents the characterization of the nano-metal oxides (ZnO and Fe_3O_4) developed using *Helichrysum odoratissimum* aqueous extracts and a plausible mechanism for their formation. These nano-metal oxides' morphology (shape, size, and composition) and crystal structure are

	provided.
5	Presents the characterization of the metal oxide-encapsulated chitosan nanocomposites. For this purpose, several techniques were used, including electron microscopy, dynamic light scattering, Fourier-transform infrared spectroscopy, thermogravimetry, and X-ray photoelectron spectroscopy. The cation release behaviour of these nanocomposites is also discussed.
6	Displays the effects of the developed zinc oxide and zinc-loaded chitosan nanoparticles on the germination of maize seeds under no stress and salinity conditions.
7	Presents the antifungal potential of the developed iron oxide and iron-loaded chitosan nanoparticles against six phytopathogenic fungi, that is, *Aspergillus niger*, *Aspergillus flavas*, *Alternaria solani*, *Fusarium oxysporum*, *Fusarium solani*, and *Fusarium verticillioides*.
8	Summarises the findings of the study and suggests future research to be taken.

REFERENCES

1. Manzeke, M. G.; Mtambanengwe, F.; Watts, M. J.; Hamilton, E. M.; Lark, R. M.; Broadley, M. R. & Mapfumo, P. 2019. Fertilizer management and soil type influence grain zinc and iron concentration under contrasting smallholder cropping systems in Zimbabwe. *Scientific Reports*, 9(1), 1-13.

2. Saha, S.; Saha, B.; Seth, T.; Dasgupta, S.; Ray, M.; Pal, B. & Hazra, G. 2019. Micronutrients availability in soil–plant system in response to long-term integrated nutrient management under rice–wheat cropping system. *Journal of Soil Science and Plant Nutrition*, 19(4), 712-724.

3. Shahid, M.; Shukla, A. K.; Bhattacharyya, P.; Tripathi, R.; Mohanty, S.; Kumar, A. & Nayak, A. K. 2016. Micronutrients (Fe, Mn, Zn and Cu) balance under long-term application of fertilizer and manure in a tropical rice-rice system. *Journal of Soils and Sediments*, 16(3), 737-747.

4. Goudia, B. D. & Hash, C. T. 2015. Breeding for high grain Fe and Zn levels in cereals. *International Journal of Innovation and Applied Studies*, 12(2), 342-354.

5. Hacisalihoglu, G. 2020. Zinc (Zn): The last nutrient in the alphabet and shedding light on Zn efficiency for the future of crop production under suboptimal Zn. *Plants*, 9(11), 1471.

6. Gregory, P. J.; Wahbi, A.; Adu-Gyamfi, J.; Heiling, M.; Gruber, R.; Joy, E. J. & Broadley, M. R. 2017. Approaches to reduce zinc and iron deficits in food systems. *Global Food Security*, 15, 1-10.

7. Mwangi, M. N.; Mzembe, G.; Moya, E. & Verhoef, H. 2021. Iron deficiency anaemia in sub-Saharan Africa: a review of current evidence and primary care recommendations for high-risk groups. *The Lancet Haematology*, 8(10), 732-743.

8. Wawire, A. W.; Csorba, Á.; Tóth, J. A.; Michéli, E.; Szalai, M.; Mutuma, E. & Kovács, E. 2021. Soil fertility management among smallholder farmers in Mount Kenya East region. *Heliyon*, 7(3), 06488.

9. Kihara, J.; Bolo, P.; Kinyua, M.; Rurinda, J. & Piikki, K. 2020. Micronutrient deficiencies in African soils and the human nutritional nexus: opportunities with staple crops. *Environmental Geochemistry and Health*, 42(9), 3015-3033.

10. Mayo-Wilson, E.; Junior, J. A.; Imdad, A.; Dean, S.; Chan, X. H. S.; Chan, E. S. & Bhutta, Z. A. 2014. Zinc supplementation for preventing mortality, morbidity, and growth failure in children aged 6 months to 12 years of age. *Cochrane Database of Systematic Reviews*, (5).

11. Rahman, M. M.; Abe, S. K.; Rahman, M. S.; Kanda, M.; Narita, S.; Bilano, V. & Shibuya, K. 2016. Maternal anemia and risk of adverse birth and health outcomes in low-and middle-income countries: systematic review and meta-analysis, 2. *The American Journal of Clinical Nutrition*, 103(2), 495-504.

12. Darnton-Hill, I. 2019. Public health aspects in the prevention and control of vitamin deficiencies. *Current Developments in Nutrition*, 3(9), nzz075.

13. Prasad, A. S. 1998. Zinc deficiency in humans: a neglected problem. *Journal of the American College of Nutrition*, 17(6), 542-543.

14. Maret, W. & Sandstead, H. H. 2006. Zinc requirements and the risks and benefits of zinc supplementation. *Journal of Trace Elements in Medicine and Biology*, 20(1), 3-18.

15. Prasad, A. S. 2017. Discovery of zinc for human health and biomarkers of zinc deficiency. In Molecular, Genetic, and Nutritional Aspects of Major and Trace Minerals. *Academic Press*, 22, 241-260.

16. Hafeez, B. M. K. Y.; Khanif, Y. M. & Saleem, M. 2013. Role of zinc in plant nutrition-a review. *American Journal of Experimental Agriculture*, 3(2), 374.

17. Akhtar, S.; Ismail, T.; Atukorala, S. & Arlappa, N. 2013. Micronutrient deficiencies in South Asia – Current status and strategies. *Trends in Food Science & Technology*, 31(1), 55- 62.

18. Stephen, G.; Mgongo, M.; Hussein Hashim, T.; Katanga, J.; Stray-Pedersen, B. & Msuya, S. E. 2018. Anaemia in pregnancy: prevalence, risk factors, and adverse perinatal outcomes in Northern Tanzania. *Anemia*, 1-9.

19. Stevens, G. A.; Finucane, M. M.; De-Regil, L. M.; Paciorek, C. J.; Flaxman, S. R.; Branca, F.; Peña-Rosas, J.P.; Bhutta, Z.A. Ezzati, M. & nutrition impact model study group. 2013. Global, regional, and national trends in haemoglobin concentration and prevalence of total and severe anaemia in children and pregnant and non-pregnant women for 1995–2011: A systematic analysis of population-representative data. *The Lancet Global Health*, 1(1), 16-25.

20. World Health Organization. Anaemia in Women and Children: WHO Global Anaemia Estimates. 2021. *World Health Organization*: Available online:https://www.who.int/data/gho/data/themes/topics/anaemia_in_women_and_children.

21. FAO; IFAD; UNICEF; WFP; WHO. The State of Food Security and Nutrition in the World. 2020. Transforming Food Systems for Affordable Healthy Diets. *Food and Agriculture Organization of the United Nations*: Rome, Italy, 2017.

22. Black, R.E.; Victora, C.G.; Walker, S.P.; Bhutta, Z.A.; Christian, P.; De Onis, M.; Ezzati, M.; Grantham-McGregor, S.; Katz, J. & Martorell, R. 2013. Maternal and child undernutrition and overweight in low-income and middle-income countries. *Lancet*, 382, 427–451.

23. World Health Organization. 2015. The Global Prevalence of Anaemia in 2011. *World Health Organization* Available online: https://apps.who.int/iris/handle/10665/177094.

24. Gautam, S.; Min, H.; Kim, H. & Jeong, H.-S. 2019. Determining factors for the prevalence of anemia in women of reproductive age in Nepal: Evidence from recent national survey data. *PLoS ONE*, 14, 0218288.

25. Simbauranga, R.H.; Kamugisha, E.; Hokororo, A.; Kidenya, B.R. & Makani, J. 2015. Prevalence and factors associated with severe anaemia amongst under-

five children hospitalized at Bugando Medical Centre, Mwanza, Tanzania. *BMC Hematology*, 15, 13.

26. Stoltzfus, R.J.; Mullany, M.L. & Black, R.E. 2004. Iron deficiency anaemia. In Comparative Quantification of Health Risks: Global and Regional Burden of Disease Attributable to Selected Major Risk Factors. *World Health Organization*, 1, 163-209.

27. Asiwe, J. N. A. 2022. Determination of quality traits, and the nutrient and mineral contents of cowpea varieties in South Africa. *African Journal of Food, Agriculture, Nutrition and Development*, 22(5), 20331-20348.

28. Stewart, W. M. & Roberts, T. L. 2012. Food security and the role of fertilizer in supporting it. *Procedia Engineering*, 46, 76-82.

29. Ben Hassen, T. & El Bilali, H. 2022. Impacts of the Russia-Ukraine war on global food security: Towards more sustainable and resilient food systems?. Foods, 11(15), 2301.

30. Dhlamini, B.; Paumo, H. K.; Kamdem, B. P.; Katata-Seru, L. & Bahadur, I. 2022. Nano-engineering metal-based fertilizers using biopolymers: An innovative strategy for a more sustainable agriculture. *Journal of Environmental Chemical Engineering*, 10, 107729

31. Broadley, M.; Brown, P.; Cakmak, I.; Rengel, Z. & Zhao, F. 2012. Function of nutrients: Micronutrients. In Marschner's mineral nutrition of higher plants. *Academic Press*, 191-248.

32. Ahmed, A. M. H.; Khalil, M. K.; Abd El-Rahman, A. M. & Nadia, A. H. 2012. Effect of zinc, tryptophan and indole acetic acid on growth, yield and chemical composition of Valencia orange trees. *Journal of Applied Sciences Research*, 901-914.

33. Jin, H. X.; Jiang, M.; Yang, J. F.; Wu, Z. H.; Ma, L. L.; Wang, C. C.; Liang, C.; Ning, X. Y.; Ge, L. F. & Chen, S. 2022. A survey of enhanced cold tolerance and low-temperature-induced anthocyanin accumulation in a novel *Zoysia japonica* biotype. *Plants*, 11(3), 429.

34. Castillo-González, J.; Ojeda-Barrios, D.; Hernández-Rodríguez, A.; González-Franco, A. C.; Robles-Hernández, L. & López-Ochoa, G. R. 2018. Zinc metalloenzymes in plants. *Interscience*, 43(4), 242-248.

35. Broadley, M. R.; White, P. J.; Hammond, J. P.; Zelko, I. & Lux, A. 2007. Zinc in plants. *New Phytologist*, 173(4), 677-702.

36. Begum, M. C.; Islam, M.; Sarkar, M. R.; Azad, M. A. S.; Huda, A. N. & Kabir, A. H. 2016. Auxin signaling is closely associated with Zn-efficiency in rice (*Oryza sativa* L.). *Journal of Plant Interactions*, 11(1), 124-129.

37. Jerlin, B.; Sharmila, S.; Kathiresan, K. & Kayalvizhi, K. 2017. Zinc solubilizing bacteria from rhizospheric soil of mangroves. *Journal of Microbiology and Biotechnology*, 2(3), 148-155.

38. https://crops.zinc.org/wp-content/uploads/sites/11/2016/12/Zinc-Fertilizer-Overview-General-Pop-June-2015.

39. Rout, G. R. & Sahoo, S. 2015. Role of iron in plant growth and metabolism. *Reviews in Agricultural Science*, 3, 1-24.

40. Schmidt, W.; Thomine, S. & Buckhout, T. J. 2020. Iron nutrition and interactions in plants. *Frontiers in Plant Science*, 10, 1670..

41. Grotz, N. & Guerinot, M. L. 2006. Molecular aspects of Cu, Fe and Zn homeostasis in plants. *Biochimica et Biophysica Acta (BBA)-Molecular Cell Research*, 1763(7), 595-608.

42. Briat, J. F.; Duc, C.; Ravet, K. & Gaymard, F. 2010. Ferritins and iron storage in plants. *Biochimica et Biophysica Acta (BBA)-General Subjects*, 1800(8), 806-814.

43. Zuo, Y. & Zhang, F. 2011. Soil and crop management strategies to prevent iron deficiency in crops. *Plant and Soil*, 339(1), 83-95.

44. Samaranayake, P.; Peiris, B. D. & Dssanayake, S. 2012. Effect of excessive ferrous (Fe^{2+}) on growth and iron content in rice (*Oryza sativa*). *International Journal of Agriculture and Biology*, 14(2).

45. Alcañiz, S.; Jordá, J. D. & Cerdán, M. 2017. Effectiveness of iron ethylenediamine-*N*,*N*′-bis(hydroxyphenylacetic) acid (*o,o*-EDDHA/Fe^{3+}) formulations with different ratios of meso and *d,l*-racemic isomers as iron fertilizers. *Journal of Agricultural and Food Chemistry*, 65(2), 253-259.

46. Li, J., Cao, X., Jia, X., Liu, L., Cao, H., Qin, W. & Li, M. 2021. Iron deficiency leads to chlorosis through impacting chlorophyll synthesis and nitrogen metabolism in *Areca catechu* L. *Frontiers in Plant Science*, 12, 710093.

47. Bashir, K.; Rasheed, S.; Kobayashi, T.; Seki, M. & Nishizawa, N. K. 2016. Regulating subcellular metal homeostasis: The key to crop improvement. *Frontiers in Plant Science*, 7, 1192.

48. Hurrell, R. F.; Trinidad, T. P.; Mallillin, A. C.; Sagum, R. S.; Foman, J. T.; Li, Q., Zedar, C.; Kastenmayer, P., Rytz, A., Sabatier, M. & Egli, I. 2022. Iron bioavailability from ferrous ammonium phosphate, ferrous sulfate, and ferric pyrophosphate in an instant milk drink — A stable isotope study in children. *Nutrients*, 14(8), 1640.

49. Potarzycki, J. & Grzebisz, W. 2009. Effect of zinc foliar application on grain yield of maize and its yielding compone. *Plant, Soil and Environment*, 55(12), 519-527.

50. Aliyu, K. T.; Huising, J.; Kamara, A. Y.; Jibrin, J. M.; Mohammed, I. B.; Nziguheba, G.; Adam, A. M. & Vanlauwe, B. 2021. Understanding nutrient imbalances in maize (*Zea mays* L.) using the diagnosis and recommendation integrated system (DRIS) approach in the maize belt of Nigeria. *Scientific Reports*, 11, 16018.

51. Black, M. M. 2003. The evidence linking zinc deficiency with children's cognitive and motor functioning. *The Journal of Nutrition*, 133(5), 1473S-1476S.

52. Noor, R. A.; Abioye, A. I.; Darling, A. M.; Hertzmark, E.; Aboud, S.; Premji, Z. & Fawzi, W. 2020. Prenatal zinc and vitamin A reduce the benefit of iron on maternal hematologic and micronutrient status at delivery in Tanzania. *The Journal of Nutrition*, 150(2), 240-248.

53. Fançony, C.; Soares, Â.; Lavinha, J. & Brito, M. 2022. Zinc deficiency interacts with intestinal/urogenital parasites in the pathway to anemia in preschool children, Bengo–Angola. *Nutrients*, 14(7), 1392.

54. Piperno, D. R. & Flannery, K. V. 2001. The earliest archaeological maize (*Zea mays* L.) from highland Mexico: new accelerator mass spectrometry dates and their implications. *Proceedings of the National Academy of Sciences of the United States of America*, 98(4), 2101–2103.

55. Chisanga, C. B. 2014. Evaluation of the Ceres-Maize model in simulating maize (*Zea mays* L.) growth, development and yield at different planting dates and nitrogen rates in a subtropical environment of Zambia. *The University of Zambia*.

56. Courtman, C.; Van Ryssen, J. B. J. & Oelofse, A. 2012. Selenium concentration of maize grain in South Africa and possible factors influencing the concentration. *South African Journal of Animal Science*, 42(5), 454-458.

57. Cammarano, D.; Valdivia, R. O.; Beletse, Y. G.; Durand, W.; Crespo, O.; Tesfuhuney, W. A.; Jones, M. R.; Walker, S.; Mpuisang, T. N.; Nhemachena, C.; Ruane, A. C.; Mutter, C.; Rosenzweig, C. & Antle, J. 2020. Integrated assessment of climate change impacts on crop productivity and income of commercial maize farms in northeast South Africa. *Food Security*, 12(3), 659-678.

58. Gwirtz, J. A. & Garcia-Casal, M. N. 2014. Processing maize flour and corn meal food products. *Annals of the New York Academy of Sciences*, 1312(1), 66-75.

59. Hossain, F.; Sarika, K.; Muthusamy, V.; Zunjare, R. U. & Gupta, H. S. 2019. “Quality protein maize for nutritional security” in Quality breeding in field crops. Ed. Qureshi, A. M. I.; Dar, Z. A. and Wani, S. H. (India: Springer), 217-237.

60. Dao A.; Sanou, J.; Gracen, V. & Danquah E. Y. 2015. Indentifying farmers’ preferences and constraints to maize production in two agro-ecological zones in Burkina Faso. *Agriculture and Food Security*, 4, 13.

61. Law-Ogbomo, K. E. & Law-Ogbomo, J. E. 2009. The performance of *Zea mays* as influenced by NPK fertilizer application. *Notulae Scientia Biologicae*, 1(1), 59-62.

62. Zafar-ul-Hye, M.; Muhammad, H.; Zahir, F.; Ahmad, Z.; Hussain, M. & Hussain, A. 2014. Application of ACC-deaminase containing rhizobacteria with fertilizer improves maize production under drought and salinity stress. *International Journal of Agriculture and Biology*, 16(3), 591-596.

63. Zewide, I. & Melash, W. 2021. Review on macronutrient in agronomy crops. *Journal of Nutrition and Food Processing*, 4(6), 848-856.

64. Kahsay, W. S. 2019. Effects of nitrogen and phosphorus on potatoes production in Ethiopia: A review. *Cogent Food & Agriculture*, 5(1), 1572985.

65. Zhang, X.; Wu, H.; Chen, L.; Liu, L. & Wan, X. 2018. Maintenance of mesophyll potassium and regulation of plasma membrane H^+-ATPase are associated with physiological responses of tea plants to drought and subsequent rehydration. *The Crop Journal*, 6(6), 611-620.

66. Park, S.; Kang, T. S.; Kim, C. K.; Han, J. S.; Kim, S.; Smith, R. H.; Pike, L.M. & Hirschi, K. D. 2005. Genetic manipulation for enhancing calcium content in potato tuber. *Journal of Agricultural and Food Chemistry*, 53(14), 5598-5603.

67. Grobler, L.; Bloem, A. A. & Claassens, A. S. 1999. A critical soil sulphur level for maize (*Zea mays* L.) grown in a glasshouse. *South African Journal of Plant and Soil*, 16(4), 204-206.

68. Luyckx, M.; Hausman, J. F.; Lutts, S. & Guerriero, G. 2017. Silicon and plants: Current knowledge and technological perspectives. *Frontiers in Plant Science*, 8, 411.

69. Rastogi, A.; Tripathi, D. K.; Yadav, S.; Chauhan, D. K.; Živčák, M.; Ghorbanpour, M.; El-Sheery, N.I. & Brestic, M. 2019. Application of silicon nanoparticles in agriculture. *3 Biotech*, 9(3), 1-11.

70. Attia, E. A. & Elhawat, N. (2021). Combined foliar and soil application of silica nanoparticles enhances the growth, flowering period and flower characteristics of marigold (*Tagetes erecta* L.). *Scientia Horticulturae*, 282, 110015.

71. Mahler, R. L. Nutrients Plants Require for Growth. 2004. Retrieved from https://www.extension.uidaho.edu/publishing/pdf/CIS/CIS1124.pdf

72. Arif, N.; Yadav, V.; Singh, S.; Singh, S.; Ahmad, P.; Mishra, R. K.; Sharma, S.; Tripathi, D. K.; Dubey, N. K. & Chauhan, D. K. 2016. Influence of high and low levels of plant-beneficial heavy metal ions on plant growth and development. *Frontiers in Environmental Science*, 4, 69.

73. Souri, M. K. 2016. Aminochelate fertilizers: the new approach to the old problem; A review. *Open Agriculture*, 1, 118-123.

74. Shang, Y.; Hasan, M.; Ahammed, G. J.; Li, M.; Yin, H. & Zhou. 2019. Applications of nanotechnology in plant growth and crop protection: A review. *Molecules*, 24, 2558.

75. Rozo, G.; Bohorques, L. & Johanna Santamaría, J. 2019. Controlled release fertilizer encapsulated by a κ-carrageenan hydrogel. *Polímeros*, 29, 2019033.

76. Islam, M. A.; Ferdous, G.; Akter, A.; Hossain, M. M. & Nandwani, D. 2017. Effect of organic, inorganic fertilizers and plant spacing on the growth and yield of cabbage. *Agriculture*, 7, 31.

77. Nookabkaew, S.; Rangkadilok, N.; Prachoom, N. & Satayavivad, J. 2016. Concentrations of trace elements in organic fertilizers and animal manures and feeds and cadmium contamination in herbal tea (*Gynostemma pentaphyllum* Makino). *Journal of Agriculture and Food Chemistry*, 64, 3119-3126.

78. Brandt, K.; Leifert, C.; Sanderson, R. & Seal, C. J. 2011. Agroecosystem management and nutritional quality of plant foods: The case of organic fruits and vegetables. *Critical Reviews in Plant Sciences*, 30, 177-197.

79. Yamulki, S. 2006. Effect of straw addition on nitrous oxide and methane emissions from stored farmyard manures. *Agriculture, Ecosystems & Environment*, 112, 140-145.

80. Cifuentes-Torres, L.; Mendoza-Espinosa, L. G.; Correa-Reyes, G. & Daesslé, L. W. 2021. Hydroponics with wastewater: a review of trends and opportunities. *Water and Environmental Journal*, 35, 166-180.

81. Duhan, J. S.; Kumar, R.; Kumar, N.; Kaur, P.; Nehra, K. & Duhan, S. 2017. Nanotechnology: The new perspective in precision agriculture. *Biotechnology Reports*, 15, 11-23.

82. Mali, S. C.; Raj, S. & Trivedi, R. 2020. Nanotechnology a novel approach to enhance crop productivity. *Biochemistry and Biophysics Reports*, 24, 100821.

83. Kalwani, M.; Chakdar, H.; Srivastava, A.; Pabbi, S. & Shukla, P. 2022. Effects of nanofertilizers on soil and plant-associated microbial communities: Emerging trends and perspectives. *Chemosphere*, 287, 132107.

84. Ghormade, V.; Deshpande, M. V. & Paknikar, K. M. 2011. Perspectives for nano-biotechnology enabled protection and nutrition of plants. *Biotechnology Advances*, 29, 792-803.

85. Kah, M.; Kookana, R. S.; Gogos, A. & Bucheli, T. D. 2018. A critical evaluation of nanopesticides and nanofertilizers against their conventional analogues. *Nature Nanotechnology*, 13(8), 677-684.

86. DeRosa, M. C.; Monreal, C.; Schnitzer, M.; Walsh, R. & Sultan, Y. 2010. Nanotechnology in fertilizers. *Nature Nanotechnology*, 5(2), 91-91.

87. Lin, W.; Lin, M.; Zhou, H.; Wu, H.; Li, Z. & Lin, W. 2019. The effects of chemical and organic fertilizer usage on rhizosphere soil in tea orchards. *PloS One*, 14(5), 0217018.

88. Innes, R. 2013. Economics of agricultural residuals and overfertilization: Chemical fertilizer use, livestock waste, manure management, and

environmental impacts. Encyclopedia of energy, natural resource, and environmental economics. *Elsevier Science, Waltham, MA*, 50-57.

89. Haj-Amor, Z.; Araya, T.; Kim, D. G. & Bouri, S. 2023. Climate change effects on soil salinity in rainfed maize areas: a case study from South Africa. *Water Supply*, 23(6), 2447-2465.

90. Nell, J. P. & Van Huyssteen, C. W. 2018. Prediction of primary salinity, sodicity and alkalinity in South African soils. *South African Journal of Plant and Soil*, 35(3), 173-178.

91. Mabidi, A.; Bird, M. S. & Perissinotto, R. 2018. Increasing salinity drastically reduces hatching success of crustaceans from depression wetlands of the semi-arid Eastern Cape Karoo region, South Africa. *Scientific Reports*, 8(1), 5983.

92. Dabrowski, J. M.; Shadung, J. M. & Wepener, V. 2014. Prioritizing agricultural pesticides used in South Africa based on their environmental mobility and potential human health effects. *Environment International*, 62, 31-40.

93. Manzoor, M. A.; Shah, I. H.; Sabir, I. A.; Ahmad, A.; Albasher, G.; Dar, A. A.; Altaf, M.A. & Shakoor, A. 2023. Environmental sustainable: Biogenic copper oxide nanoparticles as nano-pesticides for investigating bioactivities against phytopathogens. *Environmental Research*, 231, 115941.

94. Batsmanova, L.; Taran, N.; Konotop, Y.; Kalenska, S. & Novytska, N. 2020. Use of a colloidal solution of metal and metal oxide-containing nanoparticles as fertilizer for increasing soybean productivity. *Journal of Central European Agriculture*, 21(2), 311-319.

CHAPTER 2
LITERATURE REVIEW

2.1 Metal-based nanoparticles in agriculture

Mineral fertilizers are subjected to chemical processing to fulfil crop needs and provide nutrients in predetermined amounts. Studies have shown that nanoscale mineral fertilizers promote the availability of representative nutrients through adhesion on plant surfaces and rapid uptake. The nanomaterial interactions with plant surfaces reduce nutrient leaching and increase efficiency [1]. Chemical solution deposition is a procedure that can be used to produce the nanoparticles (NPs) of mineral fertilizers. The production of potassium ferrite ($KFeO_2$) NPs, for example, was achieved by reacting aqueous solutions of potassium nitrate (KNO_3) and ferric nitrate [$Fe(NO_3)$], in the presence of citric acid [$HOC(CO_2H)(CH_2CO_2H)_2$], in ethylene glycol at eighty to eighty five degrees Celsius [2]. During this reaction, citric acid acts as a chelating agent for binding the metal ions. Wax was further used to coat the as-developed nanoparticles on bulk diammonium phosphate [$(NH_4)_2HPO_4$] and yield the mineral fertilizers with Fe, N, P, and K slow-release rates. The soil supplementation of Fe and a gradual release of nitrogen and phosphorus nutrients for up to 1 440 hours (60 days) was reported throughout the soil treatment trial. Also described by Abdel-Aziz et al. [3], is the nanoformulation of a bio-based controlled-release NPK fertilizer. This nanomaterial was produced by ball-milling the chemically treated shrimp shells, squid pins, bovine bones, and banana peels. It was then utilized as an effective growing medium for *Capsicum annum*. The outcomes demonstrated a remarkable enhancement in length of shoot, leaf quantity, area, respiration rate and fruit shape index.

Numerous reports of using metallic minerals in NPs as fertilizers in agriculture are mentioned (Table 2.1). These inputs can improve the availability of nutrients to plants, their biological health, growth, and yields [4]. Delfani and co-workers (2014) examined the foliar application of Fe and Mg NPs on the growth of legume black-eyed pea plants. While Mg NPs aided in the uptake of Mg, Fe NPs substantially increased the leaf chlorophyll concentration and seed protein percentage. However, in contrast to the of $MgSO_4$ solution, the Mg NPs triggered detrimental effects on the

plasma membrane [5]. Likewise, a study by Pradhan et al. (2013) [6] on the influence of Mn NPs on mung bean plants' growth, revealed a higher photosynthetic rate than $MnSO_4$. It should be noted that at 1 mg L^{-1}, the latter inhibited the development of plants. Shah and Belozerova (2009) [7] reported in a different study that adding metallic Pd and Cu NPs to the soil effectively enhanced the ratio of shoots to roots for the growth of lettuce, a leafy vegetable. It has also been reported that Cu NPs exhibit fascinating bactericidal activities [8]. These can trigger the production of ROS that cause DNA damage in bacteria. Chemical reduction, bio-reduction, and hydro-/solvo-thermal techniques can all be used to synthesize metal nanoparticles [9,10]. In the hydro-/solvo-thermal process, nanocrystals are formed at high pressure and temperature from a solution containing metal precursors. Reductants are used in the chemical reduction procedure to change the metal cations into zero-valent metal nanoparticles. Similar to this, green methods that make use of phytoconstituents and living organisms (e.g. fungi and bacteria)have also been reported to produce metallic nanoparticles (Figure 2.1) [11,12].

A study by Thakur and colleagues (2018) [13] demonstrated the nematicidal effects of bio-developed gold NPs (20-45 nm) and their merits on tomato plant development. The *Bacillus licheniformis* strain GPI-2 was used to convert Au^{3+} from a chloride solution into the corresponding NPs. Findings from that study revealed that solutions of this nanomaterial improved the germination of tomato seeds and decreased the survival rate of the root-knot nematode*Meloidogyne incognita*. In the presence of silver ions, *Cordia myxa* leaf extract has been found to produce silver nanoparticles NPs with an average size of 5.8 nm, according to a recent publication by Akbarnejad-Samani et al. (2020) [14]. The prepared nanomaterial improved the onion's antioxidant capacity and germination indices and more than its chemically fabricated counterpart. The phyto-assisted procedure represents a more cost-effective and environmentally friendly technique than other biological methods for synthesising nanomaterials. Moreover, large-scale preparation of mineral nanofertilizers can be achieved using this method. The ability of plant biomass or extracts to reduce metal ions has been common knowledge since the early 1900s, but it has been exploited only in the last decades for the reduction of metal salts. The fundamental principle behind this technology is based on the presence of hydroxyl-rich phytochemicals and secondary metabolites with nucleophilic (–C–O–, –C=O, –

C–O–C–, and –C=C–) functional groups that act as reducers for the conversion of metal ions and stabilizers for the developing nanostructures. Furthermore, unlike microorganisms, plants' terpenoids, flavonoids, phenols, and carboxylic acids can reduce metal ions in a shorter exposure period [15].

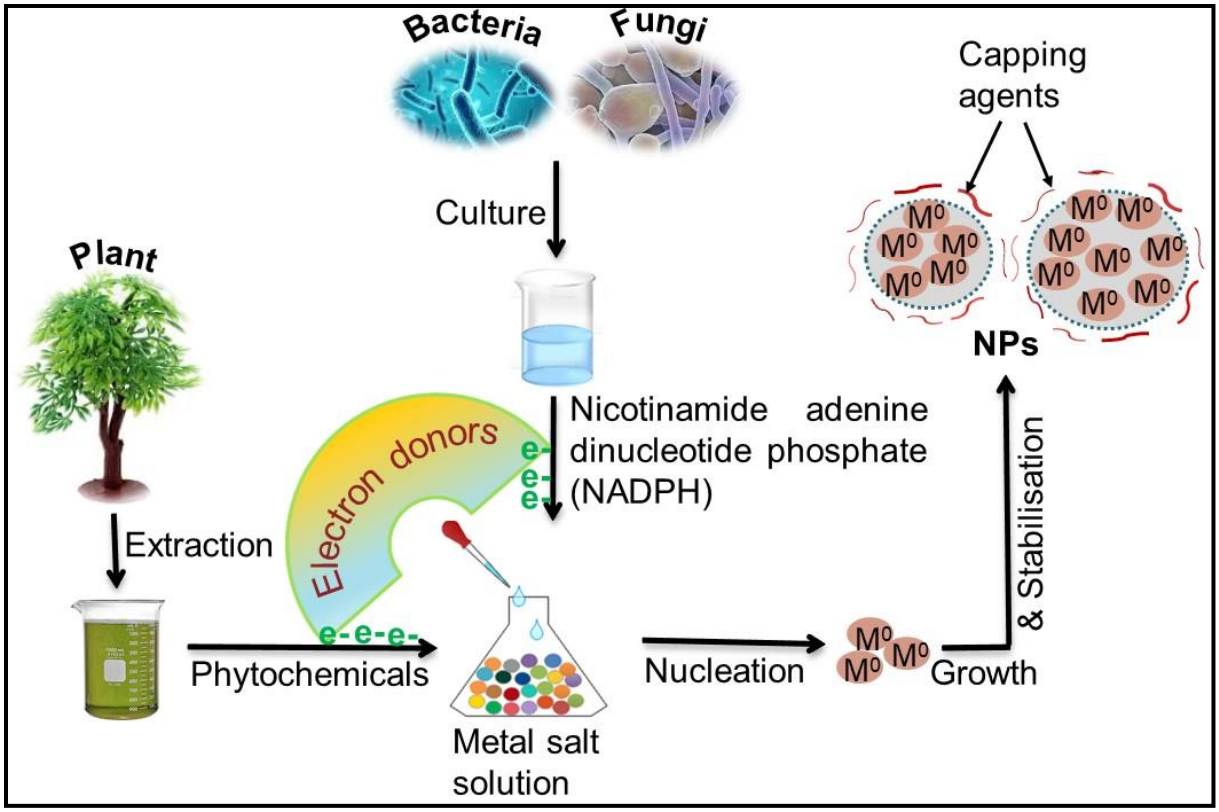


Figure 2. 1: Preparation of metal-rich nanofertilizers by biological means.

The important nano-oxide components that have been described to stimulate plant growth are oxides of silicon (SiO_2 NPs), titanium (TiO_2 NPs), cerium (CeO_2 NPs), copper (CuO NPs), zinc (ZnO NPs), and iron (Fe_2O_3 and Fe_3O_4 NPs) [16–18]. Due to their entomotoxic characteristics and potential to instigate ROS production, these nanomaterials have also been commended for their pesticide activities. Plant extracts-mediated method, gas-phase synthesis, ultrasound-assisted technique, and chemical processes such as sol-gel, precipitation, liquid impregnation, and hydrothermal procedure can prepare the metal oxide nanoparticles (Figure 2.2). The titania powder impregnation in liquid [19] and the sol-gel processing of titanium tetrachloride ($TiCl_4$) [20], for example, afforded the TiO_2 NPs that can promote the phytoavailability of phosphate ions in the soil. A study by Hanif and co-workers (2015) [19] showed that the nano-TiO_2 (size > 65 nm, dosage 100 mg/Kg soil)

increased plant phosphorus availability by 5 times, leading to better lettuce development. The anatase structure of this nano-metal oxide (size: 23 nm) can also interact with Cu(II) ions to reduce their toxicity in hydroponically grown soybean plants [21].

Recently, it was found that chlorophyll content, relative water content (RWC), and morphological traits of *Triticum aestivum* under water stress could be improved by a blended $Ca_3(PO_4)_3$ and nano-TiO_2 developed using *Moringa oleifera* leaf extract [22]. According to a study by Mariz-Ponte's research team [23], the commercially obtainable titanium oxide (P25) nanoparticles, which consist of rutile and anatase phases, can reduce the phytotoxicity caused by Al and Pb metal ions. On the other hand, it has been argued that the foliar application of nano-SiO_2 enhances N and P uptake by cucumber plants under salt stress [24]. Data from this experiment also showed that plants treated with NPK fertilizer-SiO_2 NPs exhibited an increased number of leaves and fruits. Salt stress hinders plants from growing and developing because it encourages Na^+ and/or Cl^- toxicity, water deficiency, and nutritional imbalances [25,26]. The Fe_2O_3, TiO_2, and SiO_2 NPs can mitigate the stress caused by salinity during plant growth [27]. Research on these nano-oxides has also been extended to pesticidal activities. For example, nanosilica produced by the sol-gel method employing tetra alkyl silicate precursors has been identified as an efficient pesticide against the crop pests *Spodoptera litura*, *Lipaphis pseudobrassicae*, *Tribolium castaneum*, *and Sitophilus oryzae*.

Aloe barbadensis Mill leaf extract has generated zinc oxide NPs (average size 30–40 nm) [29]. This nanomaterial was compared *via* zinc fertilization with its chemically (sol-gel) produced counterpart (average size 48 nm), and treatment of wheat seeds with the biogenic ZnO NPs (concentration 62 mg/L) yielded the most enhanced germination and early growth. Rai-Kalal and Jajoo [30] reported a similar observation after using the seed priming technique. This pre-sowing strategy activates a seed's metabolic processes and increases the germination rate [31]. In cereal crops, ZnO NPs (average size 18 nm, concentration 5 mg/Kg soil) have been linked to boost N uptake and grain yield under drought conditions [32]. In addition, research demonstrated that ZnO NPs could up-regulate the plant defence system [33,34]. It has been suggested that foliar ZnO NPs sprays (100 mg/L of deionized water)

decreased *Tomato mosaic virus* infection in tomato plants [35]. This result is attributed to an increment in the non-enzymatic antioxidant ascorbic acid and glutathione contents and a rise in the antioxidant enzyme activity. These metal oxide nanoparticles could equally cause an improvement of tomato plant growth under salt stress [36]. A mixture of ZnO NPs and 24-epibrassinolide, a naturally occurring plant hormone, increased the photosynthetic rate of tomato plants under Cu^{2+} stress [37]. A foliar treatment of *Nicotiana benthamiana* using Fe_3O_4 NPs (average size 20 nm; concentration 100 µg/mL of deionized water) increased the activities of antioxidant enzymes [38]. This improved the ability of plants to defend themselves against the *Tobacco mosaic virus. Syzygium cumini* seed extract and ferric chloride salt were used as substrates to synthesize the as-described nanoparticles. Nanoparticles of metal and metal oxide have been exposed to offer physiological and morphological advantages in several plant model systems, yet at higher doses, they have also been shown to cause genotoxicity and stress [39,40].

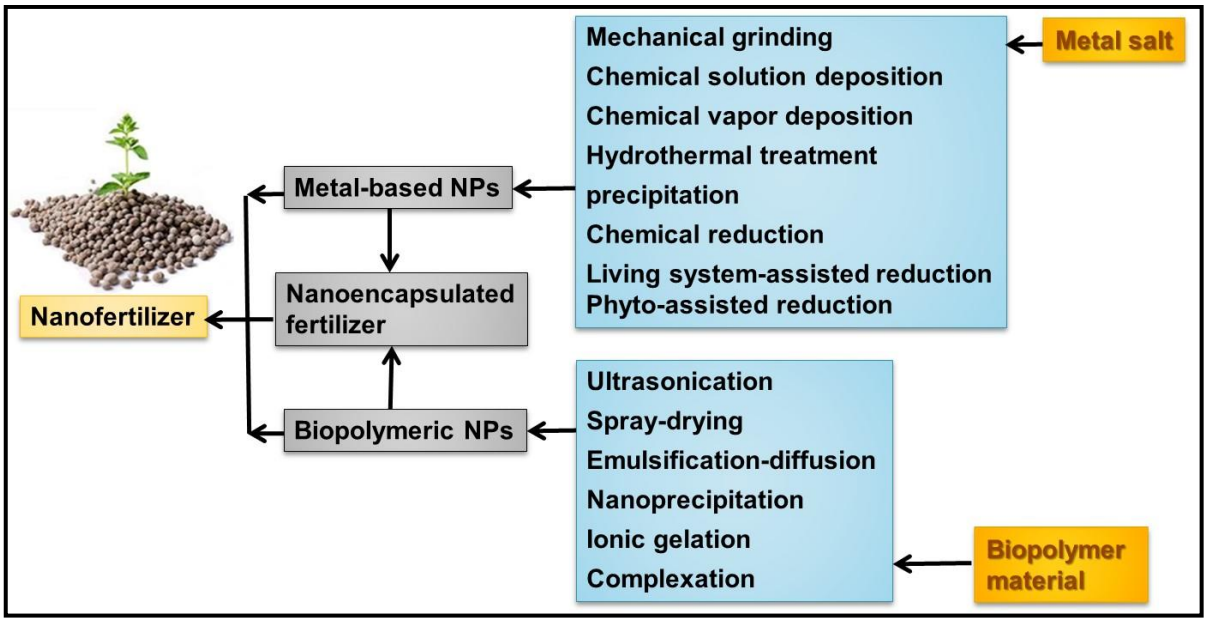


Figure 2. 2: Techniques reported for the preparation of nanofertilizers.

Table 2. 1: Reported metal-based nanoparticles for plant growth and development.

Metal/ metal oxide NPs	Method	Plant model	Effects	Ref.
Ag NPs (5 nm)	Bio-synthesized using the *Cordia myxa* leaf extract	*Allium cepa* (Onion)	Improve the seed germination	[14]
Au NPs (20-45 nm)	Bio-synthesized using the *Bacillus licheniformis* strain GPI-2	*Solanum lycopersicum* (Tomato)	Increase the seed germination and shoot length Protection against *Meloidogyne Meloidogyne incognita* nematodes	[13]
Au NPs (27 nm)	Bio-synthesized using the leaves of Wheat (*Triticum aestivum*)	*Triticum aestivum* (Wheat)	Up-regulate the defense systems under salinity	[41]
Cu NPs	NR	*Lactuca sativa* (Lettuce)	Increase the shoot/root ratio	[7]
Mixed Cu-Ag NPs	Bio-synthesized using the *Moringa oleifera* leaf extract	*Artemisia absinthium* (Wormwood)	Increase the antioxidant enzyme activities and occurrence of secondary metabolites	[42]
Fe/Co NPs (30-70 nm)	Chemical reduction	*Zea mays* (Maize)	Increase the antioxidant	[43]

			enzyme activities and germination rate	
Mg and Fe NPs	NR	*Vigna unguiculata* (Black-eyed pea)	Increase the yield and chlorophyll content	[5]
Mn NPs (20 nm)	NR	*Vigna radiata* (Mung bean)	Increase the length of the shoot, root, and chlorophyll content	[6]
Si NPs	NR	*Cymbopogon flexuosus* (Lemongrass)	Increase the leaf area, chlorophyll content, plant height, transpiration rate, and superoxide dismutase activity	[44]
CuO NPs (30 nm)	Gas phase procedure	*Elodea densa*	Increase the antioxidant enzyme activities	[45]
Fe_2O_3 NPs (20 nm)	NR	*Arachis hypogaea* (Peanut)	Up-regulate the antioxidant enzyme activity and phytohormone contents	[46]
SiO_2 NPs	Sol-gel process using a solution of sodium meta-silicate and HCl,	*Musa acuminata* (Banana)	Enhance the photosynthetic rate under salt stress and/or drought	[47]

	then calcination at 600 °C		conditions	
MgO NPs	Sol-gel process using magnesium nitrate and NaOH, then calcination at 400 °C	*Vigna unguiculata* (Cowpea)	Increase the nitrogen and chlorophyll contents	[48]
ZnO NPs (20 nm)	NR	*Cicer arietinum* (Chickpea) and *Vigna radiata* (Mung bean)	Increase the root and shoot length	[49]
ZnO NPs (25 nm)	Decomposition of zinc oxalate in air at 500 °C	*Zea mays* (Maize)	Increase the Zn content of grains and leaf area	[50]
ZnO NPs (35 nm)	Bio-synthesized using *Aloe barbadensis Mill* leaf extract	*Triticum aestivum* (Wheat)	Increase the root and shoot length	[29]
ZnO NPs (38 nm)	Sol-gel process using a solution of zinc acetate and citric acid, then calcination at 530 °C	*Glycine max* (Soybean)	Increase the yield and production of antioxidant enzymes	[51]
TiO_2 NPs (25 nm)	Hydrothermal process using titanium isopropoxide at	*Solanum lycopersicum* (Tomato)	increase root length, biomass, plant height, and fruit yield	[52]

	240 °C			
TiO_2 NPs (<65 nm)	Liquid impregnation using titania and calcination at 400 °C	*Lactuca sativa* (Lettuce)	Increase the root and shoot length, and phytoavailable phosphate in soil	[19]
CeO_2 NPs (16-25 nm)	Laser ablation	*Brassica oleracea* (Cabbage)	Increase the chlorophyll content, head circumference, and yield	[53]

2.2 Metal-based nanoparticles and their phytotoxicity

Numerous studies show how directly exposing plants to nano-metal and nano-metal oxide particles can greatly increase phytotoxicity, underscoring the necessity of their eco-friendly use. Several plants, including *A. thaliana*, *O. sativa*, *V. faba*, *C. pepo*, *A. cepa*, *T. aestivum*, *C. annuum*, and *Z. mays,* were found to be adversely affected by Ag NPs, as shown in Table 2.2. In *T. aestivum*, Zn NPs (size <100 nm) at 500 mg/kg soil, caused a delay in root growth and a decrease in the content of chlorophyll [54]. The mitotic index significantly decreased in *A. cepa* treated using copper NPs (size 17-93 nm) with escalating dosages (10-100 µg/ml) for a longer period [55]. According to Taylor and co-workers [56], the root lengths of *A. thaliana* seedlings were reduced by 75% when exposed to Au NPs (size 7-108 nm) at 100 mg/ml. Rajeshwari et al. (2016) [57] recorded elevated levels of ROS in *A. cepa* exposed to higher concentrations of nanosized gold particles. This study also demonstrated that the phytotoxicity of gold NPs is inversely correlated with their size. Treatment of *A. thaliana* seeds with 400, 2000, and 4000 mg/L of ZnO NPs decreased germination rate, root elongation and the number of leaves [58]. This nano-metal oxide has also

been reported to instigate dose-dependent cell dysfunction [59,60] and root length inhibition on *A. cepa* [61].

A cognate study on *O. sativa* revealed that 1000 mg/L of CuO NPs (size <50 nm) could cause a decline in photosynthetic and transpiration rates [62]. Similar results were observed when magnesium NPs (size <50 nm) interacted with *A. cepa* root cells. This interaction was described to increase ROS formation in a dose-related manner [63]. As the dose of MgO NPs was increased, the levels of hydroxyl (•OH) and superoxide ($\bullet O_2^-$) radicals and hydrogen peroxide (H_2O_2) also all ascended. Plants' physiological and genetic responses to TiO_2 NPs revealed a dose-dependent toxicity as well [64,65]. Dissolution and release of metal ions in soil are common for metal-based NPs. According to a study by Garca-Gómez et al. (2018) [66], soil acidity is a major contributing factor to metal phytotoxicity. In amended acidic soils, metal oxide NPs quickly release metal ions, making them readily available in high concentrations. Cellular damage, decreased germination rate, and a decline in growth metrics, including shoot and root length, are the well-known toxic manifestations in metal and metal oxide NP-exposed plants (Table 2.2). Numerous strategies have been established in the literature to overcome the phytotoxicity of metal-based nanofertilizers in food production [67]. Among them, encapsulation within biopolymeric carriers could enable smart formulations.

Table 2. 2: Reported phytotoxicity of metal and metal-oxide NPs.

Metal-based NPs	**Plant**	**Doses**	**Toxicity signs and symptoms**	**Ref.**
Ag NPs (25 nm)	*O. sativa*	50, 500, and 1000 mg/L	Cell wall damage	[68]
Ag NPs (60 nm)	*V. faba*	12.5, 25, 50, and 100 mg/ml	Increase of chromosomal aberrations (CA), and declining in mitotic index (MI)	[69]

Ag NPs (<100 nm)	*C. pepo*	250 and 750 mg/mL	Declining in plant transpiration	[70]
Ag NPs (11 nm)	*Z. mays*	0.05, 0.1, 1, 18, 36, and 73 mg/mL	Root growth inhibition	[71]
Ag NPs (10 nm)	*A. thaliana*	0.2, 0.5, and 3 mg/mL	Root growth inhibition and drop in chlorophyll content	[72]
Ag NPs (10 nm)	*T. aestivum*	0.5, 2.5, 3.5, and 5 mg/kg	Reduction of length of roots and shoots	[73]
Ag NPs (12 nm)	*C. annuum*	0.01, 0.05, 0.1, 0.5, 1 mg/L	Decrease in plant growth	[74]
Au NPs (7-108 nm)	*A. thaliana*	100 mg/mL	Reduction in root growth	[56]
Au NPs (15-40 nm)	*A. cepa*	0.1, 1, and 10 µg/mL	Increase in CA and ROS with increasing doses	[57]
Cu NPs (17-93 nm)	*A. cepa*	10-100 µg/ml	Increase in CA and decrease in MI with increasing doses	[55]
Zn NPs (<100 nm)	*T. aestivum*	500 mg/kg	Reduction in root growth, increased lipid peroxidation and oxidized glutathione in roots Decrease in chlorophyll content	[54]
Al_2O_3 NPs	*A. cepa*	0.01, 0.1, 1, 10,	Decrease of MI	[75]

(<50 nm)		and 100 µg/mL		
CuO NPs (<50 nm)	*H. vulgare*	200, 400, 600, 800, 1000 mg/L	Dose-dependent a decrease in shoot and root growth Increase in ROS	[76]
CuO NPs (<50 nm)	*O. sativa*	2.5, 10, 50, 100, 1000 mg/L	Decrease in thylakoid number, photosynthetic and transpiration rates	[62]
CuO NPs (30 nm)	Transgenic and conventional cotton	10, 200, and 1000 mg/l	Decrease in growth	[77]
CuO NPs (<50 nm)	*T. aestivum*	3, 10, 30, and 300 mg/kg	Inhibition of the root growth at 30 and 300 mg/kg	[78]
CuO NPs (25 nm)	*G. max*	0, 50, 100, 200 and 500 mg/kg	Reduction in yield at higher concentrations	[79]
α-Fe_2O_3 NPs (14 nm)	*H. vulgare*	50, 100, 200, and 400 mg/L	Reduction in germination rate and chlorophyll contents at 400 mg/L	[80]
MgO NPs (<50 nm)	*A. cepa*	12, 25, 50, and 100 µg/mL	DNA damage, increase in CA, and decrease of MI	[63]
ZnO NPs (44 nm)	*A. thaliana*	400, 2000, and 4000 mg/L	Decrease in germination rate and	[58]

			root elongation	
ZnO NPs (3-5 nm)	*A. sativum*	10, 20, 30, 40, and 50 mg/L	Dose dependent inhibition of root growth, and mitotic aberrations	[81]
ZnO NPs (50 nm)	*C. sativus*	10, 50, 100, 500, 1000 mg/L	Decrease in seedling biomass.	[82]
ZnO NPs (<50 nm)	*P. sativum*	250, 500, 750, 1000 mg/L	Inhibition of root growth	[83]
ZnO NPs (<50 nm)	*A. cepa*	10, 100, and 1000 mg/L	Dose dependent cell injury	[59]
ZnO NPs (<50 nm)	*O. sativa* and *Z. mays*	500, 1000, and 2000 mg/L	Inhibition of root growth at 2000 mg/L	[84]
TiO_2 NPs (25 nm)	*Z. mays*	300 mg/mL	Inhibition of leaf growth and transpiration	[85]
TiO_2 NPs (25 nm)	*V. narbonensis*	2000, 10000, 20000, and 40000 mg/mL	Decrease in root elongation, increase in the aberration index, and decrease of MI	[86]
TiO_2 NPs (<25 nm)	*A. cepa*	12, 25, 50 and 100 µg/mL	Decrease of the MI	[64]
TiO_2 NPs (90 nm)	*A. cepa*	0.001, 1, 100, and 10000 µg/mL	Decrease in root length	[65]

TiO_2 NPs (26 nm)	*O. sativa*	500 and 750 mg/kg	Leaf membrane injury and increase production of H_2O_2	[87]

2.3 Biopolymer-based nanomaterials for agricultural practices

Various versatile materials known as biopolymers have gained attention in food packaging and agriculture [88]. These are known to breakdown in the environment and are composed of polysaccharides and proteins. In agricultural sciences, the most popular biopolymers include chitosan (CS), alginate (ALG), and zein (Figure 2.3). These inexpensive materials have ionizable functional groups ($–NH_2$, $–COO^-$, –OH) that enable ionic bonding and electrostatic complexation with opposite charges to generate nanostructured particulates. In this respect, ionic crosslinking of polyelectrolytes and complexation processes are typically used to prepare biopolymeric NPs. There have also been reports on using precipitation, emulsification-diffusion, and spray-drying procedures to afford biopolymeric NPs (Figure 2.2).

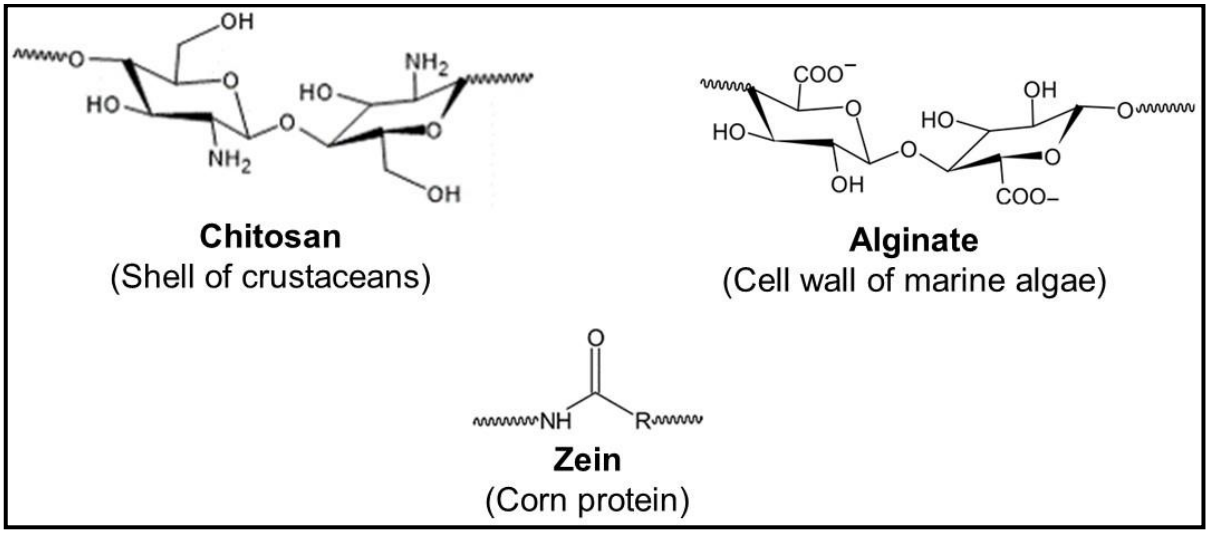


Figure 2. 3: The main functional groups in CS, ALG, and zein biopolymers.

The capacity of the nano-engineered biopolymer materials to promote plant development, control plant diseases, and preserve agricultural crop harvest has

been discussed in the literature [89]. The efficacy of these NPs in lowering the negative effects of water deficit in soil has also been described. The drought conditions inhibit the volume expansion and division of cells, which are mediated by turgor pressure [90,91]. It has been reported that the CS NPs (size > 100 nm), produced by ultrasonically treating and grinding chitosan powder, improve the leaf area, RWC, and chlorophyll content in wheat under water deficit [92]. The results also indicated that significantly greater doses of CS NPs (30, 60, and 90 ppm) achieved better outcomes in wheat plants. A study by Salinas et al. (2021) [93] provides support of a similar observation. As detailed in Table 2.3, soybean plants exposed to different doses (0.02, 0.2, and 2 mg/mL) of zein NPs (141 nm), displayed more chlorophyll, longer roots, and increased dry mass at the highest dose. The emulsification-diffusion procedure was employed to synthesize these biopolymeric NPs. This method is based on thermodynamic principles that make use of partly water-soluble solvent containing the biopolymer in equilibrium with an aqueous phase containing a stabilizer. Zein NPs are formed by the amphiphilic nature of zein polymer and their capacity to aggregate in stabilized acetone/water emulsion droplets.

The encapsulation of nutrients within biopolymeric nanostructures demonstrates a fundamental change toward sustainable farming. These nanoformulated inputs have the ability to regulate nutritional dose at the necessary concentrations throughout a predetermined period, hence lowering environmental losses. Such a strategy also ensures that nutrients remain available to plants for prolonged duration. Recently, our research group assessed the impact of SNPK nutrients loaded in CS NPs for maize growth [94]. This original nanocomposite was developed by ionic gelation, and the release ratio of total nutrients within a week was less than 60% in an aqueous solution. Another composite material consisting of ZnO NPs loaded in alginate-polyvinyl alcohol (ALG-PVA) has been shown to exhibit a slow release of Zn nutrients in addition to a remarkable water intake capacity [95]. This Zn fertilizer was also prepared by the ionic gelation method in the presence of PVA, which helped increase the yielded material's hydrophilicity. Ionic gelation offers a valuable nutrient-loading approach in encapsulated systems [96]. The synthesis of Cu-containing CS NPs through the ionic gelation of CS, tripolyphosphate (TPP), and Cu^{2+} has also been described in the literature [97]. The as-prepared nanomaterial was reported to

serve as a potent antifungal agent at the field level. The polyelectrolyte complexation process has been used to entrap CuO NPs into CS-ALG nanostructures [98]. This nanoformulated composite exhibited efficacy in increasing the seed germination of *Fortunella margarita* Swingle and achieved 80 percent of copper release within 22 days.

As depicted in Figure 2.4 [99,100], various environmental conditions can cause the release of nutrients from systems that are nano-encapsulated. Using enzymatic mechanisms, bacteria, fungi, and algae can degrade the biopolymeric chains. Moisture, heat, soil texture, light irradiation, and pH variation are non-enzymatic factors that equally promote the breakdown of biopolymeric carriers [101,102]. To slowly degrade CS and ALG particulates, protonation of the glycosidic oxygen can occur in an acidic environment, followed by heterolytic fission of the resulting conjugate acids [103,104]. Additionally, water can pass through the membrane of biopolymeric NPs that is semi-permeableand initiate the slow release of nutrient entrapped by osmotic pressure. Sunlight can also initiate their photo-oxidative decomposition due to UV rays [105,106]. Besides the ability to serve as slow-release carriers, biopolymeric-based NPs display anti-pathogenic activities [107-110].

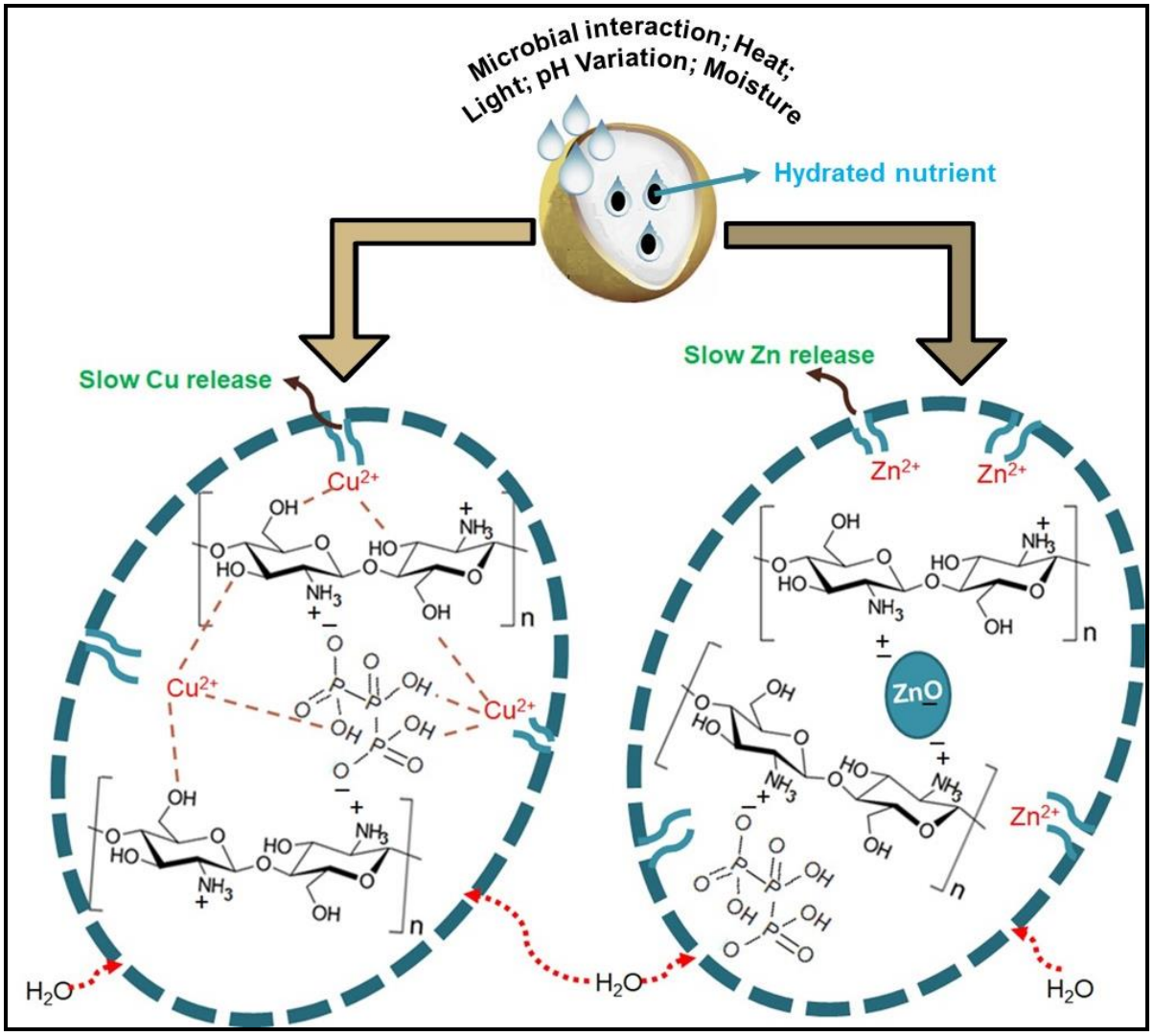


Figure 2. 4: Hypothetical illustrations of ZnO- and Cu^{2+}-entrapped CS NPs indicating the metal chelation, ionic interactions, and nutrient release.

Table 2. 3: Reported biopolymeric nanomaterials for plant development and growth.

Biopolymer-based NPs	Methods	Plant	Effects on plant growth & development	Ref.
CS NPs (420-970 nm)	Nano spraying method	*C. canephora*	Increase the nutrient uptake and chlorophyll content	[111]
CS NPs (> 100 nm)	Ultrasonication and grinding	*T. aestivum*	Improve the antioxidant defence system	[92]

			activities, and increase the water content and yield	
CS/TPP NPs (145-450 nm)	Ionic gelation	*Z. mays*	Increase the plant height and number of leaves	[94]
Zein NPs (50-230 nm)	Emulsification-diffusion process	*S. officinarum*	Promote the adherence/absorption of zein biopolymer in the roots	[112]
Zein NPs (141 nm)	Emulsification-diffusion using zein and DDMAB	*G. max*	Increase root length and the chlorophyll content	[93]
NPK nutrients-encapsulated CS/PMAA NPs	Polymerization	*T. aestivum*	Increase the shoot length, leaf area, root, and water content	[113]
NPK nutrients-encapsulated CS/TPP NPs (300-750 nm)	Ionic gelation	*Coffea arabica*	Improve the nutrient uptake and chlorophyll content	[114]
NPKS nutrients-encapsulated CS/TPP NPs (200-530 nm)	Ionic gelation	*Z. mays*	Achieve the slow release of nutrients	[94]

Cu(II)-laden CS/TPP NPs (374 nm)	Ionic gelation	*S. lycopersicum*	Improve the seed germination; increase fresh and dry weight; inhibit the activities of *Alternaria solani* and *Fusarium oxysporum*	[97]
SiO_2-encapsulated CS/TPP NPs (360 nm)	ionic gelation	*Z. mays*	Improve the seedling growth, chlorophyll content, and defense systems	[115]
Zn(II)-laden CS/TPP NPs (250-300 nm)	Ionic gelation	*T. aestivum*	Show a slow delivery of Zn	[116]
Zn(II)-laden CS/TPP NPs (387 nm)	Ionic gelation	*Z. mays*	Inhibit the activities of *Cochliobolus lunata*	[117]
Chitosan-coated ZnO NPs	Precipitation	*P. nigrum*	Improve the chlorophyll content	[118]
CuO-encapsulated ALG/CS- NPs (309 nm)	Polyelectrolyte complexation	*F. margarita*	Achieve a slow release of Cu and enhance the seed germination	[98]

2.4 Nanomaterials and their pesticidal activity

Global use of chemical pesticides is estimated to be more than 2.8 million tons per year [119]. Nevertheless, it has been argued that less than 10% of the chemical pesticides applied reach their target. Over 90% of the pest control agents are

dispersed in the environment [120] and these are potential contaminants of surface and groundwater [121]. The key aspects that govern the potential for water contamination by the conventional pesticides are their mobility and persistence. Pesticides play an essential role in controlling plant diseases and maximizing agricultural production. Several strategies have been reported recently to limit the non-target effects of pesticides [122, 123]. The development of new pest control agents has long been a field of intensive research. By virtue of the nanomaterial-associated properties (leaf adhesion, stability, and bioavailability), nanotechnology can help reducing the amount of pesticides loss in run-off event. In the literature, materials tested as nanopesticides consist of particles that present colloidal behaviour within the size range of 1-1000 nm [123]. Nano-metals, nano-metal oxides, and nano-polymeric materials have frequently been found to significantly inhibit the growth of fungal plant pathogens in a dose-dependent manner, showcasing their potential as eco-friendly alternatives to the traditional pesticides [124, 125, 126].

The treatment of a cupric nitrate solution with glycine, enhanced the effectiveness of the nanoparticles of CuO/Cu_2O, which were found to inhibit growth of the phytopathogens *Fusarium solani* and *Aspergillus niger* and Gram-negative bacteria *Escherichia coli* and *Pseudomonas aeruginosa* [127]. Earlier, Nazish and co-workers (2023) evaluated the pesticidal potential of the 95.7 nm ZnO NPs, obtained using the *Silybum marianum* seed extract [128]. The as-synthesized nanomaterial showed a significant inhibitory effect against the Gram-negative *Pseudomonas syringae* and Gram-positive *Clavibacter michiganensis* bacteria and two fungal strains (*Fusarium oxysporum* and *A. niger*). The 14.9 nm ZnO NPs, developed using the Gram-negative *P. aeruginosa* bacteria, have been described to display efficacy against the human fungal pathogen *Candida albicans* [129]. The inhibitory effects of iron oxide NPs, against a range of plant pathogens, are also well-reported in literature. The reaction of an aqueous solution of $FeCl_3$ and *Mentha spicata* leaf extract under reflux, afforded the 21-82 nm Fe_2O_3 NPs activity against the fungus-like *Phytophthora infestans* [130]. The treatment of an aqueous solution of $FeCl_3/FeCl_2$ system with seed methanol extract of *Cuminum cyminum*, generated the Fe_3O_4 NPs stabilized by phytochemicals. The as-prepared material achieved 100% mortality of the pest *Phthorimaea operculella* [131]. A recent study by Zaheer and co-workers

(2022) on the pesticidal potential of magnesium oxide, zinc oxide, and iron oxide NPs, reported the lowest lethal concentrations with iron oxide NPs. These nanomaterials were chemically produced and tested against *Hyalomma* ticks. The *Brassica oleracea*-mediated Fe_3O_4 NPs coated with chitosan polysaccharide under stirring at 60 °C for 15 h, have been found to display a greater inhibition of *Staphylococcus aureus* and *E. coli* than bare Fe_3O_4 NPs [132]. Findings from this study included the synergistic effects of chitosan and Fe_3O_4. The antimicrobial properties of chitosan biopolymer against phytopathogens (bacteria and fungi) have been reviewed previously [133]. Engineered NPs of this polysaccharide have also been reported as a carrier for the development of nanoencapsulated pesticide formulations [134, 120, 122].

REFERENCES

1. Bhardwaj, A. K.; Arya, G.; Kumar, R.; Hamed, L.; Pirasteh-Anosheh, H.; Jasrotia, P.; Kashyap, P. L. & Singh, G. P. 2022. Switching to nanonutrients for sustaining agroecosystems and environment: The challenges and benefits in moving up from ionic to particle feeding. *Journal of Nanobiotechnology*, 20, 19.

2. Saleem, I.; Maqsood, M. A.; ur Rehman, M. Z.; Aziz, T.; Bhatti, I. A. & Ali, S. 2021. Potassium ferrite nanoparticles on DAP to formulate slow release fertilizer with auxiliary nutrients. *Ecotoxicology and Environtment Safety*, 215, 112148.

3. Abdel-Aziz, H. M.; Soliman, M. I.; Abo Al-Saoud, A. M. & El-Sherbeny, G. A. 2021. Waste-derived NPK nanofertilizer enhances growth and productivity of *capsicum annuum* L. *Plants*, 10, 1144.

4. Haydon, M. J. & Cobbett, C. S. 2007. Transporters of ligands for essential metal ions in plants. *New Phytologist*, 174, 499-506.

5. Delfani, M.; Firouzabadi, M. B.; Farrokhi, N. & Makarian, H. 2014. Some physiological responses of black-eyed pea to iron and magnesium nanofertilizers. *Communications in Soil Science and Plant Analysis*, 45, 530-540.

6. Pradhan, S.; Patra, P.; Das, S.; Chandra, S.; Mitra, S.; Dey, K. K.; Akbar, S.; Palit, P. & Goswami, A. 2013. Photochemical modulation of biosafe manganese nanoparticles on *Vigna radiata*: A detailed molecular, biochemical, and biophysical study. *Environmental Science and Technology*, 47, 13122-13131.

7. Shah, V. & Belozerova, I. 2009. Influence of metal nanoparticles on the soil microbial community and germination of lettuce seeds. *Water, Air and Soil Pollution*, 197, 143-148.

8. VandeVoort, A. R. & Arai, Y. 2018. Macroscopic observation of soil nitrification kinetics impacted by copper nanoparticles: Implications for micronutrient nanofertilizer. *Nanomaterials*, 8, 927.

9. Jamkhande, P. G.; Ghule, N. W.; Bamer, A. H. & Kalaskar, M. G. 2019. Metal nanoparticles synthesis: An overview on methods of preparation, advantages and disadvantages, and applications. *Journal of Drug Delivery Science and Technology*, 53, 101174.

10. Zhang, D.; Ma, X.-L.; Gu, Y.; Huang, H. & Zhang, G.-W. 2020. Green synthesis of metallic nanoparticles and their potential applications to treat cancer. *Frontiers Chemistry*, 8, 799.

11. Narayanan, K. B. & Sakthivel, N. 2010. Biological synthesis of metal nanoparticles by microbes. *Advances in Colloid and Interface Science*, 156, 1-13.

12. Santhoshkumar, J.; Rajeshkumar, S. & Kumar, S. V. 2017. Phyto-assisted synthesis, characterization and applications of gold nanoparticles – A review. *Biochemistry and Biophysics Reports*, 11, 46-57.

13. Thakur, R.; Dhirta, B. & Shirkot, P. 2018. Studies on nano toxicity effect of gold nanoparticles on *M. incognita* and tomato plants growth and development. *Annals of Nanoscience and Nanotechnology*, 2, 1005.

14. Akbarnejad-Samani, Z.; Shamili, M. & Samari, F. 2020. The toxicity potential of Ag nanoparticles synthesized from *Cordia myxa* L. *Advances in Horticultural Science*, 34, 93-104.

15. Singh, J.; Dutta, T.; Kim, K.-H.; Rawat, M.; Samddar, P. & Kumar, P. 2018. Green synthesis of metals and their oxide nanoparticles: applications for environmental remediation. *Journal of Nanobiotechnology*, 16, 84.

16. Karunakaran, G.; Suriyaprabha, R.; Manivasakan, P.; Rajendran, V. & Kannan, N. 2014. Influence of nano and bulk SiO_2 and Al_2O_3 particles on PGPR and soil nutrient contents. *Current Nanoscience*, 10, 604-612.

17. Siddiqui, M. H. & Al-Whaibi, M. H. 2014. Role of nano-SiO_2 in germination of tomato (*Lycopersicum esculentum* seeds Mill.). *Saudi Journal of Biological Sciences*, 21, 13-17.

18. Younes, N.; Hassan, H. S.; Elkady, M. F.; Hamed, A. & Dawood, M. F. 2020. Impact of synthesized metal oxide nanomaterials on seedlings production of three *Solanaceae* crops. *Heliyon* , 6, e03188.

19. Hanif, H. U.; Arshad, M.; Ali, M. A.; Ahmed, N. & Qazi, I. A. 2015. Phyto-availability of phosphorus to *Lactuca sativa* in response to soil applied TiO_2 nanoparticles. *Pakistan Journal of Agricultural Sciences*, 52, 177-182.

20. Zahra, Z.; Arshad, M.; Rafique, R.; Mahmood, A.; Habib, A.; Qazi, I. A. & Khan, S. A. 2015. Metallic nanoparticle (TiO_2 and Fe_3O_4) application modifies rhizosphere phosphorus availability and uptake by *Lactuca sativa*. *Journal of Agricultural and Food Chemistry*, 63, 6876-6882.

21. Xiao, Y.; Du, Y.; Xiao, Y.; Zhang, X.; Wu, J.; Yang, G.; He, Y. & Zhou, Y.; Peijnenburg, W. J. G. M. & Luo, L. 2021. Elucidating the effects of TiO_2 nanoparticles on the toxicity and accumulation of Cu in soybean plants (*Glycine max* L.). *Ecotoxicology and Environmental Safety*, 219, 112312.

22. Mustafa, H.; Ilyas, N.; Akhtar, N.; Raja, N. I.; Zainab, T.; Shah, T.; Ahmad, A. & Ahmad, P. 2021. Biosynthesis and characterization of titanium dioxide nanoparticles and its effects along with calcium phosphate on physicochemical attributes of wheat under drought stress. *Ecotoxicology and Environmental Safety*, 223, 112519.

23. Mariz-Ponte, N.; Dias, C. M.; Silva, A. M.; Santos, C. & Silva, S. 2021. Low levels of TiO_2-nanoparticles interact antagonistically with Al and Pb alleviating their toxicity. *Plant Physiology and Biochemistry*, 167, 1-10.

24. Yassen, A.; Abdallah, E.; Gaballah, M. & Zaghloul, S. 2017. Role of silicon dioxide nano fertilizer in mitigating salt stress on growth, yield and chemical composition of cucumber (*Cucumis sativus* L.) *International Journal of Agricultural and Research*, 12, 130-135.

25. Isayenkov, S. V. & Maathuis, F. J. 2019. Plant salinity stress: Many unanswered questions remain. *Fronier in Plant Sciences*, 10, 80.

26. Zulfiqar, F. & Ashraf, M. 2021. Nanoparticles potentially mediate salt stress tolerance in plants. *Plant Physiology and Biochemistry*, 160, 257-268.

27. El-Saadony, M. T.; Desoky, E.-S. M.; Saad, A. M.; Eid, R. S. M.; Selem, E. & Elrys, A. S. 2021. Biological silicon nanoparticles improve *Phaseolus vulgaris* L. yield and minimize its contaminant contents on a heavy metals-contaminated saline soil. *Journal of Environmental Sciences*, 106, 1-14.

28. Goswaml, A.; Roy, I.; Sengupta, S. & Debnath, N. 2010. Novel applications of solid and liquid formulations of nanoparticles against insect pests and pathogens. *Thin Solid Films*, 519, 1252-1257.

29. Singh, J.; Kumar, S.; Alok, A.; Upadhyay, S. K.; Rawat, M.; Tsang, D. C.; Bolan, N. & Kim, K.-H. 2019. The potential of green synthesized zinc oxide nanoparticles as nutrient source for plant growth. *Journal of Cleaner Production*, 214, 1061-1070.

30. Rai-Kalal, P. & Jajoo, A. 2021. Priming with zinc oxide nanoparticles improve germination and photosynthetic performance in wheat. *Plant Physiology and Biochemistry*, 160, 341-351.

31. Shah, T.; Latif, S.; Saeed, F.; Ali, I.; Ullah, S.; Alsahli, A. A.; Jan, S. & Ahmad, P. 2021. Seed priming with titanium dioxide nanoparticles enhances seed vigor, leaf water status, and antioxidant enzyme activities in maize (*Zea mays* L.) under salinity stress. *Journal of King Saud University Science*, 33, 101207.

32. Dimkpa, C. O.; Singh, U.; Bindraban, P. S.; Elmer, W. H.; Gardea-Torresdey, J. L. & White, J. C. 2019. Zinc oxide nanoparticles alleviate drought-induced alterations in sorghum performance, nutrient acquisition, and grain fortification. *Science of Total Environment*, 688, 926-934.

33. Kalia, A.; Abd-Elsalam, K. A. & Kuca K. 2020. Zinc-based nanomaterials for diagnosis and management of plant diseases: Ecological safety and future prospects. *Journal of Fungi*, 6, 222.

34. Nandhini, M.; Rajini, S.; Udayashankar, A.; Niranjana, S.; Lund, O. S.; Shetty, H. & Prakash, H. 2019. Biofabricated zinc oxide nanoparticles as an eco-

friendly alternative for growth promotion and management of downy mildew of pearl millet. *Crop Protection*, 121, 103-112.

35. Sofy, A. R.; Sofy, M. R.; Hmed, A. A.; Dawoud, R. A., Alnaggar, A. E.-A. M.; Soliman, A. M. & El-Dougdoug, N. K. 2021. Ameliorating the adverse effects of *tomato mosaic tobamovirus* infecting tomato plants in Egypt by boosting immunity in tomato plants using zinc oxide nanoparticles. *Molecules*, 26, 1337.

36. Faizan, M.; Bhat, J. A.; Chen, C.; Alyemeni, M. N.; Wijaya, L.; Ahmad, P. & Yu, F. 2021. Zinc oxide nanoparticles (ZnO-NPs) induce salt tolerance by improving the antioxidant system and photosynthetic machinery in tomato. *Plant Physiology and Biochemistry*, 161, 122-130.

37. Faizan, M.; Bhat, J. A.; Noureldeen, A.; Ahmad, P. & Yu, F. 2021. Zinc oxide nanoparticles and 24-epibrassinolide alleviates Cu toxicity in tomato by regulating ROS scavenging, stomatal movement and photosynthesis. *Ecotoxicology and Environmental Safety*, 218, 112293.

38. Cai, L.; Cai, L.; Jia, H.; Liu, C.; Wang, D. & Sun, X. 2020. Foliar exposure of Fe_3O_4 nanoparticles on *Nicotiana benthamiana*: Evidence for nanoparticles uptake, plant growth promoter and defense response elicitor against plant virus. *Journal of Hazardous Materials*, 393, 122415.

39. Rizwan, M.; Ali, S.; Qayyum, M. F.; Ok, Y. S.; Adrees, M.; Ibrahim, M.; Zia-ur-Rehman, M.; Farid, M. & Abbas, F. 2017. Effect of metal and metal oxide nanoparticles on growth and physiology of globally important food crops: A critical review. *Journal of Hazardous Materials*, 322, 2-16.

40. Ranjan, A.; Rajput, V. D.; Minkina, T.; Bauer, T.; Chauhan, A. & Jindal, T. 2021. Nanoparticles Induced Stress and Toxicity in Plants. *Environmental Nanotechnology, Monitring & Management*, 15, 100457.

41. Wahid, I.; Rani, P.; Kumari, S.; Ahmad, R.; Hussain, S. J.; Alamri, S.; Tripathy, N. & Khan, M. I. R. 2022. Biosynthesized gold nanoparticles maintained nitrogen metabolism, nitric oxide synthesis, ions balance, and stabilizes the

defense systems to improve salt stress tolerance in wheat. *Chemosphere*, 287, 132142.

42. Hayat, K.; Ali, S.; Ullah, S.; Fu, Y. & Hussain, M. 2021. Green synthesized silver and copper nanoparticles induced changes in biomass parameters, secondary metabolites production, and antioxidant activity in callus cultures of *Artemisia absinthium* L. *Green Processing and Synthesis*, 10, 61-72.

43. Hoang, S. A.; Nguyen, L. Q.; Nguyen, N. H.; Tran, C. Q.; Nguyen, D. V.; Le, N. T.; Ha, C. V.; Vu, Q. N. & Phan, C. M. 2019. Metal nanoparticles as effective promotors for Maize production. *Science Reports*, 9, 13925.

44. Mukarram, M.; Khan, M. M. A. & Corpas, F. J. 2021. Silicon nanoparticles elicit an increase in lemongrass (*Cymbopogon flexuosus* (Steud.) Wats) agronomic parameters with a higher essential oil yield. *Journal of Hazardous Materials*, 412, 125254.

45. Nekrasova, G. F.; Ushakova, O. S.; Ermakov, A. E.; Uimin, M. A. & Byzov, I. V. 2011. Effects of copper (Ⅱ) ions and copper oxide nanoparticles on *Elodea densa Planch*. *Russian Journal of Ecology* , 42, 458-463.

46. Rui, M.; Ma, C.; Hao, Y.; Guo, J.; Rui, Y.; Tang, X.; Zhao, Q.; Fan, X., Zhang, Z. & Hou, T. Zhu, S. 2016. Iron oxide nanoparticles as a potential iron fertilizer for peanut (*Arachis hypogaea*). *Frontier in Plant Science*, 7, 815.

47. Mahmoud, L. M.; Dutt, M.; Shalan, A. M.; El-Kady, M. E.; El-Boray, M. S.; Shabana, Y. M. & Grosser, J. W. 2020. Silicon nanoparticles mitigate oxidative stress of in vitro-derived banana (*Musa acuminata* 'Grand Nain') under simulated water deficit or salinity stress. *South African Journal of Botany*, 132, 155-163.

48. Tauseef, A.; Hisamuddin; Khalilullah, A. & Uddin, I. 2021. Role of MgO nanoparticles in the suppression of Meloidogyne incognita, infecting cowpea and improvement in plant growth and physiology. *Experimental Parasitology*, 220, 108045.

49. Mahajan, P.; Dhoke, S. K.; Khanna, A. S. & Tarafdar, J. C. 2011. Effect of nano-ZnO on growth of mung bean (*vigna radiata*) and chickpea (*cicer arietinum*) seedlings using plant agar method. *Applied Biological Research*, 13, 54-61.

50. Subbaiah, L. V.; Vara Prasad, T. N. V. K.; Krishna, T. G.; Sudhakar, P.; Reddy, B. R. & Pradeep, T. 2016. Novel effects of nanoparticulate delivery of zinc on growth, productivity, and zinc biofortification in maize (*Zea mays* L.). *Journal of Agricultural and Food Chemistry*, 64, 3778-3788.

51. Yusefi-Tanha, E.; Fallah, S.; Rostamnejadi, A. & Pokhrel, L. R. 2020. Zinc oxide nanoparticles (ZnONPs) as a novel nanofertilizer: Influence on seed yield and antioxidant defense system in soil grown soybean (*Glycine max* cv. Kowsar). *Science of the Total Environment*, 738, 140240.

52. Raliya, R.; Nair, R., Chavalmane, S.; Wang, W.-N. & Biswas, P. 2015. Mechanistic evaluation of translocation and physiological impact of titanium dioxide and zinc oxide nanoparticles on the tomato (*Solanum lycopersicum* L.) plant. *Metallomics*, 7, 1584-1594.

53. Abdulhameed, M. F.; Taha, A. A. & Ismail, R. A. 2021. Improvement of cabbage growth and yield by nanofertilizers and nanoparticles. *Environmental Nanotechnology, Monitoring and Management*, 15, 100437.

54. Dimkpa, C. O.; Mclean, J. E.; Latta, D. E.; Manangón, E.; Britt, D. W.; Johnson, W. P.; Boyanov, M. I. & Anderson, A. J. 2012. CuO and ZnO nanoparticles: phytotoxicity, metal speciation, and induction of oxidative stress in sand-grown wheat. *Journal of Nanoparticle Research*,14, 1125.

55. Nagaonkar, D.; Shende, S. & Rai, M. 2015. Biosynthesis of copper nanoparticles and its effect on actively dividing cells of mitosis in *Allium cepa*. *Biotechnology Progress*, 31, 557-565.

56. Taylor, A. F.; Rylott, E. L.; Anderson, C. W. & Bruce, N. C. 2014. Investigating the toxicity, uptake, nanoparticle formation and genetic response of plants to gold. *PLoS One*, 9, e93793.

57. Rajeshwari, A.; Suresh, S.; Chandrasekaran, N. & Mukherjee, A. 2016. Toxicity evaluation of gold nanoparticles using an *Allium cepa* bioassay. *RSC Advances*, 6, 24000-24009.

58. Lee, C. W.; Mahendra, S.; Zodrow, K.; Li, D.; Tsai, Y.-C.; Braam, J. & Alvarez, P. J. J. 2010. Developmental phytotoxicity of metal oxide nanoparticles to *Arabidopsis thaliana*. *Environmental Toxicology and Chemistry*, 29, 669-675.

59. Demir, E.; Kaya, N. & Kaya, B. 2014. Genotoxic effects of zinc oxide and titanium dioxide nanoparticles on root meristem cells of *Allium cepa* by comet assay. *Turkish Journal of Biology*, 38, 31-39.

60. Kumari, M.; Khan, S. S.; Pakrashi, S.; Mukherjee, A. & Chandrasekaran, N. 2011. Cytogenetic and genotoxic effects of zinc oxide nanoparticles on root cells of *Allium cepa*. *Journal of Hazardous Materials*, 190, 613-621.

61. Ghodake, G.; Seo, Y. D. & Lee, D. S. 2011. Hazardous phytotoxic nature of cobalt and zinc oxide nanoparticles assessed using *Allium cepa*. *Journal of Hazardous Materials*, 186, 952-955.

62. Da Costa, M. V. J. & Sharma, P. K. 2016. Effect of copper oxide nanoparticles on growth, morphology, photosynthesis, and antioxidant response in *Oryza sativa*. *Photosynthetica*, 54, 110-119.

63. Mangalampalli, B.; Dumala, N. & Grover, P. 2018. *Allium cepa* root tip assay in assessment of toxicity of magnesium oxide nanoparticles and microparticles. *Journal of Environmental Sciences*, 66, 125-137.

64. Pakrashi, S.; Jain, N.; Dalai, S.; Jayakumar, J.; Chandrasekaran, P. T.; Raichur, A. M.; Chandrasekaran, N. & Mukherjee, A. 2014. In vivo genotoxicity assessment of titanium dioxide nanoparticles by *Allium cepa* root tip assay at high exposure concentrations. *PloS One*, 9, e87789.

65. Pittol, M.; Tomacheski, D.; Simões, D. N.; Ribeiro, V. F. & Santana, R. M. C. 2017. Macroscopic effects of silver nanoparticles and titanium dioxide on edible plant growth. *Environmental Nanotechnology, Monitoring and Management*, 8, 127-133.

66. García-Gómez, C.; García, S.; Obrador, A. F.; González, D.; Babín, M. & Fernández, M. D. 2018. Effects of aged ZnO NPs and soil type on Zn availability, accumulation and toxicity to pea and beet in a greenhouse experiment. *Ecotoxicology and Environmental Safety*, 160, 222-230.

67. Ahmed, T.; Noman, M.; Manzoor, N.; Shahid, M.; Hussaini, K. M.; Rizwan, M.; Ali, S.; Maqsood, A. & Li, B. 2021. Green magnesium oxide nanoparticles-based modulation of cellular oxidative repair mechanisms to reduce arsenic uptake and translocation in rice (*Oryza sativa* L.) plants. *Environmental Pollution*, 288, 117785.

68. Mazumdar, H. & Ahmed, G. 2011. Phytotoxicity effect of silver nanoparticles on *Oryza sativa*. *International Journal of Chemtech Research*, 3, 1494-1500.

69. Patlolla, A. K.; Berry, A.; May, L. & Tchounwou, P. B. 2012. Genotoxicity of silver nanoparticles in Vicia faba: a pilot study on the environmental monitoring of nanoparticles. *International Journal of Environmental Research and Public Health*, 9, 1649-1662.

70. Hawthorne, J.; Musante, C.; Sinha, S. K. & White, J. C. 2012. Accumulation and phytotoxicity of engineered nanoparticles to *Cucurbita pepo*. *International Journal of Phytoremediation*, 14, 429-442.

71. Pokhrel, L. R. & Dubey, B. 2013. Evaluation of developmental responses of two crop plants exposed to silver and zinc oxide nanoparticles. *Science of the Total Environment*, 452, 321-332.

72. Qian, H.; Peng, X.; Han, X.; Ren, J.; Sun, L. & Fu, Z. 2013. Comparison of the toxicity of silver nanoparticles and silver ions on the growth of terrestrial plant model *Arabidopsis thaliana*. *Journal of Environmental Sciences*, 25, 1947-1956.

73. Dimkpa, C. O.; Mclean, J. E.; Martineau, N.; Britt, D. W.; Haverkamp, R. & Anderson, A. J. 2013. Silver nanoparticles disrupt wheat (*Triticum aestivum* L.) growth in a sand matrix. *Environmental Science and Technology*, 47, 1082-1090.

74. Vinković, T.; Novák, O.; Strnad, M.; Goessler, W.; Jurašin, D. D.; Parađiković, N. & Vrček, I. V. 2017. Cytokinin response in pepper plants (*Capsicum annuum* L.) exposed to silver nanoparticles. *Environmental Research*, 156, 10-18.

75. Rajeshwari, A.; Kavitha, S.; Alex, S. A.; Kumar, D.; Mukherjee, A.; Chandrasekaran, N. & Mukherjee, A. 2015. Cytotoxicity of aluminum oxide nanoparticles on *Allium cepa* root tip — Effects of oxidative stress generation and biouptake. *Environmental Science and Pollution Research International*, 22, 11057-11066.

76. Shaw, A. K.; Ghosh, S.; Kalaji, H. M.; Bosa, K.; Brestic, M.; Zivcak, M. & Hossain, Z. 2014. Nano-CuO stress induced modulation of antioxidative defense and photosynthetic performance of Syrian barley (*Hordeum vulgare* L.). *Environmental and Experimental Botany*, 102, 37-47.

77. Van, N. L.; Ma, C.; Shang, J.; Rui, Y.; Liu, S. & Xing, B. 2016. Effects of CuO nanoparticles on insecticidal activity and phytotoxicity in conventional and transgenic cotton. *Chemosphere*, 144, 661-670.

78. Adams, J.; Wright, M.; Wagner, H.; Valiente, J.; Britt, D. & Anderson, A. 2017. Cu from dissolution of CuO nanoparticles signals changes in root morphology. *Plant Physiology and Biochemistry*, 110, 108-117.

79. Yusefi-Tanha, E.; Fallah, S.; Rostamnejadi, A. & Pokhrel, L. R. 2020. Particle size and concentration dependent toxicity of copper oxide nanoparticles (CuONPs) on seed yield and antioxidant defense system in soil grown soybean (*Glycine max* cv. Kowsar). *Science of the Total Environment*, 715, 136994.

80. Tombuloglu, H.; Slimani, Y.; Alshammari, T. M.; Bargouti, M.; Ozdemir, M.; Tombuloglu, G.; Akhtar, S.; Sabit, H.; Hakeem, K. R. & Almessiere, M. 2020. Uptake, translocation, and physiological effects of hematite (α-Fe_2O_3) nanoparticles in barley (*Hordeum vulgare* L.). *Environmental Pollution*, 266, 115391.

81. Shaymurat, T.; Gu, J. X.; Xu, C. S.; Yang, Z. K.; Zhao, Q.; Liu, Y. X. & Liu, Y. C. 2012. Phytotoxic and genotoxic efects of ZnO nanoparticles on garlic (*Allium sativum* L.): A morphological study. *Nanotoxicology*, 6, 241-248.

82. Kim, S.; Lee, S. & Lee, I. 2012. Alteration of phytotoxicity and oxidant stress potential by metal oxide nanoparticles in *Cucumis sativus*. *Water, Air & Soil Pollution*, 223, 2799-2806.

83. Huang, Y. C.; Fan, R.; Grusak, M. A.; Sherrier, J. D. & Huang, C. 2014. Effects of nano-ZnO on the agronomically relevant Rhizobium–legume symbiosis. *Science of the Total Environment*, 497-498, 78-90.

84. Yang, Z.; Chen, J.; Dou, R.; Gao, X.; Mao, C. & Wang, L. 2015. Assessment of the phytotoxicity of metal oxide nanoparticles on two crop plants, maize (*Zea mays* L.) and rice (*Oryza sativa* L.). *International Journal of Environment Research and Public Health*, 12, 15100-15109.

85. Asli, S. & Neumann, P. M. 2009. Colloidal suspensions of clay or titanium dioxide nanoparticles can inhibit leaf growth and transpiration *via* physical effects on root water transport. *Plant, Cell & Environment*, 32, 577-584.

86. Castiglione, M. R.; Giorgetti, L.; Geri, C. & Cremonini, R. 2011. The effects of nano-TiO_2 on seed germination, development and mitosis of root tip cells of *Vicia narbonensis* L. and *Zea mays* L. *Journal of Nanoparticle Research*, 13, 2443-2449.

87. Waani, S. P. T.; Irum, S.; Gul, I.; Yaqoob, K.; Khalid, M. U.; Ali, M. A.; Manzoor, U.; Noor, T.; Ali, S.; Rizwan, M. & Arshad, M. 2021. TiO_2 nanoparticles dose, application method and phosphorous levels influence genotoxicity in Rice (*Oryza sativa* L.), soil enzymatic activities and plant growth. *Ecotoxicology and Environmental Safety*, 213, 111977.

88. Kumar, S. & Maiti, P. 2016. Controlled biodegradation of polymers using nanoparticles and its application. *RSC Advances*, 6, 67449-67480.

89. Chouhan, D. & Mandal, P. 2021. Applications of chitosan and chitosan based metallic nanoparticles in agrosciences-A review. *International Journal of Biological Macromolecules*, 166, 1554-1569.

90. Medeiros, D. B.; da Silva, E. C.; Santos, H. R. B.; Pacheco, C. M.; Musser, R. S. & Nogueira, R. J. M. C. 2012. Physiological and biochemical responses to drought stress in Barbados cherry. *Brazillian Journal of Plant Physiology*, 24, 181-192.

91. Ali, E. F.; El-Shehawi, A. M.; Ibrahim, O. H. M.; Abdul-Hafeez, E. Y.; Moussa, M. M. & Hassan, F. A. S. 2021. A vital role of chitosan nanoparticles in improvisation the drought stress tolerance in *Catharanthus roseus* (L.) through biochemical and gene expression modulation. *Plant Physiology and Biochemistry*, 161, 166-175.

92. Behboudi, F.; Tahmasebi-Sarvestani, Z.; Kassaee, M. Z.; Modarres-Sanavy, S. A. M.; Sorooshzadeh, A. & Mokhtassi-Bidgoli, A. 2019. Evaluation of chitosan nanoparticles effects with two application methods on wheat under drought stress. *Journal of Plant Nutrition*, 42, 1439-1451.

93. Salinas, F.; Astete, C. E.; Waldvogel, J. H.; Navarro, S.; White, J. C.; Elmer, W.; Tamez, C.; Davis, J. A. & Sabliov, C. M. 2021. Effects of engineered lignin-graft-PLGA and zein-based nanoparticles on soybean health. *NanoImpact*, 23, 100329.

94. Dhlamini, B. C.; Paumo, H. K.; Katata-Seru, L. & Kutu, F. R. 2020. Sulphate-supplemented NPK nanofertilizer and its effect on maize growth. *Materials Research Express*, 7, 095011.

95. Knijnenburg, J. T.; Kasemsiri, P.; Amornrantanaworn, K.; Suwanree, S.; lamamornphan, W.; Chindaprasirt, P. & Jetsrisuparb, K. 2021. Entrapment of nano-ZnO into alginate/polyvinyl alcohol beads with different crosslinking ions for fertilizer applications. *International Journal of Biological Macromolecules*, 181, 349-356.

96. Mikolajczyk, A.; Gajewicz, A.; Rasulev, B.; Schaeublin, N.; Maurer-Gardner, E.; Hussain, S.; Leszczynski, J. & Puzyn, T. 2015. Zeta potential for metal oxide nanoparticles: A predictive model developed by a nano-quantitative structure–property relationship approach. *Chemistry of Materials*, 27, 2400-2407.

97. Saharan, V.; Sharma, G.; Yadav, M.; Choudhary, M. K.; Sharma, S. S.; Pal, A.; Raliya, R. & Biswas, P. 2015. Synthesis and *in vitro* antifungal efficacy of Cu–chitosan nanoparticles against pathogenic fungi of tomato. *International Journal of Biological Macromolecules*, 75, 346-353.

98. Leonardi, M.; Caruso, G. M.; Carroccio, S. C.; Boninelli, S.; Curcuruto, G.; Zimbone, M.; Allegra, M.; Torrisi, B.; Ferlito, F. & Miritello, M. 2021. Smart nanocomposites of chitosan/alginate nanoparticles loaded with copper oxide as alternative nanofertilizers. *Environmental Science: Nano*, 8, 174-187.

99. Mohanan, N.; Montazer, Z.; Sharma, P. K. & Levin, D. B. 2020. Microbial and enzymatic degradation of synthetic plastics. *Frontiers in Microbiology*, 11, 2837.

100. Sarkhel, R.; Sengupta, S.; Das, P. & Bhowal, A. 2020. Comparative biodegradation study of polymer from plastic bottle waste using novel isolated bacteria and fungi from marine source. *Journal of Polymer Research*, 27, 16.

101. Siracusa, V. 2019. Microbial degradation of synthetic biopolymers waste. *Polymers*, 11, 1066.

102. Lawrencia, D.; Wong, S. K.; Sern Low, D. Y.; Goh, B. H.; Goh, J. K.; Ruktanonchai, U. R.; Soottitantawat, A.; Lee, L. H. & Tang, S. Y. 2021. Controlled release fertilizers: A review on coating materials and mechanism of release. *Plants*, 10, 238.

103. Holtan, S.; Zhang, Q.; Strand, W. I. & Skjåk-Bræk, G. 2006. Characterization of the hydrolysis mechanism of polyalternating alginate in weak acid and assignment of the resulting MG-oligosaccharides by NMR spectroscopy and ESI-mass spectrometry. *Biomacromolecules*, 7, 2108-2121.

104. Kasaai, M. R.; Arul, J. & Charlet, G. 2013. Fragmentation of chitosan by acids. *The Scientific World Journal*, 508540, 1-11.

105. Yousif, E. & Haddad, R. 2013. Photodegradation and photostabilization of polymers, especially polystyrene: review. *Springerplus*, 2, 398.

106. Mittelman, A. M.; Fortner, J. D. & Pennell, K. D. 2015. Effects of ultraviolet light on silver nanoparticle mobility and dissolution. *Environmental Science: Nano*, 2, 683-691.

107. Chugh, G.; Siddique, K. H. M. & Solaiman, Z. M. 2021. Nanobiotechnology for agriculture: Smart technology for combating nutrient deficiencies with nanotoxicity challenges. *Sustainability*, 13, 1781.

108. Vanti, G. L.; Masaphy, S.; Kurjogi, M.; Chakrasali, S. & Nargund, V. B. 2020. Synthesis and application of chitosan-copper nanoparticles on damping off causing plant pathogenic fungi. *International Journal of Biological Macromolecules*, 156, 1387-1395.

109. Helander, I. M.; Nurmiaho-Lassila, E.-L.; Ahvenainen, R.; Rhoades, J. & Roller, S. 2001. Chitosan disrupts the barrier properties of the outer membrane of Gram-negative bacteria. *International Journal of Food Microbiology*, 71, 235-244.

110. Xing, Y.; Xu, Q.; Li, X.; Chen, C.; Ma, L.; Li, S.; Che, Z. & Lin, H. 2016. Chitosan-based coating with antimicrobial agents: Preparation, property, mechanism, and application effectiveness on fruits and vegetables. *International Journal of Polymer Science*, 4851730, 1-25.

111. Van, S. N.; Minh, H. D. & Anh, D. N. 2013. Study on chitosan nanoparticles on biophysical characteristics and growth of Robusta coffee in green house. *Biocatalysis and Agricultural Biotechnology*, 2, 289-294.

112. Prasad, A.; Astete, C. E.; Bodoki, A. E.; Windham, M.; Bodoki, E. & Sabliov, C. M. 2018. Zein nanoparticles uptake and translocation in hydroponically grown sugar cane plants. *Journal of Agricultural and Food Chemistry*, 66, 6544-6551.

113. Abdel-Aziz, H. M.; Hasaneen, M. N. A. & Omer, A. M. 2016. Nano chitosan-NPK fertilizer enhances the growth and productivity of wheat plants grown in sandy soil. *Spanish Journal of Agricultural Research*, 14, e0902.

114. Ha, N. M. C.; Nguyen, T. H.; Wang, S.-L. & Nguyen, A. D. 2019. Preparation of NPK nanofertilizer based on chitosan nanoparticles and its effect on biophysical characteristics and growth of coffee in green house. *Research on Chemical Intermediates*, 45, 51-63.

115. Kumaraswamy, R. V.; Saharan, V.; Kumari, S., Choudhary, R. C.; Pal, A.; Sharma, S. S.; Rakshit, S.; Raliya, R. & Biswas, P. 2021. Chitosan-silicon nanofertilizer to enhance plant growth and yield in maize (*Zea mays* L.). *Plant Physiology and Biochemistry*, 159, 53-66.

116. Deshpande, P.; Dapkekar, A.; Oak, M. D.; Paknikar, K. M. & Rajwade, J. M. 2017. Zinc complexed chitosan/TPP nanoparticles: A promising micronutrient nanocarrier suited for foliar application. *Carbohydrate Polymers*, 165, 394-401.

117. Choudhary, R. C.; Kumaraswamy, R.; Kumari, S.; Sharma, S. S.; Pal, A.; Raliya, R.; Biswas, P. & Saharan, V. 2019. Zinc encapsulated chitosan nanoparticle to promote maize crop yield. *International Journal of Biological Macromolecules*, 127, 126-135.

118. Asgari-Targhi, G.; Iranbakhsh, A.; Ardebili, Z. O. & Tooski, A. H. 2021. Synthesis and characterization of chitosan encapsulated zinc oxide (ZnO) nanocomposite and its biological assessment in pepper (*Capsicum annuum*) as an elicitor for *in vitro* tissue culture applications. *International Journal of Biological Macromolecules*, 189, 170-182.

119. Alavanja, M. C. 2009. Introduction: Pesticides use and exposure, extensive worldwide. *Reviews on Environmental Health*, 24(4), 303-310.

120. Zhao, X.; Cui, H.; Wang, Y.; Sun, C.; Cui, B. & Zeng, Z. 2017. Development strategies and prospects of nano-based smart pesticide formulation. *Journal of Agricultural and Food Chemistry*, 66(26), 6504-6512.

121. Horrigan, L.; Lawrence, R. S. & Walker, P. 2002. How sustainable agriculture can address the environmental and human health harms of industrial agriculture. *Environmental Health Perspectives*, 110(5), 445-456.

122. Nuruzzaman, M. D.; Rahman, M. M.; Liu, Y. & Naidu, R. 2016. Nanoencapsulation, nano-guard for pesticides: a new window for safe application. *Journal of Agricultural and Food Chemistry*, 64(7), 1447-1483.

123. Li, N.; Sun, C.; Jiang, J.; Wang, A.; Wang, C.; Shen, Y. & Wang, Y. 2021. Advances in controlled-release pesticide formulations with improved efficacy and targetability. *Journal of Agricultural and Food Chemistry*, 69(43), 12579-12597.

124. Kah, M.; Beulke, S.; Tiede, K. & Hofmann, T. 2013. Nanopesticides: state of knowledge, environmental fate, and exposure modeling. *Critical Reviews in Environmental Science and Technology*, 43(16), 1823-1867.

125. Arruda, S. C. C.; Silva, A. L. D.; Galazzi, R. M.; Azevedo, R. A. & Arruda, M. A. Z. 2015. Nanoparticles applied to plant science: a review. *Talanta*, 131, 693-705.

126. Ayoub, H. A.; Khairy, M.; Elsaid, S.; Rashwan, F. A. & Abdel-Hafez, H. F. 2018. Pesticidal activity of nanostructured metal oxides for generation of alternative pesticide formulations. *Journal of Agricultural and Food Chemistry*, 66(22), 5491-5498.

127. Manjunatha, K. B.; Bhat, R. S.; Shashidhara, A.; Kumar, H. A. & Nagashree, S. 2021. Antimicrobial and nonlinear optical studies of copper oxide nanoparticles. *Journal of Electronic Materials*, 50, 3415-3421.

128. Jahan, N.; Rasheed, K.; Hazafa, A.; Saleem, A.; Alamri, S.; Iqbal, M. O. & Rahman, M. A. 2023. Green inspired synthesis of zinc oxide nanoparticles using *Silybum marianum* (milk thistle) extract and evaluation of their potential pesticidal and phytopathogens activities. *PeerJ*, 11, e15743.

129. Abdo, A. M.; Fouda, A.; Eid, A. M.; Fahmy, N. M.; Elsayed, A. M.; Khalil, A. M. A. & Soliman, A. M. 2021. Green synthesis of zinc oxide nanoparticles (ZnO-NPs) by *Pseudomonas aeruginosa* and their activity against pathogenic microbes and common house mosquito, *Culex pipiens*. *Materials*, 14(22), 6983.

130. Khan, S.; Bibi, G.; Dilbar, S.; Iqbal, A.; Ahmad, M.; Ali, A. & Ali, I. 2022. Biosynthesis and characterization of iron oxide nanoparticles from *Mentha spicata* and screening its combating potential against *Phytophthora infestans*. *Frontiers in Plant Science*, 13, 1001499.

131. Khorrami, F.; Ojaghi Aghbash, K.; Soleymanzade, A.; Forouzan, M. & Ghosta, Y. 2019. *Cuminum cyminum* methanolic extract–Fe_3O_4 nanocomposite: A novel and efficient insecticide against the potato tuber moth (Lepidoptera: Gelechiidae) to protect potatoes. *Acta Phytopathologica et Entomologica Hungarica*, 54(2), 243-251.

132. Appu, M.; Lian, Z.; Zhao, D. & Huang, J. 2021. Biosynthesis of chitosan-coated iron oxide (Fe_3O_4) hybrid nanocomposites from leaf extracts of *Brassica oleracea* L. and study on their antibacterial potentials. *3 Biotechnology*, 11, 1-14.

133. Xing, K.; Zhu, X., Peng, X. & Qin, S. 2015. Chitosan antimicrobial and eliciting properties for pest control in agriculture: a review. *Agronomy for Sustainable Development*, 35, 569-588.

134. Ghormade, V.; Deshpande, M. V. & Paknikar, K. M. 2011. Perspectives for nano-biotechnology enabled protection and nutrition of plants. *Biotechnology Advances*, 29(6), 792-803.

CHAPTER 3
RESEARCH METHODOLOGY

3.1 Materials

The dried *Helichrysum odoratissimum* plant material (aerial part) was obtained from a local producer in Rustenburg (North-West, South Africa); global positioning system coordinates grid 25.6628° S, 27.2356° E. This was further identified in the Department of Crop Science, North-West-University, South Africa. Sodium tripolyphosphate, zinc nitrate hexahydrate ($Zn(NO_3)_2.6H_2O$), ferrous sulphate heptahydrate ($FeSO_4.7H_2O$), low-molecular weight chitosan, ferric chloride ($FeCl_3$), mercuric chloride ($HgCl_2$), potassium Iodide (KI), and NaOH of high grade of purity were procured from Sigma-Aldrich, Johannesburg, South Africa. These chemicals were used as purchased from the supplier without further purification. All experiments for the preparation of *H. odoratissimum* aqueous extract, ZnO NPs, and Fe_3O_4 NPs were carried out in deionized water.

3.2 Experimental methods

3.2.1 Preparation and characterization of *H. odoratissimum* aqueous extract

The plant material was washed several times with distilled water, air-dried, and crushed into fine powder. 5, 10, and 15 g of this material were macerated in 100 ml of deionized water at 70 ºC for 1 h and filtered through Whatman filter papers. A qualitative phytoconstituents screening of these extracts was performed following the procedure described elsewhere [1,2]. This analysis was based on colourimetric assessments and included the Salkowski's test, alkaline experiment, ferric chloride test, and Mayer's assay. The *H. odoratissimum* aqueous extracts (2 mL) were treated with chloroform (1 mL) and sulfuric acid (1 mL) to test the presence of terpenoids. Flavonoids were detected in these extracts by adding 2% NaOH (2 mL) while phenols and tannins were established by adding 2% ferric chloride (4 drops) to the filtrates. The plant extracts were also mixed with concentrated HCl (2 mL) and few drops of Mayer's reagent to assess the presence of alkaloids.

The extracts were also diluted to a ratio of 1:10 with water and scanned in the wavelength range 200-700 nm using a UV-Vis spectrophotometer - PerkinElmer Lambda 365 (Waltham, Massachusetts, USA). The phytochemicals in *H. odoratissimum* aqueous extracts are expected to undergo electronic transitions on absorbing light in the UV-Vis regions of the electromagnetic spectrum. Fingerprinting of these extracts was performed by the high-performance thin layer chromatography (HPTLC) technique using a CAMAG HPTLC system (Muttenz, Switzerland). 6 µl of the aqueous extracts were applied as bands on the 10 x 10 silica gel 60 F254 HPTLC plate using a syringe and the automatic TLC sampler 4. The plate was kept in a development chamber and saturated for 20 min with ethyl acetate-methanol-deionized water (ratio 5:1:2 v/v/v) mobile phase. The CAMAG TLC scanner was used to perform densitometric scanning. The plate was visualised using the CAMAG visualizer, and imaging was achieved under white light, 254 nm UV light and 366 nm UV light.

3.2.2 *H. odoratissimum* aqueous extract-mediated synthesis of nano-metal oxides (ZnO and Fe_3O_4)

The nano-zinc and -iron oxides were prepared following the phyto-assisted procedure adapted from [3]. The three filtrates characterized were treated at 50 ºC with 50 ml of aqueous zinc (II) ions solution, obtained from the complete dissolution of 1 g zinc salt in 50 ml deionized water. The different mixtures were stirred constantly (300 rpm) for 2 h, and then aged for 24 h. Subsequently, the pH of each solution was adjusted to 10, and the resultant suspensions were centrifuged at 6 000 rpm for 20 min, washed with deionized water, and dried at 80 °C for 24 h. The products were subjected to thermal annealing at 400 °C for 2 h and labelled and labelled ZnO[5s], ZnO[10s], and ZnO[15s] based on the amount of plant material used for substrate extraction.

Stirred (300 rpm) mixtures of the filtrates characterized (100 mL) and aqueous iron (II) ions solution (1 g of $FeSO_4.7H_2O$ in 50 ml deionized water) were treated as described for the preparation of ZnO NPs. Work-up and thermal annealing afforded the products designated as Fe_3O_4[5s], Fe_3O_4[10s], and Fe_3O_4[15s]. The prepared nano-metal oxides were stored in air-tight containers. Figure 3.1 provides an

overview of the steps undertaken in transforming the metal ions (Zn^{2+} and Fe^{-2+}) into oxide nanoparticles.

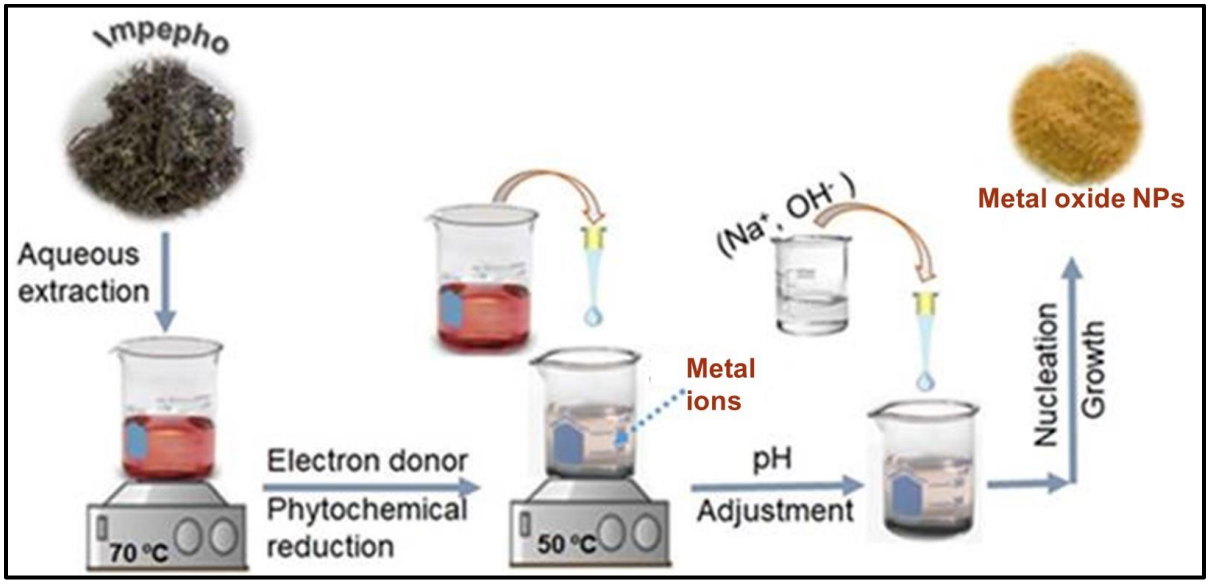


Figure 3. 1: Schematic presentation of the preparation of ZnO NPs and Fe_3O_4 NPs.

3.2.3 Encapsulation of the pre-synthesized metal oxides within chitosan nanoparticles

The nano-metal oxides ZnO and Fe_3O_4 were treated with CS solution in the presence of TPP dissolved in water (Figure 3.2). A series of chitosan-based nanoparticles (CS/TPP NPs and nutrient-loaded CS/TPP NPs) were fabricated by the ionic gelation method in accordance with the procedure proposed previously by Dhlamini et al. (2020) in the research group [4], with slight modifications. In a typical procedure, 0.3 g CS powder was dissolved in 25 mL of acetic acid (1%, v/v) under magnetic stirring at room temperature. Subsequently, 0.10 g of metal oxide NPs (ZnO[5s], ZnO[10s], ZnO[15s], Fe_3O_4[5s], Fe_3O_4[10s], or Fe_3O_4[15s]) were slowly added, and the mixture was treated with 5 ml of TPP (1%, w/v) dropwise under continuous stirring (300 rpm) for 30 min. Thereafter, the opalescent solution was centrifuged at 6 000 rpm, and the precipitate obtained was washed several times with deionized water and freeze-dried to generate the ZnO- and Fe_3O_4-encapsulated CS/TPP NPs.

A mixture of 0.10 g metal salt ($Zn(NO_3)_2.6H_2O$ or $FeSO_4.H_2O$) and 0.3 g CS powder in 25 mL of acetic acid (1%, v/v), followed by the addition of 5 ml of TPP (1%, w/v) was also treated as for the synthesis of ZnO- and Fe_3O_4-encapsulated CS/TPP NPs. Work-up afforded the Zn(II)- or Fe(II)-laden CS/TPP NPs. Considering that the micronutrients were introduced as ionic species in this case, the complexation efficiency (CE) was determined as follows:

$$CE\ (\%) = \frac{TM - FM}{TM} \times 100$$

where, TM and FM denote the total amount of metal ions used during the preparation of metal(II)-laden CS/TPP NPs and the fraction of free metal ions in the supernatant after centrifugation. FM was obtained via an inductively coupled plasma-mass spectrometer (ICP-MS) equipment (Agilent 7500 series). The pristine CS/TPP NPs were also prepared upon mixing the biopolymer solution and TPP crosslinker. All CS/TPP NPs and nutrient-loaded CS/TPP NPs were stored in air-tight sample vials.

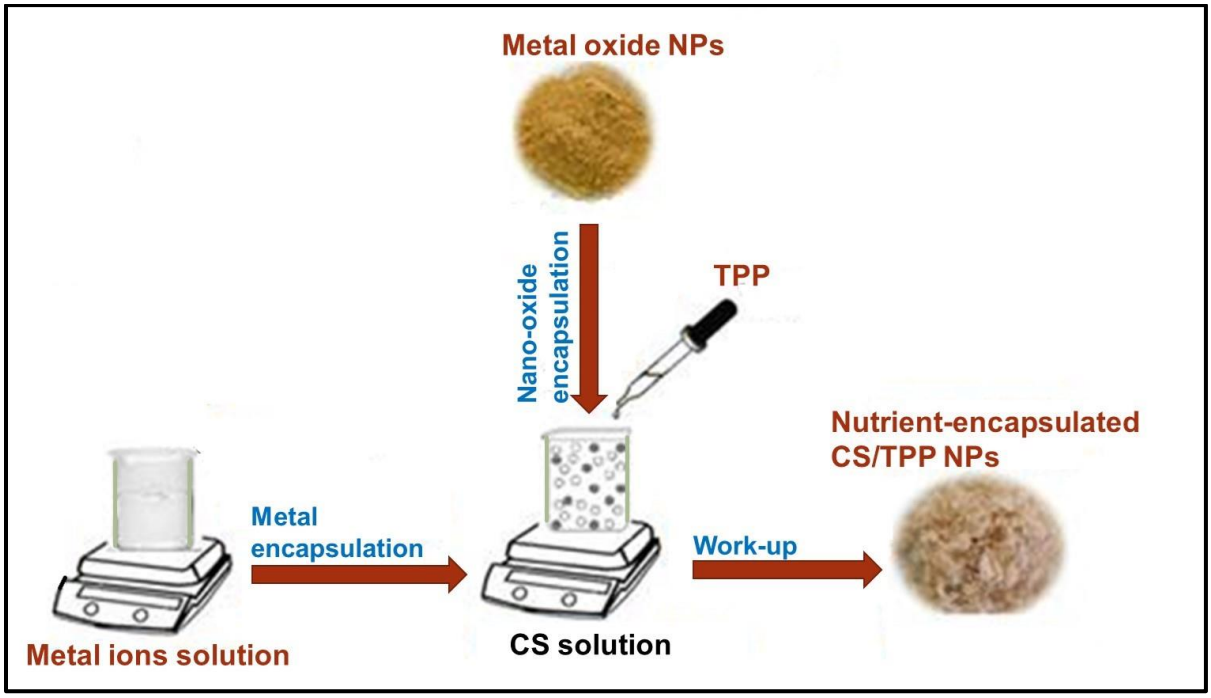


Figure 3. 2: Schematic illustration of the development of nutrient-loaded CS/TPP NPs.

3.3 Characterization of nano-metal oxides (ZnO and Fe_3O_4) and nutrient-loaded chitosan nanoparticles

3.3.1 Electrochemical measurements

The electron transfer activity is particularly interesting for transforming metal ions to nano-oxides [5]. Cyclic voltammetry is a well-known technique for studying the redox property of a species in solution. This electrochemical method was used to obtain information about the development of nano-metal oxides in the solution initiated by the *H. odoratissimum* aqueous extracts. This was conducted by measuring the current response as the potential varied. The experiment was performed with a three-electrode system consisting of bare glassy carbon (working electrode), platinum wire (counter electrode), and Ag/AgCl (reference electrode). The extract was mixed with 0.1 mol/L KCl (buffer) and the measurements were accomplished at the scan rate of 25 mV/s with an Autolab potentiostat operated by the Nova 1.10 software.

3.3.2 Dynamic light scattering (DLS) and zeta potential

DLS is a technique used to determine size particles less than a micron in dimensions by measuring their Brownian motion in suspensions. The speed of spherical particles going through Brownian motion and the fluctuations of scattered light can provide information about their hydrodynamic diameter and surface charge. The size distributions of the prepared nano-metal oxides and nutrient-loaded CS/TPP NPs were measured by the Malvern Zetasizer Nano ZS instrument. The level of accuracy in DLS measurements depends on particle concentration [6]. Extremely low concentration leads to weak scattering, while high concentration results in particle-particle interactions. One milligram of the sample was placed into a 1 mL cuvette filled with deionised water and then sonicated for 5 min. Nanoparticles were filtered by using a PTFE 0.2 µL pore size membrane to remove possible dust particles before analysis. The measurements were carried out in triplicate.

3.3.3 Fourier transform infrared spectroscopy (FTIR)

The FTIR spectroscopy is concerned with the distinct vibrational modes of functional groups. This well-established technique is based on light absorption in the infrared region of the electromagnetic spectrum, and is frequently used to gain information about the molecular structure of organic and inorganic materials. There is a correlation between the structure of a molecule and the wavenumbers at which it absorbs infrared radiation. In the current study, FTIR spectroscopy was employed to investigate the bonding of the ZnO and Fe_3O_4 nanostructures. The chemical composition of the nutrient-loaded CS/TPP NPs was also analysed through this technique. The spectra were acquired on a Perkin Elmer spectrum 100 FTIR spectrophotometer (USA). The powder samples of the prepared nanoparticles were placed onto a sample holder and scanned over the 4000 to 400 cm^{-1} range at a resolution of 4 cm^{-1}.

3.3.4 X-ray diffraction spectroscopy (XRD)

The XRD spectroscopy is a valuable technique to identify a material's composition and crystal quality. When impacted by electromagnetic radiation (X-rays), a three-dimensional array of atoms causes a constructive interference, as W. H. Bragg and W. L. Bragg reported in 1913. The following equation expresses this behaviour:

$$n\lambda = 2\ d\ sin\theta$$

where, λ, d, and Θ represent the wavelength of radiation used, the interplanar spacing of the diffracting planes, and the angle between the incident radiation and the diffracting planes. The intensity of the diffracted rays detected by varying the angle of incidence and the angle of diffraction/yields the characteristic pattern of a sample. The metal oxide nanoparticles prepared using *H. odoratissimum* extracts and their encapsulated CS derivatives were characterized by XRD, using a Bruker-D8 Advance diffractometer operated with Cu Kα radiation (λ = 0.154 nm) at 40 kV voltage and 30 mA.

3.3.5 Electron microscopy

Scanning and transmission electron microscopy (SEM and TEM) are the most representative microscopy techniques employed to examine the morphology and

size of a solid sample. These utilise a beam of electrons to generate images from the surface of a material. In SEM analysis, these images are created by the reflected electrons. On the other hand, TEM process uses electrons that pass through the sample to produce images; hence this technique can provide valuable information on the internal structure of a material. The energy dispersive X-ray (EDX) spectroscopy is usually combined with SEM and TEM for the surface elemental analysis. The field emission SEM apparatus, Zeiss Ultra Plus, was fitted with an Oxford EDX spectrometer for morphological analysis and elemental characterisation of the nanomaterials prepared in this investigation. TEM imaging was performed on a JEOL-JEM 2100 equipment, operating at 200 keV. Samples were dissolved in ethanol, sonicated for about 20 minutes and dispersed on a carbon coated copper grid for analysis.

3.3.6 X-ray photoelectron spectroscopy (XPS)

XPS is a surface sensitive technique that can provide accurate information on the elemental composition and chemical state of the outermost layers of materials. It is based on the ability of electrons at the surface of a solid sample to absorb energy upon irradiation with a beam of X-rays and get ejected. Because the chemical environment influences the binding energy of an atom, XPS enables the identification of chemical states of all elements present on the surface of a sample. The escape depth of the photoelectrons ranges from 2 to 10 nm. XPS spectra are obtained through the intensity of the escaping electrons and their binding energies. The composition of the nutrient-loaded CS/TPP NPs prepared in this investigation was analysed from XPS spectra. These were acquired on a Thermo Fisher Scientific spectrometer ESCAlab 250Xi with a monochromatic Al kα (1486,7 eV) X-ray source. The survey spectra were obtained at a pass energy of 100 eV, while high-resolution spectra were obtained at 20 eV.

3.3.7 Thermogravimetric analysis (TGA)

TGA is one of the methods used primarily to study the thermal decomposition/stability of solids. This technique has been widely exploited for characterising experimental polymeric materials [7]. The decomposition pattern can

give useful information on the filler content in composites. The thermal decomposition characteristics of nutrient-loaded CS/TPP NPs were studied by TGA-differential scanning calorimetry and runs were carried out in an SDT-Q600 simultaneous thermal analyser. Sample (10 milligram) were placed in a furnace and the experiments performed at a heating rate of 10 °C/min under a nitrogen atmosphere with a 60 cm^3/min flow rate. The ZnO-loaded CST/PP NPs was chosen as a specimen.

3.4 Release behaviour of the prepared nanomaterials in water

This study was conducted using the tea bag technique adopted from [8]. The ZnO[15S], ZnO-loaded CS/TPP, and Zn(II)-laden CS/TPP NPs were chosen as specimens. 30 mg of each sample was lodged into an empty teabag, placed in a beaker containing 50 ml of deionized water (pH 7.8-8.1), and then allowed to settle. The variation in the Zn concentration was assessed for 2 weeks, and each experiment was carried out thrice. After 01, 05, 24, 48,168, 240, and 336 h, aliquots (10 ml) were collected using the ICP-MS technique for Zn analysis. Each time an aliquot was removed, deionized water of the same volume was added to the beaker to keep the volume constant.

3.5 Seed germination study

3.5.1 Seed decontamination and stratification

The *Zea mays* seeds of an R450w/uo2250w CML550 variety were provided by Molelwane Farm, Department of Crop Science, North-West-University, South Africa. A total of 117 seeds were then selected. The seeds were surface-cleaned by placing them into falcon tubes, followed by the addition of 30 ml 70% (v/v) ethanol and vortexing for 2 min. The used ethanol was then discarded, and 30 ml of sterilizing buffer: (0.02% (v/v) Triton X-100 and 1.25% (v/v) sodium hypochlorite solution (commercial bleach)) was added, and the mixture was allowed to stand for 15 min before being vortexed for extra 2 min. After decontamination, the seeds were

immediately rinsed three times with deionized water. The washed seeds were then covered with sterile deionized water (20 ml) and placed in a fridge at 4°C for 48 hours for stratification. The importance of stratification is to promote uniform and synchronized germination.

3.5.2 Seed priming

The ZnO NPs prepared in this work were used as a priming agent and dispersed in deionized water at two concentrations (0.01 and 0.04%) using ultrasonic vibration (100 w, 42 kHz) for 20 min. The acquired zinc salt ($Zn(NO_3)_2.6H_2O$) and deionized water were also employed for seed priming assays, where the latter treatment was considered as a control. A total of 9 decontaminated and stratified seeds per treatment group were soaked in deionized H_2O, 0.01% ZnO, 0.04% ZnO, 0.01% $ZnNO_3.6H_2O$, 600 mM NaCl, and 600 mM NaCl + 0.01% ZnO priming solutions at 25 ºC for 4 h. Afterward, these imbibed seeds were arranged as triplicate experimental lines in a complete randomized design (CRD). Similarly, solutions of CS/TPP NPs, ZnO-loaded CS/TPP NPs, and Zn(II)-laden CS/TPP NPs were used for seed priming. The seeds imbibed in deionized water, and 600 mM NaCl solution were considered as control treatments while the rest were the experimental lines.

The germination study was carried out at the Plant Biotechnology Research Lab, North-West University, South Africa, for 10 days within a growth chamber system GC-300TL (Jeiotech, Korea) in petri dishes (90 x 15 mm), following irrigation with 1 ml of deionized water daily within time range 9:00–10:00 am and 16:00–17:00 pm. The chamber was set to maintain greenhouse conditions of an average daily temperature of 23 °C; a relative humidity of 70%; a daily irradiance of 150-650 $\mu mol \cdot s^{-1} \cdot m^{-2}$; and a CO_2 concentration range of 380-390 ppm.

The following parameters were measured after the 10-day germination period: radicle length (RL), number of lateral roots (NLR) on the radicle, and number of roots (NR) additional to the radicle, length of roots (LoR), shoot length (SL), coleoptile length (CL), radicle dry weight (RDW), coleoptile dry weight (CDW), shoot dry weight (SDW), and root dry weight (RDW). The time of germination was recorded as the day when the radicle emerged from the seed. All lengths were measured with a ruler

at a mm scale. All dry weights were obtained after oven-drying the tissues at 40 °C for 72 h. The results were subjected to a one-way analysis of variance using the Super-ANOVA software (Version 7, Stats graphics). The significant levels of difference for all measured traits were calculated, and means were compared and separated by the *post hoc* Student–Newman–Keuls (SNK) multiple range test ($P \leq 0,05$).

3.6 Antifungal activity

Cultures of *Aspergillus niger* (PPRI 3390), *A. flavas* (PPRI 26007), *Alternaria solani* (PPRI 25681), *Fusarium oxysporum* (PPRI 18679), *F. solani* (PPRI 19147), and *F. verticillioides* (PPRI 9278) were obtained from the Agricultural Research Council - Plant Health and Protection, Pretoria, South Africa. The fungal cultures were prepared on potato dextrose agar (PDA) as described by Seepe et al. [9]. The prepared NPs were dispersed in distilled water to give a stock concentration of 20 mg/mL. The biological activity against the six fungal pathogens was evaluated using the microplate dilution assay, as detailed by Seepe et al. [9]. Each set of NPs was evaluated in triplicate. Amphotericin B was used as a positive control, and potato dextrose broth (PDB) was the negative control. Lack of change in the colour of the microplate well, indicated fungal growth inhibition after adding 50 µL of 0.5 mg/mL *p*-iodonitrotetrazolium chloride to each well and further overnight incubation. The lowest concentration of each sample that inhibited fungal growth was recorded as the minimum inhibitory concentration (MIC).

The antifungal activity of the prepared NPs against human pathogens, *Candida tropicalis* and *C. glabrata*, was also determined. The samples were subjected to serial dilutions into 96-well microplates containing Sabouraud dextrose broth (SDB) culture medium (50 µL per well), and the fungal suspensions were added at a concentration of $2x10^4$ cells/mL (50 µL per well) to duplicate microplates. The positive control consisted of the culture medium, inoculum and fluconazole. The microplates were incubated at 37 °C for 48 hours, and each well was then treated with 10 µL of a freshly prepared resazurin solution (0.015%). The microplates were further incubated for an additional 1 hour to observe colour change. After incubation, the lowest concentrations with no change in colouration were scored as MIC values.

The treatments tested for antifungal activities were Fe_3O_4[10s] NPs, Fe_3O_4[15s] NPs, Fe_3O_4[10s]-loaded CS/TPP NPs, Fe_3O_4[15s]-loaded CS/TPP NPs, and Fe(II)-laden CS/TPP NPs.

REFERENCES

1. Victor, B. K. & Hamed, A. S. 2014. Preliminary phytochemical screening and evaluation of in vitro antioxidant activity of Iraqi species of *Hypericum perforatum* aerial part. *International Research Journal of Pharmacy*, 5(5), 369-373.

2. Bargah, R. K. 2015. Preliminary test of phytochemical screening of crude ethanolic and aqueous extract of *Moringa pterygosperma Gaertn*. *Journal of Pharmacognosy and Phytochemistry*, 4(1), 07-09.

3. Sharma, G.; Soni, R. & Jasuja, N. D. 2017. Phytoassisted synthesis of magnesium oxide nanoparticles with *Swertia chirayaita*. *Journal of Taibah University for Science*, 11(3), 471-477.

4. Dhlamini, B.; Paumo, H. K.; Katata-Seru, L. & Kutu, F. R. 2020. Sulphate-supplemented NPK nanofertilizer and its effect on maize growth. *Materials Research Express*, 7(9), 095011.

5. Jeevanandam, J.; Chan, Y. S. & Danquah, M. K. 2016. Biosynthesis of metal and metal oxide nanoparticles. *ChemBioEng Reviews*, 3(2), 55-67.

6. Austin, J.; Minelli, C.; Hamilton, D.; Wywijas, M. & Jones, H. J. 2020. Nanoparticle number concentration measurements by multi-angle dynamic light scattering. *Journal of Nanoparticle Research*, 22, 108.

7. Doyle C. D. 1961. Estimating thermal stability of experimental polymers by empirical thermogravimetric analysis. *Analytical Chemistry*, 33(1), 77-79.

8. Ekanayake, S. A. & Godakumbura, P. I. 2021. Synthesis of a dual-functional nanofertilizer by embedding ZnO and CuO nanoparticles on an alginate-based hydrogel. *ACS Omega*, 6(40), 26262-26272.

9. Seepe, H. A.; Amoo, S. O.; Nxumalo, W. & Adeleke, R. A. 2020. Sustainable use of thirteen South African medicinal plants for the management of crop diseases caused by Fusarium species - An in vitro study. *South African Journal of Botany*, 130, 456-464.

CHAPTER 4

CHARACTERIZATION OF *H. ODORATISSIMUM* EXTRACT-MEDIATED NANO-METAL OXIDES

The important nano-oxide inputs that have been described to stimulate plant growth are oxides of silicon (SiO_2 NPs), titanium (TiO_2 NPs), cerium (CeO_2 NPs), copper (CuO NPs), zinc (ZnO NPs), and iron (Fe_2O_3 and Fe_3O_4 NPs) [1–3]. Metal oxide nanoparticles have been shown to offer physiological and morphological advantages in several plant model systems [4]. ZnO represents one of the most explored alternatives to zinc fertilizers like zinc nitrate, zinc sulphate, and zinc carbonate for plant treatment [5].

Chemical reduction mediated by plant extracts is an eco-friendly approach to developing metal oxide nanoparticles. The electron-rich biomolecules in selected plant extracts can interact with metal ions to transform to the corresponding metal or metal oxide nanostructures. The phyto-assisted preparation of nanomaterials does not require additional capping agents and/or surfactants as stabilizing reagents. This denotes a cheap, simple, and less toxic synthetic approach to metal oxide nanoparticles [6]. Due to their entomotoxic characteristics and potential to instigate ROS production, these nanomaterials have also been commended for their pesticide activities.

4.1 Phytochemical screening of *H. Odoratissimum* aqueous extract

H. odoratissimum Sweet is a popular, aromatic, and perennial herb belonging to the Asteraceae's family. This plant species is native to southern Africa and is widely distributed across Africa. It is characterized by small silvery leaves and yellow flowers at the ends of the twigs, as presented in Figure 4.1. This plant is commonly used to manage health conditions like acne, diabetes, coughs, and menstrual disorders [7,8]. The methanol extract of *H. odoratissimum* has been found to inhibit the growth of *Cutibacterium acnes* bacteria at a minimum concentration of 7.81 µg/ml [9]. The bactericidal activity of the essential oil of *H. odoratissimum* has also been reported against numerous bacteria, including *Staphylococcus aureus*, *Streptococcus faecalis*, *Escherichia coli*, and *Kiebsiella pneumoniae,* with minimum

inhibitory concentrations ranging from 0.6 to 2.5 mg/mL [10]. Better known under the name of “Imphepho” in South Africa due to its strong smell, *H. odoratissimum* is also believed to serve for the communication with the ancestors and is often charred for cultural rites.



Figure 4. 1: Image of *H. odoratissimum* grown in South Africa.

The medicinal properties of plant species are often ascribed to their different phytochemical constituents. The qualitative phytoconstituents screening of the *H. odoratissimum* aqueous extracts is presented in Figure 4.2 and Table 4.1. Under the action of chloroform and H_2SO_4, a reddish-brown colour developed to reveal a positive result for terpenoids (test tube 1). A reddish-orange colour upon adding NaOH solution to the *H. odoratissimum* extract, which turns colourless when a few drops of dilute HCl are added, suggests the presence of flavonoids (test tube 2). The development of a bluish-black colour immediately after treating the extract with $FeCl_3$ solution shows the presence of phenols and tannins (test tube 3). A cream precipitate observed after adding Mayer’s reagent in acidified medium indicates the co-existence of alkaloids (test tube 4).

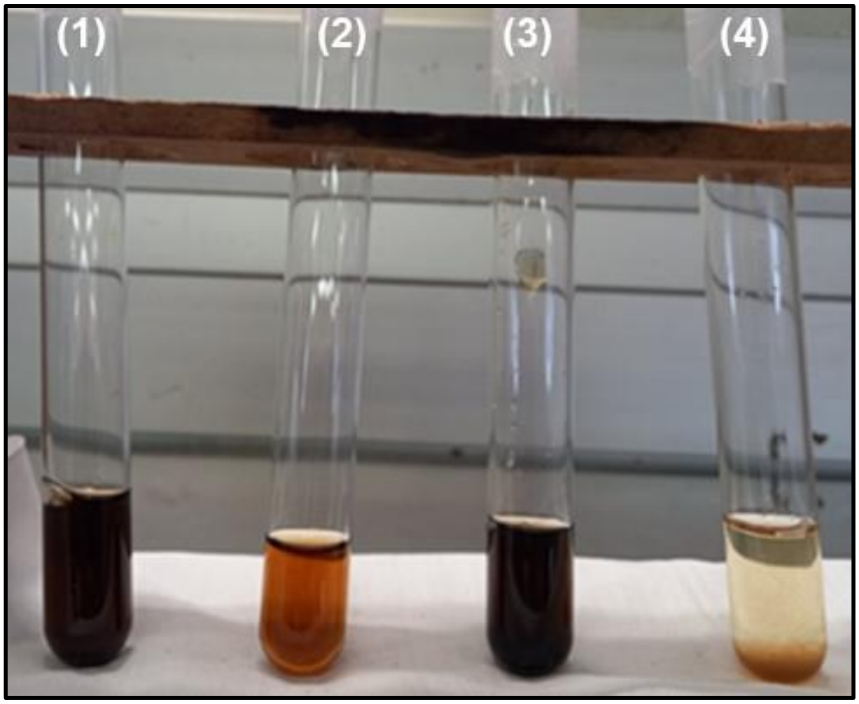


Figure 4. 2: Colourimetric test for the phytoconstituents (terpenoids (1), flavonoids (2), phenols and tannins (3), and alkaloids (4)).

Table 4. 1: Phytochemical screening results.

Phytochemicals	**Test**	**Outcome**
Terpenoids (**1**)	$CHCl_3$ and Conc. H_2SO_4	+
Flavonoids (**2**)	2% of NaOH	+
Phenols and Tannins (**3**)	2% of $FeCl_3$	+
Alkaloids (**4**)	Mayer's reagent	+

The UV-Vis absorption spectrum of the *H. odoratissimum* extract (Figure 4.3(a)) shows a prominent band at 283 and a shoulder at 333 nm, which are attributed to phenolic compounds and flavonoids [11], in agreement with the positive result for the ferric chloride test. Based on empirical research studies, typical absorption spectra of phenols and flavonoids exhibit two bands in the UV region with maximum in the ranges λ 240-285 nm and 300-400 nm [12, 13]. The electronic transitions recorded were fundamentally of the π–π* type. Phenolic compounds and flavonoids

demonstrated commendable antioxidant properties due to their ability to act as reducing agents. The HPTLC profiles of samples, prepared using 5, 10, and 15 g material, exhibit intense blue emission at retention factors of 0.05 to 0.11 under long wavelength UV light (Figure 4.3(b)), indicating high levels of phenolic acids and flavonoids. This observation is consistent with previous literature on the chemical profiling of *H. odoratissimum* species. Chemical studies on twelve samples collected in the Western Cape province, South Africa, have been previously carried out by the HPTLC and ultra performance liquid chromatography-mass spectrometry (UPLC-MS) methods. These revealed the presence of dicaffeoylquinic acid derivatives as the predominant phytochemicals [14]. The gas chromatography-mass spectrometry (GC-MS) analysis of samples from the Limpopo province has exposed high concentrations of 6-hydroxy-4-methoxy-2,3-dimethyl-benzaldehyde and tau-cadinol [15]. A specimen collected in the KwaZulu-Natal and characterized using the GC-MS method, showed the presence of prevailing palmitic acid, oxalic acid, oleic acid amide, and linoleic acid, [16]. In that respect, the bio-reducing potential of the prepared extracts was tested to convert Zn^{2+} ions to nano-oxide particulates.

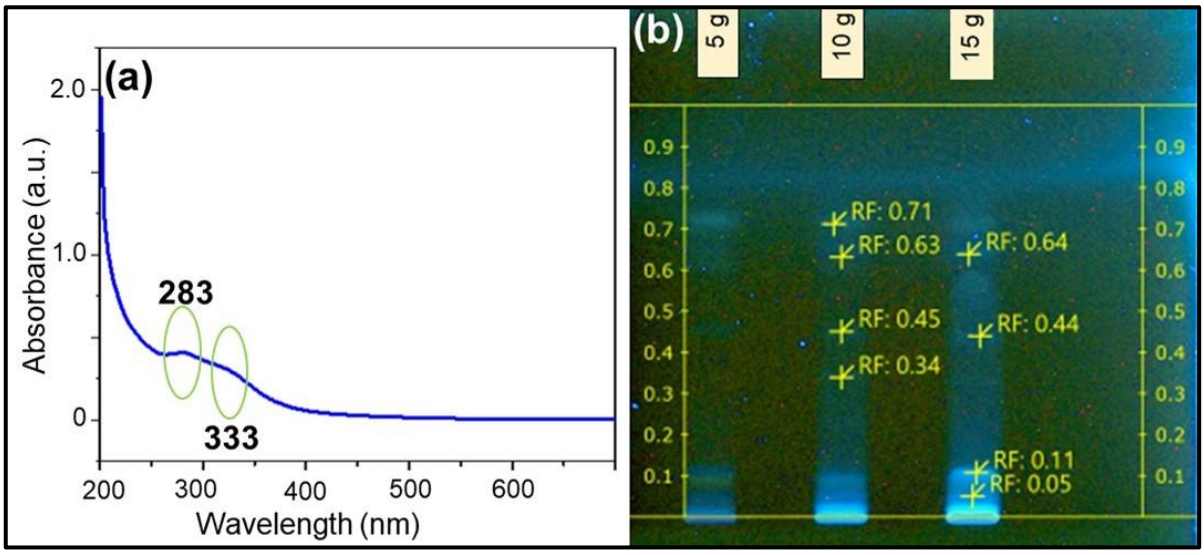


Figure 4. 3: (a) UV-Vis absorption spectrum of *H. odoratissimum* extract and (b) HPTLC fingerprints observed under UV light 366 nm.

4.2 Reduction potential of *H. Odoratissimum* aqueous extract and time monitoring for the formation of nanoparticles using absorption spectra

Cyclic voltammetry was used to explore the redox behaviour of Zn species in the presence of *H. odoratissimum* phytochemicals in 0.1 mol/L KCl at the scan rate of 25 mV/s within the potential range of -1.7 to 0.9 V at 25 °C (Figure 4.4). With no plant extract, the zinc nitrate solution exhibited 2 peaks between -1.2 and -1.0 V due to the redox reaction of NO_3^- ions [17]. The reduction peak at a potential of -1.5 V and oxidation at -0.2 V is assigned to the redox reactions of Zn(II) ions in the salt solution. The solution's free Zn(II) ions are reduced to zero-valent Zn and oxidized back. After treatment of the zinc solution with plant extract and stirring for 20 min and 2 h, the Zn(II)-extract system showed a cathodic wave at -1.3 V and the disappearance of the peak corresponding to Zn oxidation. This observation is presumably attributed to the coordination between the electron-donor phytochemicals and metal ions. The interaction is anticipated to improve the stability of Zn(II) ions and, at the same time, promote their reduction to Zn(0) complexes. Previously, a similar observation was reported for the formation of ZnO in the presence of sodium ethylenediaminetetraacetate (Na_2EDTA) [18]. After aging for 24 hours, the system displayed a small oxidation peak at -0.8 V. This probably corresponds to the oxidation of small amounts of Zn(0) complexes developed in the solution. However, adding NaOH solution to the Zn-extract system after 24 hours, resulted in a significant reduction peak at around -0.5 mV, presumably due to the catalytic reduction of phenolic compounds at the surface of the developed ZnO NPs [19]. The OH^- species introduced in the process can react with the Zn(II) complexes to generate the hydroxide intermediate, which decomposes to ZnO nanostructures [20].

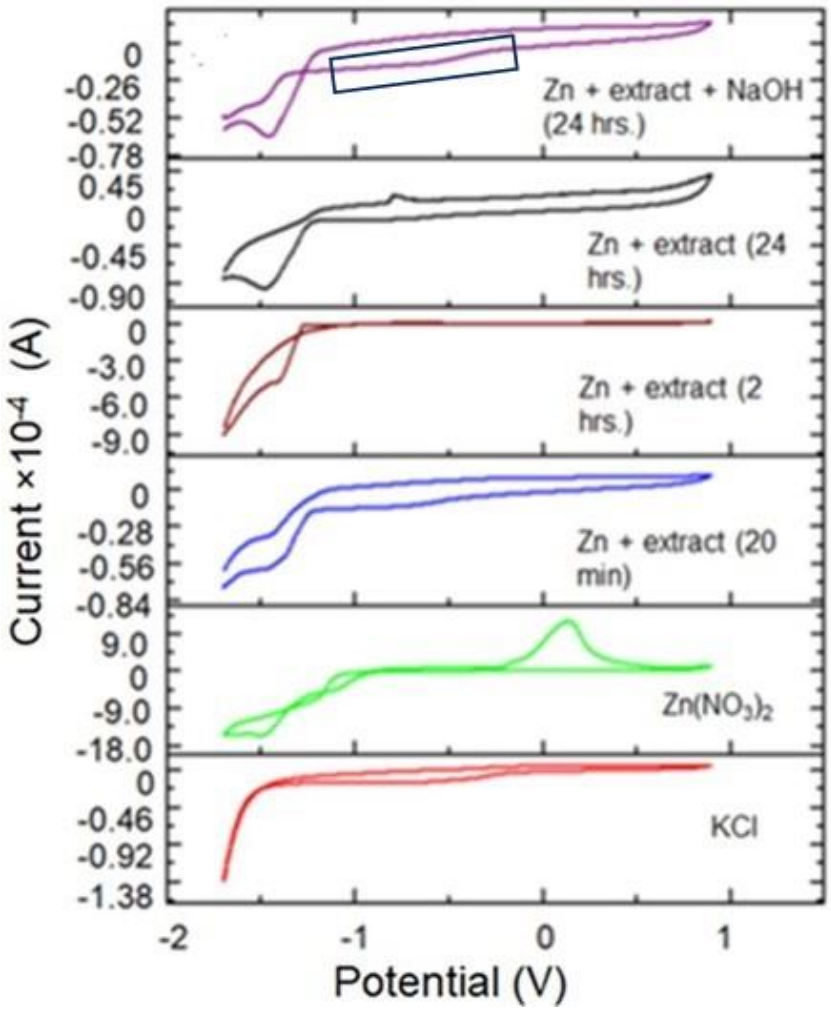


Figure 4. 4: Voltammetric characterization of solutions obtained after 20 min, 2 h stirring and 24 h aging in a three-electrode system at a scan rate of 25 mV/s.

The absorption spectroscopy was then carried out to examine the development of metal oxide nanostructures in *H. odoratissimum* extract, and the spectra obtained are shown in Figure 4.5. For this classic analysis, a characteristic absorption band is observed at 370 nm for Zn(II)-extract system owing to surface plasmon resonance (SPR). Singh et al. (2019) [21] and Santhoshkumar et al. [22] reported similar bands for the phyto-assisted synthesis of ZnO NPs with aqueous extract of *Aloe barbadensis Mill* (360 nm) and *Passiflora caerulea* leaves (380 nm). The Fe(II)-extract, on the other hand, exhibits a band at 416 nm. According to a report by Abdallah and Al-Haddad (2021) [23], the UV-Vis absorption curve of iron ions-carob leaf extract displayed the SPR peak in the region 290-480 nm due to the formation of Fe_3O_4 NPs. The collective oxillation of free electrons in the nano-metal oxide surface layer, and their interaction with the incident electromagnetic wave gave rise to surface plasmon bands in the UV-Vis spectrum [24, 25]. Plant metabolites such as

flavonoids, carboxylic acids, and phenols are well reported as proton-donating phytochemicals for reducing metal ions [26]. The aqueous and methanol extracts of *H. odoratissimum* have been reported for the reduction of Au(Ⅲ) ions and the production of Au NPs [27]. As compared to the SPR band associated with ZnO, the broadening in the SPR band observed for Fe_3O_4, suggested an increase in diameter of their particles. Furthermore, the developed materials might be containing particle aggregates resulting in polydispersity. This physical attribute is known to increase the width of the plasmon band [28, 29].The characteristics of the nano-oxides prepared with aqueous extracts of *H. odoratissimum* are assessed in the following sections.

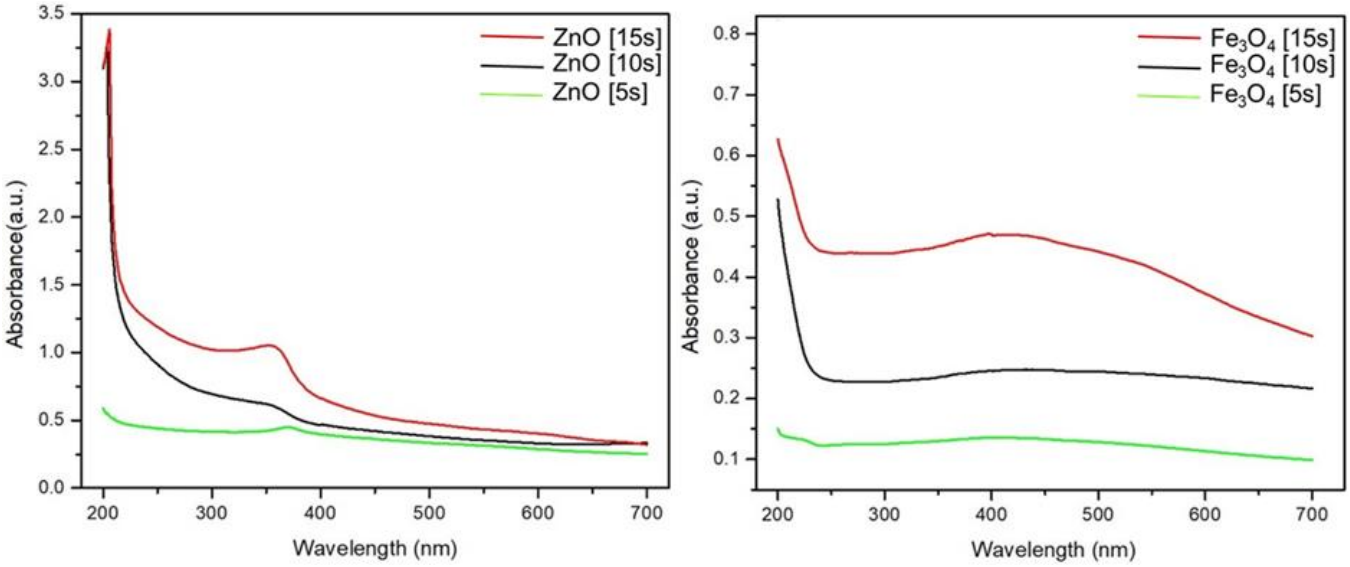


Figure 4. 5: UV-Vis absorption spectra of the ZnO NPs and Fe_3O_4 NPs developed in *H. odoratissimum* extract by monitoring time.

4.3 Microscopic and spectroscopic analysis of the nano-metal oxides (ZnO & Fe_3O_4)

4.3.1 Electron microscopy

Figures 4.6 and 4.7 displays the SEM and TEM micrographs of the zinc oxides and iron oxides obtained using *H. odoratissimum*. The SEM images indicate nearly spherical nanoparticles of various sizes. On the other hand, their topological analysis using TEM exhibits black spots representing the nano-sized metal oxides (ZnO and

Fe_3O_4) and a stabilizing light-coloured layer originating from the organic *H. odoratissimum* extract. Also, it could be observed that the developed metal oxides tended to form nano-agglomerates entangled with transparent sheet reflecting the organic materials.

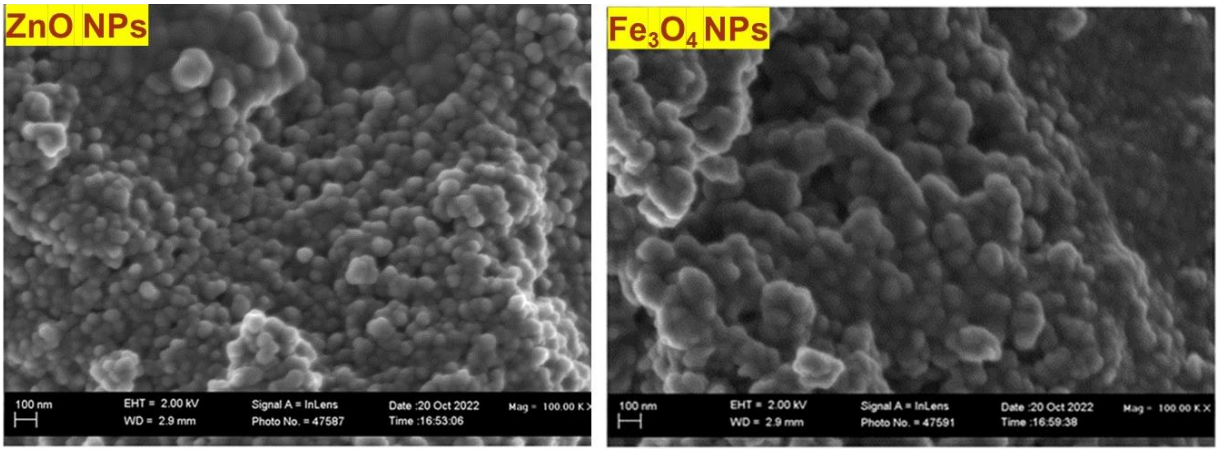


Figure 4. 6: SEM images of the developed nano-metal oxides.

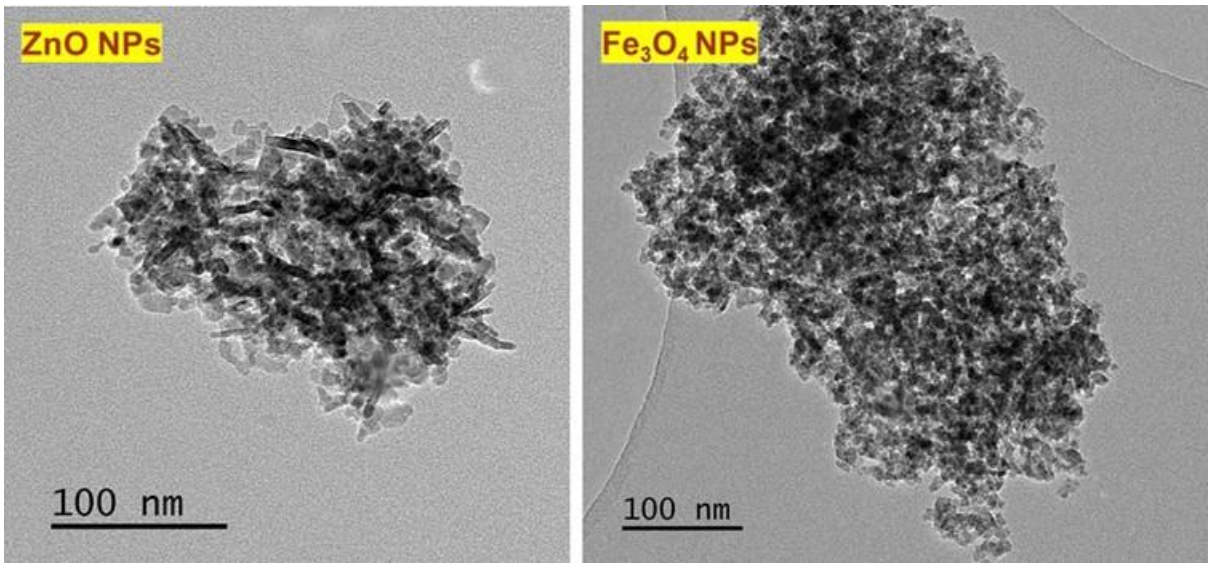


Figure 4. 7: TEM images of the developed zinc and iron nano-metal oxides.

4.3.2 Average particle size and surface charge

Data obtained from DLS analysis using different amounts of plant material to prepare the nano-metal oxides are given in Figures 4.8 and 4.9, and Table 4.2 (see Appendix). In colloidal suspension, the mean particle size of ZnO NPs ranges from 144.6 ± 2.6 to 321.2 ± 6.2 nm, with surface charge varying from -26.6 mV for

ZnO[10s] to -34.2 for ZnO[15s]. This technique also reveals average particle sizes of 210.3 ± 7.8, 203.2 ± 10.5, and 183.8 ± 2.1 nm for Fe_3O_4[5s], Fe_3O_4[10s], and Fe_3O_4[15s]. In agreement with the UV-Vis absorption spectral analysis, the average size of the Fe_3O_4 NPs was larger than that of the ZnO NPs. This is presumably ascribed to the presence of a layer of bound sulfur and residual sulfate at the surface of the *H. odoratissimum*-mediated Fe_3O_4 particles. The starting material for this sample is basically a flocculated sol; and the individual sol particles are developed from Fe ions, phytochemicals, and hydroxyl ions. It is anticipated that these particles would be stabilized by an excess of phytochemicals and Fe ions with sulfate ions as counter-ions.

An increase in the concentration of *H. odoratissimum* extract leads to reduced particle size. This is attributed to a faster rate of interaction between the metal ions and the phytocompounds in excess and stabilization of the developed smaller particles. In accordance with the UV-Vis absorption spectra of the two sets of metal oxides, the reaction rate increases with higher concentration of phytochemicals as the intensity of the SPR band also increases. Similar observation has been noted by Chauhan and Upadhyay for the conversion of ferrous sulfate to iron oxide NPs in the presence of *Lawsonia inermis* extract [30]. The presence of phytocompounds at the surface of metal oxide NPs limits their agglomeration and improves their stability, as supported by the highest zeta potential values of ZnO[15s] and Fe_3O_4[15s]. The prepared nanoparticles display moderate polydispersity index (PDI) values fluctuating from 0.136 to 0.467.

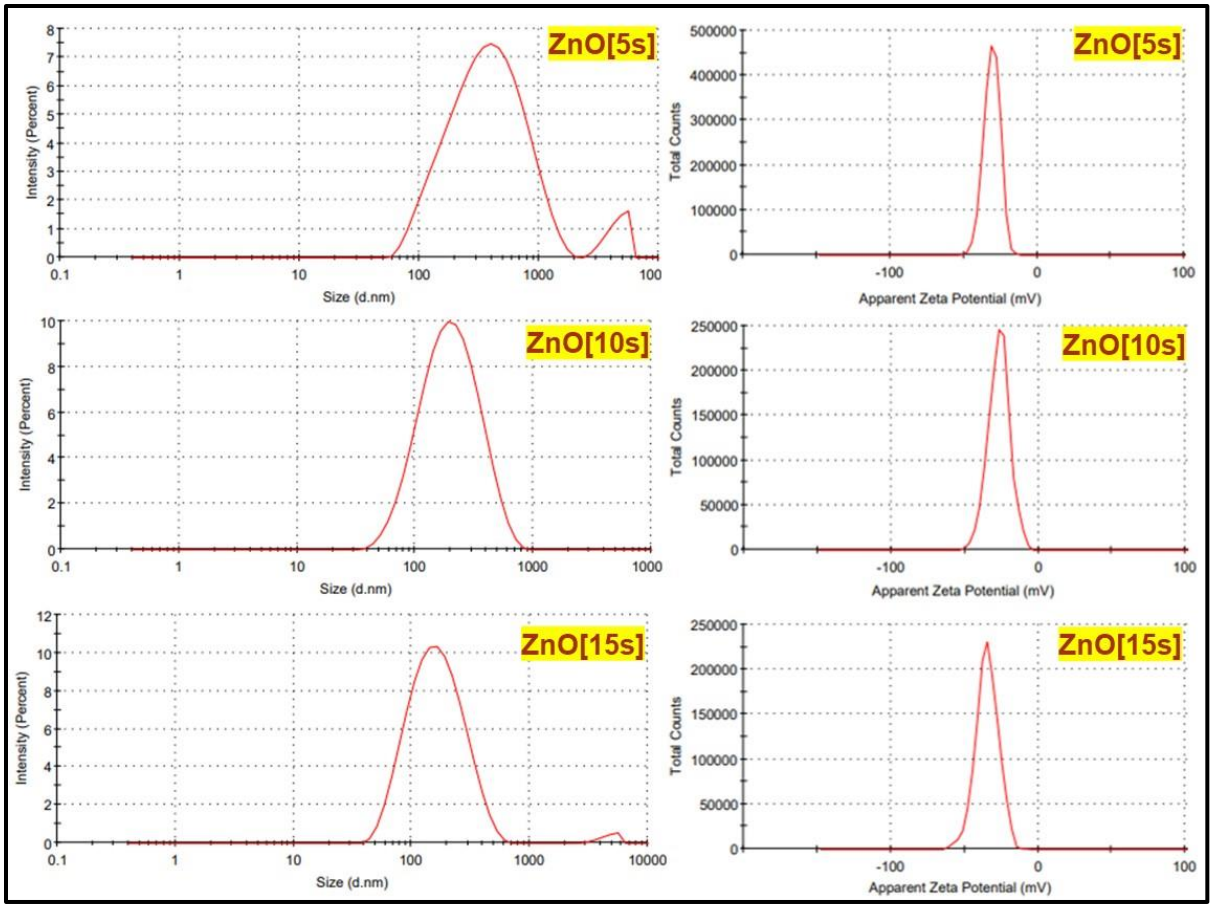


Figure 4. 8: DLS and zeta potential analysis of the nano-zinc oxides.

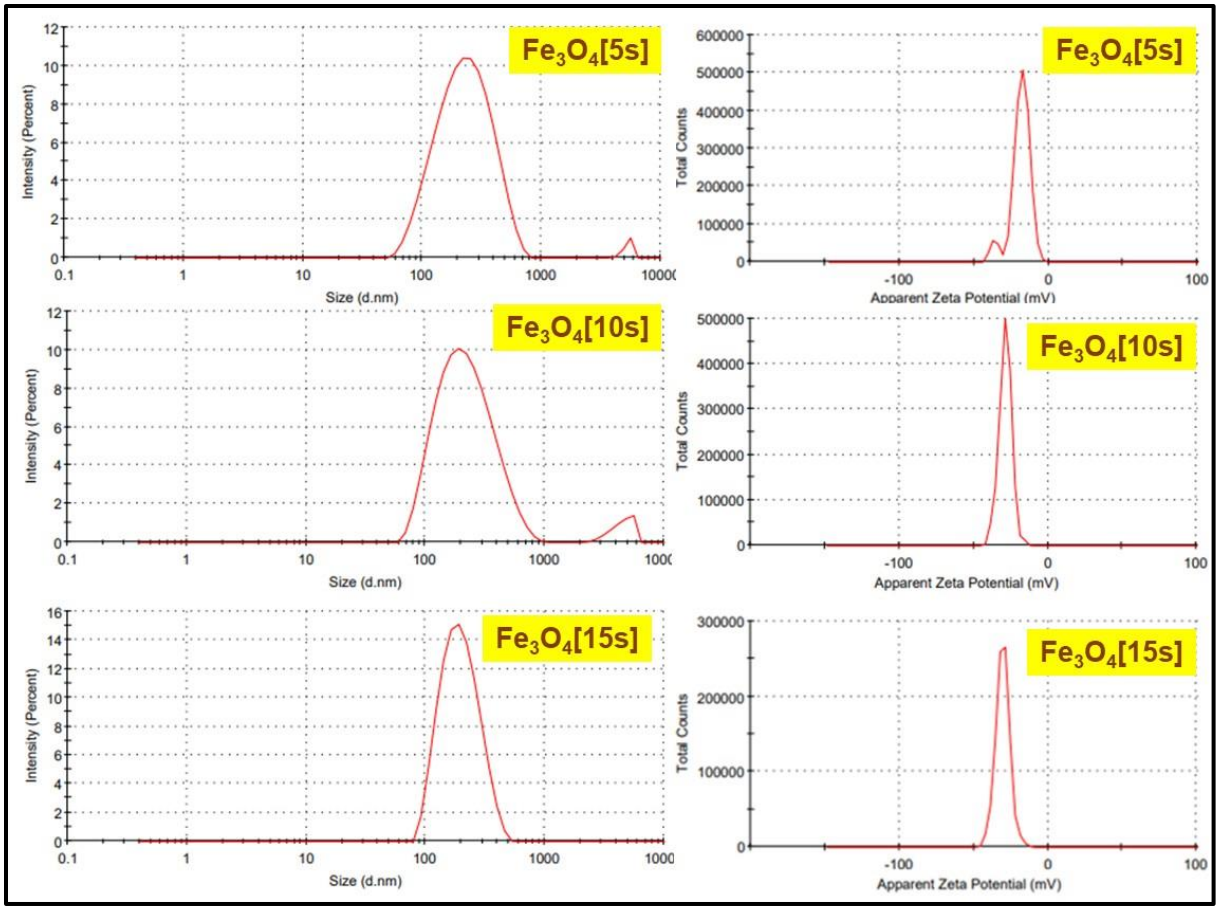


Figure 4. 9: DLS and zeta potential analysis of the nano-iron oxides.

4.3.3 FTIR spectral analysis

The FTIR spectra of bulky zinc nitrate and ZnO NPs are given in Figure 4.10. The typical absorption bands corresponding to NO_3^- ions at 814 and 1336 cm^{-1} undergo modification in the spectrum of ZnO NPs. While a shift to 1403 cm^{-1} is observed with the latter, the former tends to disappear, suggesting a transformation of zinc salt. Moreover, in the FTIR spectrum of ZnO NPs, a peak reflecting the occurrence of Zn–O stretching vibration is recorded at 486 cm^{-1}, a value consistent with previous literature [31]. Also, the typical peak of iron oxides, that is, Fe-O at 538 cm^{-1} [32] is evidenced in the FTIR spectrum (Figure 4.10) of the sample developed in the Fe(II)-extract system. The formation of ZnO NPs and Fe_3O_4 NPs isolated from aqueous *H. odoratissimum* extract has been displayed by the vibration of the Zn–O and Fe–O stretching bands. The nanomaterials' spectra also display vibration modes characteristic for organic functional groups in the region of 750-1300 cm^{-1} [32]. This region of the IR spectrum is notable for bands corresponding to , to C–C, C–O, and

C–N bonds. This confirms the presence of adsorbed phytochemicals at the surface of the nano-oxides.

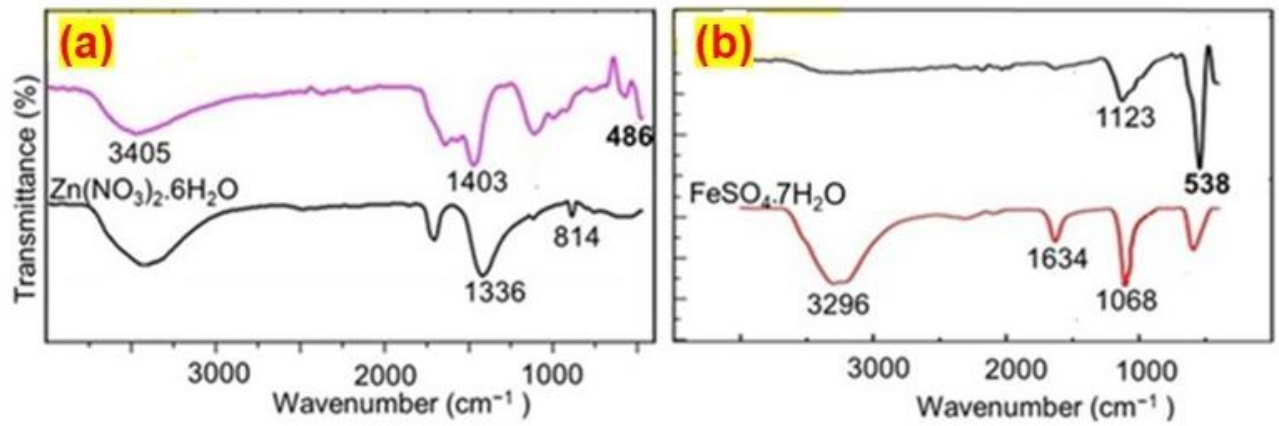


Figure 4. 10: FTIR spectra of the developed nano-metal oxides (a) ZnO and (b) Fe_3O_4.

4.3.4 XRD patterns analysis

X-ray diffraction identified the crystalline phase of the prepared ZnO NPs and Fe_3O_4 NPs; the patterns acquired are shown in Figure 4.11. For ZnO NPs, strong diffraction peaks are observed at 2θ values 31.74°, 34.38°, 36.30°, 47.51°, 56.51, 62.81°, and 68.98°, corresponding to (100), (002), (101), (102), (110), (103), and (112) lattice planes of ZnO with hexagonal wurtzite arrangement [33]. This usually consists of a Zn^{2+} cation surrounded by four O^{2-} anions at the corners of a tetrahedron and vice versa (Figure 4.12). From the pattern of Fe_3O_4 NPs, a set of characteristic peaks (220), (311), (400), (422), (511), and (440), which are consistent with the inverse cubic spinel phase of Fe_3O_4 (magnetite), are detected at 2θ 30.16°, 35.76°, 43.56°, 53.91°, 57.34°, and 63.33°. These peaks are like those described in the literature for magnetite NPs obtained using *Kappaphycus alvarezii* extract [34], and match with the Joint Committee on Powder Diffraction Standards (JCPDS) file 75-1609 reported by Liang et al. (2020) [35].

The unassigned peak observed at ~10.0° in the patterns of nano-iron oxides is likely due to impurities produced from the iron hydroxide and the oxidized carbon and sulphur during thermal annealing in air [36]. A study by Jamzad and Bidkorpeh (2020) [37], on the green preparation of iron oxide NPs using the *Laurus nobilis* L.

Leaf extract, described a comparable peak at 2θ 11.2°. This was attributed to the presence of iron hydroxide NPs, which have not been converted to nano-oxides. The inverse spinel structure consist of $(Fe^{3+}_{tetrahedral})(Fe^{2+}_{octahedral}, Fe^{3+}_{octahedral})O_4$ with a face centred cubic lattice of O^{2-} (Figure 4.12) [38]. It has been reported that Fe^{2+} occupies half of the octahedral sites while Fe^{3+} cations reside in the tetrahedral sites and the remaining octahedral lattice sites. In several reports, attempts have been made to identify α-Fe_2O_3 and γ-Fe_2O_3 with XRD analysis by the JCPDS files 33-0664 and 39-1346, respectively [39-42].

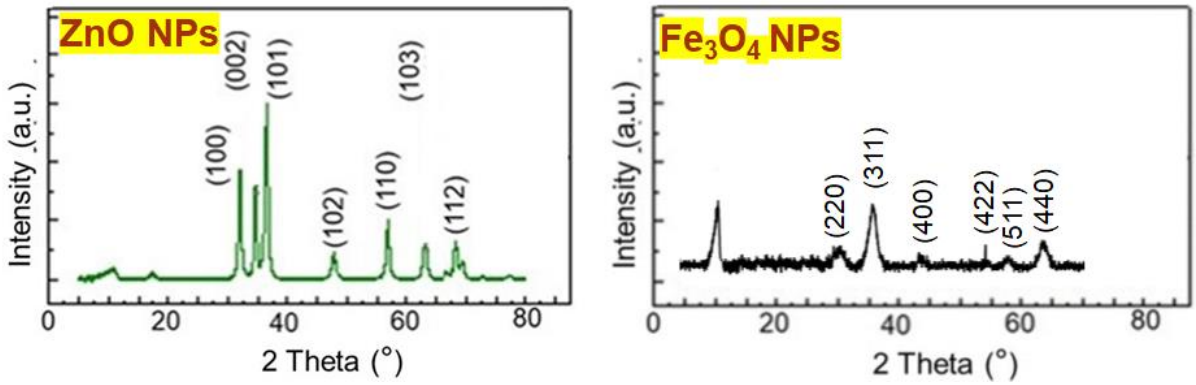


Figure 4. 11: XRD patterns of the developed nano-metal oxides.

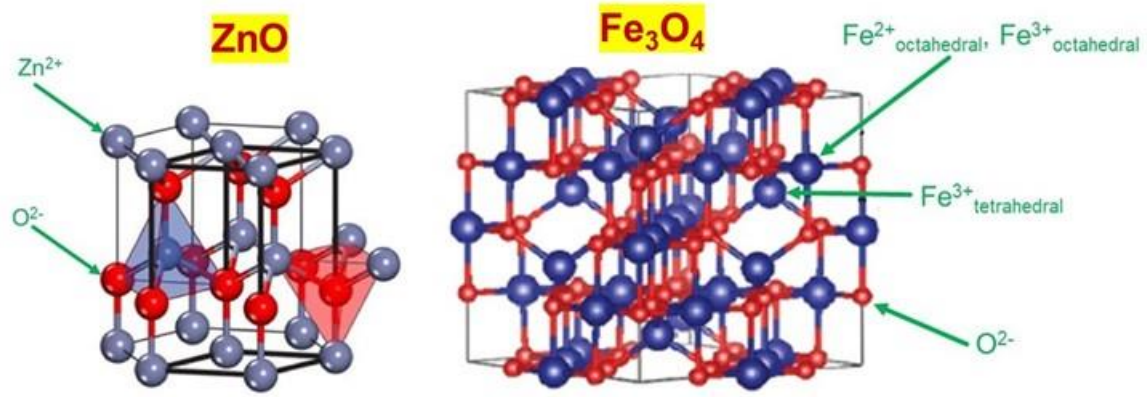
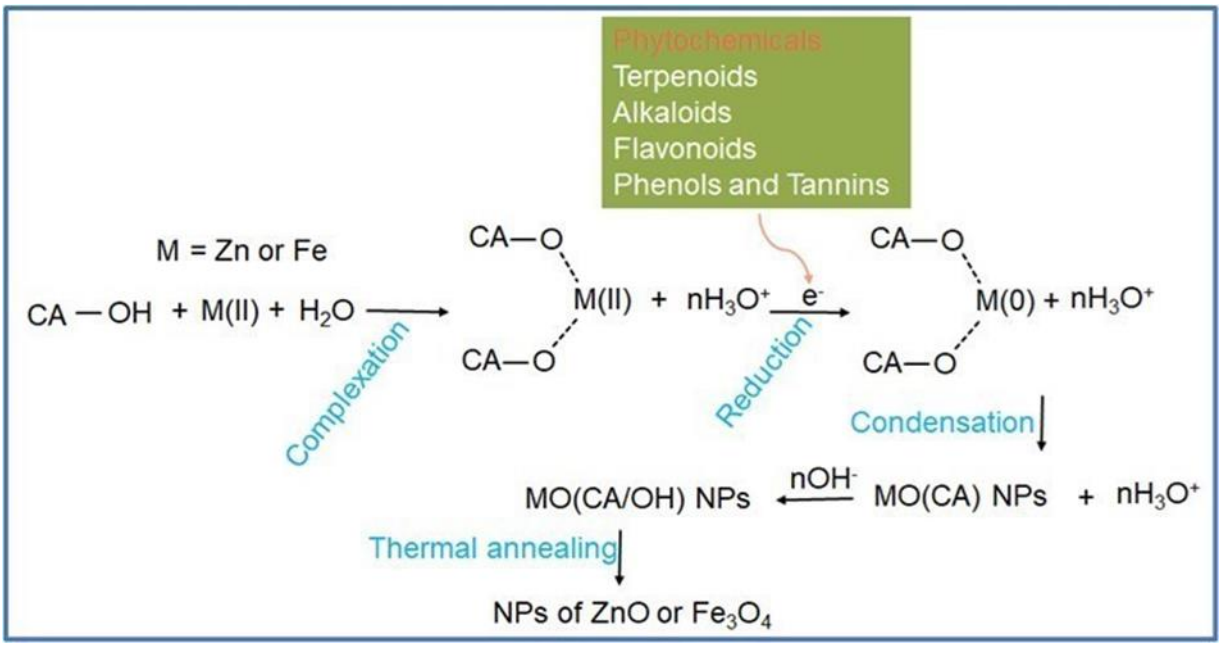


Figure 4. 12: Wurtzite ZnO structure and inverse spinel structure of Fe_3O_4.

It is anticipated that the divalent metal ions, Zn(II) and Fe(II), coordinate with the phytochemicals present in the *H. odoratissimum* extract, followed by their reduction to zero-valent metal and condensation of the metal clusters formed during the aging process [43]. The hydronium ions released are neutralized during pH adjustment, and the hydrous metal oxide NPs stabilized with phytochemicals are exposed. The

initial development of metastable intermediates, such as the amorphous metal clusters, that crystallize through non-classical pathways can lead to the precipitation of nano-zinc and -iron oxides (ZnO and FeO). A mechanistic study proposed by Sun and co-workers (2012) [44] also showed that FeO nanostructures are converted to Fe_3O_4 NPs by hetero-nucleation in the presence of oleic acid. A study by Hou et al. (2007) on the chemical conversion of FeO NPs also showed that these nanostructures undergo chemical and structural changes into various iron oxide nanoparticles (Fe_3O_4, α-Fe_2O_3, and γ-Fe_2O_3) at elevated temperatures [45]. Iron is a highly reactive transition metal that can form the oxides FeO, Fe_2O_3 and Fe_3O_4, with the latter being described as the most stable iron oxide [46].

Aging solutions have been used in complement to the precipitation and sol-gel methods for the preparation of nano-metal oxides such as TiO_2, CeO_2, Fe_3O_4, and ZnO [47-50]. This slow process controls the nucleation and chemical composition of the solid phase in solutions [49]. The reaction of an aqueous solution of $FeSO_4.7H_2O$ salt with the leaf extract of *Ziziphus mauritiana* has recently been reported by Karu et al. (2022) for the development of FeO NPs [51]. Considering the above information from the literature, the high concentrations of compounds with higher proton-donating capacities (CA) in *H. odoratissimum* extract, and the structural results of the prepared oxides, a plausible mechanism for developing metal oxide NPs is proposed.



Scheme 4. 1: A plausible reaction mechanism for the development of metal oxide (MO) NPs in *H. odoratissimum* extract.

REFERENCES

1. Karunakaran, G.; Suriyaprabha, R.; Manivasakan, P.; Rajendran, V. & Kannan, N. 2014. Influence of nano and bulk SiO_2 and Al_2O_3 particles on PGPR and soil nutrient contents. *Current Nanoscience*, 10, 604-612.

2. Siddiqui, M. H. & Al-Whaibi, M. H. 2014. Role of nano-SiO_2 in germination of tomato (*Lycopersicum esculentum* seeds Mill.). *Saudi Journal of Biological Sciences*, 21, 13-17.

3. Younes, N.; Hassan, H. S.; Elkady, M. F.; Hamed, A. & Dawood, M. F. 2020. Impact of synthesized metal oxide nanomaterials on seedlings production of three *Solanaceae* crops. *Heliyon* , 6, e03188.

4. Ahmad, A.; Hashmi, S.S.; Palma, J.M. & Corpas, F.J. 2022. Influence of metallic, metallic oxide, and organic nanoparticles on plant physiology. *Chemosphere*, 290, 133329.

5. Al Jabri, H.; Saleem, M.H.; Rizwan, M.; Hussain, I.; Usman, K. & Alsafran, M. 2022. Zinc oxide nanoparticles and their biosynthesis: Overview. *Life 12*, 594.

6. Vijayaram, S.l; Razafindralambo, H.; Sun, Y.Z.; Vasantharaj, S.; Ghafarifarsani, H.; Hoseinifar, S.H. & Raeeszadeh, M. 2023. Applications of green synthesized metal nanoparticles—A review. *Biological Trace Element Research*, 1-27.

7. Asekun, O. T.; Grierson, D. S. & Afolayan, A. J. 2007. Characterization of essential oils from *Helichrysum odoratissimum* using different drying methods. *Journal of Applied Sciences*, 7, 1005-1008.

8. Odeyemi, S. & Bradley, G. 2018. Medicinal plants used for the traditional management of diabetes in the Eastern Cape, South Africa: Pharmacology and toxicology. *Molecules*, 23, 2759.

9. De Canha, M. N.; Komarnytsky, S.; Langhansova, L. & Lall, N. 2020. Exploring the anti-acne potential of Impepho [*Helichrysum odoratissimum* (L.) Sweet] to combat *Cutibacterium acnes* virulence. *Frontiers in Pharmacology*, 10, 1559.

10. Lawal, O. A.; Ogunwande, I. A.; Kasali, A. A.; Opoku, A. R. & Oyedeji, A. O. 2015. Chemical composition, antibacterial and cytotoxic activities of essential oil from the leaves of *Helichrysum odoratissimum* grown in South Africa. *Journal of Essential Oil Bearing Plants*, 18(1), 236-241.

11. Plonska-Brzezinska, M. E.; Bobrowska, D. M.; Sharma, A.; Rodziewicz, P.; Tomczyk, M.; Czyrko, J. & Brzezinski K. 2015. Triple helical collagen-like peptide interactions with selected polyphenolic compounds. *RSC Advances*, 5(116), 95443-95453.

12. Markham, K. R. 1982. Techniques of flavonoid identification. *Academic Press*, 113.

13. Souza, M.; José Comin, J.; Moresco, R.; Maraschin, M.; Kurtz, C.; Emílio Lovato, P.; Rogério Lourenzi, C.; Pilatti, F.K., Loss, A. & Kuhnen, S. 2021. Exploratory and discriminant analysis of plant phenolic profiles obtained by UV–vis scanning spectroscopy. *Journal of Integrative Bioinformatics*, 18(3), 20190056.

14. Serabele, K.; Chen, W.; Tankeu, S.; Combrinck, S.; Veale, C. G. L.; van Vuuren, S.; Chaudhary, S. K. & Viljoen, A. 2021. Comparative chemical profiling and antimicrobial activity of two interchangeably used 'Imphepho' species (*Helichrysum odoratissimum* and *Helichrysum petiolare*). *South African Journal of Botany*, 137, 117-132.

15. Twilley, D.; Moodley, D.; Rolfes, H.; Moodley, I.; McGaw, L. J.; Madikizela, B. & Lall, N. 2021. Ethanolic extracts of South African plants, *Buddleja saligna* Willd. and *Helichrysum odoratissimum* (L.) Sweet, as multifunctional ingredients in sunscreen formulations. *South African Journal of Botany*, 137, 171-182.

16. De Canha, M. N.; Komarnytsky, S.; Langhansova, L. & Lall, N. 2020. Exploring the anti-acne potential of Impepho [*Helichrysum odoratissimum* (L.) sweet] to combat *Cutibacterium acnes* virulence. *Frontiers in Pharmacology*, 10, 1559.

17. Bandeira, M.; Possan, A. L.; Pavin, S. S.; Raota, C. S.; Vebber, M. C.; Giovanela, M.; Roesch-Ely, M.; Devine, D. M. & Crespo, J. S. 2020.

Mechanism of formation, characterization and cytotoxicity of green synthesized zinc oxide nanoparticles obtained from *Ilex paraguariensis* leaves extract. *Nano-Structures & Nano-Objects*, 24, 100532.

18. Martynova, N. A.; Umedov, S. T.; Lepnev, L. S.; Komarova, M. Y. & Grigorieva, A. V. 2020. Electrochemicaly formed ZnO and Au/ZnO opal films. *SN Applied Sciences*, 2, 560.

19. Zhang, W. & Lai, E. P. C. 2020. Electrochemical detection of zinc oxide nanoparticles in water contamination analysis based on surface catalytic reactivity. *Journal of Nanoparticle Research*, 22, 95.

20. Patil, S. A.; Shinde, D. V.; Ahn, D. Y.; Patil, D. V.; Tehare, K. K.; Jadhav, V. V.; Lee, J. K.; Mane, R. S.; Shrestha, N. K. & Han, S.-H. 2014. A simple, room temperature, solid-state synthesis route for metal oxide nanostructures. *Journal of Materials Chemistry A*, 2(33) 13519-13526.

21. Singh, J.; Kumar, S.; Alok, A.; Upadhyay, S. K.; Rawat, M.; Tsang, D. C. W.; Bolan, N. & Kim, K.-H. 2019. The potential of green synthesized zinc oxide nanoparticles as nutrient source for plant growth. *Journal of Cleaner Production*, 214, 1061-1070.

22. Santhoshkumar, J.; Kumar, S. V. & Rajeshkumar, S. 2017. Synthesis of zinc oxide nanoparticles using plant leaf extract against urinary tract infection pathogen. *Resource-Efficient Technologies*, 3(4), 459-465.

23. Abdallah R. M. & S Al-Haddad R. M. 2021. Optical and morphology properties of the magnetite (Fe_3O_4) nanoparticles prepared by green method. *Journal of Physics: Conference Series*, 1829, 012022.

24. Krajczewski, J.; Kołątaj, K. & Kudelski, A. 2017. Plasmonic nanoparticles in chemical analysis. *RSC Advances*, 7(28), 17559-17576.

25. Rhodes, C.; Franzen, S.; Maria, J. P.; Losego, M.; Leonard, D. N.; Laughlin, B. & Weibel, S. 2006. Surface plasmon resonance in conducting metal oxides. *Journal of Applied Physics*, 100(5).

26. El-Seedi, H. R.; El-shabasy, R. M.; Khalifa, S. A. M.; Saeed, A.; Shah, A.; Shah, R.; Iftikhar, F. J.; Abdel-Daim, M. M.; Omri, A.; Hajrahand, N. H.; Sabir, J. S. M.; Zou, X.; Halabi, M. F.; Sarhan, W. & Guo W. 2019. Metal nanoparticles fabricated by green chemistry using natural extracts: Biosynthesis, mechanisms, and applications. *RSC Advances*, 9(42), 24539-24559.

27. De Canha, M. N.; Thipe, V. C.; Katti, K. V.; Mandiwana, V.; Kalombo, M. L.; Ray, S. S.; Rikhotso, R.; van Vuuren, A. J. & Lall, N. 2021. The activity of gold nanoparticles synthesized using *Helichrysum odoratissimum* against *Cutibacterium acnes* biofilms. *Frontiers in Cell and Developmental Biology*, 9, 675064.

28. Adams, S. A.; Hauser, J. L.; Allen, A. L. C.; Lindquist, K. P.; Ramirez, A. P.; Oliver, S. & Zhang, J. Z. 2018. Fe_3O_4@ SiO_2 nanoparticles functionalized with gold and poly (vinylpyrrolidone) for bio-separation and sensing applications. *ACS Applied Nano Materials*, 1(3), 1406-1412.

29. Schwartzberg, A. M.; Grant, C. D.; Wolcott, A.; Talley, C. E.; Huser, T. R.; Bogomolni, R. & Zhang, J. Z. 2004. Unique gold nanoparticle aggregates as a highly active surface-enhanced Raman scattering substrate. *The Journal of Physical Chemistry B*, 108(50), 19191-19197.

30. Chauhan, S. & Upadhyay, L. S. B. 2019. Biosynthesis of iron oxide nanoparticles using plant derivatives of *Lawsonia inermis* (Henna) and its surface modification for biomedical application. *Nanotechnology for Environmental Engineering*, 4, 1-10.

31. Bundit, O. & Wongsaprom, K. 2018. Shape control in zinc oxide nanostructures by precipitation method. *Journal of Physics: Conference Series*, 1144, 012044.

32. Lesiak, B.; Rangam, N.; Jiricek, P.; Gordeev, I.; Tóth, J.; Kövér, L.; Mohai, M. & Borowicz, P. 2019. Surface study of Fe_3O_4 nanoparticles functionalized with biocompatible adsorbed molecules. *Frontiers in Chemistry*, 7, 642.

33. Padalia, H. & Chanda, S. 2017. Characterization, antifungal and cytotoxic evaluation of green synthesized zinc oxide nanoparticles using *Ziziphus*

nummularia leaf extract. *Artificial Cells, Nanomedicine, and Biotechnology*, 45(8), 1751-1761.

34. Yew, Y. P.; Shameli, K.; Miyake, M.; Kuwano, N.; Bt Ahmad Khairudin, N. B.; Bt Mohamad, S. E. & Lee K. X. 2016. Green synthesis of magnetite (Fe_3O_4) nanoparticles using seaweed (*Kappaphycus alvarezii*) extract. *Nanoscale Research Letters*, 11, 276.

35. Liang, H.; Xing, H.; Qin, M. & Wu, H. 2020. Bamboo-like short carbon fibers@ Fe_3O_4@ phenolic resin and honeycomb-like short carbon fibers@ Fe_3O_4@ FeO composites as high-performance electromagnetic wave absorbing materials. *Composites Part A: Applied Science and Manufacturing*, 135, 105959.

36. Khan, M. R.; Hoque, S. M.; Binte Hossain, K. F.; Bakar Siddique, M. A.; Uddin, M. K. & Rahman, M. M. 2020. Green synthesis of silver nanoparticles using *Ipomoea aquatica* leaf extract and its cytotoxicity and antibacterial activity assay. *Green Chemistry Letters and Reviews*, 13(4), 39-51.

37. Jamzad, M. & Kamari Bidkorpeh, M. 2020. Green synthesis of iron oxide nanoparticles by the aqueous extract of *Laurus nobilis* L. leaves and evaluation of the antimicrobial activity. *Journal of Nanostructure in Chemistry*, 10, 193-201.

38. Taimoory S. M.; Trant, J. F.; Rahdar, A.; Aliahmad, M.; Sadeghfar, F. & Hashemzaei, M. 2017. Importance of the inter-electrode distance for the electrochemical synthesis of magnetite nanoparticles: synthesis, characterization, computational modelling, and cytotoxicity. *e-Journal of Surface Science and Nanotechnology*, 15, 31-39.

39. Han, Q.; Liu, Xu, Y.; Chen, Wang & Zhang, H. 2007. Growth and properties of single-crystalline γ-Fe_2O_3 nanowires. *The Journal of Physical Chemistry C*, 111(13), 5034-5038.

40. Ajinkya, N.; Yu, X.; Kaithal, P.; Luo, H.; Somani, P. & Ramakrishna, S. 2020. Magnetic iron oxide nanoparticle (IONP) synthesis to applications: present and future. *Materials*, 13(20), 4644.

41. Wang, F.; Qin, X. F.; Meng, Y. F.; Guo, Z. L.; Yang, L. X. & Ming, Y. F. 2013. Hydrothermal synthesis and characterization of α-Fe_2O_3 nanoparticles. *Materials Science in Semiconductor Processing*, 16(3), 802-806.

42. Cao, D.; Li, H.; Pan, L.; Li, J.; Wang, X.; Jing, P.; Jing, P.; Wang, J. & Liu, Q. 2016. High saturation magnetization of γ-Fe_2O_3 nanoparticles by a facile one-step synthesis approach. *Scientific Reports*, 6(1), 32360.

43. Dupuis, R.; Ho Hahn, S.; van Duin, A. C. T.; Pellenq, R. J.-M. & Poulesquen, A. 2022. Condensation and growth of amorphous aluminosilicate nanoparticles via an aggregation process. *Physical Chemistry Chemical Physics*, 24(16), 9229-9235.

44. Sun, H.; Chen, B.; Jiao, X.; Jiang, Z.; Qin, Z. & Chen, D. 2012. Solvothermal synthesis of tunable electroactive magnetite nanorods by controlling the side reaction. *Journal of Physical Chemistry C*, 116(9), 5476-5481.

45. Hou, Y.; Xu, Z. & Sun, S. 2007. Controlled synthesis and chemical conversions of FeO nanoparticles. *Angewandte Chemie International Edition*, 46(33), 6329-6332.

46. Genuzio, F.; Sala, A.; Schmidt, T.; Menzel, D. & Freund, H. J. 2014. Interconversion of α-Fe_2O_3 and Fe_3O_4 thin films: mechanisms, morphology, and evidence for unexpected substrate participation. *The Journal of Physical Chemistry C*, 118(50), 29068-29076.

47. Chigondo, M.; Paumo, H. K.; Bhaumik, M.; Pillay, K. & Maity, A. 2018. Hydrous CeO_2-Fe_3O_4 decorated polyaniline fibers nanocomposite for effective defluoridation of drinking water. *Journal of Colloid and Interface Science*, 532, 500-516.

48. Mukhopadhyay, K.; Ghosh, A.; Das, S. K.; Show, B.; Sasikumar, P. & Ghosh, U. C. 2017. Synthesis and characterisation of cerium(IV)-incorporated hydrous iron(III) oxide as an adsorbent for fluoride removal from water. *RSC Advances*, 7, 26037-26051.

49. Jasbi, N. E. & Dorranian, D. 2016. Effect of aging on the properties of TiO_2 nanoparticle, *Journal of Theoretical and Applied Physics*, 10, 157-161.

50. Sheikhi, S.; Aliannezhadi, M. & Tehrani, F. S. 2022. Effect of precursor material, pH, and aging on ZnO nanoparticles synthesized by one-step sol–gel method for photodynamic and photocatalytic applications, *The European Physical Journal Plus*. 137, 60.

51. Karu, E.; Magaji, B. & Bello, A. M. 2022. Green synthesis, spectroscopic analysis, and stabilisation energy of iron oxide nanoparticles from aqueous Ziziphus leaf extract. *Bima Journal of Science and Technology* (2536-6041), 6(03), 40-49.

CHAPTER 5

CHARACTERIZATION OF NUTRIENT-LOADED CHITOSAN NANOPARTICLES

Biopolymers are gaining close attention for the development of eco-friendly and sustainable products due to their innocuous nature, biodegradability, and large volume availability of the bio precursors [1]. Among these, chitosan represents one of the most abundant materials with versatile applications, including food packaging, beverages, pharmaceuticals, textiles, cosmetics, and agriculture [2]. Chitosan is obtained from the structural modification (*N*-deacetylation) of chitin, a constituent of the extracellular matrix of arthropods, sponges, and fungi. Its molecular structure consists of *β*-(1→4)-2-acetamido-*D*-glucose and *β*-(1→4)-2-amino-*D*-glucose repeating units. The presence of hydroxyl and amino groups along the polymeric chain of chitosan influences its solubility and manipulation. The hydrogen bonding network of chitosan material is responsible for its low solubility in water, representing a major limitation in agricultural applications [3]. However, in an acidic *milieu*, the amino groups get protonated and increase the solubility of chitosan. The prompted cationic matrix can interact with crosslinking agents to generate chitosan nanoscale particles with high sorption capability toward the water. This process can also be exploited to encapsulate potentially toxic nutrients plants need and achieve nanofertilizers with slow-release conduct. The positively charged chitosan can adhere to the negatively charged surface of the nano-metal oxides and facilitate their encapsulation in polymeric nanostructures. This project adopted the ionic gelation process because of its simplicity and high reactivity.

5.1 Microscopic and spectroscopic analysis of the nutrient-loaded chitosan nanoparticles

5.1.1 Electron microscopy

The morphological characteristic of the CS/TPP NPs and nutrient-loaded CS/TPP NPs was examined using SEM imaging, as shown in Figures 5.1, 5.2, and 5.4. These exhibited spherically shaped NPs of various sizes. Images of the metal oxide-loaded CS/TPP NPs presented uneven nano-aggregate shapes, suggesting a higher degree of electrostatic attraction at some areas of the visualized sample. This

evidence, complemented by TEM (Figure 5.3), establishes the efficacy of the ionic gelation procedure to induce the agglomeration of nanostructures during the introduction of the metal oxide nano-powders. Contrastingly, SEM images of the Zn(II)-laden CS/TPP NPs and Fe(II)-laden CS/TPP NPs show spherical-like shapes in superior gelling systems. The divalent metal ions (Zn(II) and Fe(II)) undergo complexation with the amino and hydroxyl groups on the chitosan, increasing the viscosity of the polymeric solution and organization of the CS/TPP network [4]. The small radius-to-charge ratio of these metal ions is accountable for their pronounced Lewis acid property, and this justifies their ability to stabilize with N- and O-donors of the CS/TPP matrix. The complexation efficiency calculations show that 46.1% of Zn and 32.6% of Fe were available in the integrated form within the CS/TPP NPs for Zn(II)-laden CS/TPP NPs and Fe(II)-laden CS/TPP NPs, respectively.

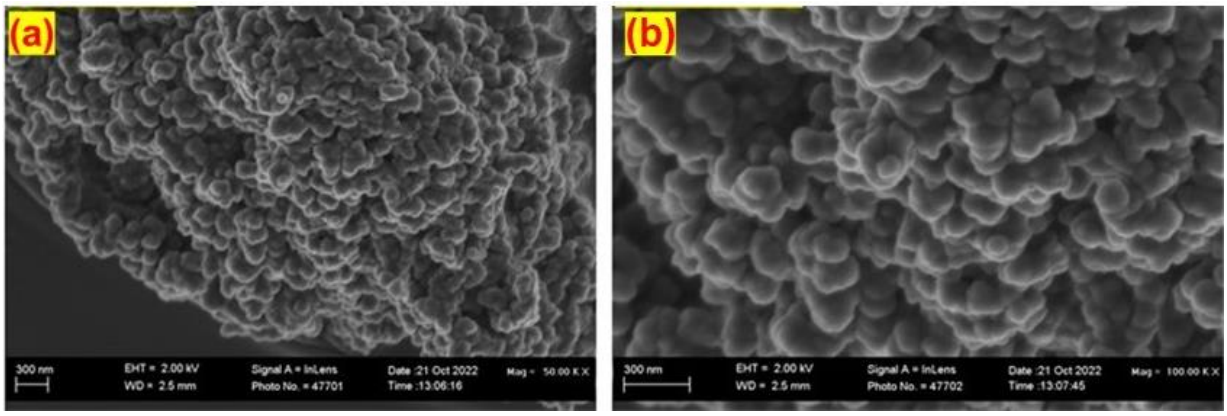


Figure 5. 1: SEM images of CS/TPP NPs at two different magnifications of (a) 50 and (b) 100.

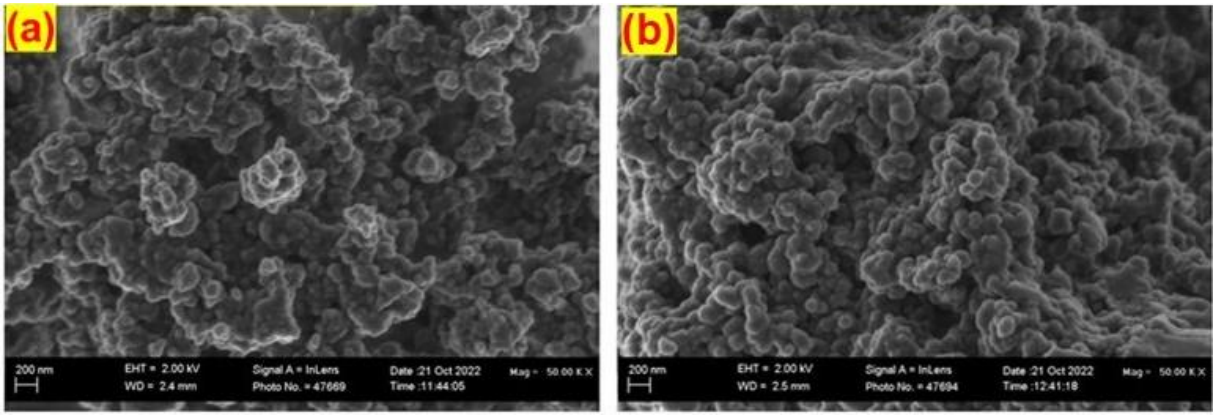


Figure 5.2: SEM images of (a) ZnO-loaded CS/TPP NPs and (b) Fe_3O_4-loaded CS/TPP NPs.

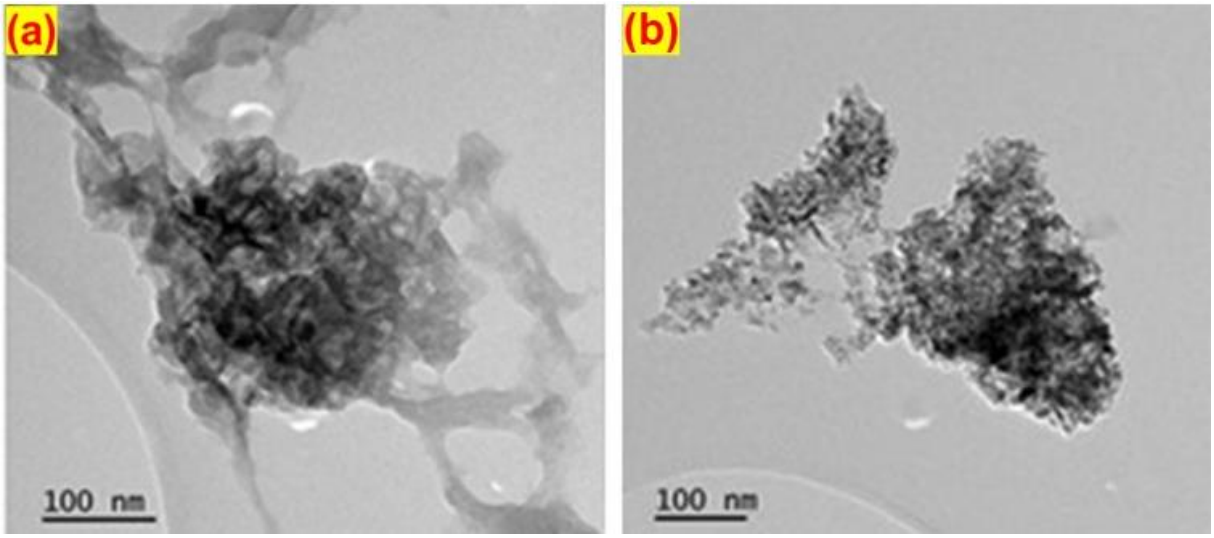


Figure 5. 3: TEM images of (a) ZnO-loaded CS/TPP NPs and (b) Fe_3O_4-loaded CS/TPP NPs.

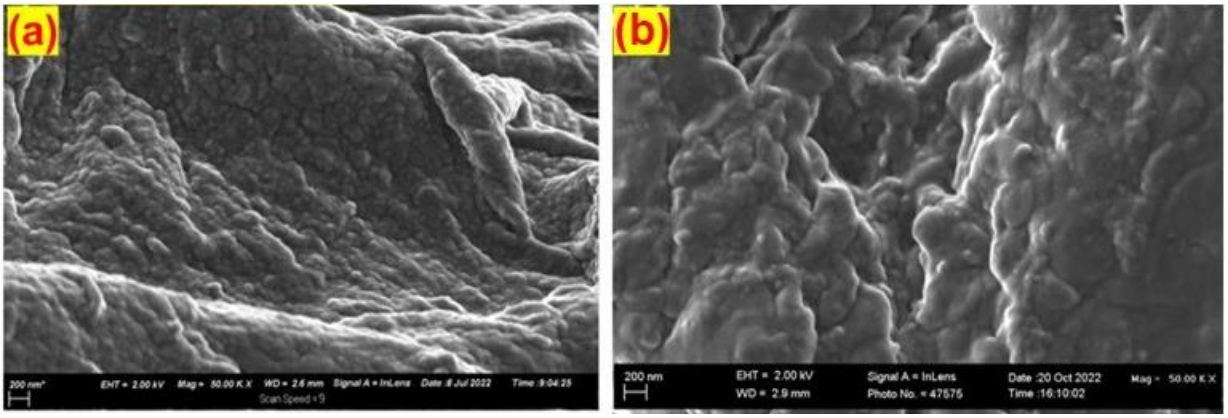


Figure 5. 4: SEM images of Zn(II)-laden CS/TPP and Fe(II)-laden CS/TPP NPs.

To analyse the distribution of nutrients on the loaded CS/TPP NPs, the elemental mapping of Zn(II)-laden CS/TPP NPs was conducted, and the images are shown in Figure 5.5. These reveal a uniform distribution of Zn, P, O, and C. Peaks conforming to these elements are detected at energy values of 1.012, 2.013, 0.525, and 0.277 keV, respectively.

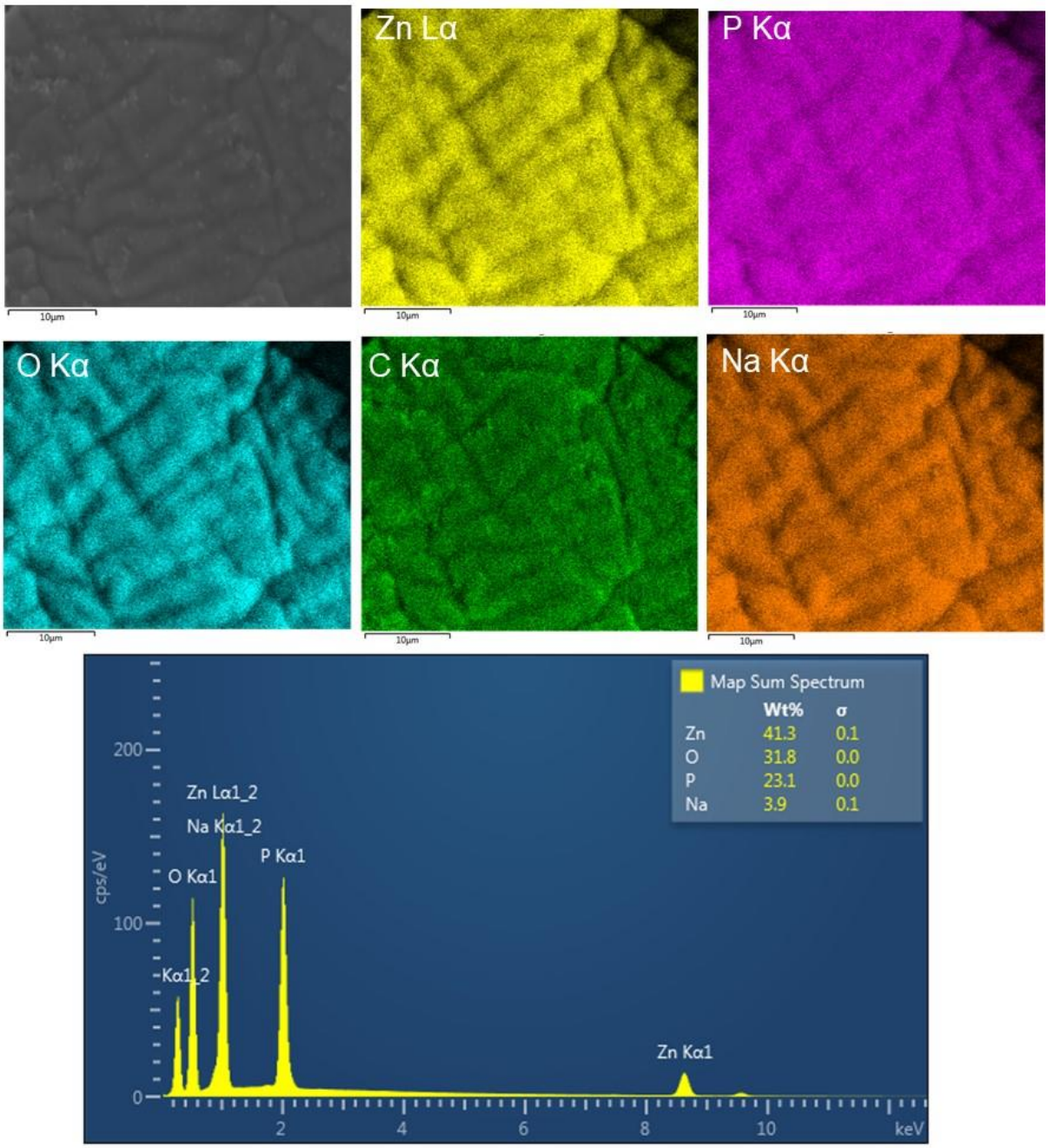


Figure 5. 5: Elemental maps (Zn, P, O, C, and Na) and EDX spectrum of Zn(II)-laden CS/TPP NPs.

5.1.2 Average particle size and surface charge

CS/TPP NPs are forming instantly through the Coulombic interaction between the positively charged amino groups of chitosan and the negatively charged phosphate groups of TPP. The average hydrodynamic size and zeta potential of CS/TPP NPs prepared in this study are 149.4 ± 22.3 nm and 19.7 mV, respectively (Table 5.1, see Appendix). Treatment of the nano-metal oxides or their precursors (Zn^{2+}/Fe^{2+}) with

chitosan solution in the presence of TPP crosslinking agent, generated particles with larger sizes 195.0-498.8 nm, as compared to pristine CS/TPP NPs (Figure 5.6 and 5.7). The PDI value ranges from 0.197 to 0.410. These are more often considered acceptable for polymeric nanomaterials [5]. The Fe_3O_4[10s]-, Fe_3O_4[15s]-, and Fe(II)-laden CS/TPP NPs showed the highest stability in aqueous solution, as made evident by their surface potential 24.4, 27.3, and 27.4 mV, respectively. This characteristic is considered a significant determinant of the biological interactions of NPs and their permeability across physiological barriers [6]. A study by Arakha and colleagues (2015) [7] reported the enhanced antibacterial activity of chitosan-coated Fe_3O_4 NPs with a surface charge of 36.3 mV. The free ZnO and Fe_3O_4 NPs showed a negative surface charge, while the CS/TPP NPs, ZnO-loaded CS/TPP NPs, Zn(II)-laden CS/TPP NPs, Fe_3O_4-loaded CS/TPP NPs, Fe(II)-laden CS/TPP NPs exhibited a positive charge due to the presence of ionized amino groups of chitosan, which formed the shell of the CS/TPP NPs. These developed through the formation of CS-TPP complexes, which are further bridge crosslinked into ordered colloids by excess TPP.

Entrapment of the prepared metal oxides within polysaccharide-based nanoparticles takes place through mechanisms like (i) the condensation of their surface hydroxyl groups and the hydroxyl groups of CS and TPP, and (ii) the coordination of the metal atoms to the P=O groups of TPP (Scheme 5. 1) [8, 9].

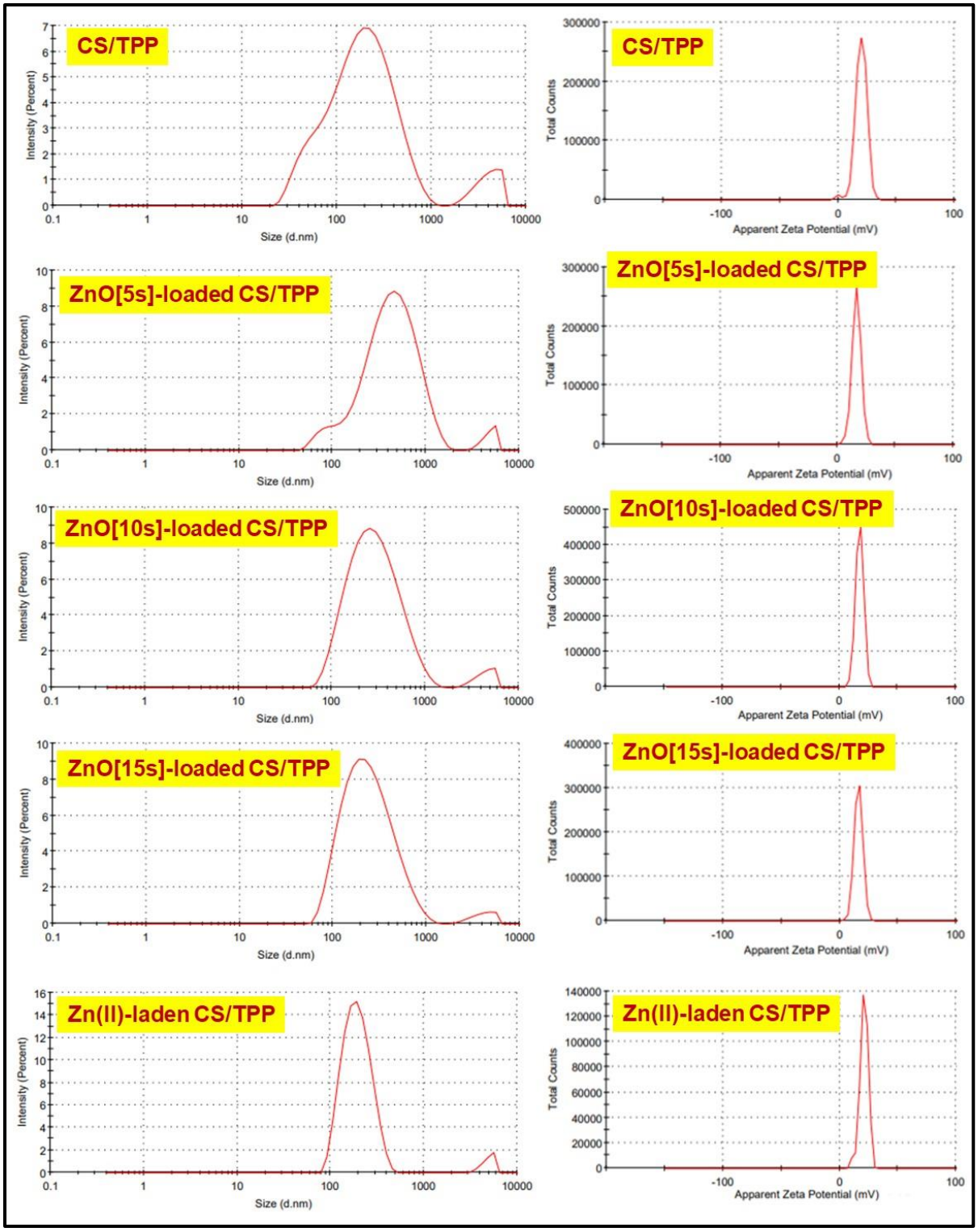


Figure 5. 6: DLS and zeta potential analysis of the CS/TPP, ZnO-loaded CS/TPP, and Zn(II)-laden CS/TPP NPs.

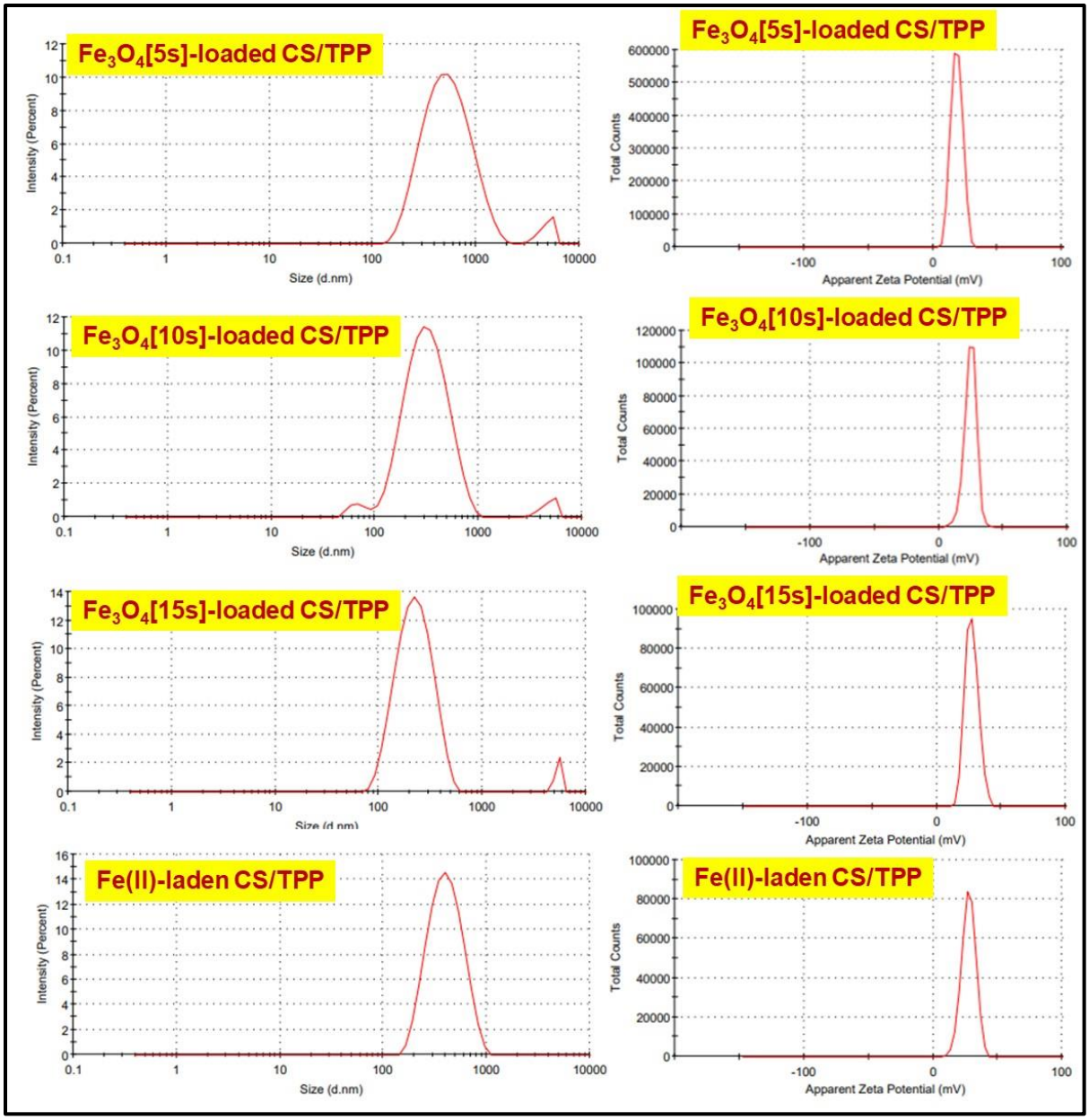
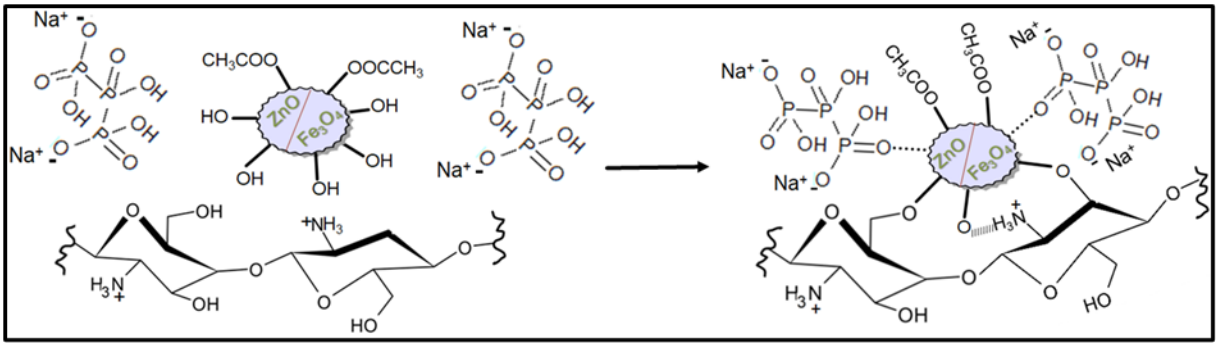


Figure 5. 7: DLS and zeta potential analysis of the Fe_3O_4-loaded CS/TPP and Fe(II)-laden CS/TPP NPs.



Scheme 5. 1: Interactions of the metal oxide surface with CS and TPP under acidic conditions.

5.1.3 FTIR spectral analysis

The FTIR spectra of CS/TPP, Zn(II)-laden CS/TPP, ZnO-loaded CS/TPP, Fe(II)-laden CS/TPP, and Fe_3O_4-loaded CS/TPP NPs were recorded and are presented in Figure 5.8. The CS/TPP NPs spectrum displays a broad band at 3177 cm^{-1} due to the combined stretches of O–H and N–H bonds in the biopolymer matrix, which matched with several studies [10, 11]. The small frequency at 2883 cm^{-1} is associated with the asymmetric and symmetric C–H stretching [12]. The bands at 1533 and 1392 cm^{-1} are assigned to C=O and C–N stretching modes, respectively. The bands detected at 1052 and 1008 cm^{-1} indicate the presence of TPP crosslinker [13,14]. These bands are attributed to the stretching vibration of the P=O and P–O bonds. The main differences observed between the spectrum of the CS/TPP NPs and the spectra of the metal ions-laden CS/TPP NPs include a drop in intensity of the bands corresponding to O–H/N–H and C=O/C–N vibrations, reflecting the complexation of metal ions with the heteroatoms of these functional groups. Also, characteristic bands attributed to Zn–O and Fe–O stretching modes are evidenced in the spectra of the ZnO-loaded CS/TPP NPs and Fe_3O_4-loaded CS/TPP NPs, respectively. These also show a significant change in the intensity of bands attributed to O–H/N–H and C=O/C–N stretching due to the electrostatic interaction of their postively charged forms with the negatively charged metal oxide.

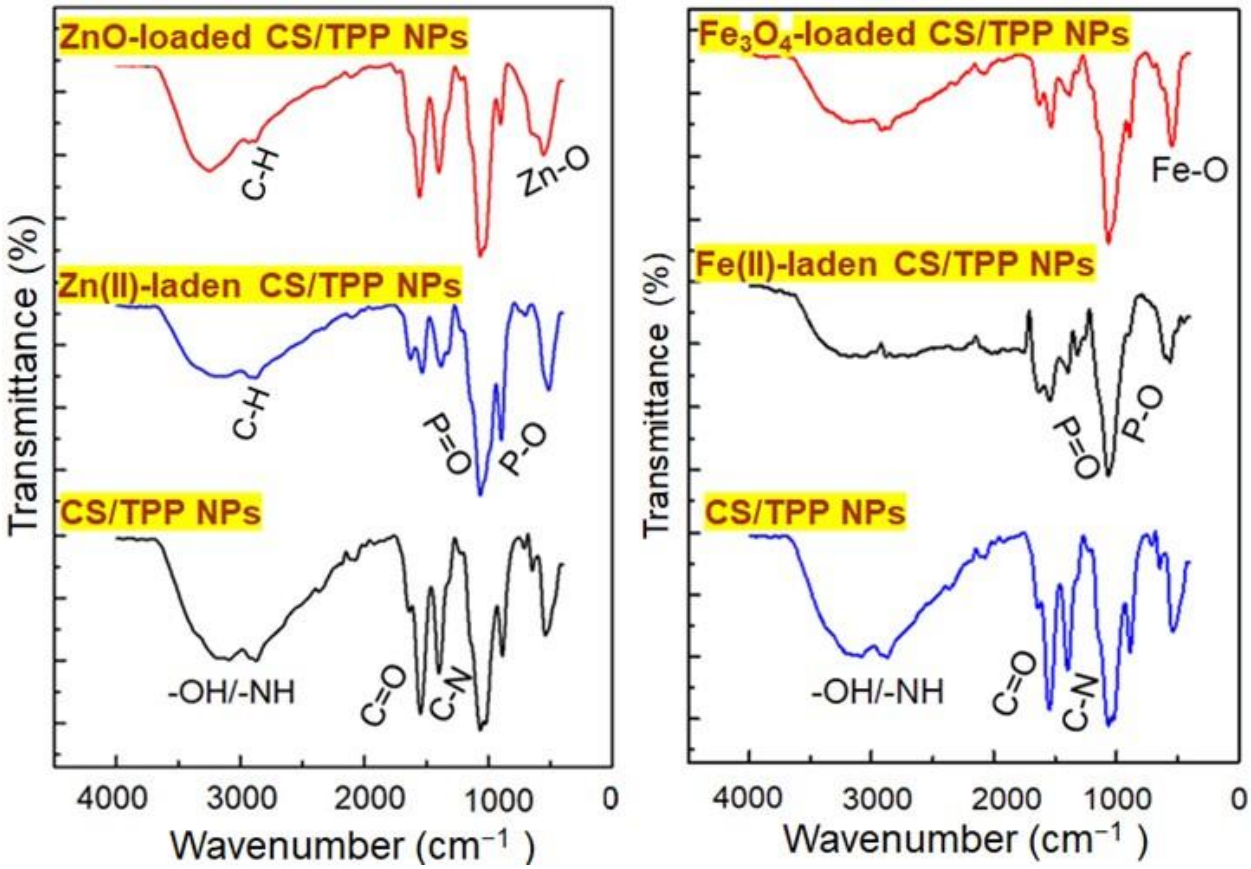


Figure 5. 8: FTIR spectra of pristine CS/TPP NPs and nutrient-loaded CS/TPP NPs.

5.1.4 Thermogravimetric analysis

TGA-DSC thermograms of ZnO-loaded CS/TPP NPs are presented in Figure 5.9. The thermal decomposition pattern observed is divided into several key stages. An initial mass loss of 12.6% between 25 and 180 °C is due to the loss of surface and absorbed water molecules [15]. The hygroscopic nature of CS/TPP nanostructures is responsible for the ability of nutrient-loaded-CS/TPP to absorb moisture. The most apparent weight loss stage of 31.4% recorded around 200-300 °C is attributed to ether bond cleavage in the chitosan skeleton [16]. The weight loss (5.3%) over the temperature range of 300-400 °C is most likely due to the cleavage of O–H and N–H bonds [17]. Above 400 °C, no further change in mass occurred. This thermal analysis indicated that the CS/TPP NPs were successfully modified with metal oxides.

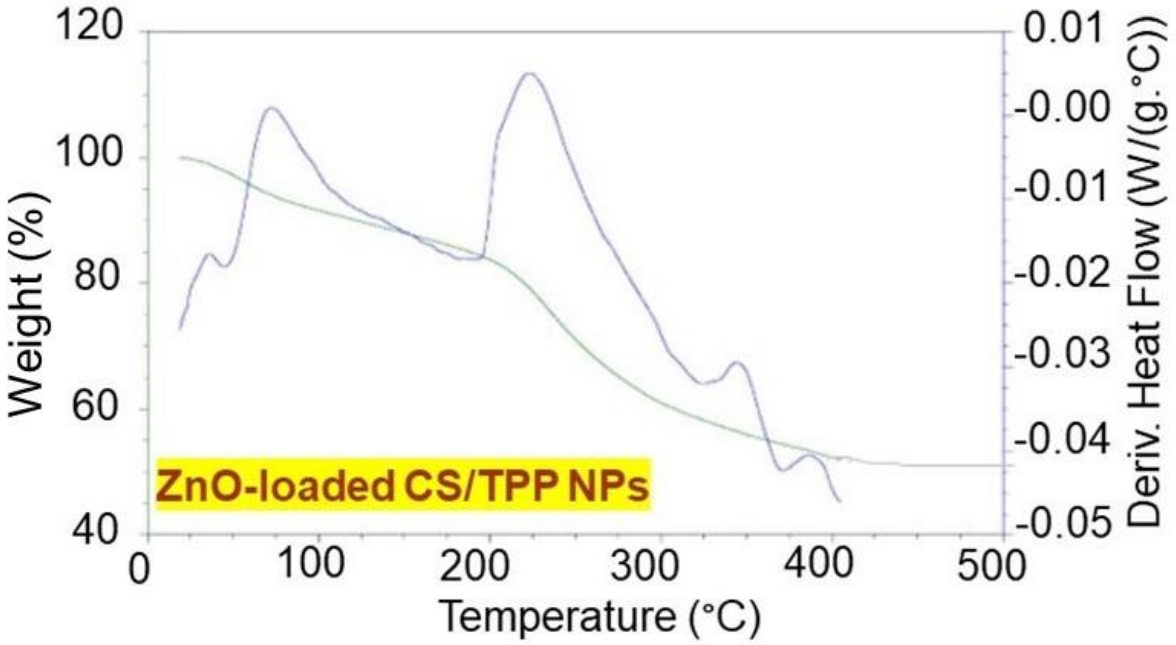


Figure 5. 9: TGA-DSC thermograms of ZnO-loaded CS/TPP NPs.

5.1.5 XPS spectra analysis

Data from the XPS spectra analysis were used to confirm the composition of the nutrient-loaded CS/TPP NPs. The XPS survey spectra of ZnO-loaded CS/TPP (Figures 5.10) and Zn(II)-laden CSTPP NPs (Figure 5.11) show the presence of zinc, oxygen, carbon, phosphorus, nitrogen, and sodium at their surface. These were evidenced by the presence of Zn 2s, Zn 2p, Zn 3p, C 1s, O 1s, O 2s, N 1s, P 2s, P 2p, P 3p, C Auger, O Auger, and Zn Auger peaks. In addition, contributions to the Na 1s and Na Auger peaks were also detected. These originated from an excess crosslinking agent in the synthesized NPs even after washing several times with deionized water. Figure 5.12 displays the XPS spectra of ZnO-loaded CS/TPP NPs at the core-level C 1s, O 1s, N 1s, and Zn 2p peaks. The C 1s peak was resolved into C=C (284.1 eV), C–C (284.7 eV), C–O (286.3 eV), C=O (287.1 eV), and O–C=O (288.1 eV) bonds [18]. The N 1s spectrum exhibits two deconvoluted peaks at 399.7 and 401.6 eV, contributions of $–NH_2$ and protonated $–NH_3^+$ amine groups [19, 20]. The high-resolution spectrum of O 1s was deconvoluted into three peaks at 528.3, 531.2, and 532.8 eV assigned to Zn–O, C–O, and C=O bonds, respectively [21]. The peaks at 133.6 and 1022.0 eV are contributions by P 2p of phosphate [22] and Zn $2p^{3/2}$ of Zn^{2+} in the ZnO lattice [23].

Table 5.2 (see Appendix) summarizes the location and assignment of characteristic peaks for ZnO-loaded CS/TPP NPs. Similar parameters are recorded with Zn(II)-laden CS/TPP NPs except for data obtained from the curve fitting of O 1s and spectrum of Zn 2p. While no deconvoluted peak attributed to the Zn–O bond (O^{2-} ions of ZnO structure) is observed, the high-resolution Zn 2p spectrum of Zn(II)-laden CS/TPP NPs can be deconvoluted to two peaks at 1022.4 and 1024.1 eV, suggesting dative coordination bonds of Zn^{2+} to N- and O-containing functional groups [20]. The parameters obtained through the individual peak profile fittings are shown in Figure 5.13 and summarized in Table 5.3 (see Appendix). From the C 1s characteristics shown in Tables 5.2 and 5.3, a significant decrease in atomic percentages corresponding to C–O and O–C=O bonds confirmed the presence of *H. odoratissimum* mediated metal oxide for ZnO-loaded CS/TPP nanoparticles, in comparison with Zn(II) laden CS/TPP NPs.

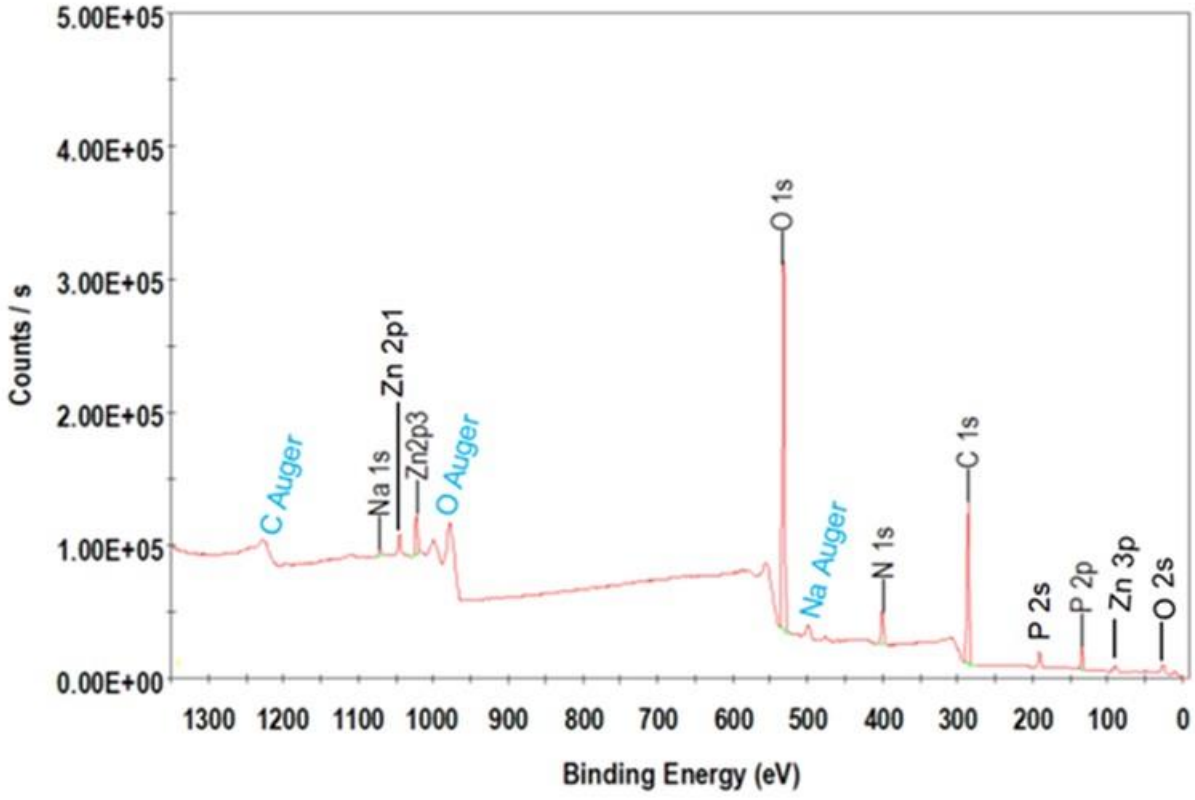


Figure 5. 10: XPS survey spectrum of ZnO-loaded CS/TPP NPs.

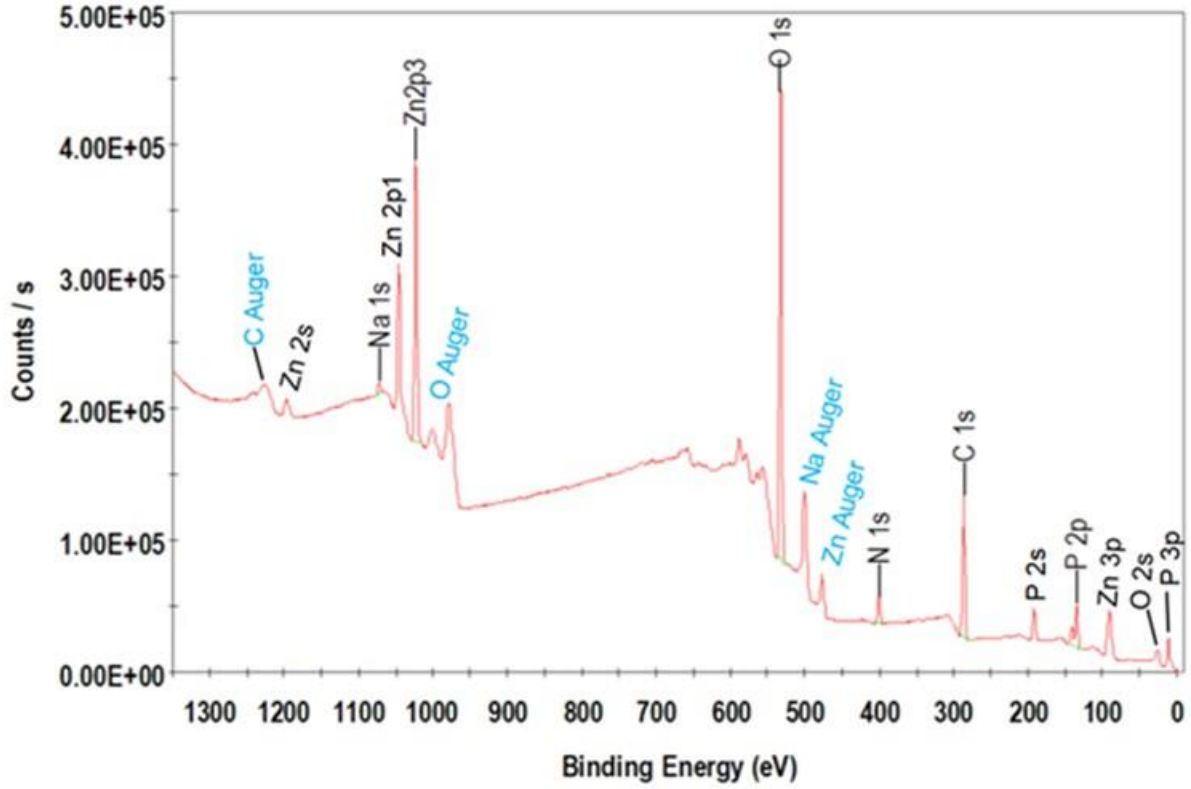


Figure 5. 11: XPS survey spectrum of Zn(II)-laden CS/TPP NPs.

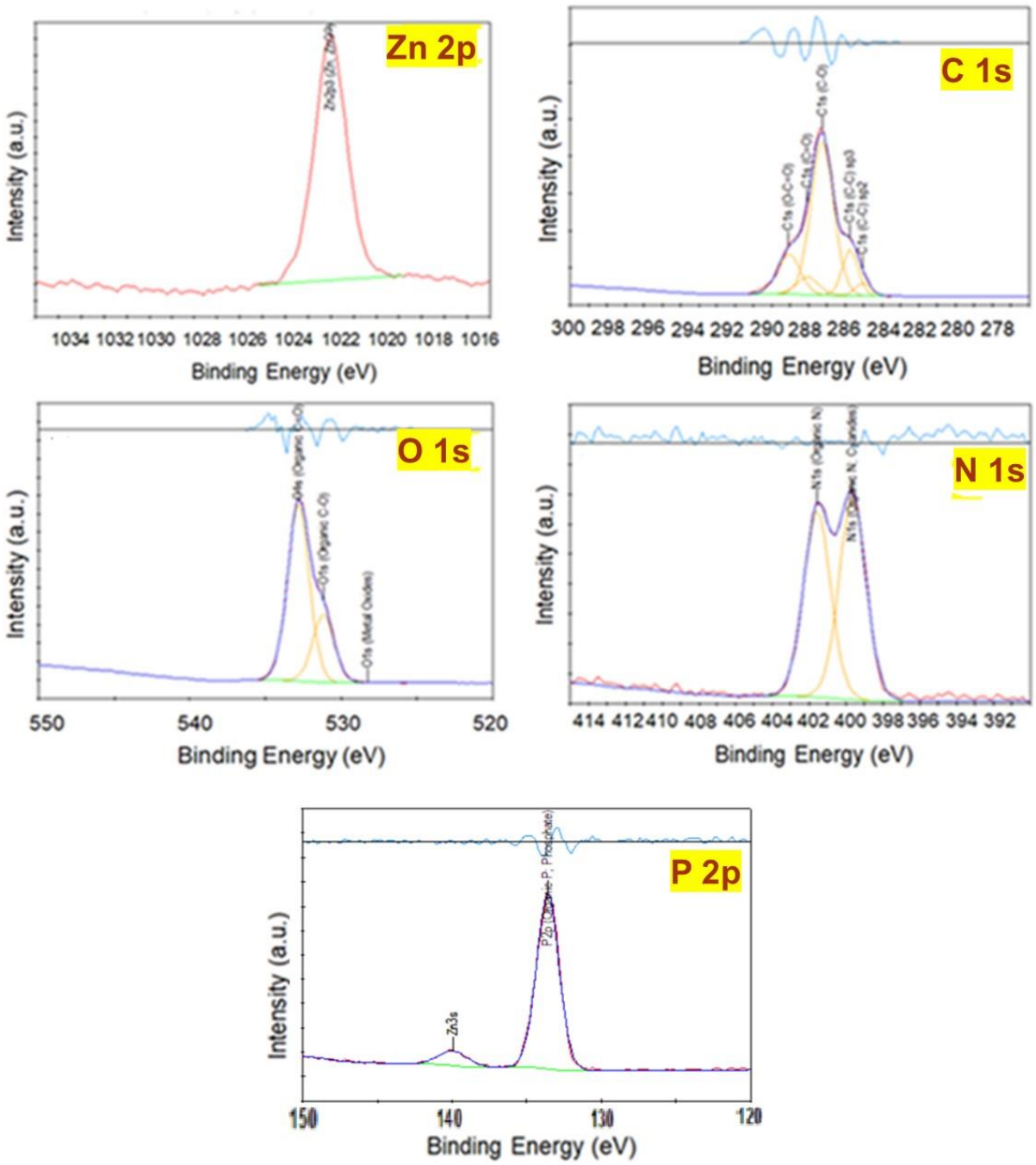


Figure 5. 12: High-resolution XPS spectra of Zn 2p, C 1s, O 1 s, N 1s, and P 2p of ZnO-loaded CS/TPP NPs.

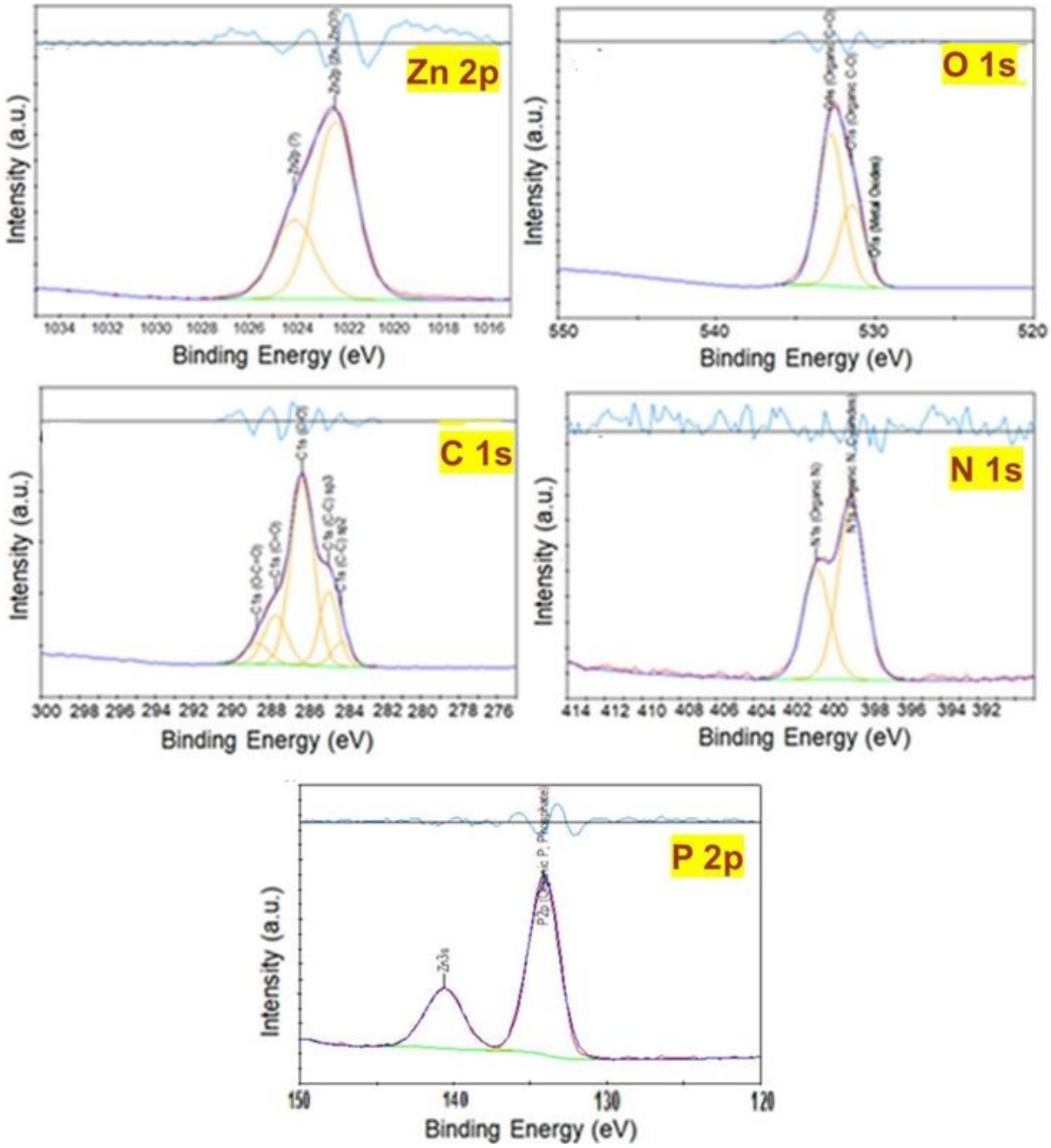


Figure 5. 13: High-resolution XPS spectra of Zn 2p, C 1s, O 1 s, and N 1s of Zn(Ⅱ)-laden CS/TPP NPs.

Figures 5.14 and 5.15 also display the representative survey scan of Fe_3O_4-loaded CS/TPP NPs and the high-resolution spectra of Fe 2p, O 1s, N 1s, and C 1s peaks. The Fe 2p high-resolution spectrum of this nanocomposite displays two distinctive photoelectron peaks at 710.8 and 724.6 eV corresponding to Fe $2p^{3/2}$ and Fe $2p^{1/2}$ states in iron oxide materials. In previous reports, It has been demostrated that the peak positions of Fe $2p^{3/2}$ and Fe $2p^{1/2}$ relate to the ionic states of Fe. Binding energy of Fe $2p^{3/2}$ is around 711 eV for Fe^{3+} and 709 eV for Fe^{2+} [24, 25]. The main Fe $2p^{3/2}$ signal observed at 710.8 eV binding energy indicates the coexistence of both Fe^{3+} and Fe^{2+} ions. Additionally, it is well-known that the XPS spectra of iron oxides display satellite features, which are very sensitive to the oxidation states of iron. Consequently, the satellite structures are often exploited as fingerprints to establish the iron oxide phases. The less resolved satellite peaks at 718.0 and 733 eV, typical of the Fe^{3+} ions [26, 27], confirm that a number of Fe^{2+} ions were converted to Fe^{3+} ions during preparation of our nano-iron oxides. It should be recalled in this regard that the *H. odoratissimum*-mediated Fe_3O_4 NPs described in this research were prepared using a solution of $FeSO_4.7H_2O$ salt and further subjected to thermal annealing treatment in air. The Fe $2p^{3/2}$ and Fe $2p^{1/2}$ binding energy positions recorded in this study are in good agreement with previous literature on the XPS analysis of iron oxide Fe_3O_4 [28].

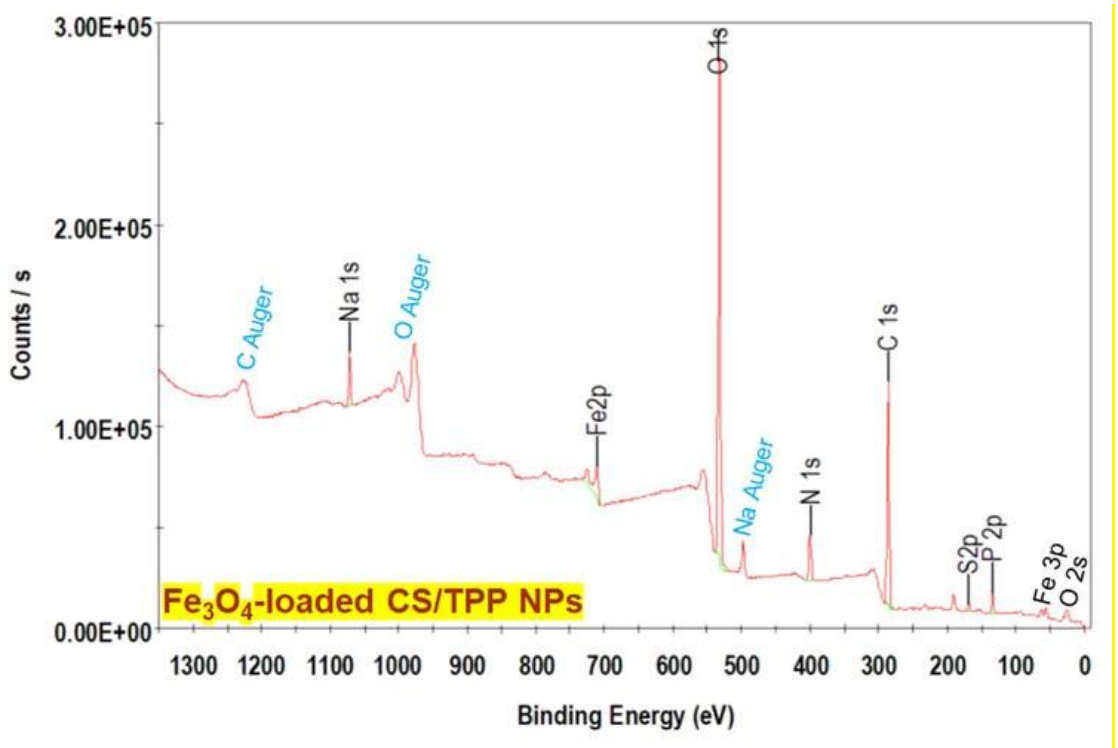


Figure 5. 14: XPS survey spectrum of Fe_3O_4-loaded CS/TPP NPs.

The deconvolution of the O 1s high-resolution spectrum reveals three sub-peaks at 530.4, 531.3, and 532.7 eV (Table 5.4, see Appendix). The component at lower binding energy indicates the Fe–O bond [29]. The presence of S 2p in Figure 5.14 is due to bound sulphur at the surface of the developed nanoparticles. From residual sulfate at the surface of the *H. odoratissimum*-mediated Fe_3O_4 NPs, an active form of sulfur is likely to interact with phytochemicals and CS/TPP complexes. The XPS results obtained in this investigation confirm that the combinative ZnO/CS, Zn(II) ions/CS, Fe_3O_4/CS, and Fe(II) ions/CS NPs have been developed successfully.

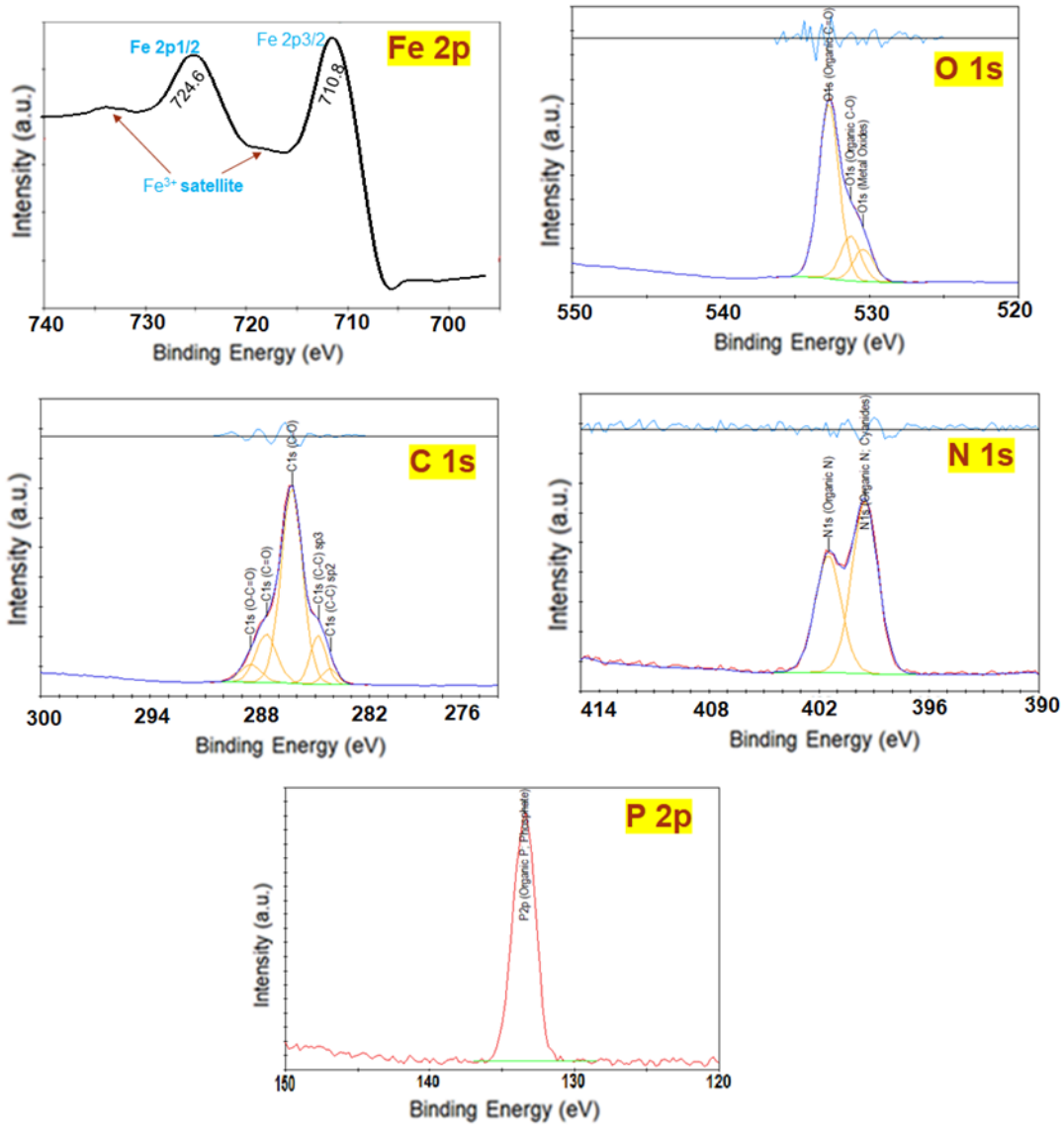


Figure 5. 15: High-resolution XPS spectra of Fe 2p, C 1s, O 1s, N 1s, and P 2p of Fe_3O_4-loaded CS/TPP NPs.

5.2 Nutrient release behaviour in water

Inputs with slow-release properties have been the focus of ongoing research to promote the efficiency and sustainability of agricultural practices [30-32]. Slow delivery systems aim towards adequate amounts of nutrients and pesticides over a period of time, to achieve the fullest biological efficacy and abate the harmful effects. Accordingly, the application of slow-release inputs, especially nanoformulations, is considered a best management practice tool for crop production. The nanofertilizer application consists of three main techniques, namely, foliar, soil treatment, and seed priming. The micronutrient release behaviour of the developed nanomaterials, placed in empty tea bag filter disposable and steeped in aqueous solutions, was examined.

This analysis was found to be of significant interest to consider these nanomaterials in priming technology and provide a plausible path for improving seed germination and post-germination growth. Figure 5.16 illustrates the change in zinc concentrations for the prepared ZnO NPs, ZnO-loaded CS/TPP NPs, and Zn(II)-laden CS/TPP NPs suspended in deionized water for 2 weeks (336 h). Throughout the experiment, the amount of Zn^{2+} ions released was relatively low for the ZnO NPs compared to the nutrient-loaded CS/TPP NPs. This difference in behaviour is undoubtedly due to the reduced solubility of crystalline ZnO NPs in water under the experimental conditions (pH 7.8-8.1). A study by Omar et al. (2014) indicates that ZnO NPs exhibit a dissolution region between pH 3.7 and 6.7 [33]. It has been reported that water solubility of metal oxide NPs can be stimulated by silanization, surface modification with water-soluble ligands, or encapsulation within block-copolymer micelles [34]. Indeed, the solubility is modulated for ZnO-loaded CS/TPP NPs.The entrapment of ZnO NPs during crosslinking reaction in an acidic *milieu* makes it low in crystallinity and improves their solubility [35]. The protonation of surface O^{2-} anions of the presynthesized metal oxides, and coordination of the acetate base species of the acid to their surface cations (Scheme 5.1) is thought to be responsible for their transformation into amorphous phases [36, 37]. The overall structure of amorphous metal oxides consists of a superposition of random atomic arrangements.

Relatively high levels of Zn^{2+} ions were observed for the Zn(II)-laden CS/TPP NPs after 1, 5, and 24 h of steeping. The 48, 168, 240, and 336 h release diagrams displayed higher Zn concentrations for the ZnO[15s]-loaded CS/TPP NPs. Moreover, solutions containing this nanocomposite showed a gradual increase in Zn levels while their Zn(II)-laden counterparts exhibited a quick release of Zn. The early burst release behavior of Zn(II)-laden CS/TPP NPs can be attributed to the diffusion of Zn at the surface of the particles. The slow change in Zn concentration of the ZnO[15s]-loaded CS/TPP NPs in water is due to CS/TPP swelling, dissolution of the amorphous ZnO, and diffusion of Zn from the swollen matrix in analogy with the literature precedent for the alginate-polyvinyl alcohol loaded with ZnO NPs [38]. Ekanayake and Godakumbura (2021) demonstrated that metal oxide NPs integrated into the alginate matrix are held by weaker interactions (e.g. hydrogen bonding) [39]. Earlier, evidence on the slow P release in soil from the 430 nm CS/TPP-ZnO nanocomposites was also reported by Dimkpa et al. (2023) [40]. These nanomaterials were developed by the ionic gelation method in the presence of the commercially available 18 nm ZnO NPs .

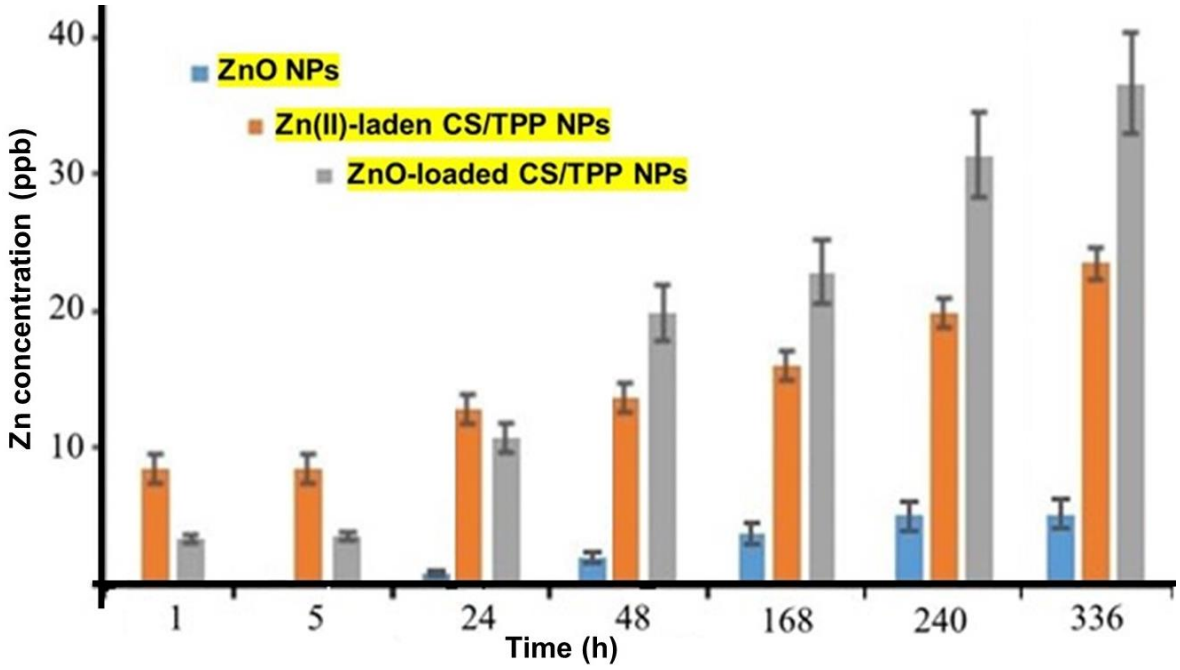


Figure 5. 16: Plot depicting the release behaviour of the synthesized ZnO[15s], ZnO[15s]-loaded CS/TPP NPs, and Zn(II)-laden CS/TPP NPs in deionized water showing the variation of zinc concentration for 2 weeks.

REFERENCES

1. Oladzadabbasabadi, N.; Nafchi, A. M.; Ariffin, F.; Jeevani Osadee Wijekoon, M. M.; Al-Hassan, A. A.; Dheyab, M. A. & Ghasemlou, M. 2022. Recent advances in extraction, modification, and application of chitosan in packaging industry. *Carbohydrate Polymers*, 277, 118876.

2. Morin-Crini, N.; Lichtfouse, E.; Torri, G. & Crini, G. 2019. Applications of chitosan in food, pharmaceuticals, medicine, cosmetics, agriculture, textiles, pulp and paper, biotechnology, and environmental chemistry. *Environmental Chemistry Letters*, 17, 1667-1692.

3. Li, B.; Wang, J.; Moustafa, M. E. & Yang, H. 2019. Ecofriendly method to dissolve chitosan in plain water, *ACS Biomaterials Science & Engineering*, 5, 6355-6360.

4. Xing, Q.; Yates, K.; Vogt, C.; Qian, Z.; Frost, M. C. & Zhao, F. 2014. Increasing mechanical strength of gelatin hydrogels by divalent metal ion removal. *Scientific Reports*, 4, 4706.

5. Danaei, M.; Dehghankhold, M.; Ataei, S.; Davarani, F. H.; Javanmard, R.; Dokhani, A.; Khorasani S. & Mozafari, M. R. 2018. Impact of particle size and polydispersity index on the clinical applications of lipidic nanocarrier systems. *Pharmaceutics* 10(2), 57.

6. Liu, Q.; Li, H.; Xia, Q.; Liu, Y.; Xiao, K. 2015. Role of surface charge in determining the biological effects of CdSe/ZnS quantum dots. *International Journal of Nanomedicine*, 10, 7073-7088.

7. Arakha, M.; Pal, S.; Samantarrai, D.; Panigrahi, T. K.; Mallick, B. C.; Pramanik, K.; Mallick, B. & Jha, S. 2015. Antimicrobial activity of iron oxide nanoparticle upon modulation of nanoparticle-bacteria interface. *Scientific Reports*, 5(1), 1-12.

8. Pauly, C. S.; Genix, A. C.; Alauzun, J. G.; Sztucki, M.; Oberdisse, J. & Mutin, P. H. 2015. Surface modification of alumina-coated silica nanoparticles in aqueous

sols with phosphonic acids and impact on nanoparticle interactions. *Physical Chemistry Chemical Physics*, 17(29), 19173-19182.

9. Queffélec, C.; Petit, M.; Janvier, P.; Knight, D. A. & Bujoli, B. 2012. Surface modification using phosphonic acids and esters. *Chemical Reviews*, 112(7), 3777-3807.

10. Qi, L.; Xu, Z.; Jiang, X.; Hu, C. & Zou, X. 2004. Preparation and antibacterial activity of chitosan nanoparticles. *Carbohydrate Research*, 339(16), 2693-2700.

11. Dudhani, A. R. & Kosaraju, S. L. 2010. Bioadhesive chitosan nanoparticles: Preparation and characterization. *Carbohydrate Polymers*, 81(2), 243-251.

12. Ríos-Caloch, G.; Santes, V.; Escobar, J.; Pérez-Romo, P.; Díaz, L. & Lartundo-Rojas, L. 2016. Effect of chitosan on the performance of NiMoP-supported catalysts for the hydrodesulfurization of dibenzothiophene. *Journal of Nanomaterials*, 2016, 17-17.

13. Aşık, M. D.; Kaplan, M.; Çetin, B. & Sağlam, N. 2021. Synthesis of iron oxide core chitosan nanoparticles in a 3D printed microfluidic device. *Journal of Nanoparticle Research*, 23(3), 1-11.

14. Rahmani, O.; Bouzid, B. & Guibadj, A. 2017. Extraction and characterization of chitin and chitosan: applications of chitosan nanoparticles in the adsorption of copper in an aqueous environment. *e-Polymers*, 17(5), 383-397.

15. Chigondo, M.; Paumo, H. K.; Bhaumik, M.; Pillay, K. & Maity, A. 2018. Hydrous CeO_2-Fe_3O_4 decorated polyaniline fibers nanocomposite for effective defluoridation of drinking water. *Journal of Colloid and Interface Science*, 532, 500-516.

16. Naushad, M.; Ahamad, T. & Al-Sheetan, K. M. 2021. Development of a polymeric nanocomposite as a high-performance adsorbent for Pb (II) removal from water medium: Equilibrium, kinetic and antimicrobial activity. *Journal of Hazardous Materials*, 407, 124816.

17. Kahdestani, S. A.; Shahriari, M. H. & Abdouss, M. 2021. Synthesis and characterization of chitosan nanoparticles containing teicoplanin using sol–gel. *Polymer Bulletin*, 78, 1133-1148.

18. Rathore, B. S.; Singh Chauhan, N. P.; Jadoun, S.; Ameta, S. C. & Ameta, R. 2021. Synthesis and characterization of chitosan-polyaniline-nickel(II) oxide nanocomposite. *Journal of Molecular Structure*, 1242, 130750.

19. Zaman, H. G.; Baloo, L.; Aziz, F.; Kutty, S. R. & Ashraf, A. 2022. COD adsorption and optimization from produced water using chitosan–ZnO nanocomposite. *Applied Nanoscience*, 12(6), 1885-1898.

20. Frindy, S.; el Kadib, A.; Lahcini, M.; Primo, A. & García, H. 2015. Copper nanoparticles stabilized in a porous chitosan aerogel as a heterogeneous catalyst for C− S cross-coupling. *ChemCatChem*, 7(20), 3307-3315.

21. Daniyal, W. M. E. M. M.; Fen, Y. W.; Saleviter, S.; Chanlek, N.; Nakajima, H.; Abdullah, J. & Yusof, N. A. 2021. X-ray photoelectron spectroscopy analysis of chitosan–graphene oxide-based composite thin films for potential optical sensing applications. *Polymers*, 13, 478.

22. Qiao, X.; Liao, S.; You, C. & Chen, R. 2015. Phosphorus and nitrogen dual doped and simultaneously reduced graphene oxide with high surface area as efficient metal-free electrocatalyst for oxygen reduction. *Catalysts*, 5, 981-991.

23. Abdullin, K. A.; Gabdullin, M. T.; Zhumagulov, S. K.; Ismailova, G. A.; Gritsenko, L. V.; Kedruk, Y. Y. & Mirzaeian, M. 2021. Stabilization of the surface of ZnO films and elimination of the aging effect. *Materials*, 14, 6535.

24. Fujii, T.; De Groot, F. M. F.; Sawatzky, G. A.; Voogt, F. C.; Hibma, T. & Okada, K. 1999. In situ XPS analysis of various iron oxide films grown by NO_2- assisted molecular-beam epitaxy. *Physical Review B*, 59(4), 3195.

25. Li, P.; Jiang, E. Y. & Bai, H. L. 2011. Fabrication of ultrathin epitaxial γ-Fe_2O_3 films by reactive sputtering. *Journal of Physics D: Applied Physics*, 44(7), 075003.

26. Ai, Q.; Yuan, Z.; Huang, R.; Yang, C.; Jiang, G.; Xiong, J. & Yuan, S. 2019. One-pot co-precipitation synthesis of Fe_3O_4 nanoparticles embedded in 3D carbonaceous matrix as anode for lithium-ion batteries. *Journal of Materials Science*, 54(5), 4212-4224.

27. Nene, A. G.; Takahashi, M. & Somani, P. R. 2016. Fe_3O_4 and Fe nanoparticles by chemical reduction of $Fe(acac)_3$ by ascorbic acid: role of water. *World Journal of Nano Science and Engineering*, 6(1), 20-28.

28. Yamashita, T. & Hayes, P., 2008. Analysis of XPS spectra of Fe^{2+} and Fe^{3+} ions in oxide materials. *Applied Surface Science*, 254(8), 2441-2449.

29. Sathishkumar, G.; Logeshwaran, V.; Sarathbabu, S.; Pradeep, K. J.; Jeyaraj M.; Rajkuberan, C.; Senthilkumar, N. & Sivaramakrishnan, S. 2018. Green synthesis of magnetic Fe_3O_4 nanoparticles using *Couroupita guianensis* Aubl. fruit extract for their antibacterial and cytotoxicity activities. *Artificial Cells, Nanomedicine, and Biotechnology*, 46 (3), 589-598.

30. Ghormade, V.; Deshpande, M. V. & Paknikar, K. M. 2011. Perspectives for nano-biotechnology enabled protection and nutrition of plants. *Biotechnology Advances*, 29(6), 792-803.

31. Dimkpa, C. O. & Bindraban, P. S. 2017. Nanofertilizers: new products for the industry? *Journal of Agricultural and Food Chemistry*, 66(26), 6462-6473.

32. Li, N.; Sun, C.; Jiang, J.; Wang, A.; Wang, C.; Shen, Y. & Wang, Y. 2021. Advances in controlled-release pesticide formulations with improved efficacy and targetability. *Journal of Agricultural and Food Chemistry*, 69(43), 12579-12597.

33. Omar, F. M.; Aziz, H. A. & Stoll, S. 2014. Aggregation and disaggregation of ZnO nanoparticles: influence of pH and adsorption of Suwannee River humic acid. *Science of the Total Environment*, 468, 195-201.

34. Vaseem, M.; Umar, A. & Hahn, Y.B. 2010. ZnO nanoparticles: growth, properties, and applications. *Metal Oxide Nanostructures and their Applications*, 5(1),10-20.

35. Matsumoto, T.; Okazaki, M.; Inoue, M.; Hamada, Y.; Taira, M. & Takahashi, J. 2002. Crystallinity and solubility characteristics of hydroxyapatite adsorbed amino acid. *Biomaterials*, 23(10), 2241-2247.

36. Barteau, M. A. 1996. Organic reactions at well-defined oxide surfaces. *Chemical Reviews*, 96(4), 1413-1430.

37. Brown Jr, G. E.; Henrich, V.; Casey, W.; Clark, D.; Eggleston, C.; Andrew Felmy, A. F. & Zachara, J. M. 1999. Metal oxide surfaces and their interactions with aqueous solutions and microbial organisms. *Chemical Reviews*, 99, 77-174.

38. Knijnenburg, J. T.; Kasemsiri, P.; Amornrantanaworn, K.; Suwanree, S.; Iamamornphan, W.; Chindaprasirt, P. & Jetsrisuparb, K. 2021. Entrapment of nano-ZnO into alginate/polyvinyl alcohol beads with different crosslinking ions for fertilizer applications. *International Journal of Biological Macromolecules*, 181, 349-356.

39. Ekanayake, S. A. & Godakumbura, P. I. 2021. Synthesis of a dual-functional nanofertilizer by embedding ZnO and CuO nanoparticles on an alginate-based hydrogel. *ACS Omega 6*, 26262-26272.

40. Dimkpa, C. O.; Deng, C.; Wang, Y.; Adisa, I. O.; Zhou, J. & White, J. C. 2023. Chitosan and zinc oxide nanoparticle-enhanced tripolyphosphate modulate phosphorus leaching in soil. *ACS Agricultural Science & Technology*, 3, 487-498.

CHAPTER 6

EFFECTS OF DEVELOPED ZINC OXIDE AND ZINC LOADED CHITOSAN NANOPARTICLES ON MAIZE SEED GERMINATION

6.1 Nanopriming technology for enhancing seed germination in sustainable agriculture

The agricultural sector is increasingly facing the negative impacts of climate change due to various stress conditions. To curb this scenario, economical and low-risk practices such as decreasing fertilizer inputs and seed priming have been promoted [1,2]. Seed priming is a pre-sowing method established to control the hydration of seeds and initiate the metabolic events needed for energy generation [3]. This strategy is well-reported in several approaches, including seed soaking in water and nutrient-containing solutions. The latter represents a value-added procedure that can meet plant micronutrient requirements, with no impact on the natural environment. The conventional techniques of supplying micronutrients, i.e., foliar spraying and soil fertilization, are reliant on environmental conditions that can lessen their efficiency. High soil pH, for example, limits the availability of micronutrients. Low moisture, on the other hand, may restrict their uptake by plants. In the foliar-sprayed method, there is a high risk of phytotoxicity as multiple treatments are often required [4].

Seed priming in a solution containing nanoparticles (nanopriming) is an innovative technique to accelerate and synchronise germination. This seed treatment under controlled conditions before sowing can also enhance plant growth and increase their resistance to biotic or abiotic stress conditions. In so doing, nanopriming can help reduce the over application of fertilizers. The prominent features of NPs in cereal seed priming have been argued to increase water uptake, establish electron exchange, and activate the production of ROS in seeds [5,6]. These species initiate cell wall loosening for rapid degradation of starch. Hydroxyl (•OH) and superoxide ($\bullet O_2^-$) radicals and hydrogen peroxide (H_2O_2) increased the dynamics of seed germination in several crops [7]. For example, the Ag NPs (6-36 nm), developed in leaf extract of kaffir lime and used to prime seeds of *Oryza sativa*, have been reported to enhance water uptake and germination [8]. The internalization of NPs on

the seed coat leads to the accumulation of ROS that activate several downstream events.

Seed germination is an essential process in the plant's life cycle and future development [9]. This developmental process begins with water absorption by the dormant seed and ends with the protrusion of the radicle through the seed coat and the embryonic axis elongation [10]. During seed germination, the physiological and morphological alterations result in embryo activation. In the germination's last phase, the seedling structure's expansion occurs from continued cell growth and division (Figure 6.1). This denotes the determining biological and morphological traits that define the plant establishment. Delayed germination and inhibition of radicle protrusion are common conditions encountered with the seeds under abiotic stress.

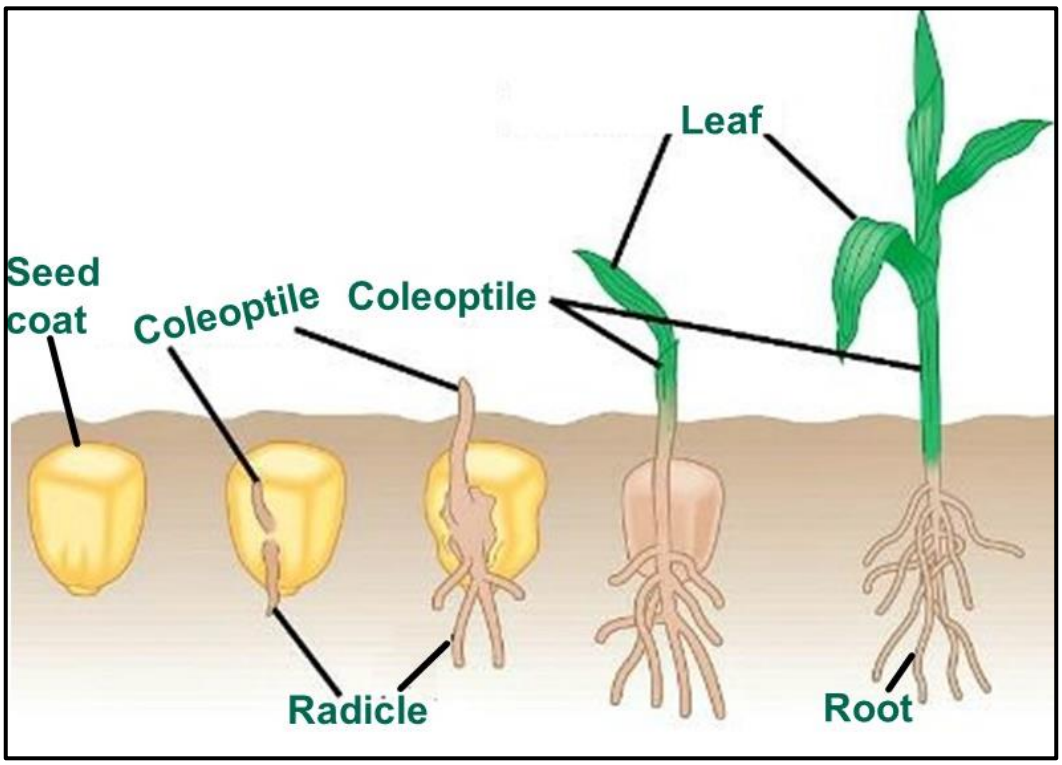


Figure 6. 1: Germination process of maize seed.

Abiotic stresses, especially drought and salinity, significantly impact seed germination, plant growth, and crop productivity. Salt stress on crops can occur from high fertility routine with NPK inputs, deficit irrigation and/or frequent irrigation with saline water [11,12]. Studies have shown that this condition inhibits seed germination, causes nutritional imbalance in plants, and persuades the excessive production of ROS, which can degrade proteins and DNA structures [13,14].

The increasing popularity of ZnO fertilizer is attributed to its high percentage of Zn content that acts as a regulatory co-factor of a multiplicity of enzymes, including oxidoreductases, hydrolases, ligases, transferases, and isomerases [15]. It has been reported that priming lupine seeds under salt stress with ZnO NPs (21 nm; concentrations 20, 40, and 60 mg/L in distilled water) increased the root length, shoot length, and fresh weight in 20 days old seedlings [16]. Higher germination and increased radical length have also been reported in the salinized bean seeds primed with TPP-crosslinked CS NPs (46 nm; concentrations 0.1%, 0.2% and 0.3%) [17].

The aqueous extract of *H. odoratissimum* Sweet was used in this investigation to develop the ZnO[5s] (321.2 nm; -30.8 mV), ZnO[10s] (173.5 nm; -26.6 mV), and ZnO[15s] (144.6 nm; -34.2 mV) NPs. These nano-metal oxides were further encapsulated in TPP-crosslinked CS nanostructures to afford the ZnO[5s]-loaded CS/TPP (351.5 nm, 16,5 mV), ZnO[10s]-loaded CS/TPP (257.3 nm, 17,8 mV), and ZnO[15s]-loaded CS/TPP (207.2 nm, 16.0 mV) nanocomposites, respectively. Based on their excellent stability in aqueous solution and relatively reduced size, ZnO[15s], ZnO[10s]-loaded CS/TPP, and ZnO[15s]-loaded CS/TPP nanoproducts were selected and then used at two concentrations (0.01 and 0.04%) to prime two groups of *Z. mays* seeds (non-stressed and salt-stressed). The pristine CS/TPP and Zn(II)-laden CS/TPP NPs were also applied in the nanopriming procedure. At first glance, these treatments stimulated germination and seedling growth, as shown in Figure 6.2.

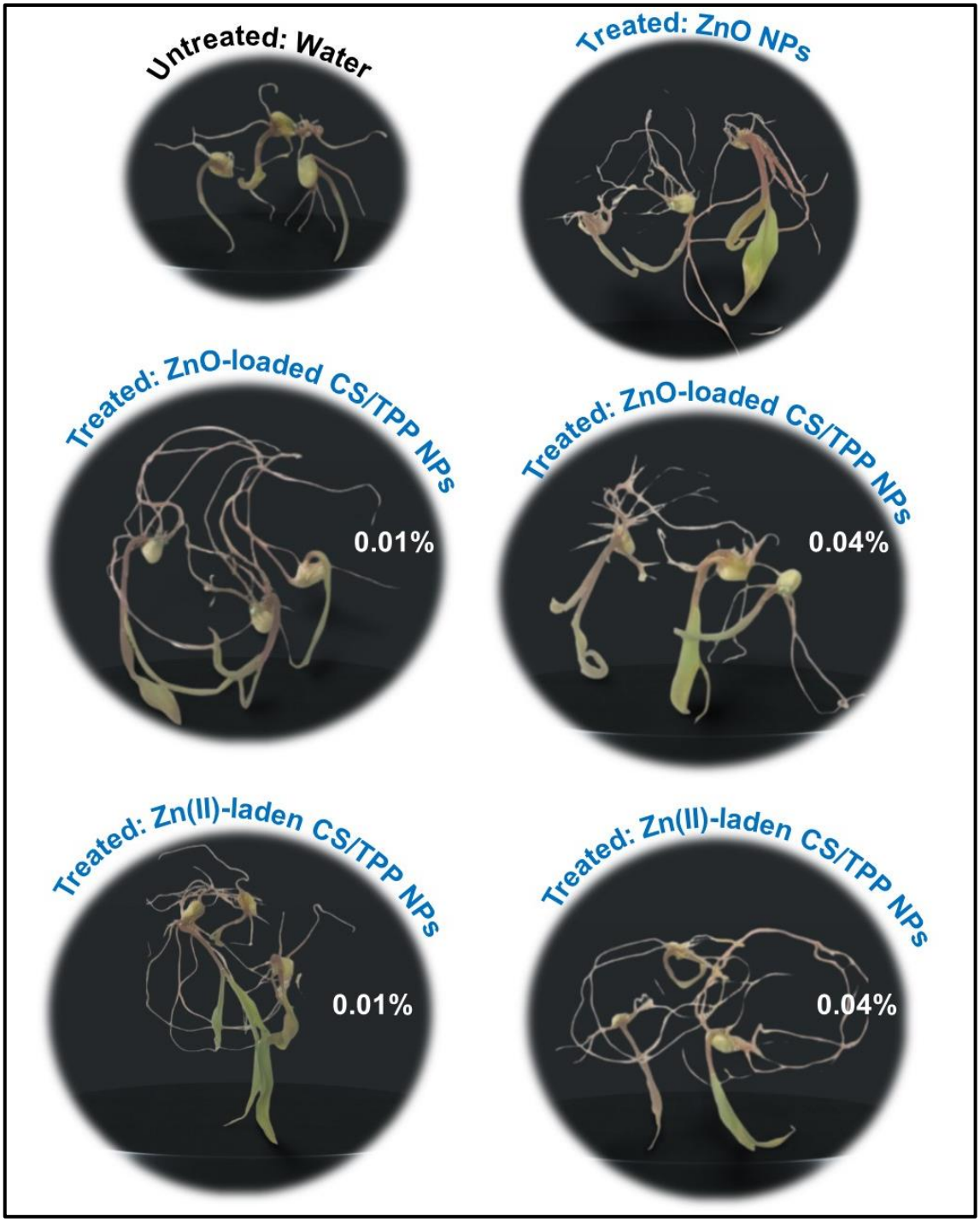


Figure 6. 2: Effects of the seed nanopriming with ZnO NPs and Zn-loaded CS/TPP NPs.

6.2 Germination traits of maize seeds primed with ZnO nanoparticles

6.2.1 Effects on germination of non-stressed seeds

Priming treatments with the biogenic ZnO NPs (0.01% & 0.04%) and its salt precursor (0.01%) had significant effects on coleoptile length (CL) and length of roots (LoR) (Figure 6.3); number of lateral roots (NLR) on radicle and number of roots (NR) additional to radicle (Figure 6.4); radicle length (RL) and shoot length (SL) (Figure 6.5) and mean dry matter yield (Table 6.1) in comparison with the control in deionized water. Priming the maize seeds with ZnO NPs 0.04% and $Zn(NO_3)_2$ 0.01% enhanced CL and LoR throughout the growth period. On the 10^{th} day (termination day), these treatments averaged CL 18.8 and 16.2 mm, respectively. The average LoR of seedlings was recorded to be 36.5 mm for seeds primed with ZnO NPs 0.04% and 24.8 mm for seeds treated with $Zn(NO_3)_2$ 0.01%. ZnO NPs 0.04% showed the best performance in both growth attributes, followed by the zinc nitrate solution. The least value was recorded with ZnO NPs 0.01% treatment. In comparison with the control and $Zn(NO_3)_2$ treatment, ZnO NPs 0.01% could promote toxicity on the seedling root elongation. A literature precedent suggests that after penetrating the seed coats, the emerging radicles promptly absorb water and nutrients, hence intensifying particle exposure [18].

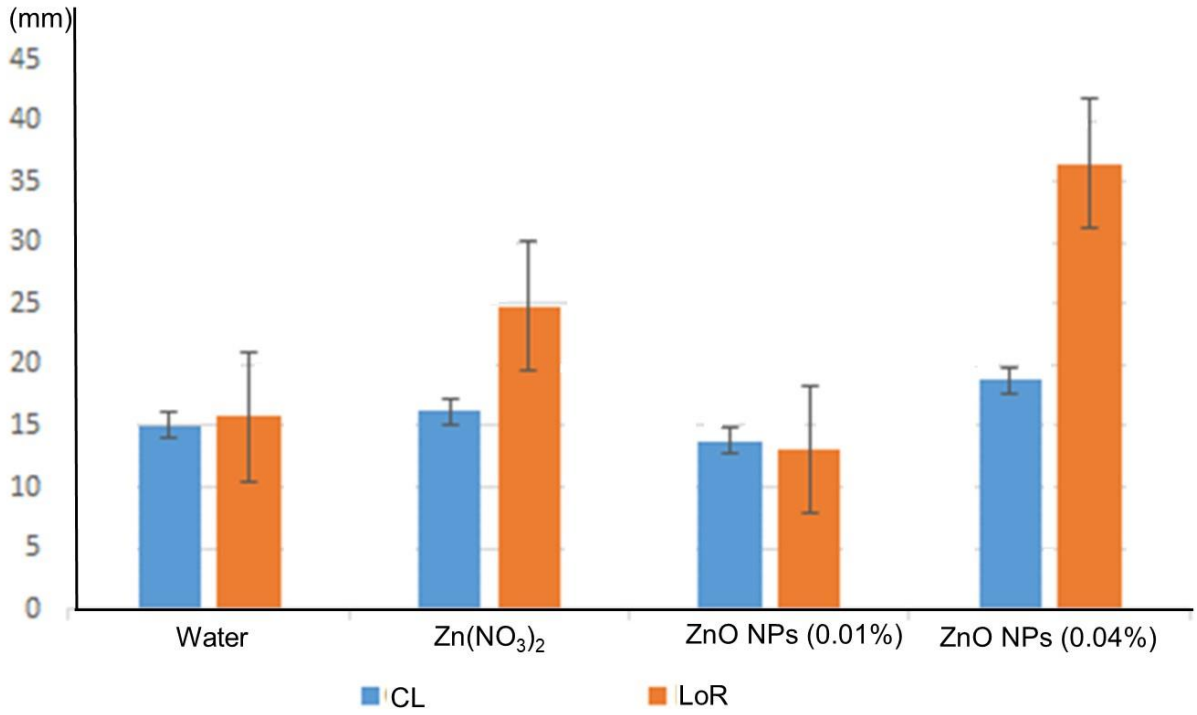


Figure 6. 3: Effects of biogenic ZnO NPs and $Zn(NO_3)_2$ on the coleoptile and roots length with a significance difference ($P \leq 0.05$).

Seed priming with ZnO NPs (0.01% & 0.04%) and $Zn(NO_3)_2$ 0.01% significantly affected the formation of roots and the density of lateral roots (Figure 6.4). The increase in average NLR was in the order of ZnO NPs 0,04% 17.0 > $Zn(NO_3)_2$ 0.01% 13.8 > ZnO NPs 0,01% 10.2 > control 5.1. On the other hand, the highest NR was obtained from the ZnO 0.01% treated seeds. For this attribute, $Zn(NO_3)_2$ treatment performed better than ZnO NPs 0.04%. Apart from its key function in acquiring soil resources (water and nutrients), the root system is accountable for the upright position of a plant and its resistance to mechanical factors like wind [19]. In crops such as maize, wheat and rice, the responses of plants to low nutrient availability are through increased root elongation and branching [20,21].

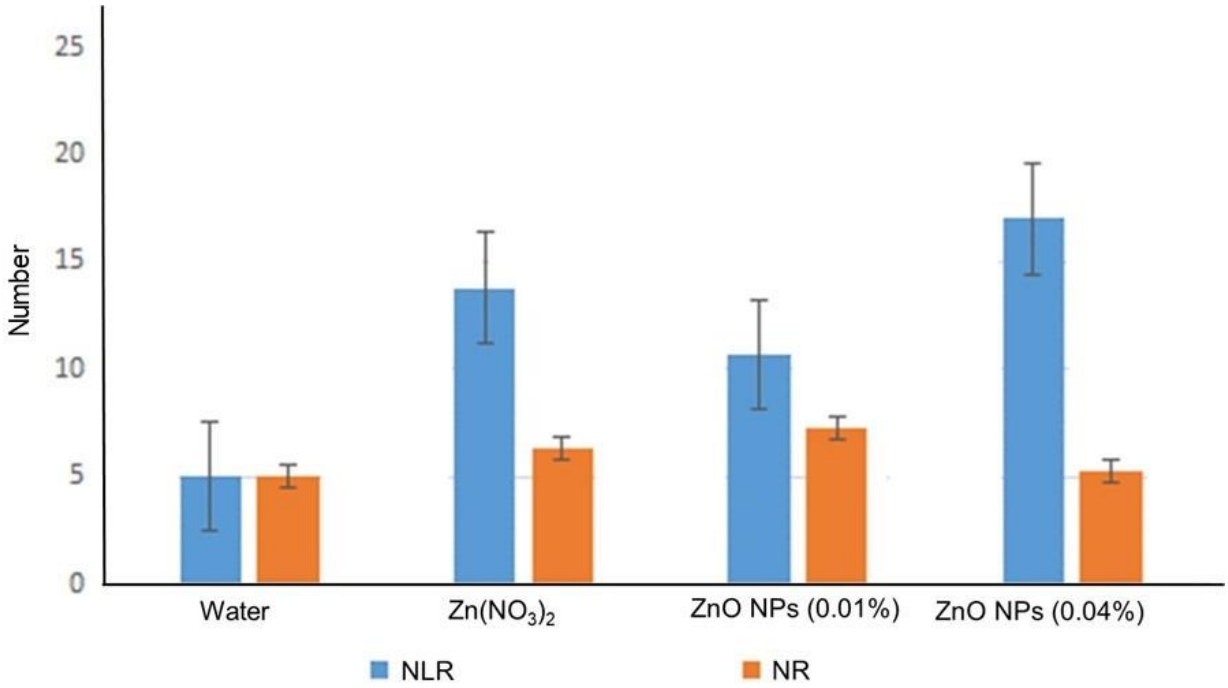


Figure 6. 4: Effects of biogenic ZnO NPs and $Zn(NO_3)_2$ on the number of roots and lateral roots with a significance difference ($P \leq 0.05$).

The radicle is the primary root emerging during the initial stages of seedling development. Its growth represents a universal and reliable parameter for the appraisal of seed vigour [22]. The shoot elongation also represents an essential characteristic of vigorous seeds. This process can improve the seedling growth ability for shoot infiltration through the obstructing soil of the seed bed [23]. The rapid germination and early growth are thought to be responsible for longer shoot length. In the current study, the average RL and SL recorded with the ZnO NPs 0.04% treatment were 64.9 and 47 mm, respectively (Figure 6.5). These indicate a more than 3-fold increase in RL value compared to the control treatment (20 mm). $Zn(NO_3)_2$ was the second-best performing treatment, with an RL value of 54.6 mm and SL of 43.2 mm. Also, the ZnO 0.01% treatment significantly affected both seedling growth parameters (RL 44.3 mm and SL 39.3 mm, respectively) and performed better than the control.

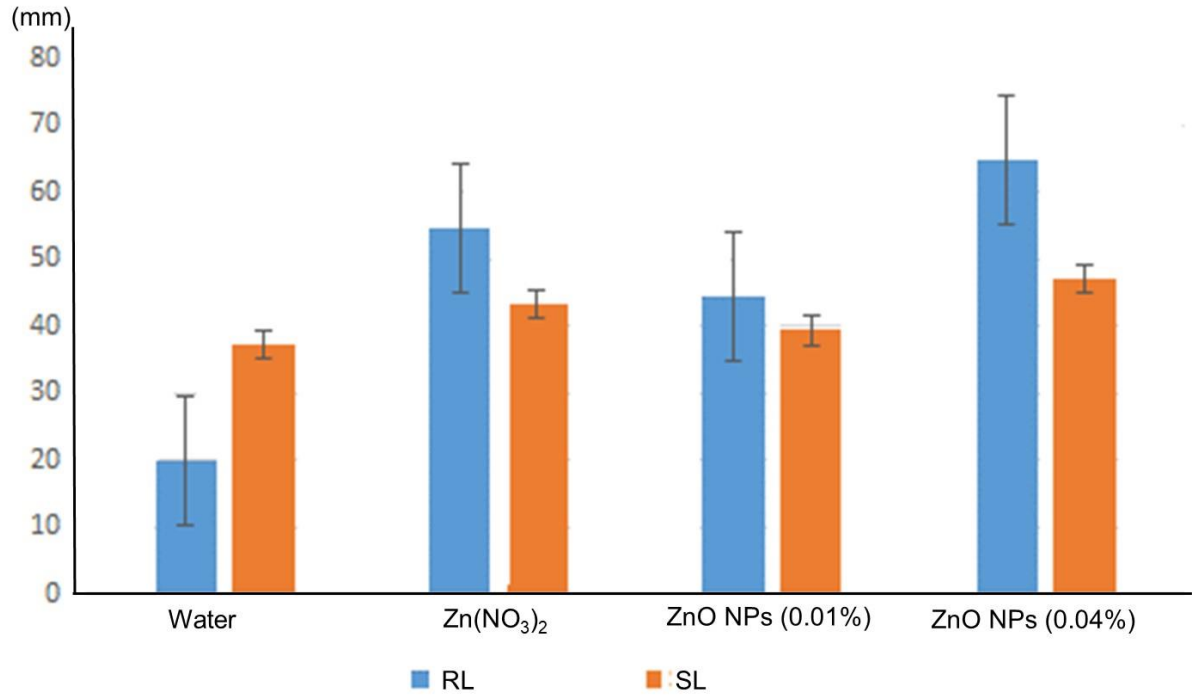


Figure 6. 5: Effects of biogenic ZnO NPs and $Zn(NO_3)_2$ on the radicle and shoot length with a significance difference ($P \leq 0.05$).

Table 6.1 shows the mean dry matter yield of the seedlings (coleoptiles dry weight CDW, radicles dry weight RDW, shoots dry weight SDW, and roots dry weight RoDW) after 10 days of seed germination under growth chamber conditions. The mean dry matter yield for the control set, ZnO NPs and zinc nitrate solution showed no significant difference for the coleoptiles. However, the least mean CDW was recorded from the ZnO 0.01% petri dish with a value of 0.022 g, while ZnO 0.04% treatment yielded the highest mean value of CDW 0.036 g. These results correlate with the data presented in Figure 6.3 owing to dry matter production with increased coleoptile elongation. For RDW, the ZnO NPs 0.04% treated seeds exhibited a maximum yield of 0.293 g and the minimum yield of 0.009 g was weighed from the untreated petri dish (water). Contrastingly, the latter treatment displayed the highest value of mean SDW. The ZnO NPs 0.01% treated seeds, on the other hand, revealed the maximum mean RoDW. As compared to the control treatment, $Zn(NO_3)_2$ priming also increased the dry matter weight of roots. The application of $ZnSO_4$ has previously been found to increase the dry matter yield of upland rice [24]. A recent report by Szulc and others (2021) [25] demonstrates that Zea mays' dry matter yield can indicate fertilization proficiency. Findings in the current study clearly show that the germination characteristics measured, increase significantly with the

increasing concentration of ZnO NPs (from 0.01 to 0.04%), except for the number of roots and their dry weight.

Table 6. 1: Effect of $Zn(NO_3)_2$ and ZnO NPs on dry matter yield (g).

Treatment	CDW	RDW	SDW	RoDW
Water	0.035^a	0.009^c	0.052^a	0.011^c
$Zn(NO_3)_2$ (0.01%)	0.029^a	0.026^a	0.032^b	0.029^b
ZnO NPs (0.01%)	0.022^a	0.220^b	0.027^c	0.039^a
ZnO NPs (0.04%)	0.036^a	0.293^a	0.037^a	0.019^c

Means with the different letters in the same column are significantly different at 5% probability level ($P \leq 0.05$).

6.2.2 Effects on germination of salt-stressed seeds

Salt stress is one of the most severe environmental factors inhibiting seed germination and plant growth [26]. The high concentration of soluble salt ions triggers osmotic stress and Na^+ and/or Cl^- toxicity. The toxicity of salt ions in plant cells results from their uptake by the roots and transportation within the transpiration stream to the shoots. The salt-persuaded osmotic stress reduces the water available to plants at the root surface [27]. The difficulty in establishing a uniform stand that has a considerable impact on crop yield might be caused by the constraint in water intake, which can severely slow down or prevent seed germination and early seedling growth. Importantly, knowledge of the stages of salt stress in maize suggests that Na^+ represents the major ion causing toxicity rather than Cl^- [28]. Consequently, ensuring better nutrition while limiting Na^+ uptake is an effective strategy that can contribute to salt stress tolerance in plants.

A rapid increase in germination and low sensitivity to salt stress of seeds and seedlings was obtained from priming with the mixture NaCl 600 mM + ZnO NPs 0.01% compared to the control and NaCl treatment. By day 10, NaCl + ZnO NPs significantly promoted root elongation (Figure 6.6), density of roots (Figure 6.7),

radicle elongation (Figure 6.8), and dry matter yield for the selected growth parameters (Table 6.2). While a 42.7% increase in LoR was observed in seeds treated with NaCl 600 mM + ZnO NPs 0.01% compared with the control, no inhibition in CL was noted. The highest average numbers of lateral (NLR) and additional roots (NR) were also recorded from this treatment (45 and 6, respectively). Comparing the control and NaCl treatment, the former had a noteworthy performance in both parameters.

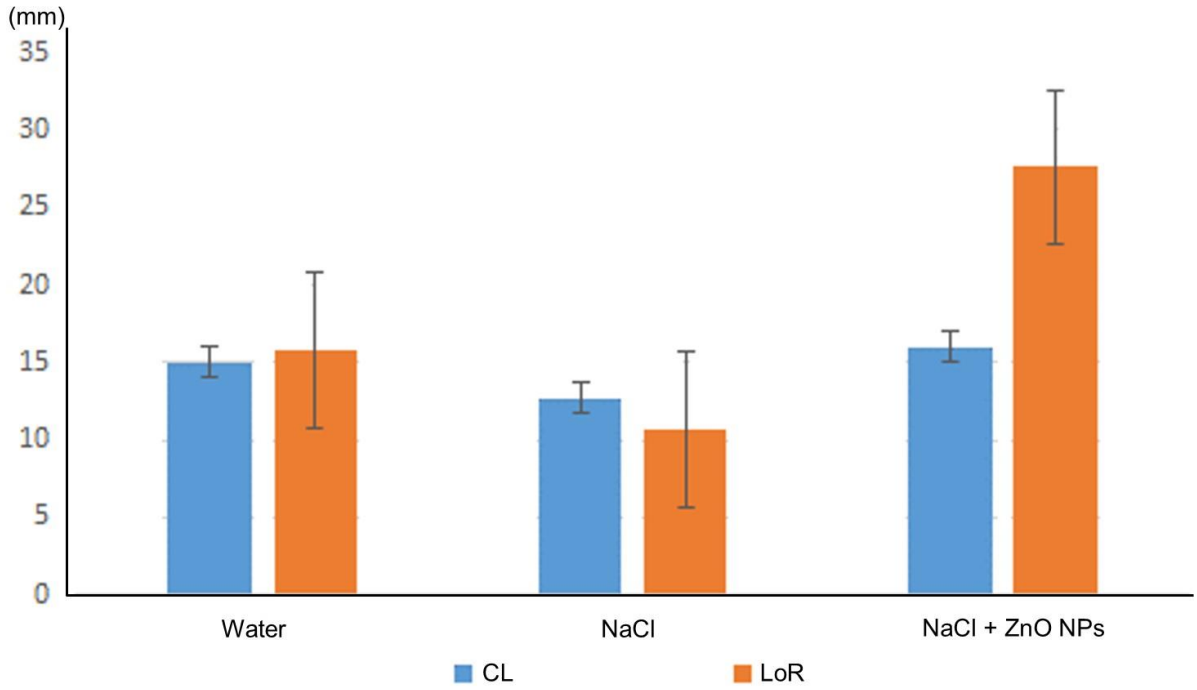


Figure 6. 6: Effects of ZnO NPs 0.01% + NaCl 600 mM on the coleoptile and roots length with a significance difference ($P \leq 0.05$).

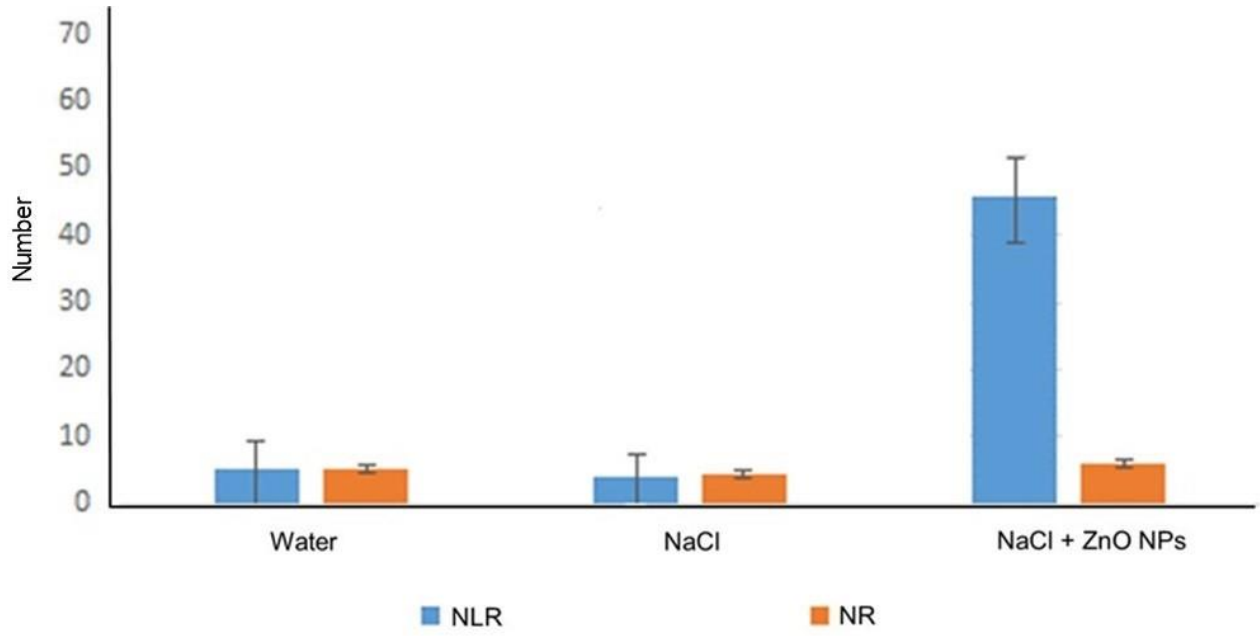


Figure 6. 7: Effects of ZnO NPs 0.01% + NaCl 600 mM on the number of roots and lateral roots with a significance difference ($P \leq 0.05$).

Exposure to NaCl 600 mM + ZnO NPs 0.01% increased the radicle elongation by 78.7 and 84.7%, relative to the control and NaCl treatment, respectively. It has been described that saline conditions often do not affect lateral root density [29]. The slight decrease in NLR observed for NaCl treatment compared to the control is attributed to the inhibition of the radicle growth, as shown in Figure 6.8. Salinity stress reduces the rate of cell division at the root meristems, thereby reducing growth.

The three treatments significantly influenced the dry matter yield of coleoptiles, radicles, shoots, and roots (Table 6.2). Seed priming with water resulted in increased CDW compared to NaCl and NaCl + ZnO NPs treatments. However, the maximum mean value from RDW (0.015 g) and RoDW (0.044 g) was obtained when seeds were treated with NaCl + ZnO NPs. The greatest shoot dry matter yield was recorded for the control treatment (0.052 g), followed by the NaCl + ZnO NPs treatment (0.048 g). A cognate study in salt-stressed *Z. mays* seeds also suggested increased dry weight of root and shoot under the influence of SiO_2 NPs [30]. It is envisaged that the biogenic ZnO NPs described in this investigation mitigate salt stress by reducing the absorption of Na^+ ions in the seedlings. These nanoparticles release Zn^{2+} ions (radius 0.074 nm) that can be easily absorbed by plant tissues than Na^+ ions (radius 0.102 nm). Due to the allelopathy effect, the aqueous extract of

H. odoratissimum is anticipated to inhibit *Z. mays'* germination and early seedling growth; hence, this treatment was not considered in this investigation. The allelochemicals are well-reported to display toxic effects on maize seed germination and seedling emergence by diminishing the uptake of water and nutrients, suppressing root and shoot growth, and decreasing the biomass production of maize seedlings [31,32].

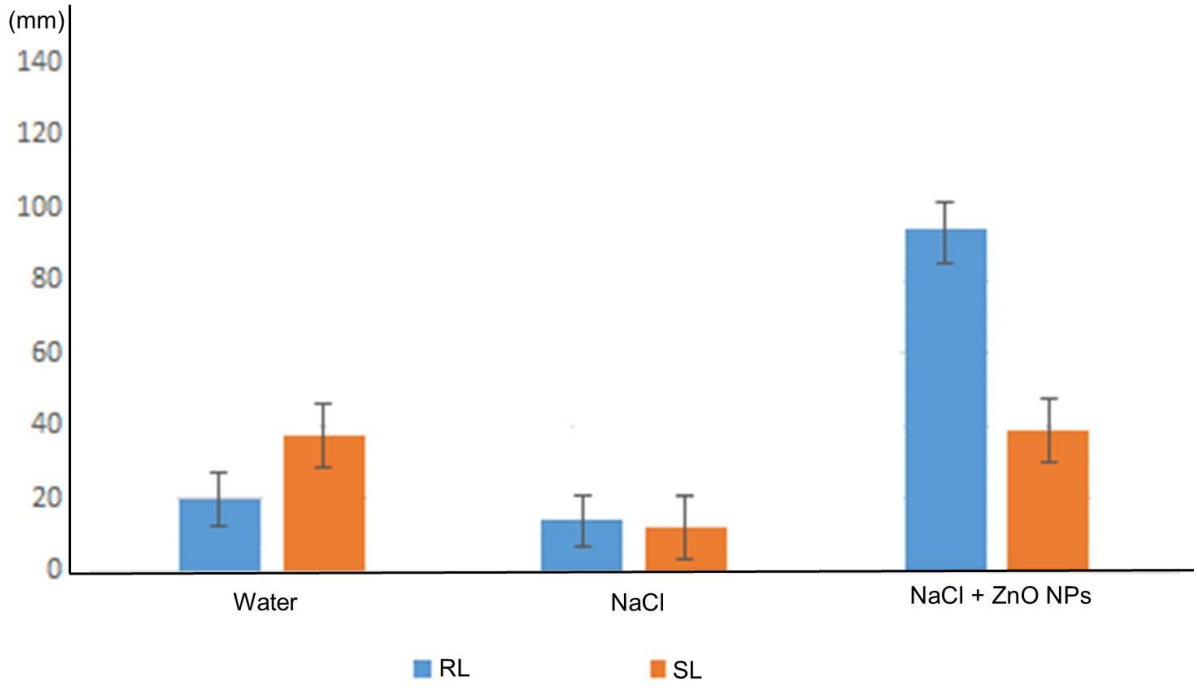


Figure 6. 8: Effects of ZnO NPs 0.01% + NaCl 600 mM on the radicle and shoot length with a significance difference (*P ≤ 0.05*).

Table 6. 2: Effects of NaCl and ZnO NPs on dry matter yield (g).

Treatment	CDW	RDW	SDW	RoDW
Water	0.0347^{a}	0.009^{c}	0.052^{a}	0.0113^{c}
NaCl (600Mm)	0.0118^{b}	0.013^{b}	0.0307^{b}	0.035^{b}
ZnO NPs (0.01%) + NaCl (600 mM)	0.0077^{c}	0.0157^{a}	0.048^{c}	0.044^{a}

Means with the different letters in the same column are significantly different at 5% probability level *(P ≤ 0.05).*

6.3 Germination traits of maize seeds primed with zinc-loaded chitosan nanoparticles

6.3.1 Effects on germination of non-stressed seeds

The seedlings from CS/TPP, Zn(II)-laden CS/TPP, ZnO[10s]-loaded CS/TPP, and ZnO[15s]-loaded CS/TPP nanopriming at 0.01% displayed significantly longer coleoptiles compared to the control set (Figure 6.9). CS/TPP NPs treatment at a higher dose of 0.04%, led to a maximum increase in mean CL of 25.2 mm (Figure 6.10). Seed priming with bulk chitosan and nano-engineered chitosan has been described for improved germination and seedling establishment [33,34]. The mean coleoptile length for the control treatment (water) was recorded to be 15.0 mm. The highest length of roots was obtained from the ZnO[15s]-loaded CS/TPP and ZnO[10s]-loaded CS/TPP treatments at 0.04%. A research by Ozturk et al. (2006) [35] noted that high zinc concentrations are required in highly metabolically active differentiating cells. Zn is essential for the developing stages of plants and has a high mobility in germinating seeds.

The mean LoR from these nanopriming procedures was recorded to be 77.4 and 69.8 mm, respectively. Maximum NLR 20.0 was found from the seeds treated with ZnO[10s]-loaded CS/TPP NPs at 0.01%. The control treatment showed the least average NLR, 5.0. The NLR in *A. thaliana* seedlings exposed to 2.1 µm CS/TPP (10 µg/mL) for 48 hours was increased by 60% relative to untreated seedlings, as reported by Iglesias et al. (2019) [36]. This modulation of the root system architecture was attributed to the activation of the auxin signaling response.

At 0.01% of a nanopriming agent, the highest average NR was obtained from the CS/TPP treatment (10.3), followed by Zn(II)-laden CS/TPP (9.3). Previously, Choudhary et al. (2019) [37] reported that nanopriming maize seeds with the 387 nm Zn(II)-laden CS/TPP NPs (0.01%) could stimulate an increase in the NR in 9-day-old seedlings (6.0) compared to water as a control (5.6). This literature highlighted that the developed chitosan-based nanomaterial triggers higher activities of α-amylase and and protease enzymes in seeds. Notably, ZnO[10s]-loaded CS/TPP NPs 0.01%

led to more than a 2-fold increment in the radicle and shoot elongation compared to the control.

At an increased concentration of 0.04%, the highest NR was counted from the seed treated with CS/TPP NPs (9.3). The ZnO[15s]-loaded CS/TPP and ZnO[10s]-loaded CS/TPP treatments at 0.04% also promoted maximum radicle length of 99.7 and 95.0 mm, respectively. The average shoot length was significantly higher from the Zn(II)-laden CS/TPP 0.01% (81.7 mm), ZnO[10s]-loaded CS/TPP 0.01% (79.0 mm), ZnO[10s]-loaded CS/TPP 0.04% (74.0 mm), and ZnO[15s]-loaded CS/TPP 0.04% (72.7 mm) compared to the control group 42.4 mm. In terms of the growth parameters LoR, RL, and SL, the ZnO[15s]- and ZnO[10s]-loaded CS/TPP NPs at 0.04%, achieved the best results. The overall growth traits presented in Table 6.3 showed that while the pristine CS/TPP NPs and ZnO[15s]-loaded CS/TPP NPs achieved superior promoting impact from 0.01% to 0.04%, the ZnO[10s]-loaded CS/TPP NPs would tend to be less effective at 0.04%. This finding revealed that considerable inhibitory effects could be seen on maize seed germination and plant growth at greater concentrations (> 0.04%) of the ZnO[10s]-loaded CS/TPP NPs [38]. One may wonder if the toxicity of this nanocomposite could be from the physico-chemical interferences of the carrier-free nano-oxide with the germinating embryonic roots. *Z. mays* seed coat has been argued to provide protection from the 30 nm ZnO NPs entering seeds due to selective permeability, and in so doing, mitigate their toxicity [39]. A study by Lin et al. (2008) [40] showed that a single particle of the 279 nm ZnO NPs could enter into the root cell of *Lolium perenne* and suppress seedling growth. Therefore, the toxicity of the engineered 257 nm ZnO[10s]-loaded CS/TPP NPs could be related to the free ZnO[10s]. Nonetheless, this postulation deserves further investigation as the Zn(II)-laden CS/TPP NPs priming solution also showed lower growth attributes at 0.04% compared to 0.01%.

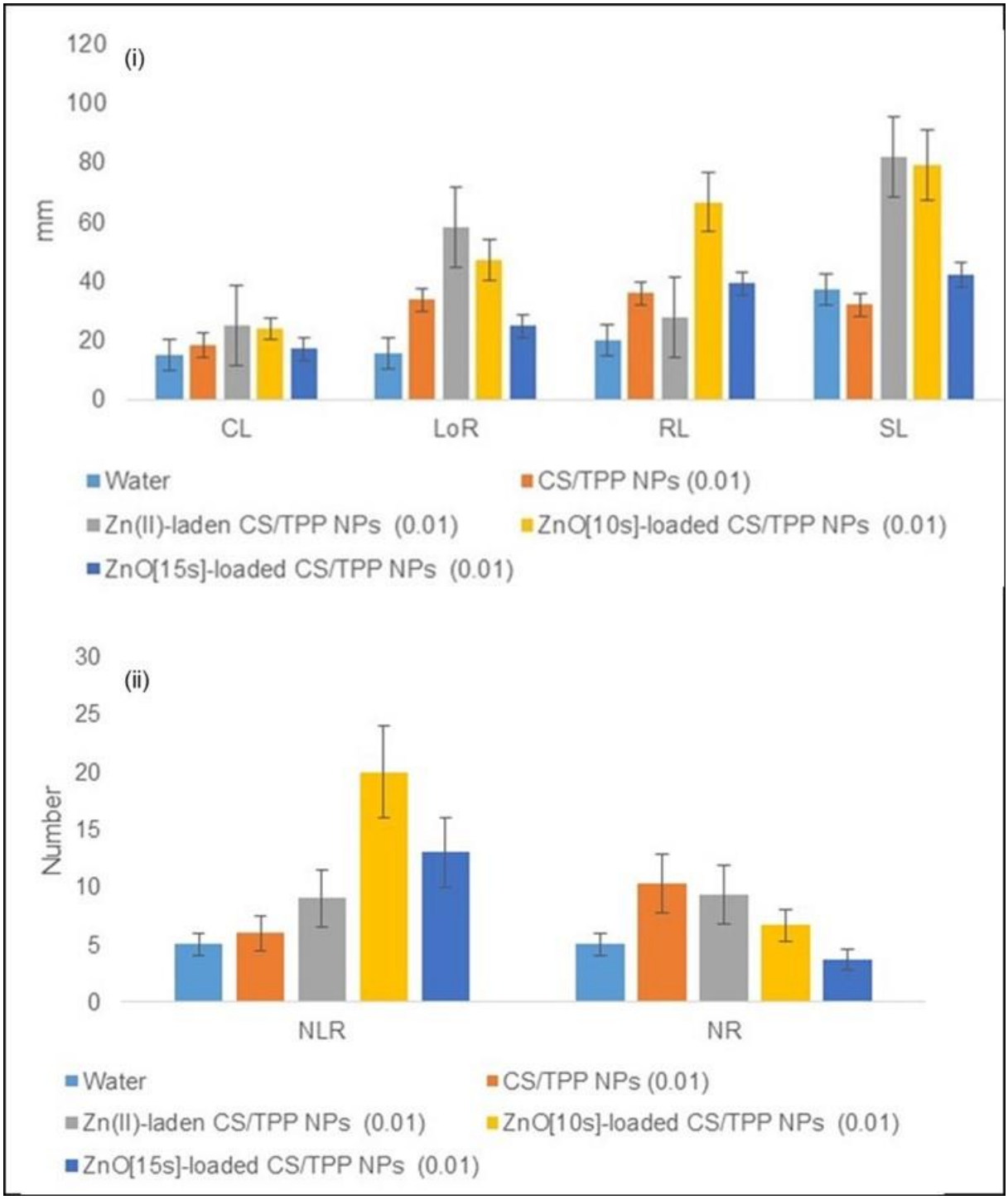


Figure 6. 9: Effects of the prepared CS/TPP, Zn(II)-laden CS/TPP, and ZnO-loaded CS/TPP NPs at 0.01% on selected growth parameters with a significance difference ($P \leq 0.05$).

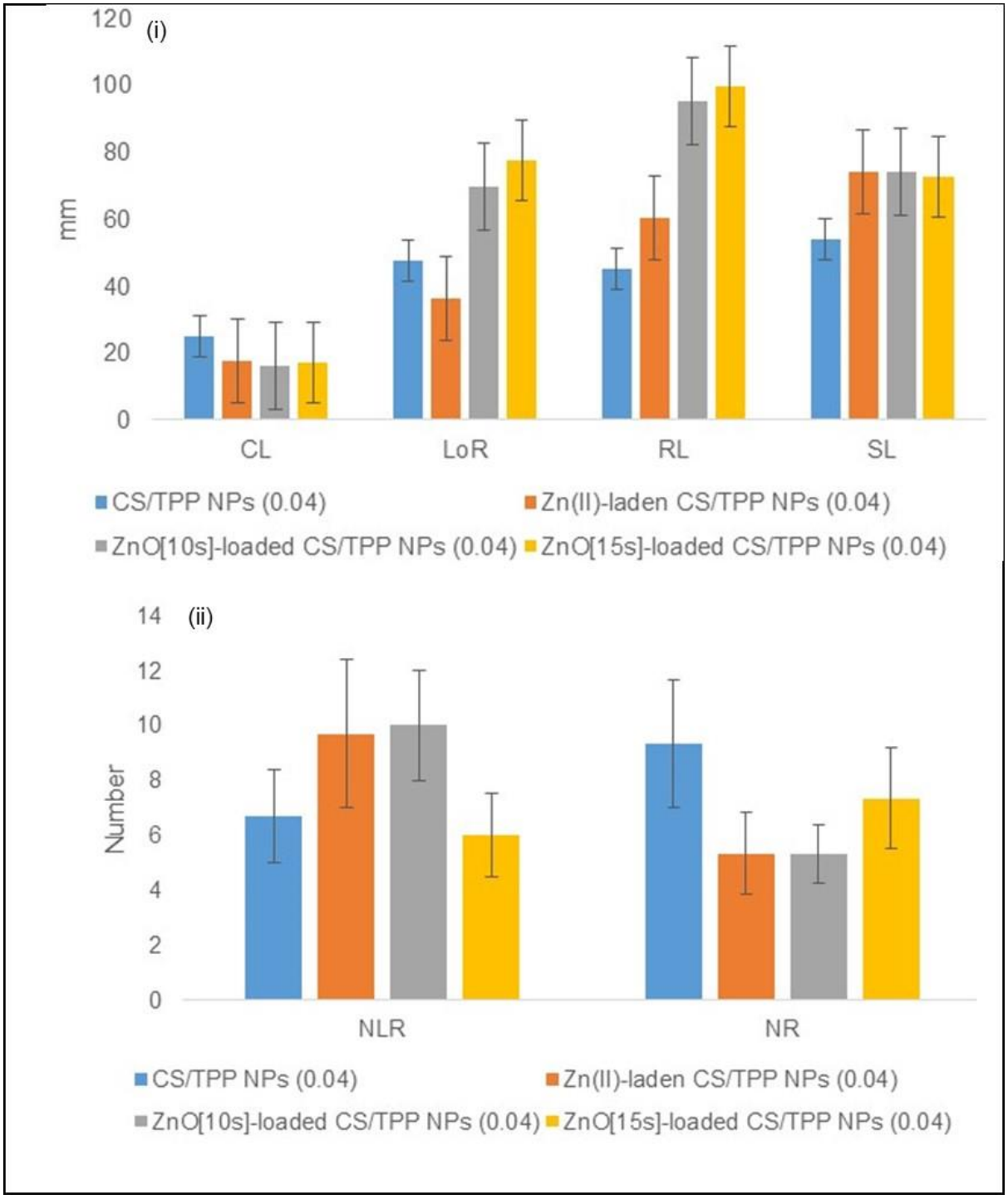


Figure 6. 10: Effects of the prepared CS/TPP, Zn(II)-laden CS/TPP, and ZnO-loaded CS/TPP NPs at 0.04% on selected growth parameters with a significance difference ($P \leq 0.05$).

Table 6. 3: Growth traits for 10-day-old seedlings under non-stress conditions.

Treatment	CL	LoR	NLR	NR	RL	SL
Water	15.00[b]	15.80[c]	5.00[a]	5.00[b]	20.00[a]	37.30[b]
CS/TPP NPs (0.01%)	18.30[a]	33.60[b]	6.02[a]	10.33[a]	35.70[a]	32.00[b]
Zn(II)-laden CS/TPP NPs (0.01%)	25.00[a]	58.10[a]	9.00[a]	9.33[a]	27.70[a]	81.70[a]
ZnO[10s]-loaded CS/TPP NPs (0.01%)	23.70[a]	46.90[b]	20.00[a]	6.67[b]	66.30[a]	79.00[a]
ZnO[15s]-loaded CS/TPP NPs (0.01%)	17.01[a]	24.71[b]	13.00[a]	3.66[b]	39.00[a]	42.00[a]
CS/TPP NPs (0.04%)	25.00[a]	47.60[b]	6.70[a]	9.33[a]	45.00[a]	54.00[a]
Zn(II)-laden CS/TPP NPs (0.04%)	17.70[a]	36.40[a]	9.70[a]	5.33[b]	60.30[a]	74.00[a]
ZnO[10s]-loaded CS/TPP NPs (0.04%)	16.00[a]	69.80[a]	10.00[a]	5.33[b]	95.00[a]	74.00[a]
ZnO[15s]-CS/TPP NPs (0.04%)	16.99[a]	77.41[a]	6.00[a]	7.32[a]	99.70[a]	72.70[a]

Variables with different letters in the same column are significantly different at 5% probability level *($P \leq 0.05$).*

The coleoptile, radicle, shoot, and root dry mater productions were also significantly affected in the nanopriming systems compared to the control (Table 6.4). The seeds treated with only water (control) exhibited increased CDW (0.035 g) and SDW (0.052 g) as compared with the seeds exposed to nanoparticles. The second highest CDW and SDW were averaged to be 0.032 g for seeds treated with ZnO[10s]-loaded CS/TPP NPs 0.01%. A comparable mass (0.031 g) was also recorded using Zn(II)-laden CS/TPP NPs 0.04%. The highest mean RDW (0.015 g) and RoDW (0.033 g) were found from seeds primed with ZnO[10s]-loaded CS/TPP NPs 0.01% and Zn(II)-laden CS/TPP NPs 0.01%, respectively. Seed priming with Zn(II)-laden CS/TPP NPs 0.01%, ZnO[10s]-loaded CS/TPP NPs 0.01%, CS/TPP NPs 0.04%, ZnO[15s]-loaded CS/TPP NPs 0.04% showed a significant increase (> 2-fold) in the dry weight of the roots in 10 day-old seedlings in comparison with the control.

Table 6. 4: Effects of pristine chitosan NPs and Zn-loaded chitosan NPs on dry matter yield (g) for the seeds germinated under normal conditions.

Treatment	CDW	RDW	SDW	RoDW
Water	0.035^{a}	0.009^{c}	0.052^{a}	0.011^{c}
CS/TPP NPs (0.01%)	0.014^{c}	0.006^{d}	0.012^{d}	0.018^{b}
Zn(II)-laden CS/TPP NPs (0.01%)	0.027^{b}	0.005^{e}	0.024^{c}	0.033^{a}
ZnO[10s]-loaded CS/TPP NPs (0.01%)	0.032^{a}	0.015^{a}	0.032^{b}	0.028^{a}
ZnO[15s]-loaded CS/TPP NPs (0.01%)	0.018^{c}	0.007^{a}	0.008^{c}	0.007^{c}
CS/TPP NPs (0.04%)	0.018^{c}	0.008^{c}	0.020^{c}	0.021^{b}
Zn(II)-laden CS/TPP NPs (0.04%)	0.012^{c}	0.011^{b}	0.031^{b}	0.012^{c}
ZnO[10s]-loaded CS/TPP NPs (0.04%)	0.012^{c}	0.010^{b}	0.020^{c}	0.018^{b}
ZnO[15s]-loaded CS/TPP NPs (0.04%)	0.015^{c}	0.008^{c}	0.020^{c}	0.025^{b}

Variables with different letters in the same column are significantly different at 5% probability level *($P \leq 0.05$).*

6.3.2 Effects on germination of salt-stressed seeds

The seeds primed with Zn(II)-laden CS/TPP NPs (0.01 and 0.04%), ZnO[10s]-loaded CS/TPP NPs 0.01%, ZnO[15s]-loaded CS/TPP NPs 0.04% and CS-TPP 0.04% under salt stress had the longest mean CL 31.0, 25.7, 25.1, 27.3, 25, and 24.3 mm, respectively (Figure 6.11 and 6.12). The control group and seeds germinated under salt conditions, with no addition of nanoparticles, displayed significantly lower average CL. The length of roots was recorded from the highest performed treatment

to the least. The ZnO[10s]-loaded CS/TPP NPs 0.01% priming solution significantly increased the root length (> 75%) of seedlings developing under salt stress than the control group. The mean LoR of the seeds exposed to ZnO[10s]-loaded CS/TPP NPs 0.01%, Zn(II)-laden CS/TPP NPs 0.01%, ZnO[10s]-loaded CS/TPP NPs 0.04%, and ZnO[15s]-loaded CS/TPP NPs 0.04% were 63.4, 52.7, 46.3, and 45.8 mm, respectively. A considerable inhibition of root growth was observed with the NaCl set (LoR 13.6 mm), relative to the control group (LoR 15.8 mm). The effects of salinity slow cell division and nutrient uptake in root meristems, thereby impairing the seed germination and early seedling growth [41]. It is worth mentioning that knowledge of the stages of salt stress in *Z. mays* suggests that Na^+ ions represent the main species causing toxicity rather than Cl^- [42]. It is foreseen that the nanocomposites described in this study alleviate salt stress by lowering the absorption of Na^+ ions in the seeds and seedlings. These nanoparticles release Zn^{2+} ions (radius 0.074 nm) that can be easily absorbed by plant tissues than Na^+ ions (radius 0.102 nm).

Regarding the number of lateral roots, the CS/TPP NPs 0.04% and ZnO[10s]-loaded CS/TPP NPs 0.01% treatments resulted in better growth (NLR 19.7 and 17.0, respectively) compared to other groups. The highest average number of roots was recorded from the seed priming with Zn(II)-laden CS/TPP NPs 0.04% (10.3), followed by CS/TPP NPs 0.01% (9.3). The NaCl treatment also evidenced the root growth inhibition (NR 4.3). Furthermore, the mean radicle length from seeds primed with ZnO[10s]-loaded CS/TPP NPs 0.01%, Zn(II)-laden CS/TPP NPs 0.01%, CS/TPP NPs 0.04%, and ZnO[10s]-loaded CS/TPP NPs 0.04% was 6.7-fold, 4.0-fold, 3.7-fold, and 2.8-fold greater than the control. When analyzing the shoot length, Zn(II)-laden CS/TPP NPs 0.01%, ZnO[15s]-loaded CS/TPP NPs 0.01%, and CS/TPP NPs 0.01% treatments had the best variables (SL 49.3, 41.7 and 38.0 mm, respectively). Seed priming with CS/TPP NPs, ZnO[10s]-loaded CS/TPP NPs, and Zn(II)-laden CS/TPP NPs at 0.01%, influenced the early development of the salt-stressed seeds, mainly by increasing CL, LoR, NLR, and NR, compared to the control. It is anticipated that these chitosan-based nanostructures could counteract the inhibitory effects of salt conditions by triggering the production of intracellular messengers, H_2O_2, nitric oxide (NO), and Ca^{2+} [43, 44], which induce physiological responses. In addition, the antioxidant properties of chitosan could alleviate the oxidative stress caused by salinity [45]. In agreement with the findings presented

here, Abdel-Aziz (2019) reported that priming of *Vicia faba* seed with CS/methacrylic acid NPs 0.05% increased the activities of polyphenol oxidase, peroxidase, ascorbate peroxidase, and catalase during salt stress [46]. The scavenging activities of chitosan against ROS are attributed to the reactivity of its –OH and $–NH_2$ groups.

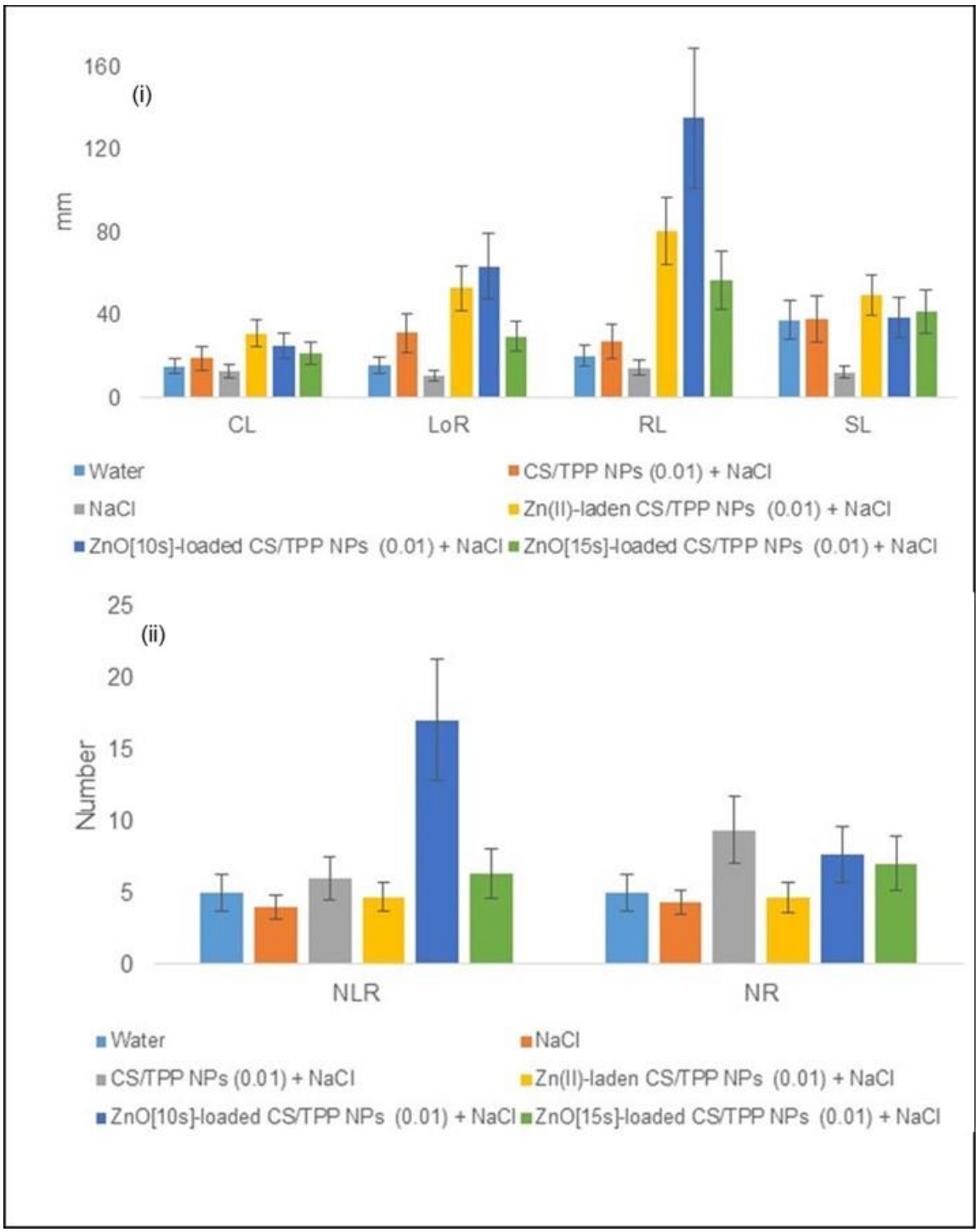


Figure 6. 11: Effects of the prepared CS/TPP, Zn(Ⅱ)-laden CS/TPP, and ZnO-loaded CS/TPP NPs at 0.01% on the growth parameters under salt stress (600 mM). Means

were recorded from replicates for each treatment and significantly different at $P \leq 0.05$.

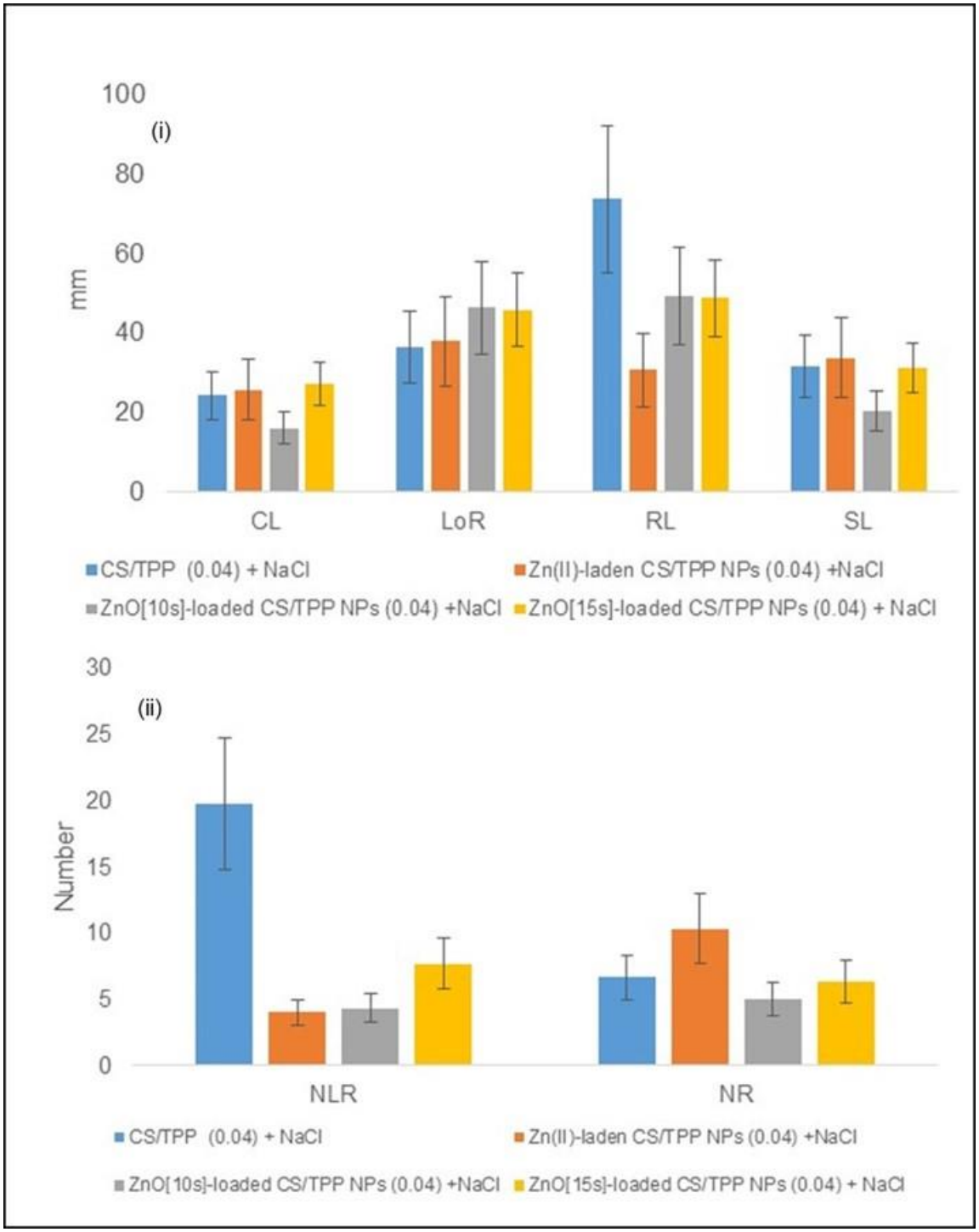


Figure 6. 12: Effects of the prepared CS/TPP, Zn(Ⅱ)-laden CS/TPP, and ZnO-loaded CS/TPP NPs at 0.04% on the growth parameters under salt stress (NaCl 600 mM). Means were recorded from replicates for each treatment and significantly different at $P \leq 0.05$.

Table 6. 5: Growth traits for 10-day-old seedlings under salt stress conditions.

Treatment	CL	LoR	NLR	NR	RL	SL
Water	15.00[b]	15.80[b]	5.00[a]	5.00[a]	20.00[c]	37.30[a]
NaCl	12.70[b]	10.60[b]	4.00[a]	4.33[a]	14.30[c]	12.30[b]
CS/TPP NPs (0.01%) + NaCl	19.00[b]	31.10[a]	6.00[a]	9.33[a]	27.30[c]	38.00[a]
Zn(II)-laden CS/TPP NPs (0.01%) + NaCl	31.00[a]	52.70[a]	4.70[a]	4.67[a]	80.30[b]	49.30[a]
ZnO[10s]-loaded CS/TPP NPs (0.01%) + NaCl	25.10[a]	63.40[a]	17.00[a]	7.67[a]	135.00[a]	38.70[a]
ZnO[15s]-loaded CS/TPP NPs (0.01%) + NaCl	21.30[a]	29.50[a]	6.30[a]	7.00[a]	56.71[b]	41.7.0[a]
CS/TPP NPs (0.04%) + NaCl	24.30[a]	36.50[a]	19.70[a]	6.67[a]	73.70[b]	31.70[a]
Zn(II)-laden CS/TPP NPs (0.04%) + NaCl	25.70[a]	37.90[a]	4.00[a]	10.33[a]	30.70[c]	33.70[a]
ZnO[10s]-loaded CS/TPP NPs (0.04%) + NaCl	16.00[b]	46.30[a]	4.30[a]	5.00[a]	49.30[b]	20.30[b]
ZnO[15s]-loaded CS/TPP NPs (0.04%) + NaCl	27.30[b]	45.80[a]	7.70[a]	6.33[a]	48.70[b]	31.30[a]

The priming treatments studied also significantly affected the dry mass of the growth parameters (Table 6.6). The results indicate higher coleoptile and shoot dry matter from the control group. The maximum radicle dry weight was recorded from ZnO[10s]-loaded CS/TPP NPs 0.04% (0.024 g), followed by CS/TPP NPs 0.04% (0.019 g), and Zn(II)-laden CS/TPP NPs 0.04% (0.017 g). The ZnO[15s]-loaded CS/TPP NPs 0.04%, on the other hand, showed the highest average dry weight of roots (0.057). Remarkably, all CS/TPP NPs and zinc-loaded CS/TPP NPs (0.01% and 0.04%) treatments increased RoDW compared to the control. These results corroborate chitosan's effectiveness in increasing seeds' germination rate, even under salt stress conditions [47].

Table 6. 6: Effects of pristine chitosan NPs and Zn-loaded chitosan NPs on dry matter yield (g) for the seeds germinated under salinity stress.

Treatment	CDW	RDW	SDW	RoDW
Water	0.035^{a}	0.009^{c}	0.052^{a}	0.011^{c}
NaCl (600 mM)	0.012^{b}	0.013^{b}	0.031^{b}	0.035^{b}
CS/TPP NPs (0.01%)	0.013^{b}	0.007^{b}	0.017^{bc}	0.022^{b}
Zn(II)-laden CS/TPP NPs (0.01%)	0.013^{b}	0.011^{b}	0.016^{c}	0.042^{ab}
ZnO[10s]-loaded CS/TPP NPs (0.01%)	0.029^{a}	0.006^{c}	0.012^{c}	0.027^{b}
ZnO[15s]-loaded CS/TPP NPs (0.01%)	0.015^{b}	0.005^{c}	0.017^{bc}	0.014^{bc}
CS/TPP NPs (0.04%)	0.010^{b}	0.019^{a}	0.015^{c}	0.014^{bc}
Zn(II)-laden CS/TPP NPs (0.04%)	0.008^{c}	0.017^{a}	0.029^{b}	0.022^{b}
ZnO[10s]-loaded CS/TPP NPs (0.04%)	0.011^{b}	0.024^{a}	0.012^{c}	0.020^{b}
ZnO[15s]-loaded CS/TPP NPs (0.04%)	0.012^{b}	0.014^{a}	0.013^{c}	0.057^{a}

Means with the different letters in the same column are significantly different at 5% probability level *($P \leq 0.05$).*

REFERENCES

1. Devika, O. S.; Singh, S.; Sarkar, D.; Barnwal, P.; Suman, J. & Rakshit, A. 2021. Seed priming: A potential supplement in integrated resource management under fragile intensive ecosystems. *Frontiers in Sustainable Food Systems*. 5, 654001.

2. Sarkar, D.; Kar, S. K.; Chattopadhyay, A.; Rakshit, A.; Tripathi, V. K.; Dubey, P. K. & Abhilash, P. C. 2020. Low input sustainable agriculture: a viable climate-smart option for boosting food production in a warming world. *Ecological Indicators*, 115, 106412.

3. Rosental, L.; Nonogaki, H. & Fait, A. 2014. Activation and regulation of primary metabolism during seed germination. *Seed Science Research*, 24, 1-15.

4. Majda, C.; Khalid, D.; Aziz, A.; Rachid, B.; Badr, A.-S.; Lotfi, A. & Mohamed, B. 2019. Nutri-priming as an efficient means to improve the agronomic performance of molybdenum in common bean (*Phaseolus vulgaris* L.). *Science of the Total Environment*, 661, 654-663.

5. Nile, S. H.; Thiruvengadam, M.; Wang, Y.; Samynathan, R.; Shariati, M. A.; Rebezov, M.; Nile, A.; Sun, M.; Venkidasamy, B.; Xiao, J. & Kai, G. 2022. Nano-priming as emerging seed priming technology for sustainable agriculture-recent developments and future perspectives. *Journal of Nanobiotechnology*, 20, 254.

6. Chandrasekaran, U.; Luo, X.; Wang, Q. & Shu, K. 2020. Are there unidentified factors involved in the germination of nano-primed seeds? *Frontiers in Plant Science*, 11, 832.

7. Wojtyla, Ł.; Lechowska, K.; Kubala, S. & Garnczarska, M. 2016. Different modes of hydrogen peroxide action during seed germination. *Frontiers in Plant Science*, 7, 66-66.

8. Mahakham, W.; Sarmah, A. K.; Maensiri, S. & Theerakulpisut, P. 2017. Nanopriming technology for enhancing germination and starch metabolism of

aged rice seeds using phytosynthesized silver nanoparticles. *Scientific Reports*, 7, 8263.

9. Anaya, F.; Fghire, R.; Wahbi, S. & Loutfi, K. 2018. Influence of salicylic acid on seed germination of *Vicia faba* L. under salt stress. *Journal of the Saudi Society of Agricultural Sciences*, 17(1), 1-8.

10. Gianinetti, A. 2020. Basic features of the analysis of germination data with generalized linear mixed models. *Data*, 5(1), 6.

11. Salika, R. & Riffat, J. 2021. Abiotic stress responses in maize: A review. *Acta Physiologiae Plantarum*, 43(9), 1-22.

12. Ding, Z.; Kheir, A. M. S.; Ali, M. G. M.; Ali, O. A. M.; Abdelaa, A. I. N.; Lin, X.; Zhou, Z.; Wang, B.; Liu, B. & He, Z. 2020. The integrated efect of salinity, organic amendments, phosphorus fertilizers, and defcit irrigation on soil properties, phosphorus fractionation and wheat productivity. *Scientific Reports*, 10, 2736.

13. Manohara, K. K.; Gireesh, C.; Anantha, M. S.; Sakhare, A. S.; Parmar, B.; Yadav, B. K.; Bandumula, N.; Raihan, F.; Zielinska-Chmielewska, A.; Meriño-Gergichevich, C.; Reyes-Díaz, M.; Khan, A.; Panfilova, O.; Fuentealba, A. S.; Romero, S. M.; Nabil, B.; Wan, C.; Shepherd, J. & Horvatinec, J. 2022. Salt stress in plants and mitigation approaches. *Plants*, 11, 717.

14. He, M.; He, C.-Q. & Ding, N.-Z. 2018. Abiotic stresses: General defenses of land plants and chances for engineering multistress tolerance. *Frontiers in Plant Science*, 9, 1771.

15. Prasad, T. N. V. K. V.; Sudhakar, P.; Sreenivasulu, Y.; Latha, P.; Munaswamy, V.; Reddy, K. R.; Sreeprasad, T. S.; Sajanlal, P. R. & Pradeep, T. 2012. Effect of nanoscale zinc oxide particles on the germination, growth and yield of peanut. *Journal of Plant Nutrition*, 35, 905-927.

16. Abdel Latef, A. A. H.; Abu Alhmad, M. F. & Abdelfattah, K. E. 2017. The possible roles of priming with ZnO nanoparticles in mitigation of salinity stress

in lupine (*Lupinus termis*) plants. *Journal of Plant growth Regulation*, 36(1), 60-70.

17. Zayed, M. M.; Elkafafi, S. H.; Zedan, A. M. G. & Dawoud, S. F. M. 2017. Effect of nano chitosan on growth, physiological and biochemical parameters of *Phaseolus vulgaris* under salt stress. *Journal of Plant Production, Mansoura University*, 8(5), 577-585.

18. Wang, Z.; Xie, X.; Zhao, J.; Liu, X.; Feng, W.; White, J. C. & Xing, B. 2012. Xylem- and phloem-based transport of CuO nanoparticles in maize (*Zea mays* L.). *Environmental Science & Technology*, 46, 4434-4441.

19. Potocka, I. & Szymanowska-Pułka, J. 2018. Morphological responses of plant roots to mechanical stress. *Annals of Botany*, 122, 711-723.

20. Li, X.; Zeng, R. & Liao, H. 2016. Improving crop nutrient efficiency through root architecture modifications. *Journal of Integrative Plant Biology*, 58, 193-202.

21. Ju, C. X.; Buresh, R. J.; Wang, Z. Q.; Zhang, H.; Liu, L. J.; Yang, J. C. & Zhang, J. H. 2015. Root and shoot traits for rice varieties with higher grain yield and higher nitrogen use efficiency at lower nitrogen rates application. *Field Crops Research*, 175, 47-55.

22. Baalbaki, R.; Chaharsoughi, S. A.; Le, V. & Koonse, S. 2018. Radicle length in agar is a reliable predictor of seed vigor. *Seed Technology*, 39 (1/2), 155-171.

23. Kazmi, R. H.; Willems, L. A. J.; van Heusden, A. W.; Ligterink, W. & Hilhorst, H. W. M. 2012. Exploring the natural variation for seedling traits and their link with seed dimensions in tomato. *PLoS ONE*, 7(8), e43991.

24. Fageria, N. K. 2002. Influence of micronutrients on dry matter yield and interaction with other nutrients in annual crops. *Pesquisa Agropecuária Brasileira*, 37(12), 1765-1772.

25. Szulc, P.; Ambrozy-Deregowska, K.; Waligóra, H.; Mejza, I.; Grzes, S.; Zielewicz, W. & Wróbel, B. 2021. Dry Matter yield of maize (*Zea mays* L.) as an indicator of mineral fertilizer efficiency. *Plants*, 10, 535.

26. Baz, H., Creech, M.; Chen, J.; Gong, H.; Bradford, K. & Huo, H. 2020. Water-soluble carbon nanoparticles improve seed germination and post-germination growth of lettuce under salinity stress. *Agronomy*, 10(8), 1192.

27. Munns, R. & Tester, M. 2008. Mechanisms of salinity tolerance. *Annual Review of Plant Biology*, 59, 651.

28. Wang, H.; An, T.; Huang, D.; Liu, R.; Xu, B.; Zhang, S.; Deng, X.; Siddique, K. H. M. & Chen, Y. 2021. Arbuscular mycorrhizal symbioses alleviating salt stress in maize is associated with a decline in root-to-leaf gradient of Na^+/K^+ ratio. *BMC Plant Biology*, 21, 457.

29. Koevoets, I. T.; Venema, J. H.; Elzenga, J. T. M. & Testerink, C. 2016. Roots withstanding their environment: exploiting root system architecture responses to abiotic stress to improve crop tolerance. *Frontiers in Plant Science*, 7, 1335.

30. Gao, X.; Zou, C.; Wang, L. & Zhang, F. 2006. Silicon decreases transpiration rate and conductance from stomata of maize plants. *Journal of Plant Nutrition*, 29(9) 1637-1647.

31. Baličević, R.; Ravlić, M.; Knežević, M. & Serezlija, I. 2014. Allelopathic effect of field bindweed (*Convolvulus arvensis* L.) water extracts on germination and initial growth of maize. *The Journal of Animal and Plant Sciences*, 24(6), 1844-1848.

32. Ayele, A.; Sharma, J.J. & Nigatu, L. 2014. The Impact of Commolina benghalensis Extract on Maize (*Zea mays* L.) Seed Germination and Early Seedling Growth. *Journal of Biology, Agriculture and Healthcare*, 4, 43-46.

33. Ling, Y.; Zhao, Y.; Cheng, B.; Tan, M.; Zhang, Y. & Li, Z. 2022. Seed priming with chitosan improves germination characteristics associated with alterations in antioxidant defense and dehydration-responsive pathway in white clover under water stress. *Plants*, 11, 2015.

34. Samaneh Attaran Dowom, S. A.; Karimian, Z.; Dehnavi, M. M. & Samiei, L. 2022. Chitosan nanoparticles improve physiological and biochemical responses of *Salvia abrotanoides* (Kar.) under drought stress. *BMC Plant Biology*, 22, 364.

35. Ozturk, L.; Yazici, M. A.; Yucel, C.; Torun, A.; Cekic, C.; Bagci, A.; Ozkan, H.; Braun, H.-J.; Sayers, Z. & Cakmak, I. 2006. Concentration and localization of zinc during seed development and germination in wheat. *Physiologia Plantarum*, 128, 144-152.

36. Iglesias, M. J.; Colman, S. L.; Terrile, M. C.; Paris, R.; Martín-Saldaña, S.; Chevalier, A. A.; Alejandra, A. V. & Casalongue, C. 2019. Enhanced properties of chitosan microparticles over bulk chitosan on the modulation of auxin signaling pathway with beneficial impacts on root architecture in plants. *Journal of Agricultural and Food Chemistry*, 67, 6911-6920.

37. Choudhary, R. C.; Kumaraswamy, R. V.; Kumari, S.; Sharma, S. S.; Pal, A.; Raliya, R.; Biswas, P. & Saharan, V. 2019. Zinc encapsulated chitosan nanoparticle to promote maize crop yield. *International Journal of Biological Macromolecules*, 127, 126-135.

38. Yang, Z.; Chen, J.; Dou, R.; Gao, X.; Mao, C. & Wang, L. 2015. Assessment of the phytotoxicity of metal oxide nanoparticles on two crop plants, maize (*Zea mays* L.) and rice (*Oryza sativa* L.). *International Journal of Environmental Research and Public Health*, 12, 15100-15109.

39. Zhang, R.; Zhang, H.; Tu, C.; Hu, X.; Li, L.; Luo, Y. & Christie, P. 2015. Phytotoxicity of ZnO nanoparticles and the released Zn (II) ion to corn (*Zea mays* L.) and cucumber (*Cucumis sativus* L.) during germination. *Environmental Science and Pollution Research*, 22, 11109-11117.

40. Lin, D. & Xing, B. 2008. Root uptake and phytotoxicity of ZnO nanoparticles. *Environmental Science & Technology*, 42, 5580-5585.

41. Ondrasek, G.; Rathod, S.; Manohara, K. K.; Gireesh, C.; Anantha, M. S.; Sakhare, A. S.; Parmar, B.; Yadav, B. K.; Bandumula, N.; Raihan, F.; Zielinska-Chmielewska, A.; Meriño-Gergichevich, C.; Reyes-Díaz, M.; Khan, A.; Panfilova, O.; Fuentealba, A. S.; Romero, S. M.; Nabil, B.; Wan, C.; Shepherd, J. & Horvatinec, J. 2022. Salt stress in plants and mitigation approaches. *Plants* 11, 717.

42. Wang, H.; An, T.; Huang, D.; Liu, R.; Xu, B.; Zhang, S.; Deng, X.; Siddique, K. H. M. & Chen, Y. 2021. Arbuscular mycorrhizal symbioses alleviating salt stress in maize is associated with a decline in root-to-leaf gradient of Na^+/K^+ ratio. *BMC Plant Biology*, 21, 457.

43. Hidangmayum, A.; Dwivedi, P.; Katiyar, D. & Hemantaranjan, A. 2019. Application of chitosan on plant responses with special reference to abiotic stress. *Physiology and Molecular Biology of Plants*, 25(2), 313-326.

44. Hu, T.; Chen, K.; Hu, L.; Amombo, E. & Fu, J. 2016. H_2O_2 and Ca^{2+}-based signaling and associated ion accumulation, antioxidant systems and secondary metabolism orchestrate the response to NaCl stress in perennial ryegrass. *Scientific Reports*, 6, 36396.

45. Jabeen, N. & Ahmad, R. 2013. The activity of antioxidant enzymes in response to salt stress in safflower (*Carthamus tinctorius* L.) and sunflower (*Helianthus annuus* L.) seedlings raised from seed treated with chitosan. *Journal of the Science of Food and Agriculture*, 93, 1699-1705.

46. Abdel-Aziz, H. M. M. 2019. Effect of priming with chitosan nanoparticles on germination, seedling growth and antioxidant enzymes of broad beans. *Catrina* 18, 81-86.

47. Mahdavi, B. & Rahimi, A. 2013. Seed priming with chitosan improves the germination and growth performance of ajowan (*Carum copticum*) under salt stress. *EurAsian Journal of BioSciences*, 7, 69-76.

CHAPTER 7

ANTIFUNGAL PROPERTIES OF THE DEVELOPED IRON OXIDE AND IRON LOADED CHITOSAN NANOPARTICLES

7.1 Antifungal potential of metal oxide and chitosan nanoparticles

Fungal pathogens contribute to over 30% of all crop diseases and cause hefty losses in crop production [1]. The impact of fungi in agricultural activities has been estimated at around 65% of pathogen-driven host loss [2]. Annually, diseases caused by these organisms also destroy up to a third of all harvests, posing a threat to food security. Current variations in climatic conditions have resulted in more emerging fungal pathogens. These produce toxins that can adversely affect the physiological functions of host plants. Generally, the secondary metabolites generated by pathogenic fungi are low molecular weight compounds that encourage symptoms such as chlorosis, wilting, necrosis, and leaf spotting [3]. These toxins mainly interact with host plants' cell membrane, chloroplasts, and mitochondria [4]. They are also well-reported in food contamination. Several mycotoxins, including aflatoxin (produced by *Aspergillus flavus*) and fumonisins (produced by *Fusarium verticillioides*), have been classified as substances with mutagenic and carcinogenic potential in humans. Aflatoxins and fumonisins are recurrent contaminants in cereals.

The dissemination of plant-harming fungi occurs by wind and water. Although fungal spores can undergo devitalization during aerial transport due to atmospheric components, many remain active. For centuries, fungicide chemicals have been used extensively to control the growth of pathogenic fungi and avoid diseases in crops. However, this control strategy is described as unsafe for the environment and for humans. Moreover, their site-specific action causes the development of resistant strains. The earliest chemical control treatments were executed with copper-containing formulations, which are still widely used today. Many reports have also been devoted to developing biological control methods based on the application of fungal antagonists or their inhibitory metabolites [5]. Nevertheless, manipulating the micro-environment to facilitate the activity of antagonists is challenging.

Lately, engineered nanomaterials consisting of metal and metal oxide NPs have garnered interest in biomedical applications; numerous reports exhibit their great potential on nutritional enhancement and disease suppression [6-8]. The most commonly studied include metals or metallic oxides of silver, copper, titanium, cerium, and zinc [9]. Nonetheless, a study by Zaheer et al. (2022) [10] on the pesticidal potential of iron oxide NPs, magnesium oxide NPs, and zinc oxide NPs showed the lowest lethal concentrations with iron oxide NPs. These have been described for their inhibitory effect on the growth of pathogenic fungi such as *Aspergillus niger*, *A. flavus*, *Penicillium chrysogenum*, *P. spinulosum*, *Trichothecium roseum*, *Cladosporium herbarum*, and *Alternaria alternata* [11,12]. The antifungal effect of nano-metal oxides correlates with the oxidative burst. The interactions between these nanoparticles and fungal cells can indirectly induce ROS formation through processes associated with surface defects, corrosion, photo-excitation, and the Fenton-like and Haber-Weiss reactions (Figure 7.1) [13]. ROS take part in lipid peroxidation and can trigger damage to proteins and DNA in pathogenic fungi. The free Fe ions are also important catalysts for the oxidative fragmentation of DNA.

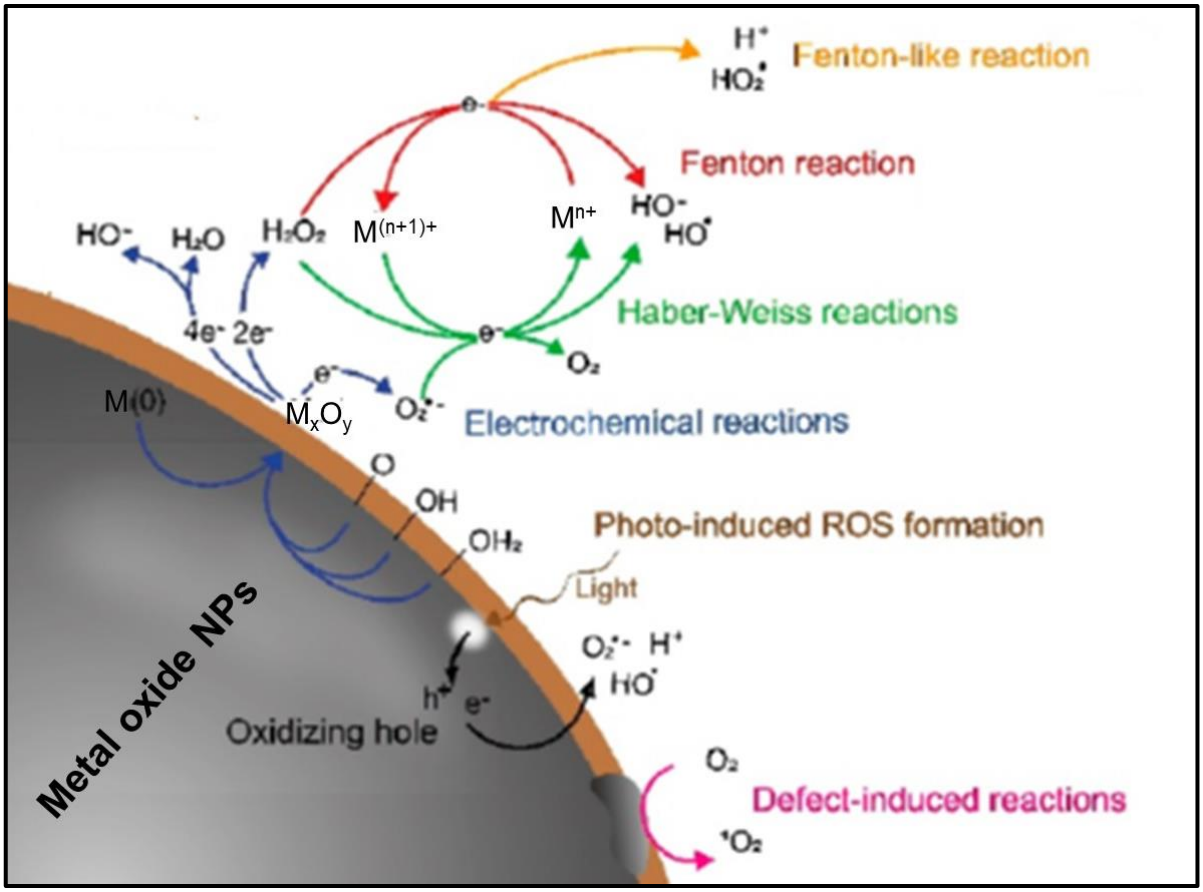


Figure 7. 1: Schematic representation of the possible processes occurring at the surface of nano-metal oxide for the formation of ROS in biological settings.

Chitosan has also been reported in agricultural commodities to control fungal plant diseases caused by *Fusarium oxysporum* [14], *A. tenuissima* [15], *P. expansum* [16], *Lasiodiplodia theobromae* [17], *A. niger*, and *A. alternata* [18]. The antifungal properties of chitosan have been ascribed to its polycationic nature that allows binding to the negatively charged functional groups of cell wall components of fungi. The nano-engineered particles of this natural polysaccharide, obtained by ionic crosslinking low-and high-molecular weight chitosan with TPP, were also proven to inhibit the growth of *F. oxysporium*, *F. sembaticum*, and *A. niger* [19,20]. The transformation of bulk chitosan into chitosan NPs can provide materials with increasing biological activity due to larger surface area and higher encapsulation efficacy [21]. Moreover, the fungicidal activity of such materials is influenced by the nanoparticles' structural and functional properties. Nanoparticles with distinct physicochemical characteristics may show different inhibition mechanisms against fungal pathogens.

In the present study, the nano-iron oxide Fe_3O_4[5s] (210.3 nm; -18.5 mV), Fe_3O_4[10s] (203.2 nm; -28.3 mV), and Fe_3O_4[15s] (183.8 nm; -30.3 mV) were prepared by a green procedure using aqueous *H. odoratissimum* extract. The as-prepared iron-based NPs were then integrated into nanostructured TPP-crosslinked chitosan to give the Fe_3O_4[5s]-loaded CS/TPP (498.8 nm; 18.6 mV), Fe_3O_4[10s]-loaded CS/TPP (281.8 nm, 24.4 mV), and Fe_3O_4[15s]-loaded CS/TPP (226.7 nm, 27.3 mV) nanocomposites. The bulk ferrous sulphate was also successfully integrated into TPP-crosslinked chitosan NPs to yield the Fe(II)-laden CS/TPP (334.1 nm, 27.4 mV) nano-product. These nanomaterials were screened for their antifungal activity against *A. niger*, *A. flavas*, *A. solani*, *F. oxysporum*, *F. solani*, and *F. verticillioides*. The emerging pathogen groups *Aspergillus*, *Fusarium*, and *Penicillium* have been described as predominant fungal genera in maize infection and post-harvest losses [22,23].

7.2 Activities against selected plant pathogenic fungi

The selected nanomaterials displayed various levels of antifungal activity, as indicated in Table 7.1, against different phytopathogenic fungi. The lower the MIC value, the stronger the antifungal activity. The Fe_3O_4[10s] NPs demonstrated remarkable antifungal activities with MIC < 1.0 mg/mL against all pathogens except *F. oxysporum*. The antipathogenic activity of the biogenic Ag NPs blended with *Pyre acantha grandiflora* extract was noteworthy when the MIC values were lower than 1.0 mg/mL [24]. As compared with the Fe_3O_4[10s] NPs, the nano-oxide Fe_3O_4[15s] exhibited stronger antifungal activities against all the pathogens except *F. solani*. On the other hand, the Fe3O4[15s]-loaded CS/TPP NPs showed stronger activities against four pathogenic fungal strains, *A. niger*, *F. solani*, *A. solani*, and *A. flavas*. This nanocomposite performed better than the analogous Fe_3O_4[10s]-loaded CS/TPP and revealed the lowest MIC (0.208 mg/mL), against *A. niger*. In contrast to the pristine Fe_3O_4[15s] NPs, the Fe_3O_4[15s]-loaded CS/TPP NPs showed superior effectiveness for *A. niger*, *F. solani*, and *A. solani,* presumably due to the combinative effect of iron-based NPs and chitosan NPs [25]. Also, the Fe(II)-laden CS/TPP NPs demonstrated stronger activities against *F. solani* (MIC 0.3125 mg/mL) and *A. flavas* (MIC 0.625 mg/mL). Although amphotericin B displayed excellent activity compared to all nanomaterials tested, the latter could enable foliar adhesion

and sustained action. A previous investigation on the foliar application of copper-containing nanoparticles ($Cu(OH)_2$ and CuO) has established that these adhere to the plant surface for many days, even after washing [26].

Of the five nanomaterials screened separately, four, three, and three nanoproducts displayed impressive activity (MIC < 1.0 mg/mL) against *A. flavas*, *A. solani*, *F. solani*, and *A. niger*, respectively. Thus, the antifungal properties demonstrated by the prepared nanoparticles indicate their potential for controlling phytopathogenic fungi associated with pre-and post-harvest losses and food contamination in agricultural production.

Table 7. 1: Antifungal activity of the prepared nanomaterials.

Nanomaterials	**MIC (mg/mL)**					
	A. niger	*F. solani*	*A. solani*	*F. verticillioides*	*A. flavas*	*F. oxysporum*
Fe_3O_4[10s] NPs	0.625	0.3125	0.625	0.3125	0.625	1.25
Fe_3O_4[15s] NPs	0.625	1.25	0.625	0.625	0.625	0.625
Fe_3O_4[10s]-loaded CS/TPP NPs	1.25	2.5	1.25	2.5	2.5	1.25
Fe_3O_4[15s]-loaded CS/TPP NPs	0.208	0.416	0.416	1.666	0.833	1.666
Fe(II)-laden CS/TPP NPs	1.25	0.3125	1.25	2.5	0.625	2.5
Amphotericin B	0.00122	0.00244	0.00488	0.00488	0.00122	0.00244

7.3 Activities against selected fungal pathogens of humans

The prevalence of fungal infections has risen dramatically in recent decades, resulting in nearly 1.7 million deaths per year worldwide [27]. This alarming situation is mainly due to the emergence of drug-resistant fungi, including *Candida* species. Although the genus *Candida* is found living in healthy humans' gastrointestinal, reproductive, and respiratory tracts, species like *C. albicans*, *C. tropicalis*, and *C. glabrata* are frequently encountered in opportunistic fungal infections [28]. The uncontrolled proliferation of fungus can lead to candidiasis, which refers to the development of infections affecting cutaneous, mucosal, and deep-seated organs [29]. Candidiasis treatment requires the use of systemic or topical antifungal agents.

The plethora of antifungal drugs would suggest that therapeutic needs for candidiasis infections are negligible. Unfortunately, there are still unmet needs. Adverse reactions such as hepatotoxicity, haemolytic anaemia, and nephrotoxicity are the most significant limitations in the current arsenal of antifungal compounds approved [30,31]. While *C. albicans* and *C. tropicalis* have emerged as the most virulent *Candida* species, the increasing prevalence of *C. glabrata* has been reported lately [32].

The Fe_3O_4[10s], Fe_3O_4[15s], Fe_3O_4[10s]-loaded CS/TPP, Fe_3O_4[15s]-loaded CS/TPP, and Fe(II)-laden CS/TPP nanomaterials were also evaluated for inhibitory activity against *C. tropicalis* and *C. glabrata,* and the results are presented in Table 7.2. The Fe_3O_4[10s] NPs showed potent antifungal activity against *C. tropicalis*, with a MIC value of 6.25 µg/ml. Previously, the biogenic iron oxide NPs developed using the aqueous leaf extract of *Rhamnus virgate* have shown potential results against *C. albicans* (MIC 62.5 µg/ml) [33]. As compared with the Fe_3O_4[10s] NPs, the nano-oxide Fe_3O_4[10s]-loaded CS/TPP demonstrated significant antifungal activities against both *Candida* species (MIC 6.25 and 25 µg/ml). The Fe_3O_4[15s]-loaded CS/TPP NPs and Fe(II)-laden CS/TPP NPs also revealed noteworthy activities against *C. tropicalis*, with a MIC value of 6.25 µg/ml. These results indicate the favourable antifungal effects of chitosan nanocarriers. In a related study, Caldeirão et al. (2021) prepared encapsulations of miconazole and fluconazole using iron oxide

NPs coated with chitosan [34]. The resulting nanomaterials showed better effects in reducing colony-forming units for *C. albicans* and *C. glabrata*.

All the selected nanomaterials, excluding Fe_3O_4[15s] NPs, showed good antifungal activity against the most virulent *Candida* species (*C. tropicalis*). The findings support the potential of the *H. odoratissimum*-mediated Fe_3O_4 NPs and Fe_3O_4-chitosan nanocomposites as novel anti-*Candida* therapeutic agents.

Table 7. 2: Antifungal activity of the prepared nanomaterials on human pathogens.

Nanomaterials	**MIC (µg/ml)**	
	C. tropicalis	*C. glabrata*
Fe_3O_4[10s] NPs	6.25	> 100
Fe_3O_4[15s] NPs	> 100	> 100
Fe_3O_4[10s]-loaded CS/TPP NPs	6.25	25
Fe_3O_4[15s] -loaded CS/TPP NPs	6.25	> 100
Fe(Ⅱ)-laden CS/TPP NPs	6.25	> 100

REFERENCES

1. Almeida, F.; Rodrigues, M. L. & Coelho, C. 2019. The still underestimated problem of fungal diseases worldwide. Frontiers in Microbiology, 10, 214.

2. Fisher, M. C.; Henk, D. A.; Briggs, C. J.; Brownstein, J. S. Madoff, L. C.; McCraw, S. L. & Gurr, S. J. 2012. Emerging fungal threats to animal, plant and ecosystem health. *Nature*, 484, 186-194.

3. Peng, Y.; Li, S. J.; Yan, J.; Tang, Y.; Cheng, J. P.; Gao, A. J.; Yao, X.; Ruan, J. J.; & Xu, B. L. 2021. Research progress on phytopathogenic fungi and their role as biocontrol agents. *Frontiers in Microbiology*, 12, 670135.

4. Tzelepis, G.; Dölfors, F.; Holmquist, L. & Dixelius, C. 2021. Plant mitochondria and chloroplasts are targeted by the *Rhizoctonia solani* RsCRP1 effector. *Biochemical and Biophysical Research Communications*, 544, 86-90.

5. Thambugala, K. M.; Daranagama, D. A.; Phillips, A. J. L.; Kannangara, S. D. & Promputtha, I. 2020. Fungi vs. fungi in biocontrol: An overview of fungal antagonists applied against fungal plant pathogens. *Frontiers in Cellular and Infection Microbiology*, 10, 604923.

6. Omran, B. A. & Baek, K.-H. 2022. Control of phytopathogens using sustainable biogenic nanomaterials: Recent perspectives, ecological safety, and challenging gaps. *Journal of Cleaner Production*, 372, 133729.

7. Khan, M. R. Siddiqui, Z. A. & Fang, X. 2022. Potential of metal and metal oxide nanoparticles in plant disease diagnostics and management: Recent advances and challenges. *Chemosphere*, 297, 134114.

8. Elmer, W.; Ma, C. & White, J. 2018. Nanoparticles for plant disease management. *Current Opinion in Environmental Science & Health*, 6, 66-70.

9. Adisa, I. O.; Pullagurala, V. L. R.; Peralta-Videa, J. R.; Dimkpa, C. O.; Elmer, W. H.; Gardea-Torresdey, J. L. & White, J. C. 2019. Recent advances in nano-enabled fertilizers and pesticides: a critical review of mechanisms of action. *Environmental Science: Nano*, 6(7), 2002-2030.

10. Zaheer, T.; Kandeel, M.; Abbas, R. Z.; Khan, S. R. & Aqib, A. I. 2022. Acaricidal potential and ecotoxicity of metallic nano-pesticides used against the major life stages of hyalomma ticks. *Life*, 12(7), 977.

11. Kessler, A.; Hedberg, J.; Blomberg, E.& Odnevall, I. 2022. Reactive oxygen species formed by metal and metal oxide nanoparticles in physiological media-A review of reactions of importance to nanotoxicity and proposal for categorization. *Nanomaterials*, 12(11), 1922.

12. Parveen, S.; Wani, A. H. Shah, M. A.; Devi, H. S.; Bhat, M. Y. & Koka, J. A. 2018. Preparation, characterization and antifungal activity of iron oxide nanoparticles. *Microbial Pathogenesis*, 115, 287-292.

13. Jamzad, M. & Bidkorpeh, M. K. 2020. Green synthesis of iron oxide nanoparticles by the aqueous extract of *Laurus nobilis* L. leaves and evaluation of the antimicrobial activity. *Journal of Nanostructure in Chemistry*, 10, 193-201.

14. Liu, Y.; Wisniewski, M.; Kennedy, J. F.; Jiang, Y.; Tang, J. & Liu, J. 2016. Chitosan and oligochitosan enhance ginger (*Zingiber officinale* Roscoe) resistance to rhizome rot caused by *Fusarium oxysporum* in storage. *Carbohydrate Polymers*, 151, 474-479.

15. Liu, J.; Zhang, X.; Kennedy, J. F.; Jiang, M.; Cai, Q. & Wu, X. 2019. Chitosan induces resistance to tuber rot in stored potato caused by *Alternaria tenuissima*. *International Journal of Biological Macromolecules*, 140, 851-857.

16. Li, H.; Wang, Y.; Liu, F.; Yang, Y.; Wu, Z.; Cai, H.; Zhang, Q.; Wang, Y. & Li, P. 2015. Effects of chitosan on control of postharvest blue mold decay of apple fruit and the possible mechanisms involved. *Scientia Horticulturae*, 186, 77-83.

17. Obianom, C.; Romanazzi, G. & Sivakumar D. 2019. Effects of chitosan treatment on avocado postharvest diseases and expression of phenylalanine ammonialyase, chitinase and lipoxygenase genes. *Postharvest Biology and Technology*, 147, 214-221.

18. Ziani, K.; Fernandez-Pan, I.; Royo, M. & Mate, J. I. 2009. Antifungal activity of films and solutions based on chitosan against typical seed fungi. *Food Hydrocolloids*, 23(8), 2309-2314.

19. Ing, L. Y.; Zin, N. M.; Sarwar, A. & Katas, H. 2012. Antifungal activity of chitosan nanoparticles and correlation with their physical properties. *International Journal of Biomaterials*, 2012, Article ID 632698, 9 pages.

20. El-Mohamedy, R. S. R.; El-Aziz, M. E. A. & Kamel, S. 2019. Antifungal activity of chitosan nanoparticles against some plant pathogenic fungi *in vitro*. *Agricultural Engineering International: CIGR Journal*, 21(4), 201-209.

21. Chouhan, D.; Dutta, A.; Kumar, A.; Mandal, P. & Choudhuri, C. 2022. Application of nickel chitosan nanoconjugate as an antifungal agent for combating *Fusarium* rot of wheat. *Scientifc Reports*, 12, 14518.

22. Xu, X.; Zhang, L.; Yang, X.; Cao, H.; Li, J.; Cao, P.; Guo, L.; Wang, X.; Zhao, J. & Xiang, W. 2022. *Alternaria* spp. associated with leaf blight of maize in Heilongjiang province, China. *Plant Disease*, 106(2), 572-584.

23. Garbaba, C. A.; Denboba, L. G.; Mendesil, E.; Ocho, F. L. Hensel, O. 2018. Actors' post-harvest maize handling practices and allied mycoflora epidemiology in southwestern Ethiopia: Potential for mycotoxin-producing fungi management. *Journal of Applied Botany and Food Quality*, 91, 237-248.

24. Murei, A.; Pillay, K.; Govender, P.; Thovhogi, N.; Gitari, W. M. & Samie, A. 2021. Synthesis, characterization and in vitro antibacterial evaluation of *Pyrenacantha grandiflora* conjugated silver nanoparticles. *Nanomaterials*, 11, 1568.

25. Rezazadeh, N. H.; Buazar, F. & Matroodi, S. 2020. Synergistic effects of combinatorial chitosan and polyphenol biomolecules on enhanced antibacterial activity of biofunctionalized silver nanoparticles. *Scientific Reports*, 10, 19615.

26. Laughton, S.; Laycock, A.; von der Kammer, F.; Hofmann, T.; Casman, E. A.; Rodrigues, S. M.; & Lowry, G. V. 2019. Persistence of copper-based

nanoparticle-containing foliar sprays in *Lactuca sativa* (lettuce) characterized by spICP-MS. *Journal of Nanoparticle Research*, 21(8):1-13.

27. Kainz, K.; Bauer, M.A.; Madeo, F. & Carmona-Gutierrez, D. 2020. Fungal infections in humans: the silent crisis. *Microbial Cell*, 7(6), 143.

28. Silva, S.; Negri, M.; Henriques, M.; Oliveira, R.; Williams, D.W. & Azeredo, J. 2012. *Candida glabrata*, *Candida parapsilosis* and *Candida tropicalis*: biology, epidemiology, pathogenicity and antifungal resistance. *FEMS Microbiology Reviews*, 36(2), 288-305.

29. Lionakis, M.S.; Drummond, R.A. & Hohl, T.M. 2023. Immune responses to human fungal pathogens and therapeutic prospects. *Nature Reviews Immunology*, 1-20.

30. Robbins, N.; Wright, G.D. & Cowen, L.E. 2016. Antifungal drugs: the current armamentarium and development of new agents. *Microbiology Spectrum*, 4(5), 4-5.

31. Celiksoy, V.; Moses, R.L.; Sloan, A.J.; Moseley, R. & Heard, C.M. 2022. Synergistic activity of pomegranate rind extract and Zn (II) against *Candida albicans* under planktonic and biofilm conditions, and a mechanistic insight based upon intracellular ROS induction. *Scientific Reports*, 12(1), 19560.

32. Meyahnwi, D.; Siraw, B.B. & Reingold, A. 2022. Epidemiologic features, clinical characteristics, and predictors of mortality in patients with candidemia in Alameda County, California; a 2017–2020 retrospective analysis. *BMC Infectious Diseases*, 22(1), 1-10.

33. Abbasi, B.A.; Iqbal, J.; Mahmood, T.; Qyyum, A. & Kanwal, S., 2019. Biofabrication of iron oxide nanoparticles by leaf extract of Rhamnus virgata: Characterization and evaluation of cytotoxic, antimicrobial and antioxidant potentials. *Applied Organometallic Chemistry*, 33(7), 4947.

34. Caldeirão, A.C.M.; Araujo, H.C.; Tomasella, C.M.; Sampaio, C.; dos Santos Oliveira, M.J.; Ramage, G.; Pessan, J.P. & Monteiro, D.R., 2021. Effects of

antifungal carriers based on chitosan-coated iron oxide nanoparticles on microcosm biofilms. *Antibiotics*, 10(5), 588.

CHAPTER 8

CONCLUSION AND PERSPECTIVES

Nanotechnology applications in the agricultural sector are regarded as an emerging approach that can foster the transformation of traditional production systems into upgraded practices with a clear articulation of the development of environmentally friendly and more efficient methodologies.

This study investigated for the first time a facile, environmentally safe, and economically viable approach for the synthesis of metal oxides (ZnO & Fe_3O_4) NPs using South Africa's sacred herb *Helichrysum odoratissimum*, followed by their integration within nanostructured chitosan. The UV-Vis absorption spectroscopy and HPTLC profiling of the aqueous extracts of *H. odoratissimum* suggested the presence of phytochemicals that can form metal complexes in the presence of Zn and Fe ionic species. The phenol reduction peak in the KCl electrolyte at around -0.5 mV in the voltammetric characterization of the Zn(II)-extract system after 24 h aging, indicated the development of metal oxide NPs in *H. odoratissimum* aqueous extract. Thus, the tested phytoconstituents acted as reducer and oxygen providers to nucleate the metal ionic species (Zn(II) and Fe(II)) and grow the corresponding oxide NPs. An increase in the concentration of *H. odoratissimum* extract (from 0.05 to 0.15 g/mL) led to reduced particle size (from 321 to 144 nm). The morphological analysis of these oxides by SEM showed spherical particles. The diffraction peaks of the prepared samples confirmed the formation of ZnO and Fe_3O_4 nanocrystalline materials. FTIR, TEM and XPS studies demonstrated the successful integration of these particles and their ionic metal precursors into nanostructured TPP-crosslinked chitosan polysaccharide. The Zn(II)- and Fe(II)-laden CS/TPP NPs were developed to compare with their oxide-loaded counterparts. The latter demonstrates a slow release of cations in the aqueous environment over 336 h, tested using the tea bag procedure. The cationic release was relatively faster with the metal ion-laden CS/TPP NPs and much too low for the crystalline metal oxide NPs.

To promote green nanotechnology applications in agriculture, aqueous suspensions of the zinc-containing NPs at two doses (0.01 and 0.04%) as nanopriming agents

were used to stimulate the germination and early seedling growth of maize seeds. The iron-containing NPs, on the other hand, were screened for potential antifungal activities against *Aspergillus niger*, *Fusarium solani*, *Alternaria solani*, *F. verticillioides*, *A. flavas*, *F. oxysporum* phytopathogens and human pathogens namely; *Candida tropicallis* and *C. glabrata*.

Zea mays seeds treated with zinc-containing materials showed most improved biophysical attributes in 10-days old seedlings. The ZnO[15s] nanopriming candidate applied at 0.04%, improved the radicle and root elongation as well as the density of lateral roots in 10-days old seedlings. Furthermore, the negative effects of NaCl on seed germination and early seedling growth were mitigated with low-concentration (0.01%) ZnO[15s] NPs. The effectiveness of the combinative ZnO-chitosan nanoproducts in increasing the germination rate of *Z. mays* seeds was also evidenced. ZnO[10s]-loaded CS/TPP NPs 0.01% led to a more than 2-times increment in the radicle and shoot elongation compared to the control. Notably, this nanocomposite enhanced the early development of salt-stressed seeds. These results demonstrated the beneficial effects of the developed nanofertilizers in increasing the germination rate of maize seeds, even under salinity conditions.

Regarding the iron-containing NPs, the Fe_3O_4[10s] and Fe_3O_4[15s] NPs exhibited efficacy against all phytopathogens except *F. oxysporum* and *F. solani*, respectively. The Fe_3O_4[15s]-loaded CS/TPP NPs revealed the lowest MIC (0.208 mg/mL) against *A. niger*, albeit non-comparable to the conventional Amphotericin B. It is worth noting that the prepared iron-containing NPs could adhere to the plant surface for many days to achieve sustained action. These could therefore, be considered for the control of several fungal diseases. Furthermore, findings also support the potential of these nanoproducts as novel anti-*Candida* therapeutic agents.

Overall, the nanomaterials developed in this study have displayed promising results in *Z. mays* growth and plant protection. It has been demonstrated that *Zea mays* seed priming with the reported nanomaterials is an effective strategy to reduce the NaCl-induced negative influence on seedlings and effectively address the environmental hazards associated with the intensive fertilization. The study may

contribute in the process of transformation towards the United Nations Sustainable Development Goals 2 and 15.

Future research from this study includes sampling the seedlings for Zn analysis in different plant parts. Foliar and soil application of ZnO NPs to maize has been found to increase shoot and grain Zn concentrations. Transplanting the germinated seedlings into plastic pots containing soil and allowing growth under greenhouse conditions will be executed. Next, the plant end-of-life height, grain, and shoot biomass will be examined. It is speculated that the Fe-containing NPs could also serve to correct Fe deficiency in *Z. may* or improve its nutritional quality of Fe. Thus, germinated seedlings transplanted into plastic pots filled with soil will be treated regularly (foliar spray) with a suspension of the Fe_3O_4[15s]-loaded CS/TPP NPs until plant maturity. Subsequently, an assessment of grain iron content will be conducted.

To further improve the properties of the mono-metal oxide-loaded CS/TPP NPs, an attempt to develop the bimetallic Fe-Zn oxide-loaded CS/TPP NPs will be performed. The *H. odoratissimum*-mediated synthesis of the bimetallic Fe-Zn nano-oxides will be experimented in dissolved Fe ($FeSO_4.H_2O$) and Zn ($Zn(NO_3)_2.6H_2O$) salts. The resultant material will be integrated into TPP-crosslinked CS NPs by the ionic gelation process. The influence of Fe-Zn oxide-loaded CS/TPP seed priming on the emergence and seedling growth of *Z. may* in pot trials under greenhouse conditions, will be evaluated. Their antifungal activities will also be reported.

APPENDIX

Table 4. 2: Average hydrodynamic size, polydispersity index (PDI) and zeta potential (ZP) of colloidal suspensions of the nano-metal oxides.

Nanomaterial	Size (nm)	PDI	ZP (mV)
ZnO[5s]	321.2 ± 6.2	0.467	-30.8
ZnO[10s]	173.5 ± 7.8	0.373	-26.6
ZnO[15s]	144.6 ± 2.6	0.226	-34.2
Fe_3O_4[5s]	210.3 ± 7.8	0.264	-18.5
Fe_3O_4[10s]	203.2 ± 10.5	0.136	-28.3
Fe_3O_4[15s]	183.8 ± 2.1	0.281	-30.3

Table 5. 1: Average hydrodynamic size, polydispersity index (PDI) and zeta potential (ZP) of colloidal suspensions of CS/TPP and nutrient-laden CS/TPP NPs.

Nanomaterial	Size (nm)	PDI	ZP (mV)
CS/TPP	149.4 ± 22.3	0.410	19.7
ZnO[5s]-loaded CS/TPP	351.5 ± 31.9	0.272	16.5
ZnO[10s]-loaded CS/TPP	257.3 ± 19.8	0.197	17.8
ZnO[15s]-loaded CS/TPP	207.2 ± 18.5	0.226	16.0
Zn(II)-laden CS/TPP	195.0 ± 6.4	0.221	21.5
Fe_3O_4[5s]-loaded CS/TPP	498.8 ± 12.3	0.423	18.6
Fe_3O_4[10s]-loaded CS/TPP	281.8 ± 6.9	0.282	24.4

Fe_3O_4[15s]-loaded CS/TPP	226.7 ± 15.0	0.308	27.3
Fe(II)-laden CS/TPP	334.1 ± 51.9	0.351	27.4

Table 5. 2: Characteristics of the XPS peaks observed for ZnO-loaded CS/TPP NPs.

Signal	Binding energy (eV)	FWHM (eV)	Atomic %
P 2p (Phosphate)	133.6	1.7	4.4
C 1s (C=C)	284.1	1.0	1.7
C 1s (C–C)	284.7	1.0	6.0
C 1s (C–O)	286.3	1.4	29.2
C 1s (C=O)	287.1	1.4	3.3
C 1s (O–C=O)	288.1	1.4	7.6
N 1s (Organic N)	399.7	1.7	3.4
N 1s (Organic N)	401.6	1.7	3.2
O 1s (Zn–O)	528.3	1.7	0.1
O 1s (C–O)	531.2	1.7	11.1
O 1s (C=O)	532.8	1.7	26.8
Zn 2p3 (Zn–O)	1022.0	1.6	2.8
Na 1s (Na TPP)	1071.4	1.8	0.3

FWHM: Full Width at Half Maximum

Table 5. 3: Characteristics of the XPS peaks observed for Zn(II)-laden CS/TPP NPs.

Signal	Binding energy (eV)	FWHM (eV)	Atomic %
P 2p (Phosphate)	134.1	2.3	7.7
Zn 3s	140.6	2.9	5.5
C 1s (C=C)	284.2	1.1	2.2
C 1s (C–C)	284.8	1.1	6.5
C 1s (C–O)	286.3	1.4	19.9
C 1s (C=O)	287.7	1.4	5.3
C 1s (O–C=O)	288.6	1.4	2.2
N 1s (Organic N)	399.8	1.7	2.8
N 1s (Organic N)	401.6	1.7	1.8
O 1s (C–O)	531.5	1.9	14.8
O 1s (C=O)	532.8	1.9	27.4
Zn 2p (Zn^{2+} complex)	1022.4	2.1	2.4
Zn 2p (Zn^{2+} complex)	1024.1	2.1	1.1
Na 1s (Na TPP)	1071.8	2.1	0.5

Table 5. 4: Characteristics of the XPS peaks observed for Fe_3O_4-loaded CS/TPP NPs.

Signal	Binding energy (eV)	FWHM (eV)	Atomic %
P 2p (Phosphate)	133.4	1.8	2.9
S 2p (Sulfate)	168.7	2.1	0.5
C 1s (C=C)	284.2	1.0	1.7
C 1s (C–C)	284.8	1.0	5.4
C 1s (C–O)	286.3	1.4	29.3
C 1s (C=O)	287.7	1.4	7.2
C 1s (O–C=O)	288.5	1.4	2.6
N 1s (Organic N)	399.5	1.7	3.9
N 1s (Organic N)	401.5	1.7	2.6
O1s (Fe–O)	530.4	1.6	5.2
O 1s (C–O)	531.3	1.6	7.2
O 1s (C=O)	532.7	1.6	26.2
Fe 2p (Fe–O)	710.8	3.4	3.3
Na 1s (Na TPP)	1071.8	1.9	0.4

A: ICP-MS analysis of Zn ionic species in tap water treated with the nano ZnO, ZnO-loaded CS/TPP, and Zn(II)-laden CS/TPP.

TotalQuant - Summary Report

Sample ID: std ms-3 at 10 ppb

Sample Date/Time: Wednesday, August 10, 2022 10:17:53
Sample Description:
Solution Type: Standard
Sample File: C:\Users\Public\Documents\PerkinElmer Syngistix\ICPMS\Sample\Dr Naomi samples.sam
Method File: C:\Users\Public\Documents\PerkinElmer Syngistix\ICPMS\Method\Dr NaomiTotalQuant.mth
Dataset File: C:\Users\Public\Documents\PerkinElmer Syngistix\ICPMS\DataSet\Default\std ms-3 at 10 ppb.1570
Response File: C:\Users\Public\Documents\PerkinElmer Syngistix\ICPMS\System\totalquant.rsp
Initial Sample Quantity (mg):
Sample Prep Volume (mL):
Aliquot Volume (mL):
Diluted to Volume (mL):
Torch Z Position (mm): 0.00

Report Concentration Unit: ppb

Analyte Intensities

Analyte	Concentration	Intensity	Intensity Comment
F		0	
Ne		0	
Na	10.00	998067	
Mg	0.00	0	
Al	10.00	654678	
Si	7.07	267400	
P	0.00	0	
S	0.00	0	
Cl	0.00	0	
Ar	0.00	0	
K	0.00	0	
Ca	10.00	7502363	
Sc	0.00	0	
Ti	0.00	0	
V	10.00	378397	
Cr	0.00	0	
Mn	10.00	260424	
Fe	0.00	0	
Co	10.00	205812	
Ni	10.00	162384	
Cu	10.00	108412	
Zn	10.00	562369	

Sample ID: cal blank

Sample Date/Time: Wednesday, August 10, 2022 10:12:36
Sample Description:
Solution Type: Blank
Sample File: C:\Users\Public\Documents\PerkinElmer Syngistix\ICPMS\Sample\Dr Naomi samples.sam
Method File: C:\Users\Public\Documents\PerkinElmer Syngistix\ICPMS\Method\Dr NaomiTotalQuant.mth
Dataset File: C:\Users\Public\Documents\PerkinElmer Syngistix\ICPMS\DataSet\Default\cal blank.1569
Response File: C:\Users\Public\Documents\PerkinElmer Syngistix\ICPMS\System\totalquant.rsp
Initial Sample Quantity (mg):
Sample Prep Volume (mL):
Aliquot Volume (mL):
Diluted to Volume (mL):
Torch Z Position (mm): 0.00

Report Concentration Unit: ppb

Analyte Intensities

Analyte	Concentration	Intensity	Intensity Comment
F		30054	
Ne		33056	
Na	**0.54**	30054	
Mg	**0.87**	38188	
Al	**0.58**	30054	
Si	**52.57**	1629710	
P	**8.83**	45902	
S	**6834.66**	34173300	
Cl	**99.48**	39791	
Ar	**4861860.95**	4861861	
K	**1.70**	32282	
Ca	**70.28**	1440738	
Sc	**0.23**	16183	
Ti	**0.79**	44163	
V	**0.53**	30127	
Cr	**2.76**	176263	
Mn	**0.72**	48578	
Fe	**35.36**	1718299	
Co	**0.04**	2137	
Ni	**0.19**	8833	
Cu	**0.61**	22807	
Zn	**2.28**	61278	

B: Assessing the concentration Zn(II) ions released by the ZnO NPs for 1 h.

Sample ID: A1 1 HRS

Sample Date/Time: Wednesday, August 10, 2022 10:29:08
Sample Description:
Solution Type: Sample
Sample File: C:\Users\Public\Documents\PerkinElmer Syngistix\ICPMS\Sample\Dr Naomi samples.sam
Method File: C:\Users\Public\Documents\PerkinElmer Syngistix\ICPMS\Method\Dr NaomiTotalQuant.mth
Dataset File: C:\Users\Public\Documents\PerkinElmer Syngistix\ICPMS\DataSet\Default\A1 1 HRS.1572
Response File: C:\Users\Public\Documents\PerkinElmer Syngistix\ICPMS\System\totalquant100822.rsp
Initial Sample Quantity (mg):
Sample Prep Volume (mL):
Aliquot Volume (mL):
Diluted to Volume (mL):
Torch Z Position (mm): 0.00

Report Concentration Unit: ppb

Analyte Intensities

Analyte	Concentration	Intensity	Intensity Comment
F		0	
Ne		0	
Na	0.00	0	
Mg	0.00	0	
Al	13.62	580999	
Si	0.00	0	
P	0.00	0	
S	0.00	0	
Cl	0.00	0	
Ar	0.00	0	
K	0.00	0	
Ca	7.24	2114702	
Sc	0.00	0	
Ti	0.00	0	
V	0.15	5354	
Cr	0.00	0	
Mn	2.26	65323	
Fe	0.00	0	
Co	0.00	38	
Ni	0.11	1669	
Cu	2.88	33802	
Zn	0.00	0	

C: Assessing the concentration Zn(II) ions released by the ZnO NPs for 5 h,

Sample ID: A1 5 HRS

Sample Date/Time: Wednesday, August 10, 2022 10:45:03
Sample Description:
Solution Type: Sample
Sample File: C:\Users\Public\Documents\PerkinElmer Syngistix\ICPMS\Sample\Dr Naomi samples.sam
Method File: C:\Users\Public\Documents\PerkinElmer Syngistix\ICPMS\Method\Dr NaomiTotalQuant.mth
Dataset File: C:\Users\Public\Documents\PerkinElmer Syngistix\ICPMS\DataSet\Default\A1 5 HRS.1575
Response File: C:\Users\Public\Documents\PerkinElmer Syngistix\ICPMS\System\totalquant100822.rsp
Initial Sample Quantity (mg):
Sample Prep Volume (mL):
Aliquot Volume (mL):
Diluted to Volume (mL):
Torch Z Position (mm): 0.00

Report Concentration Unit: ppb

Analyte Intensities

Analyte	Concentration	Intensity	Intensity Comment
F		0	
Ne		0	
Na	0.00	0	
Mg	0.00	0	
Al	10.42	444231	
Si	0.00	0	
P	0.57	2662	
S	0.00	0	
Cl	0.00	0	
Ar	0.00	0	
K	0.00	0	
Ca	5.00	1461356	
Sc	0.00	0	
Ti	0.00	0	
V	0.00	0	
Cr	0.00	0	
Mn	3.96	114602	
Fe	0.00	0	
Co	0.00	0	
Ni	0.13	1910	
Cu	2.77	32518	
Zn	0.00	0	

D: Assessing the concentration Zn(II) ions released by the ZnO NPs for 24 h.

Sample ID: A1 24 HRS

Sample Date/Time: Wednesday, August 10, 2022 11:11:32
Sample Description:
Solution Type: Sample
Sample File: C:\Users\Public\Documents\PerkinElmer Syngistix\ICPMS\Sample\Dr Naomi samples.sam
Method File: C:\Users\Public\Documents\PerkinElmer Syngistix\ICPMS\Method\Dr NaomiTotalQuant.mth
Dataset File: C:\Users\Public\Documents\PerkinElmer Syngistix\ICPMS\DataSet\Default\A1 24 HRS.1580
Response File: C:\Users\Public\Documents\PerkinElmer Syngistix\ICPMS\System\totalquant.rsp
Initial Sample Quantity (mg):
Sample Prep Volume (mL):
Aliquot Volume (mL):
Diluted to Volume (mL):
Torch Z Position (mm): 0.00

Report Concentration Unit: ppb

Analyte Intensities

Analyte	Concentration	Intensity	Intensity Comment
F		0	
Ne		0	
Na	0.00	0	
Mg	0.00	0	
Al	3.38	221400	
Si	0.00	0	
P	4.31	26335	
S	0.00	0	
Cl	0.00	0	
Ar	0.00	0	
K	0.00	0	
Ca	8.14	6104495	
Sc	0.00	0	
Ti	0.00	0	
V	0.00	0	
Cr	0.00	0	
Mn	7.32	190620	
Fe	0.00	0	
Co	0.00	0	
Ni	0.00	0	
Cu	0.55	5952	
Zn	0.79	40163	

E: Assessing the concentration Zn(II) ions released by the ZnO NPs for 48 h.

Sample ID: A1 48 HRS

Sample Date/Time: Wednesday, August 10, 2022 11:06:16
Sample Description:
Solution Type: Sample
Sample File: C:\Users\Public\Documents\PerkinElmer Syngistix\ICPMS\Sample\Dr Naomi samples.sam
Method File: C:\Users\Public\Documents\PerkinElmer Syngistix\ICPMS\Method\Dr NaomiTotalQuant.mth
Dataset File: C:\Users\Public\Documents\PerkinElmer Syngistix\ICPMS\DataSet\Default\A1 48 HRS.1579
Response File: C:\Users\Public\Documents\PerkinElmer Syngistix\ICPMS\System\totalquant.rsp
Initial Sample Quantity (mg):
Sample Prep Volume (mL):
Aliquot Volume (mL):
Diluted to Volume (mL):
Torch Z Position (mm): 0.00

Report Concentration Unit: ppb

Analyte Intensities

Analyte	Concentration	Intensity	Intensity Comment
F		0	
Ne		0	
Na	**0.00**	0	
Mg	**0.00**	0	
Al	**11.51**	753481	
Si	**0.00**	0	
P	**5.77**	35312	
S	**0.00**	0	
Cl	**0.00**	0	
Ar	**0.00**	0	
K	**0.00**	0	
Ca	**10.70**	8030351	
Sc	**0.00**	0	
Ti	**0.00**	0	
V	**0.00**	0	
Cr	**0.00**	0	
Mn	**10.89**	283541	
Fe	**0.00**	0	
Co	**0.00**	0	
Ni	**0.00**	0	
Cu	**1.32**	14269	
Zn	**2.26**	95323	

F: Assessing the concentration Zn(II) ions released by the ZnO NPs for 168 h.

Sample ID: A1 168 HRS

Sample Date/Time: Wednesday, August 10, 2022 10:55:37
Sample Description:
Solution Type: Sample
Sample File: C:\Users\Public\Documents\PerkinElmer Syngistix\ICPMS\Sample\Dr Naomi samples.sam
Method File: C:\Users\Public\Documents\PerkinElmer Syngistix\ICPMS\Method\Dr NaomiTotalQuant.mth
Dataset File: C:\Users\Public\Documents\PerkinElmer Syngistix\ICPMS\DataSet\Default\A1 168 HRS.1577
Response File: C:\Users\Public\Documents\PerkinElmer Syngistix\ICPMS\System\totalquant.rsp
Initial Sample Quantity (mg):
Sample Prep Volume (mL):
Aliquot Volume (mL):
Diluted to Volume (mL):
Torch Z Position (mm): 0.00

Report Concentration Unit: ppb

Analyte Intensities

Analyte	Concentration	Intensity	Intensity Comment
F		0	
Ne		0	
Na	0.00	0	
Mg	0.00	0	
Al	0.63	40988	
Si	0.00	0	
P	0.00	0	
S	0.00	0	
Cl	0.00	0	
Ar	0.00	0	
K	0.00	0	
Ca	13.40	10053749	
Sc	0.00	0	
Ti	0.00	0	
V	0.00	0	
Cr	0.00	0	
Mn	17.12	445733	
Fe	0.00	0	
Co	0.00	0	
Ni	0.00	0	
Cu	1.08	11672	
Zn	4.31	166335	

G: Assessing the concentration Zn(II) ions released by the ZnO NPs for 240 h.

Sample ID: A1 240 HRS

Sample Date/Time: Wednesday, August 10, 2022 11:16:49
Sample Description:
Solution Type: Sample
Sample File: C:\Users\Public\Documents\PerkinElmer Syngistix\ICPMS\Sample\Dr Naomi samples.sam
Method File: C:\Users\Public\Documents\PerkinElmer Syngistix\ICPMS\Method\Dr NaomiTotalQuant.mth
Dataset File: C:\Users\Public\Documents\PerkinElmer Syngistix\ICPMS\DataSet\Default\A1 240 HRS.1581
Response File: C:\Users\Public\Documents\PerkinElmer Syngistix\ICPMS\System\totalquant.rsp
Initial Sample Quantity (mg):
Sample Prep Volume (mL):
Aliquot Volume (mL):
Diluted to Volume (mL):
Torch Z Position (mm): 0.00

Report Concentration Unit: ppb

Analyte Intensities

Analyte	Concentration	Intensity	Intensity Comment
F		0	
Ne		0	
Na	0.00	0	
Mg	0.00	0	
Al	0.24	15388	
Si	0.00	0	
P	0.00	0	
S	0.00	0	
Cl	0.00	0	
Ar	0.00	0	
K	0.00	0	
Ca	15.27	11454587	
Sc	0.00	0	
Ti	0.00	0	
V	0.00	0	
Cr	0.00	0	
Mn	20.55	535157	
Fe	0.00	0	
Co	0.00	0	
Ni	0.00	0	
Cu	0.72	7754	
Zn	5.25	221435	

H: Assessing the concentration Zn(II) ions released by the ZnO NPs for 336 h.

Sample ID: A1 336 HRS

Sample Date/Time: Wednesday, August 10, 2022 11:00:53
Sample Description:
Solution Type: Sample
Sample File: C:\Users\Public\Documents\PerkinElmer Syngistix\ICPMS\Sample\Dr Naomi samples.sam
Method File: C:\Users\Public\Documents\PerkinElmer Syngistix\ICPMS\Method\Dr NaomiTotalQuant.mth
Dataset File: C:\Users\Public\Documents\PerkinElmer Syngistix\ICPMS\DataSet\Default\A1 336 HRS.1578
Response File: C:\Users\Public\Documents\PerkinElmer Syngistix\ICPMS\System\totalquant.rsp
Initial Sample Quantity (mg):
Sample Prep Volume (mL):
Aliquot Volume (mL):
Diluted to Volume (mL):
Torch Z Position (mm): 0.00

Report Concentration Unit: ppb

Analyte Intensities

Analyte	Concentration	Intensity	Intensity Comment
F		0	
Ne		0	
Na	0.00	0	
Mg	0.00	0	
Al	1.59	103924	
Si	0.00	0	
P	0.00	0	
S	0.00	0	
Cl	0.00	0	
Ar	0.00	0	
K	0.00	0	
Ca	20.99	15749838	
Sc	0.00	0	
Ti	0.00	0	
V	0.00	0	
Cr	0.00	0	
Mn	29.03	755902	
Fe	0.00	0	
Co	0.00	0	
Ni	0.00	0	
Cu	0.58	6289	
Zn	5.23	221402	

I: Assessing the concentration Zn(II) ions released by the Zn(II)-laden CS/TPP NPs for 1 h.

Sample ID: A2 1HRS

Sample Date/Time: Wednesday, August 10, 2022 10:34:26
Sample Description:
Solution Type: Sample
Sample File: C:\Users\Public\Documents\PerkinElmer Syngistix\ICPMS\Sample\Dr Naomi samples.sam
Method File: C:\Users\Public\Documents\PerkinElmer Syngistix\ICPMS\Method\Dr NaomiTotalQuant.mth
Dataset File: C:\Users\Public\Documents\PerkinElmer Syngistix\ICPMS\DataSet\Default\A2 1HRS.1573
Response File: C:\Users\Public\Documents\PerkinElmer Syngistix\ICPMS\System\totalquant100822.rsp
Initial Sample Quantity (mg):
Sample Prep Volume (mL):
Aliquot Volume (mL):
Diluted to Volume (mL):
Torch Z Position (mm): 0.00

Report Concentration Unit: ppb

Analyte Intensities

Analyte	Concentration	Intensity	Intensity Comment
F		0	
Ne		0	
Na	0.00	0	
Mg	21.51	1127578	
Al	3.69	157304	
Si	23.60	633235	
P	12.23	57397	
S	0.00	0	
Cl	0.00	0	
Ar	0.00	0	
K	0.00	0	
Ca	0.00	0	
Sc	0.00	0	
Ti	0.00	0	
V	0.00	0	
Cr	0.00	0	
Mn	0.34	9735	
Fe	0.00	0	
Co	0.00	6	
Ni	0.20	3031	
Cu	4.12	48325	
Zn	8.47	342353	

J: Assessing the concentration Zn(II) ions released by the Zn(II)-laden CS/TPP NPs for 5 h.

Sample ID: A3 5 HRS

Sample Date/Time: Wednesday, August 10, 2022 13:42:56
Sample Description:
Solution Type: Sample
Sample File: C:\Users\Public\Documents\PerkinElmer Syngistix\ICPMS\Sample\Dr Naomi samples.sam
Method File: C:\Users\Public\Documents\PerkinElmer Syngistix\ICPMS\Method\Dr NaomiTotalQuant.mth
Dataset File: C:\Users\Public\Documents\PerkinElmer Syngistix\ICPMS\DataSet\Default\A3 5 HRS.1599
Response File: C:\Users\Public\Documents\PerkinElmer Syngistix\ICPMS\System\totalquant100822.rsp
Initial Sample Quantity (mg):
Sample Prep Volume (mL):
Aliquot Volume (mL):
Diluted to Volume (mL):
Torch Z Position (mm): 0.00

Report Concentration Unit: ppb

Analyte Intensities

Analyte	Concentration	Intensity	Intensity Comment
F		0	
Ne		0	
Na	0.00	0	
Mg	21.69	1137052	
Al	9.71	413968	
Si	32.84	881060	
P	19.11	89680	
S	0.00	0	
Cl	0.00	0	
Ar	0.00	0	
K	0.00	0	
Ca	3.46	1011700	
Sc	0.00	0	
Ti	0.00	0	
V	0.07	2619	
Cr	0.00	0	
Mn	0.44	12614	
Fe	0.00	0	
Co	0.00	8	
Ni	0.15	2220	
Cu	3.72	43704	
Zn	8.44	342351	

K: Assessing the concentration Zn(II) ions released by the Zn(II)-laden CS/TPP NPs for 24 h.

Sample ID: A2 24 HRS

Sample Date/Time: Wednesday, August 10, 2022 11:22:06
Sample Description:
Solution Type: Sample
Sample File: C:\Users\Public\Documents\PerkinElmer Syngistix\ICPMS\Sample\Dr Naomi samples.sam
Method File: C:\Users\Public\Documents\PerkinElmer Syngistix\ICPMS\Method\Dr NaomiTotalQuant.mth
Dataset File: C:\Users\Public\Documents\PerkinElmer Syngistix\ICPMS\DataSet\Default\A2 24 HRS.1582
Response File: C:\Users\Public\Documents\PerkinElmer Syngistix\ICPMS\System\totalquant.rsp
Initial Sample Quantity (mg):
Sample Prep Volume (mL):
Aliquot Volume (mL):
Diluted to Volume (mL):
Torch Z Position (mm): 0.00

Report Concentration Unit: ppb

Analyte Intensities

Analyte	Concentration	Intensity	Intensity Comment
F		0	
Ne		0	
Na	**0.00**	0	
Mg	**0.00**	0	
Al	**6.15**	402896	
Si	**0.04**	1671	
P	**62.56**	382524	
S	**0.00**	0	
Cl	**0.00**	0	
Ar	**0.00**	0	
K	**0.00**	0	
Ca	**7.12**	5342290	
Sc	**0.00**	0	
Ti	**0.00**	0	
V	**0.00**	0	
Cr	**0.00**	0	
Mn	**0.00**	0	
Fe	**0.00**	0	
Co	**0.00**	0	
Ni	**0.00**	0	
Cu	**2.37**	25662	
Zn	**14.53**	582073	

L: Assessing the concentration Zn(II) ions released by the Zn(II)-laden CS/TPP NPs for 48 h.

Sample ID: A2 48 HRS

Sample Date/Time: Wednesday, August 10, 2022 12:44:47
Sample Description:
Solution Type: Sample
Sample File: C:\Users\Public\Documents\PerkinElmer Syngistix\ICPMS\Sample\Dr Naomi samples.sam
Method File: C:\Users\Public\Documents\PerkinElmer Syngistix\ICPMS\Method\Dr NaomiTotalQuant.mth
Dataset File: C:\Users\Public\Documents\PerkinElmer Syngistix\ICPMS\DataSet\Default\A2 48 HRS.1588
Response File: C:\Users\Public\Documents\PerkinElmer Syngistix\ICPMS\System\totalquant100822.rsp
Initial Sample Quantity (mg):
Sample Prep Volume (mL):
Aliquot Volume (mL):
Diluted to Volume (mL):
Torch Z Position (mm): 0.00

Report Concentration Unit: ppb

Analyte Intensities

Analyte	Concentration	Intensity	Intensity Comment
F		0	
Ne		0	
Na	0.00	0	
Mg	25.95	1360349	
Al	1.51	64277	
Si	20.29	544378	
P	85.05	399190	
S	0.00	0	
Cl	0.00	0	
Ar	0.00	0	
K	0.00	0	
Ca	3.49	1018483	
Sc	0.00	0	
Ti	0.00	2360	
V	0.58	20331	
Cr	0.00	0	
Mn	0.65	18752	
Fe	0.00	0	
Co	0.00	72	
Ni	0.17	2557	
Cu	3.90	45776	
Zn	16.41	647673	

M: Assessing the concentration Zn(II) ions released by the Zn(II)-laden CS/TPP NPs for 168 h.

Sample ID: A2 168 HRS

Sample Date/Time: Wednesday, August 10, 2022 12:55:24
Sample Description:
Solution Type: Sample
Sample File: C:\Users\Public\Documents\PerkinElmer Syngistix\ICPMS\Sample\Dr Naomi samples.sam
Method File: C:\Users\Public\Documents\PerkinElmer Syngistix\ICPMS\Method\Dr NaomiTotalQuant.mth
Dataset File: C:\Users\Public\Documents\PerkinElmer Syngistix\ICPMS\DataSet\Default\A2 168 HRS.1590
Response File: C:\Users\Public\Documents\PerkinElmer Syngistix\ICPMS\System\totalquant100822.rsp
Initial Sample Quantity (mg):
Sample Prep Volume (mL):
Aliquot Volume (mL):
Diluted to Volume (mL):
Torch Z Position (mm): 0.00

Report Concentration Unit: ppb

Analyte Intensities

Analyte	Concentration	Intensity	Intensity Comment
F		0	
Ne		0	
Na	0.00	0	
Mg	28.74	1506425	
Al	5.17	220341	
Si	28.57	766447	
P	129.88	609606	
S	0.00	0	
Cl	0.00	0	
Ar	0.00	0	
K	0.00	0	
Ca	8.00	2337357	
Sc	0.00	0	
Ti	0.03	15564	
V	0.00	0	
Cr	0.00	0	
Mn	0.86	24929	
Fe	0.00	0	
Co	0.01	137	
Ni	0.21	3092	
Cu	3.55	41686	
Zn	17.63	721193	

N: Assessing the concentration Zn(II) ions released by the Zn(II)-laden CS/TPP NPs for 240 h.

Sample ID: A2 240 HRS

Sample Date/Time: Wednesday, August 10, 2022 11:27:23
Sample Description:
Solution Type: Sample
Sample File: C:\Users\Public\Documents\PerkinElmer Syngistix\ICPMS\Sample\Dr Naomi samples.sam
Method File: C:\Users\Public\Documents\PerkinElmer Syngistix\ICPMS\Method\Dr NaomiTotalQuant.mth
Dataset File: C:\Users\Public\Documents\PerkinElmer Syngistix\ICPMS\DataSet\Default\A2 240 HRS.1583
Response File: C:\Users\Public\Documents\PerkinElmer Syngistix\ICPMS\System\totalquant.rsp
Initial Sample Quantity (mg):
Sample Prep Volume (mL):
Aliquot Volume (mL):
Diluted to Volume (mL):
Torch Z Position (mm): 0.00

Report Concentration Unit: ppb

Analyte Intensities

Analyte	Concentration	Intensity	Intensity Comment
F		0	
Ne		0	
Na	0.00	0	
Mg	0.00	0	
Al	10.05	657701	
Si	12.75	482037	
P	173.05	1058126	
S	0.00	0	
Cl	0.00	0	
Ar	0.00	0	
K	0.00	0	
Ca	8.60	6453992	
Sc	0.00	0	
Ti	0.03	19464	
V	0.00	0	
Cr	0.00	0	
Mn	0.00	0	
Fe	0.00	0	
Co	0.00	0	
Ni	0.00	0	
Cu	3.66	42992	
Zn	19.57	850486	

O: Assessing the concentration Zn(II) ions released by the Zn(II)-laden CS/TPP NPs for 336 h.

Sample ID: A2 336 HRS

Sample Date/Time: Wednesday, August 10, 2022 13:11:13
Sample Description:
Solution Type: Sample
Sample File: C:\Users\Public\Documents\PerkinElmer Syngistix\ICPMS\Sample\Dr Naomi samples.sam
Method File: C:\Users\Public\Documents\PerkinElmer Syngistix\ICPMS\Method\Dr NaomiTotalQuant.mth
Dataset File: C:\Users\Public\Documents\PerkinElmer Syngistix\ICPMS\DataSet\Default\A2 336 HRS.1593
Response File: C:\Users\Public\Documents\PerkinElmer Syngistix\ICPMS\System\totalquant100822.rsp
Initial Sample Quantity (mg):
Sample Prep Volume (mL):
Aliquot Volume (mL):
Diluted to Volume (mL):
Torch Z Position (mm): 0.00

Report Concentration Unit: ppb

Analyte Intensities

Analyte	Concentration	Intensity	Intensity Comment
F		0	
Ne		0	
Na	0.00	0	
Mg	26.72	1400647	
Al	10.49	447398	
Si	0.00	0	
P	263.43	1236481	
S	0.00	0	
Cl	0.00	0	
Ar	0.00	0	
K	0.00	0	
Ca	8.39	2452183	
Sc	0.00	0	
Ti	0.09	48815	
V	0.00	0	
Cr	0.00	0	
Mn	0.56	16149	
Fe	0.00	0	
Co	0.01	98	
Ni	0.08	1212	
Cu	2.76	32445	
Zn	21.46	916588	

P: Assessing the concentration Zn(II) ions released by the ZnO-loaded CS/TPP NPs for 1 h.

Sample ID: A3 1 HRS

Sample Date/Time: Wednesday, August 10, 2022 10:39:44
Sample Description:
Solution Type: Sample
Sample File: C:\Users\Public\Documents\PerkinElmer Syngistix\ICPMS\Sample\Dr Naomi samples.sam
Method File: C:\Users\Public\Documents\PerkinElmer Syngistix\ICPMS\Method\Dr NaomiTotalQuant.mth
Dataset File: C:\Users\Public\Documents\PerkinElmer Syngistix\ICPMS\DataSet\Default\A3 1 HRS.1574
Response File: C:\Users\Public\Documents\PerkinElmer Syngistix\ICPMS\System\totalquant100822.rsp
Initial Sample Quantity (mg):
Sample Prep Volume (mL):
Aliquot Volume (mL):
Diluted to Volume (mL):
Torch Z Position (mm): 0.00

Report Concentration Unit: ppb

Analyte Intensities

Analyte	Concentration	Intensity	Intensity Comment	
F		0		
Ne		0		
Na	0.00	0		
Mg	24.75	1297338	1	7401
Al	26.32	1122671	0.56	614
Si	30.82	826885	0.00	0
P	24.16	113396	11.01	854799
S	0.00	0	0.00	0
Cl	0.00	0	0.34	
Ar	0.00	0		
K	0.00	0		
Ca	2.48	724684		
Sc	0.00	0		
Ti	0.00	0		
V	0.00	0		
Cr	0.00	0		
Mn	1.18	34276		
Fe	0.00	0		
Co	0.00	44		
Ni	0.13	1910		
Cu	3.19	37455		
Zn	5.84	259466		

Q: Assessing the concentration Zn(II) ions released by the ZnO-loaded CS/TPP NPs for 5 h.

Sample ID: A3 5 HRS

Sample Date/Time: Wednesday, August 10, 2022 13:42:56
Sample Description:
Solution Type: Sample
Sample File: C:\Users\Public\Documents\PerkinElmer Syngistix\ICPMS\Sample\Dr Naomi samples.sam
Method File: C:\Users\Public\Documents\PerkinElmer Syngistix\ICPMS\Method\Dr NaomiTotalQuant.mth
Dataset File: C:\Users\Public\Documents\PerkinElmer Syngistix\ICPMS\DataSet\Default\A3 5 HRS.1599
Response File: C:\Users\Public\Documents\PerkinElmer Syngistix\ICPMS\System\totalquant100822.rsp
Initial Sample Quantity (mg):
Sample Prep Volume (mL):
Aliquot Volume (mL):
Diluted to Volume (mL):
Torch Z Position (mm): 0.00

Report Concentration Unit: ppb

Analyte Intensities

Analyte	Concentration	Intensity	Intensity Comment
F		0	
Ne		0	
Na	**0.00**	0	
Mg	**23.01**	1206057	
Al	**4.58**	195426	
Si	**34.38**	922456	
P	**46.39**	217744	
S	**0.00**	0	
Cl	**0.00**	0	
Ar	**0.00**	0	
K	**0.00**	0	
Ca	**0.00**	0	
Sc	**0.00**	0	
Ti	**0.00**	0	
V	**0.00**	0	
Cr	**0.00**	0	
Mn	**1.34**	38668	
Fe	**0.00**	0	
Co	**0.00**	0	
Ni	**0.00**	0	
Cu	**2.58**	30282	
Zn	**5.17**	216311	

R: Assessing the concentration Zn(II) ions released by the ZnO-loaded CS/TPP NPs for 24 h.

Sample ID: A3 24 HRS

Sample Date/Time: Wednesday, August 10, 2022 13:21:46
Sample Description:
Solution Type: Sample
Sample File: C:\Users\Public\Documents\PerkinElmer Syngistix\ICPMS\Sample\Dr Naomi samples.sam
Method File: C:\Users\Public\Documents\PerkinElmer Syngistix\ICPMS\Method\Dr NaomiTotalQuant.mth
Dataset File: C:\Users\Public\Documents\PerkinElmer Syngistix\ICPMS\DataSet\Default\A3 24 HRS.1595
Response File: C:\Users\Public\Documents\PerkinElmer Syngistix\ICPMS\System\totalquant100822.rsp
Initial Sample Quantity (mg):
Sample Prep Volume (mL):
Aliquot Volume (mL):
Diluted to Volume (mL):
Torch Z Position (mm): 0.00

Report Concentration Unit: ppb

Analyte Intensities

Analyte	Concentration	Intensity	Intensity Comment
F		0	
Ne		0	
Na	0.00	0	
Mg	26.54	1391057	
Al	10.24	436619	
Si	22.82	612289	
P	101.88	478198	
S	0.00	0	
Cl	0.00	0	
Ar	0.00	0	
K	0.00	0	
Ca	4.00	1169293	
Sc	0.00	0	
Ti	0.01	4989	
V	0.00	0	
Cr	0.00	0	
Mn	2.01	58224	
Fe	0.00	0	
Co	0.00	32	
Ni	0.00	0	
Cu	1.98	23233	
Zn	11.87	471298	

S: Assessing the concentration Zn(II) ions released by the ZnO-loaded CS/TPP NPs for 48 h.

Sample ID: A3 48 HRS

Sample Date/Time: Wednesday, August 10, 2022 14:09:25
Sample Description:
Solution Type: Sample
Sample File: C:\Users\Public\Documents\PerkinElmer Syngistix\ICPMS\Sample\Dr Naomi samples.sam
Method File: C:\Users\Public\Documents\PerkinElmer Syngistix\ICPMS\Method\Dr NaomiTotalQuant.mth
Dataset File: C:\Users\Public\Documents\PerkinElmer Syngistix\ICPMS\DataSet\Default\A3 48 HRS.1604
Response File: C:\Users\Public\Documents\PerkinElmer Syngistix\ICPMS\System\totalquant100822.rsp
Initial Sample Quantity (mg):
Sample Prep Volume (mL):
Aliquot Volume (mL):
Diluted to Volume (mL):
Torch Z Position (mm): 0.00

Report Concentration Unit: ppb

Analyte Intensities

Analyte	Concentration	Intensity	Intensity Comment
F		0	
Ne		0	
Na	0.00	0	
Mg	25.20	1320771	
Al	0.70	29868	
Si	14.73	395236	
P	102.78	482406	
S	0.00	0	
Cl	0.00	0	
Ar	0.00	0	
K	0.00	0	
Ca	0.21	61876	
Sc	0.00	0	
Ti	0.01	4496	
V	0.00	0	
Cr	0.00	0	
Mn	1.76	51059	
Fe	0.00	0	
Co	0.00	57	
Ni	0.00	0	
Cu	1.89	22164	
Zn	19.34	811369	

T: Assessing the concentration Zn(II) ions released by the ZnO-loaded CS/TPP NPs for 168 h.

Sample ID: A3 168 HRS

Sample Date/Time: Wednesday, August 10, 2022 14:04:08
Sample Description:
Solution Type: Sample
Sample File: C:\Users\Public\Documents\PerkinElmer Syngistix\ICPMS\Sample\Dr Naomi samples.sam
Method File: C:\Users\Public\Documents\PerkinElmer Syngistix\ICPMS\Method\Dr NaomiTotalQuant.mth
Dataset File: C:\Users\Public\Documents\PerkinElmer Syngistix\ICPMS\DataSet\Default\A3 168 HRS.1603
Response File: C:\Users\Public\Documents\PerkinElmer Syngistix\ICPMS\System\totalquant100822.rsp
Initial Sample Quantity (mg):
Sample Prep Volume (mL):
Aliquot Volume (mL):
Diluted to Volume (mL):
Torch Z Position (mm): 0.00

Report Concentration Unit: ppb

Analyte Intensities

Analyte	Concentration	Intensity	Intensity Comment
F		0	
Ne		0	
Na	0.00	0	
Mg	26.10	1368257	
Al	0.00	0	
Si	38.82	1041469	
P	122.09	573069	
S	0.00	0	
Cl	0.00	0	
Ar	0.00	0	
K	0.00	0	
Ca	1.85	542000	
Sc	0.00	0	
Ti	0.02	9574	
V	0.00	0	
Cr	0.00	0	
Mn	1.71	49531	
Fe	0.00	0	
Co	0.00	57	
Ni	0.00	0	
Cu	2.12	24856	
Zn	22.61	944892	

U: Assessing the concentration Zn(II) ions released by the ZnO-loaded CS/TPP NPs for 240 h.

Sample ID: A3 240 HRS

Sample Date/Time: Wednesday, August 10, 2022 13:27:03
Sample Description:
Solution Type: Sample
Sample File: C:\Users\Public\Documents\PerkinElmer Syngistix\ICPMS\Sample\Dr Naomi samples.sam
Method File: C:\Users\Public\Documents\PerkinElmer Syngistix\ICPMS\Method\Dr NaomiTotalQuant.mth
Dataset File: C:\Users\Public\Documents\PerkinElmer Syngistix\ICPMS\DataSet\Default\A3 240 HRS.1596
Response File: C:\Users\Public\Documents\PerkinElmer Syngistix\ICPMS\System\totalquant100822.rsp
Initial Sample Quantity (mg):
Sample Prep Volume (mL):
Aliquot Volume (mL):
Diluted to Volume (mL):
Torch Z Position (mm): 0.00

Report Concentration Unit: ppb

Analyte Intensities

Analyte	Concentration	Intensity	Intensity Comment
F		0	
Ne		0	
Na	0.00	0	
Mg	28.47	1492077	
Al	1.24	53079	
Si	30.49	818015	
P	174.72	820068	
S	0.00	0	
Cl	0.00	0	
Ar	0.00	0	
K	0.00	0	
Ca	5.55	1622271	
Sc	0.00	0	
Ti	0.05	27289	
V	0.00	0	
Cr	0.00	0	
Mn	1.92	55474	
Fe	0.00	0	
Co	0.00	19	
Ni	0.00	0	
Cu	2.10	24702	
Zn	27.40	1151352	

V: Assessing the concentration Zn(II) ions released by the ZnO-loaded CS/TPP NPs for 336 h.

Sample ID: A3 336 HRS

Sample Date/Time: Wednesday, August 10, 2022 13:16:30
Sample Description:
Solution Type: Sample
Sample File: C:\Users\Public\Documents\PerkinElmer Syngistix\ICPMS\Sample\Dr Naomi samples.sam
Method File: C:\Users\Public\Documents\PerkinElmer Syngistix\ICPMS\Method\Dr NaomiTotalQuant.mth
Dataset File: C:\Users\Public\Documents\PerkinElmer Syngistix\ICPMS\DataSet\Default\A3 336 HRS.1594
Response File: C:\Users\Public\Documents\PerkinElmer Syngistix\ICPMS\System\totalquant100822.rsp
Initial Sample Quantity (mg):
Sample Prep Volume (mL):
Aliquot Volume (mL):
Diluted to Volume (mL):
Torch Z Position (mm): 0.00

Report Concentration Unit: ppb

Analyte Intensities

Analyte	Concentration	Intensity	Intensity Comment
F		0	
Ne		0	
Na	0.00	0	
Mg	29.62	1552798	
Al	2.58	109984	
Si	33.72	904702	
P	200.78	942406	
S	0.00	0	
Cl	0.00	0	
Ar	0.00	0	
K	0.00	0	
Ca	6.99	2041642	
Sc	0.00	0	
Ti	0.06	34429	
V	0.00	0	
Cr	0.00	0	
Mn	2.07	60044	
Fe	0.00	0	
Co	0.00	92	
Ni	0.00	0	
Cu	1.24	14590	
Zn	38.43	1554565	

RANDOM IMAGES FOR SEED GERMINATION EXPERIMENT

